

Mathematical modeling with applications in biological systems, physiology,
and neuroscience

by

Tahmineh Azizi

B.Sc., Isfahan University of Technology, Iran, 2013

AN ABSTRACT OF A DISSERTATION

submitted in partial fulfillment of the
requirements for the degree

DOCTOR OF PHILOSOPHY

Department of Mathematics
College of Arts and Sciences

KANSAS STATE UNIVERSITY
Manhattan, Kansas

2021

Abstract

Dynamical systems modeling is used to describe different biological and physical systems as well as to predict the interactions between multiple components of a system over time. A dynamical system describes the evolution of a given system over time using a set of mathematical laws, typically described by differential equations. There are two main methods to model the dynamical behaviors of a system: continuous time modeling and discrete-time modeling. When the time between two measurements is negligible, the continuous time modeling governs the evolution of the system, however, when there is a gap between any two consecutive measurements, discrete-time system modeling comes into play. Differential equations are used to model continuous systems and iterated maps represent the generations in discrete-time systems. In this dissertation, we study some dynamical systems and present their applications to different problems in biological systems, physiology, and neuroscience.

In chapter one, we study the local dynamics of some interesting systems and show the local stable behavior of the system around its critical points. Moreover, we investigate the local dynamical behavior of different systems including the Hénon-Heiles system, the Duffing oscillator, and the Van der Pol equation. Furthermore, we discuss about the chaotic behavior of Hamiltonian systems using two different and new examples.

In chapter two, we consider some models in computational neuroscience. Due to the complexity of nerve systems, linear modeling methods are not sufficient to understand the various phenomena in neuroscience. We use nonlinear methods and models, which aim at capturing certain properties of the neurons and their complex dynamics. Specifically, we explore the interesting phenomenon of firing spikes and complex dynamics of the Morris-Lecar model. We consider a set of parameters such that the model exhibits a wide range of phenomenon. We investigate the influences of injected current and temperature on the spiking dynamics of Morris-Lecar model. In addition, we study bifurcations, and computational properties of

this neuron model. Moreover, we provide a bound for the membrane potential and a certain voltage value or threshold for firing the spikes. Studying the two co-dimension bifurcations demonstrates more complicated behaviors for this single neuron model. Furthermore, we describe the phenomenon of neural bursting and investigate the dynamics of Morris-Lecar model as a square-wave burster, elliptic burster and parabolic burster.

Pharmacokinetic models are mathematical models, which provide insights into the interaction of chemicals with certain biological processes. In chapter three, we consider the process of drug and nanoparticle (NPs) distribution throughout the body. We use a tri-compartmental model to study the perfusion of NPs in tissues and a six-compartmental model to study drug distribution in different body organs. We perform global sensitivity analysis by LHS Monte Carlo method using Partial Rank Correlation Coefficient (PRCC). We identify the key parameters that contribute most significantly to the absorption and distribution of drugs and NPs in different organs in the body.

In chapter four, we study two infectious disease models and use nonlinear optimization and optimal control theory to help in identifying strategies for transmission control and forecasting the spread of infectious diseases. We analyze the effect of vaccination on the disease transmission in these models. Moreover, we perform global sensitivity analysis to investigate the key parameters in these models.

In chapter five, we investigate the complex dynamics of two-species Ricker-type discrete-time competitive model. We perform local stability analysis for the fixed points of the system and discuss about its persistence for boundary fixed points. This system inherits properties of the dynamics of a one-dimensional Ricker model such as the cascade of period-doubling bifurcation, periodic windows, and chaos. We explore the existence of chaos for the equilibrium points for a specific case of this system using Marotto theorem and show the existence of snap-back repeller.

In chapter six, we study the problem of chaos synchronization in certain discrete-time dynamical systems. We introduce a drive-response discrete-time dynamical system, which is coupled using convex link function. We investigate a synchronization threshold, after which, the drive-response system uncouples and loses its synchronized behaviors. We apply this

method to the synchronized cycles of the Ricker model and show that this model displays a rich cascade of complex dynamics from a stable fixed point and cascade of period-doubling bifurcation to chaos. We numerically verify the effectiveness of the proposed scheme and demonstrate how this type of coupling affects the synchronization of the system.

In chapter seven, we study the synchronized cycles of a generalized Nicholson-Bailey model. This model demonstrates a rich cascade of complex dynamics from a stable fixed point to periodic orbits, quasi periodic orbits and chaos. We introduce a coupling of these two chaotic systems with different initial conditions and show how they synchronize over a short time. We investigate the qualitative behavior of Generalized Nicholson-Bailey model and its synchronized model using time series analysis and its long-time dynamics by using its bifurcation diagram.

Mathematical modeling with applications in biological systems, physiology,
and neuroscience

by

Tahmineh Azizi

B.Sc., Isfahan University of Technology, Iran, 2013

A DISSERTATION

submitted in partial fulfillment of the
requirements for the degree

DOCTOR OF PHILOSOPHY

Department of Mathematics
College of Arts and Sciences

KANSAS STATE UNIVERSITY
Manhattan, Kansas

2021

Approved by:

Major Professor
Dr. Bacim Alali

Copyright

© Tahmineh Azizi 2021.

Abstract

Dynamical systems modeling is used to describe different biological and physical systems as well as to predict the interactions between multiple components of a system over time. A dynamical system describes the evolution of a given system over time using a set of mathematical laws, typically described by differential equations. There are two main methods to model the dynamical behaviors of a system: continuous time modeling and discrete-time modeling. When the time between two measurements is negligible, the continuous time modeling governs the evolution of the system, however, when there is a gap between any two consecutive measurements, discrete-time system modeling comes into play. Differential equations are used to model continuous systems and iterated maps represent the generations in discrete-time systems. In this dissertation, we study some dynamical systems and present their applications to different problems in biological systems, physiology, and neuroscience.

In chapter one, we study the local dynamics of some interesting systems and show the local stable behavior of the system around its critical points. Moreover, we investigate the local dynamical behavior of different systems including the Hénon-Heiles system, the Duffing oscillator, and the Van der Pol equation. Furthermore, we discuss about the chaotic behavior of Hamiltonian systems using two different and new examples.

In chapter two, we consider some models in computational neuroscience. Due to the complexity of nerve systems, linear modeling methods are not sufficient to understand the various phenomena in neuroscience. We use nonlinear methods and models, which aim at capturing certain properties of the neurons and their complex dynamics. Specifically, we explore the interesting phenomenon of firing spikes and complex dynamics of the Morris-Lecar model. We consider a set of parameters such that the model exhibits a wide range of phenomenon. We investigate the influences of injected current and temperature on the spiking dynamics of Morris-Lecar model. In addition, we study bifurcations, and computational properties of

this neuron model. Moreover, we provide a bound for the membrane potential and a certain voltage value or threshold for firing the spikes. Studying the two co-dimension bifurcations demonstrates more complicated behaviors for this single neuron model. Furthermore, we describe the phenomenon of neural bursting and investigate the dynamics of Morris-Lecar model as a square-wave burster, elliptic burster and parabolic burster.

Pharmacokinetic models are mathematical models, which provide insights into the interaction of chemicals with certain biological processes. In chapter three, we consider the process of drug and nanoparticle (NPs) distribution throughout the body. We use a tri-compartmental model to study the perfusion of NPs in tissues and a six-compartmental model to study drug distribution in different body organs. We perform global sensitivity analysis by LHS Monte Carlo method using Partial Rank Correlation Coefficient (PRCC). We identify the key parameters that contribute most significantly to the absorption and distribution of drugs and NPs in different organs in the body.

In chapter four, we study two infectious disease models and use nonlinear optimization and optimal control theory to help in identifying strategies for transmission control and forecasting the spread of infectious diseases. We analyze the effect of vaccination on the disease transmission in these models. Moreover, we perform global sensitivity analysis to investigate the key parameters in these models.

In chapter five, we investigate the complex dynamics of two-species Ricker-type discrete-time competitive model. We perform local stability analysis for the fixed points of the system and discuss about its persistence for boundary fixed points. This system inherits properties of the dynamics of a one-dimensional Ricker model such as the cascade of period-doubling bifurcation, periodic windows, and chaos. We explore the existence of chaos for the equilibrium points for a specific case of this system using Marotto theorem and show the existence of snap-back repeller.

In chapter six, we study the problem of chaos synchronization in certain discrete-time dynamical systems. We introduce a drive-response discrete-time dynamical system, which is coupled using convex link function. We investigate a synchronization threshold, after which, the drive-response system uncouples and loses its synchronized behaviors. We apply this

method to the synchronized cycles of the Ricker model and show that this model displays a rich cascade of complex dynamics from a stable fixed point and cascade of period-doubling bifurcation to chaos. We numerically verify the effectiveness of the proposed scheme and demonstrate how this type of coupling affects the synchronization of the system.

In chapter seven, we study the synchronized cycles of a generalized Nicholson-Bailey model. This model demonstrates a rich cascade of complex dynamics from a stable fixed point to periodic orbits, quasi periodic orbits and chaos. We introduce a coupling of these two chaotic systems with different initial conditions and show how they synchronize over a short time. We investigate the qualitative behavior of Generalized Nicholson-Bailey model and its synchronized model using time series analysis and its long-time dynamics by using its bifurcation diagram.

Table of Contents

List of Figures	xiv
Acknowledgements	xxi
Dedication	xxii
1 Application of Stability Theory in Studying the Local Dynamics of Nonlinear Systems	1
1.1 Introduction	1
1.2 Dynamical systems theory	2
1.3 Application of continuous dynamical systems modeling	7
1.3.1 Hénon-Heiles system	7
1.3.2 Duffing oscillator	9
1.3.3 The Van der Pol equation	10
1.4 Chaos in continuous dynamical systems	11
1.5 Conclusion	12
2 Neural Bursting and Spiking in Neurons: the Morris-Lecar Model	17
2.1 Introduction	1
2.2 Description of model equations	2
2.3 The Hopf case	4
2.4 The SNLC case	10
2.5 The Homoclinic case	13
2.6 Two co-dimension bifurcations	16

2.7	Bursting behaviors of the Morris-Lecar model	20
2.7.1	Morris-Lecar model as a Square-Wave burster	21
2.7.2	Morris-Lecar model as an Elliptic burster	23
2.7.3	Morris-Lecar model as a Parabolic burster	23
2.8	Conclusion	25
3	Global Sensitivity Analysis in Physiological Systems	29
3.1	Introduction	1
3.2	A simple three compartmental model example for NP distribution	3
3.3	A six compartmental model example for drug distribution through body organs	8
3.4	Global sensitivity analysis	14
3.4.1	Partial Rank Correlation Coefficient (PRCC) results for tri-compartmental model (3.1)	15
3.4.2	Partial Rank Correlation Coefficient (PRCC) results for six-compartmental model (3.1)-(3.25)	16
3.5	Conclusion	17
4	Impact of Vaccination Strategies and Key Parameters on Infectious Disease Models	22
4.1	Introduction	1
4.2	Kermack-McKendrick SIR epidemic model (S-I-R Model)	4
4.2.1	Will the disease spread? What is the max number of infectives I_{max} ? How many people catch the disease?	7
4.3	The S-E-I-R model	9
4.4	Optimal control problem	13
4.4.1	Pontryagin's Maximum Principle	14
4.4.2	Existence of a finite objective functional value at the optimal control and state variables	16
4.5	An optimal control problem for S-I-R model	17

4.6	An optimal control problem for S-E-I-R model	19
4.7	Global sensitivity analysis	21
4.7.1	Partial Rank Correlation Coefficient (PRCC) results for S-I-R model (4.1)	23
4.7.2	Partial Rank Correlation Coefficient (PRCC) results for S-E-I-R model (4.5)	23
4.8	Conclusion	24
5	Chaos Induced by Snap-Back Repeller in a Two Species Competitive Model	26
5.1	Introduction	1
5.2	The two-species Ricker competitive model and its local dynamics	6
5.3	Global stability analysis using persistence theory	8
5.3.1	Boundedness of the system solutions	8
5.3.2	Persistence of the species	10
5.4	Application of snap-back repeller and Marroto chaos in study of chaotic dy- namics of system	14
5.5	Conclusion	22
6	Chaos Synchronization in Population Dynamics	24
6.1	Introduction	1
6.2	Description of the coupling method	2
6.2.1	Complete synchronization using contraction mapping theorem	3
6.2.2	Local dynamics, attractors and attracting set of drive-response system	7
6.3	Application of chaos synchronization in population dynamics	10
6.3.1	Phase and amplitude synchronization in population dynamics	15
6.3.2	Complete synchronization in population dynamics	16
6.4	Conclusion	19
7	Synchronized Cycles of Generalized Nicholson-Bailey Model	21

7.1	Introduction	1
7.2	Drive-response system derivation	3
7.2.1	Stable threshold for synchronization in discrete-time dynamical systems	9
7.3	Synchronized cycles in Generalized Nicholson Bailey (GNB) model: Description of the Model	13
7.3.1	Synchronized cycles in GNB model without parasitoid	15
7.4	Numerical simulations	17
7.5	Conclusion	21

List of Figures

1.1	$F_1(X, Y) = (-X^2 - Y^2) \exp(-X^2 - Y^2)$, local dynamics	3
1.2	$F_2(X, Y) = (X^2 + Y^2) \exp(-X^2 - Y^2)$, local dynamics	4
1.3	$F_3(X, Y) = X^2 \exp(-X^2 - Y^2)$, local dynamics	4
1.4	$Z = Y^2 \exp(-X^2 - Y^2)$, local dynamics	5
1.5	$F_5(X, Y) = (X^2 Y^2) \exp(-X^2 - Y^2)$, local dynamics	6
1.6	$F_6(X, Y) = -(X^2 Y^2) \exp(-X^2 - Y^2)$, local dynamics	6
1.7	Hénon-Heiles system phase portraits	8
1.8	Chaotic solutions of Duffing oscillator (1.20) for $amp = 0.42$, $b = 0.5$, $\alpha = -1.0$, $\beta = 1.0$, $w = 1.0$, Periodic solutions of Duffing oscillator (1.20) for $amp = 0.35$, $b = 0.75$, $\alpha = -1.0$, $\beta = 1.0$, $w = 1.0$	10
1.9	Periodic solutions of Duffing oscillator (1.20) for $amp = 0.45$, $b = 0.45$, $\alpha = -1.0$, $\beta = 1.0$, $w = 0.75$, Chaotic solutions of Duffing oscillator (1.20) for $amp = 0.4$, $b = 0.49$, $\alpha = -1.0$, $\beta = 1.0$, $w = 1.1$	11
1.10	Periodic solutions of Duffing oscillator (1.20) for $amp = 0.43$, $b = 0.51$, $\alpha = -1.0$, $\beta = 1.0$, $w = 1.05$, Chaotic solutions of Duffing oscillator (1.20) for $amp = 0.39$, $b = 0.47$, $\alpha = -1.0$, $\beta = 1.0$, $w = 0.9$	12
1.11	Solutions of Van der Pol equation (1.22) with $\mu = 0.75$ and $\mu = 5$	13
1.12	Solutions of Van der Pol equation (1.22) with $\mu = 0.5$ and $\mu = 3$	14
1.13	Solutions of Van der Pol equation (1.22) with $\mu = 0.25$ and $\mu = 10$	15
1.14	Solutions of Van der Pol equation (1.22) with $\mu = 0.1$ and $\mu = 15$	15
1.15	Dissolving the KAM tori caused by perturbation, $H_1(x, y) = -((1/2)x^2) + \epsilon(\sin((\pi/2)y) + \sin((\pi/2)(y - \beta)))$	16

1.16	Dissolving the KAM tori caused by perturbation, $H_2(x, y) = -((1/2)x^2) + \epsilon(\cos((2\pi)y) + \cos((2\pi)(y - \beta)))$	16
2.1	Equivalent circuit for model (2.1). E_K , E_{Ca} , and E_L the Nernst equilibrium potentials. I_{app} the injected current, g_L leak membrane conductance, g_K potassium membrane conductance, g_{Ca} calcium membrane conductance, C_M the total membrane capacitance.	4
2.2	Morris-Lecar parameters ³⁷	5
2.3	Nullclines of model (2.1) with $I_{app} = 0, 25, 50, 100$	5
2.4	Time series of model (2.1) with $I_{app} = 20$ left, and $I_{app} = 40$ right.	6
2.5	Trajectories of model (2.1) with $I_{app} = 87$ (up,left), $I_{app} = 88.25$ (up,right), $I_{app} = 88.3$ (down,left), $I_{app} = 90$ (down,right).	7
2.6	Threshold for firing a spike in model (2.1).	8
2.7	The Nullclines of model (2.1) in the case of SNLC bifurcation.	10
2.8	Trajectories of model (2.1) in the case of SNLC bifurcation for (up,left) $I_{app} = 5$, (up.right) $I_{app} = 30$, (down,left) $I_{app} = 42$, (down, right) $I_{app} = 100$	11
2.9	Trajectories of model (2.1) in the case of Saddle-Homoclinic bifurcation for (up,left) $I_{app} = 0$, (up.right) $I_{app} = 40$, (down,left) $I_{app} = 50$, (down, right) $I_{app} = 70$	14
2.10	Nullclines of model (2.1) with $I_{app} = 0, 25, 50, 100$	15
2.11	Continuation of equilibrium point in generalized Hopf bifurcation with $\phi = 0.30634507$	18
2.12	Continuation of equilibrium point in generalized Hopf bifurcation with $\phi = 0.30634507$	19
2.13	Continuation of limit point cycles. Influence of injected current on neuron activities, maximum and minimum voltage bound.	20
2.14	Continuation of limit point cycles. Influence of temperature on neuron activities, maximum and minimum voltage bound.	21

2.15	Equivalent circuit for model (2.33). E_K , E_{Ca} , and E_L the Nernst equilibrium potentials. I_{app} the injected current, g_L leak membrane conductance, g_K potassium membrane conductance, g_{Ca} calcium membrane conductance, C_M the total membrane capacitance.	23
2.16	Bursting parameters ³⁷	24
2.17	Continuation of equilibrium points for $I_{app} = 0, 50, 100, 150, 200$ and occurrence of cusp bifurcation with considering 2 free parameters, the horizontal curve corresponding to co-dimension two bifurcation and the vertical curves are corresponding to co-dimension one bifurcation with increasing I_{app} from left to right. Morris-Lecar model as a Square-Wave burster.	25
2.18	Continuation of equilibrium points for $I_{app} = -50, 0, 45, 100, 150, 200, 250, 300$, the horizontal curve corresponding to co-dimension two bifurcation and the vertical curves are corresponding to co-dimension one bifurcation with increasing I_{app} from left to right. Morris-Lecar model as an Elliptic burster.	26
2.19	Equivalent circuit for model (2.34), Morris-Lecar model as a Parabolic burster. E_K , E_{Ca} , and E_L the Nernst equilibrium potentials. I_{app} the injected current, g_L leak membrane conductance, g_K potassium membrane conductance, g_{Ca} calcium membrane conductance, C_M the total membrane capacitance.	27
2.20	Continuation of equilibrium points for $I_{app} = 0, 50, 100, 150, 200$ and occurrence of the zero-Hopf and Bogdanov-Takens and cusp bifurcation with considering 2 free parameters for model (2.34), the horizontal curve corresponding to co-dimension two bifurcation and the vertical curves are corresponding to co-dimension one bifurcation with increasing I_{app} from left to right. Morris-Lecar model as a Parabolic burster.	28
3.1	Endothelial cells as barriers between blood vessels and target tissue.	4

3.2	Structure of the tri-compartment pharmacokinetic model for nanoparticle disposition with considering NPs infusion, where k_{23} , k_{32} and k_{34} are transfer rate constants, k_{25} describes the rate of mass transfer from vascular (2) compartment to the venous effluent, J_{12} is the infusion drug flux, which is the product of flow (Q) and concentration (C_{12}).	5
3.3	A_{Cap} , A_{EC} and A_{DT} in model (3.1).	7
3.4	Global uncertainty and sensitivity analysis of calculated different parameters for capillary compartment of model (3.1).	16
3.5	Global uncertainty and sensitivity analysis of calculated different parameters for endothelial cell compartment of model (3.1).	17
3.6	Global uncertainty and sensitivity analysis of calculated different parameters for deep tissue compartment of model (3.1).	18
3.7	Global uncertainty and sensitivity analysis of calculated different parameters for kidney. Analysis based on parameter effects for C_k (concentration of drug in kidney). The PRCCs are compiled within the pharmacokinetic parameters ranges obtained from ⁶³⁻⁶⁵	19
3.8	Global uncertainty and sensitivity analysis of calculated different parameters for kidney. Analysis based on parameter effects for C_L (concentration of drug in liver). The PRCCs are compiled within the pharmacokinetic parameters ranges obtained from ⁶³⁻⁶⁵	19
3.9	Global uncertainty and sensitivity analysis of calculated different parameters for kidney. Analysis based on parameter effects for C_{Lu} (concentration of drug in lung). The PRCCs are compiled within the pharmacokinetic parameters ranges obtained from ⁶³⁻⁶⁵	20

3.10	Global uncertainty and sensitivity analysis of calculated different parameters for kidney. Analysis based on parameter effects for C_F (concentration of drug in fat). The PRCCs are compiled within the pharmacokinetic parameters ranges obtained from ⁶³⁻⁶⁵	20
3.11	Global uncertainty and sensitivity analysis of calculated different parameters for kidney. Analysis based on parameter effects for C_M (concentration of drug in muscle). The PRCCs are compiled within the pharmacokinetic parameters ranges obtained from ⁶³⁻⁶⁵	21
3.12	Global uncertainty and sensitivity analysis of calculated different parameters for kidney. Analysis based on parameter effects for C_V (concentration of drug in plasma). The PRCCs are compiled within the pharmacokinetic parameters ranges obtained from ⁶³⁻⁶⁵	21
4.1	The SIR schematic model for system (4.1). S :=Susceptible Compartment, I := Infective Compartment, R := Removed Compartment.	5
4.2	The time-evolution of disease over 300 days $\beta = 5 \times 10^{-9}$, $\gamma = 0.12$, $\delta = 0.016$	5
4.3	The time-evolution of disease over 300 days $\beta = 5 \times 10^{-9}$, $\gamma = 0.12$, $\delta = 0.0$	6
4.4	The time-evolution of disease over 300 days $\beta = 5 \times 10^{-9}$, $\gamma = 0.07$, $\delta = 0.0$	6
4.5	The transport diagram for S-E-I-R model (7.15). S :=Susceptible Compartment, E := Exposed Compartment, I := Infective Compartment, R := Removed Compartment.	9
4.6	The time-evolution of system (4.5) over 300 days $\beta = 5 \times 10^{-9}$, $\gamma = 0.07$, $\delta = 1/60$ and $\mu = 1/50$	13
4.7	Solutions of optimal control problem for $S-E-I-R$ model (4.1). u := Vaccination related variable, S :=Susceptible Population, I := Infective Population, R := Removed Population.	19

4.8	Solutions of optimal control problem for S-E-I-R model (4.5). u := Vaccination related variable, S :=Susceptible Population, E := Exposed Population, I := Infective Population, R := Removed Population	22
4.9	Global uncertainty and sensitivity analysis of calculated different parameters for S-I-R model (4.1).	23
4.10	Global uncertainty and sensitivity analysis of calculated different parameters for S-E-I-R model (4.5).	24
5.1	Snap-Back repeller schematic diagram.	2
5.2	Bifurcation diagram of system (5.5) when $k = 10$ and $r_1 = r_2 = r$	20
5.3	Bifurcation diagram of system (5.5) when $r_1 = 2.75$ and $r_2 = 2.5$	21
5.4	Evolution of host population X_1 and its coupled X_2 in time for system (5.5) when $k = 10$	22
6.1	The schematic diagram for complete synchronization in a discrete-time drive-response dynamical system.	8
6.2	The mean phase difference and the mean amplitude difference for drive-response system (6.10)-(6.11) when $r = 3$	16
6.3	Evolution of host population x_1 and its coupled x_2 in time with two different initial conditions for drive-response system (6.10)-(6.11) when $s = 0.5$ and $k = 10$, drive system (red color) and response system (black color).	17
6.4	Evolution of host population x_1 and its coupled x_2 in time with two different initial conditions for drive-response system (6.10)-(6.11) when $s = 0.95$ and $k = 10$, drive system (red color) and response system (black color).	18
6.5	Bifurcation diagram of Ricker model and its coupled with the error between their attractors for $s = 0.95$ and $k = 10$, drive system (red color) and response system (black color).	19

6.6	Poincaré section and spectrum for Ricker model and its coupled with corresponding error for $s = 0.95$, $r = 3$ and $k = 10$, drive system (red color) and response system (black color).	20
7.1	The schematic diagram for complete synchronization in a discrete-time drive-response dynamical system.	7
7.2	Evolution of host population x_1 and its coupled x_2 in time for drive-response system (7.30)-(7.31) when $s = 0.95$, $k = 10$	16
7.3	(a): bifurcation diagram for drive-response system (7.30)-(7.31) when $s = 0.95$, $k = 10$, red (drive system) and black (response system), (b): the error between the solutions of drive system and response system receptively, (c): the Lyapunov Exponent corresponding to drive-response system (7.30)-(7.31) when $s = 0.95$, $k = 10$, red (drive system) and black (response system).	17
7.4	Attractors for drive-response system (7.24)-(7.27) when $s = 0.5$, $a = 40$, $k = 10$, from up left side $r = 1.08, 1.087, 1.095$, and from down left side $r = 1.099, 1.1, 1.15$	18
7.5	Attractors for drive-response system (7.24)-(7.27) when $s = 0.99995$, $a = 40$, $k = 10$, from up left side $r = 1.08, 1.087, 1.095$, and from down left side $r = 1.099, 1.1, 1.15$	19
7.6	Evolution of host population x_1 and its coupled x_2 in time for drive-response system (7.24)-(7.27) when $s = 0.5$, $a = 40$, $k = 10$	20
7.7	Evolution of host population x_1 and its coupled x_2 in time for drive-response system (7.24)-(7.27) when $s = 0.95$, $a = 40$, $k = 10$	21
7.8	Up: bifurcation diagram for drive-response system (7.24)-(7.27) for $a = 40$, $s = 0.5$, $k = 10$. Down: the error between the solutions of drive system and response system receptively	22

- 7.9 Up: bifurcation diagram for drive-response system (7.24)-(7.27) for $a = 40$, $s = 0.95$, $k = 10$, red (drive system) and blue (response system). Down: the error between the solutions of drive system and response system receptively . 23
- 7.10 Attractors for drive-response system (7.24)-(7.27) when $s = 0.94$, $a = 5$, $k = 1.5$, from up left side $r = 2.0, 2.2, 2.3$, and from down left side $r = 2.5, 2.7, 2.8$. 24
- 7.11 Attractors for drive-response system (7.24)-(7.27) when $s = 0.95$, $a = 5$, $k = 1.5$, from up left side $r = 2.0, 2.2, 2.3$, and from down left side $r = 2.5, 2.7, 2.8$. 24
- 7.12 Attractors for drive-response system (7.24)-(7.27) when $s = 0.96$, $a = 5$, $k = 1.5$, from up left side $r = 2.0, 2.2, 2.3$, and from down left side $r = 2.5, 2.7, 2.8$. 25
- 7.13 Attractors for drive-response system (7.24)-(7.27) when $s = 0.99$, $a = 5$, $k = 1.5$, from up left side $r = 2.0, 2.2, 2.3$, and from down left side $r = 2.5, 2.7, 2.8$.. 25

Acknowledgments

First and foremost, praises and thanks to Dr. Santosh Aryal, his dynamism, vision, sincerity and motivation have deeply inspired me, without him I would not have been able to complete this research, and without him I would not have made it through my doctorate degree and then job.

I would like to express my deep and sincere gratitude to Dr. Bacim Alali, and also Dr. Gabriel Kerr and Dr. Majid Jaber-Douraki for giving me the opportunity to do research and providing invaluable guidance throughout this research. They have taught me the methodology to carry out the research and to present the research works as clearly as possible. It was a great privilege and honor to work and study under their guidance.

I cannot express enough thanks to my committee for their continued support and encouragement: Dr. Lizaveta Ihnatsyeva and Dr. Jingru Mu.

I am extremely grateful to my parents for their love, prayers, caring and sacrifices for educating and preparing me for my future.

I would like to say thanks to Dr. Pritam Sidhu, Dr. Hossein Amini, Dr. Miao Li, Dr. Heman Shakeri for all the support they have shown me through PhD and then job market.

I offer my sincere appreciation for the learning opportunities provided by Dr. David Auckly, Dr. Jim E. Riviere, Dr. Hans Coetzee, Dr. Nancy A. Monteiro-Riviere, Dr. Zhoumeng Lin, Dr. Henry Adams, Dr. Don Saucier, and Dr. Brooks Emerick.

Finally, my thanks go to all the people who have supported me to complete the research work directly or indirectly.

Dedication

*This dissertation is dedicated to my MOM
For her endless love, support and encouragement.*

Chapter 1

Application of Stability Theory in Studying the Local Dynamics of Nonlinear Systems

Abstract

In Chapter One, we study the local dynamics of some interesting systems and show the local stable behavior of the system around its critical points. Moreover, we investigate the local dynamical behavior of different systems including the Hénon-Heiles system, the Duffing oscillator, and the Van der Pol equation. Furthermore, we discuss about the chaotic behavior of Hamiltonian systems using two different and new examples.

1.1 Introduction

A dynamical system describes the evolution of a system over time using a set of mathematical laws. Moreover, it can be used to predict the interactions between different components of a system^{1;2}. There are two main methods to model the dynamical behaviors of a system, continuous time modeling, discrete-time modeling¹⁻³. When the time between two measurements is negligible, the continuous time modeling governs the evolution of the system, however, when there is a gap between two measurements, discrete-time system modeling comes to play. Ordinary differential equations are the tool to model a continuous system and iterated maps represent the discrete generations^{4;203}.

In this paper we will be concerned with continuous dynamical systems which are defined by differential equations. Indeed, some famous examples of dynamical systems can be written in terms of differential equations: the harmonic oscillator, the pendulum and double pendulum, or the N-body problem^{4;6-8;41;203}. A dynamical system is a triple (M, Φ_t, K) where M is called the phase space and is usually a smooth manifold or a subset of \mathbb{R}^n , $\Phi_t : M \times K \rightarrow M$, called the evolution, is a smooth action of K in M and K is either a subset of \mathbb{R} in the case of a continuous time dynamical system or a subset of \mathbb{Z} in the case of a discrete time dynamical system. The smooth action $\Phi_t(x)$ describes the evolution with time $t \in K$ of a point x in the phase space M ^{4;6;7;203}.

Stability of a system is one of the most important parts of the studying the dynamical behavior of a system. Generally speaking, an unstable and moreover a chaotic system are not useful and we like to work with a system with stable and or periodic behavior (although chaos is a known behavior for many systems and sometimes people look for different strategies for chaotification of a system for different purposes¹⁰⁻¹²).

There are different definitions for stability, however, all they have this common fact that a system is stable if perturbation, external input and or intentionally applied signals can not make the system get away from the equilibrium point^{13;14}. There are three possibilities for dynamical behavior of a system after applying a perturbation²⁰³:

1. The system state would return to the equilibrium state.

2. The system state would not return to the equilibrium state but stays near to that state.
3. The system state diverges from the equilibrium state.

Mathematically speaking, the equilibrium state x^* is stable if for each initial conditions $x(0)$ close enough to x^* , the corresponding trajectory $x(t)$ remains near x^* for all $t \geq 0$.

$$\forall \epsilon > 0 \quad \exists \delta > 0 \quad : \quad \|x(0) - x^*\| < \delta \quad \Rightarrow \quad \|x(t) - x^*\| < \epsilon, \quad \forall t \geq 0$$

In this paper, we present some results regarding the study of local dynamics of non-linear continuous time dynamical systems. We provide different examples to display stable and unstable limit cycles and we demonstrate the numerical results for each case. In addition, we study the local dynamics of three well known physical systems, Henon-Heiles system, Duffing oscillator and Van der pol equations and we display the evolution of solutions of the system in time. Finally, we discuss about the chaos in Hamiltonian systems and we provide two examples to show chaos in Hamiltonian systems.

1.2 Dynamical systems theory

When we start to analyze the local dynamics of non-linear systems, the first step is finding the critical points and then exploring how the trajectories of the system evolving in the neighborhood of critical point. This analysis helps us to find out how other solutions or trajectories of the system behave when they get close to the critical points. Another step to analyze a dynamical system is studying the trajectories which trace out a limit cycle or a closed curve. In this case, the solution $x(t)$ of the system will go around and create a closed curve C with a certain period T . Therefore, the solutions $x(t) = (x(t), y(t))$ of the system when it becomes periodic change to be $x(t+T) = x(t), y(t+T) = y(t)$ for all t . Any trajectories which are close to the limit cycle C , follow the same behavior as the limit cycle C . For instance, they can get spiral in toward C , or they can spiral away from C , which demonstrates if the closed curve C is stable or unstable. See Figure (1.1). The root point

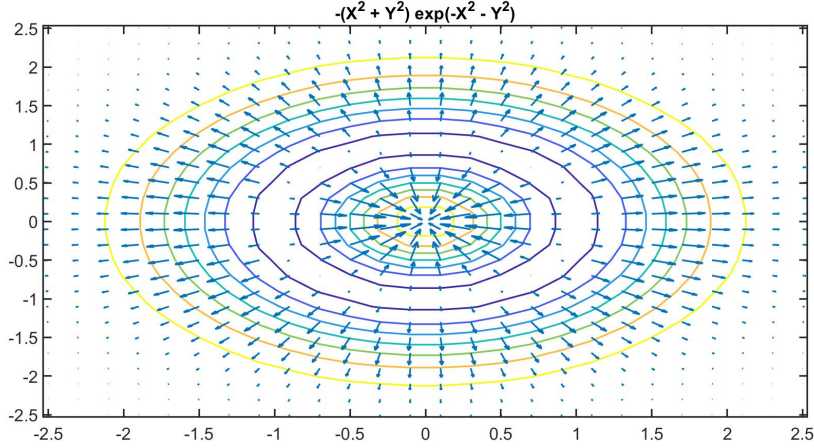


Figure 1.1: $F_1(X, Y) = (-X^2 - Y^2) \exp(-X^2 - Y^2)$, *local dynamics*

for $F_1(X, Y) = (-X^2 - Y^2) \exp(-X^2 - Y^2)$ is $(X, Y) = (0, 0)$. The Taylor expansion for $F_1(X, Y)$ at $(X, Y) = (0, 0)$ has the following form:

$$T_n(X, Y) = -Y^2 e^{-Y^2} + X^2 e^{-Y^2} (Y^2 - 1) - \frac{1}{2} X^4 e^{-Y^2} (Y^2 - 2) + O(X^5) \quad (1.1)$$

From Figure (1.1), the point $(0, 0)$ is a stable fixed point and moreover the maximum of $F_1(X, Y)$ occurs at $(X, Y) = (0, 0)$ and it is:

$$\max\{(-X^2 - Y^2) \exp(-X^2 - Y^2)\} = 0 \quad (1.2)$$

In Figure (1.2), we see $F_2(X, Y) = (X^2 + Y^2) \exp(-X^2 - Y^2)$. The root for $F_2(X, Y)$ is $(X, Y) = (0, 0)$. The Taylor expansion for $F_2(X, Y)$ at $(X, Y) = (0, 0)$ has the following form:

$$T_n(X, Y) = Y^2 e^{-Y^2} - X^2 e^{-Y^2} (Y^2 - 1) + \frac{1}{2} X^4 e^{-Y^2} (Y^2 - 2) + O(X^5) \quad (1.3)$$

The minimum of $F_2(X, Y)$ happens for $(X, Y) = (0, 0)$ which is equal to:

$$\min\{(X^2 + Y^2) \exp(-X^2 - Y^2)\} = 0 \quad (1.4)$$

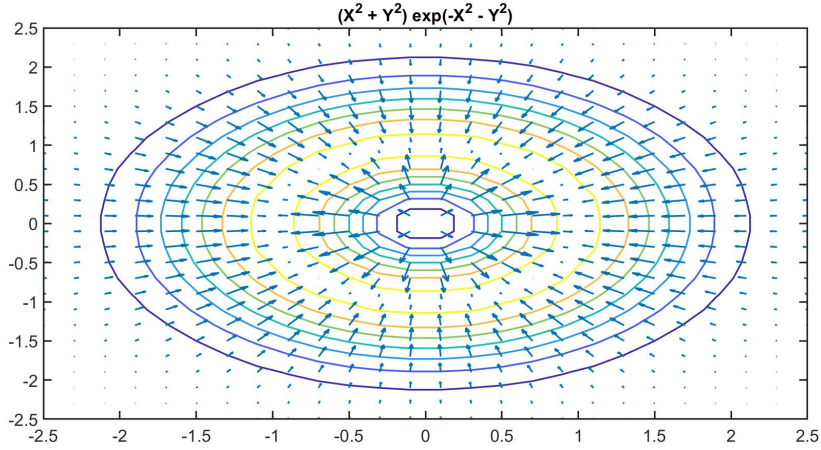


Figure 1.2: $F_2(X, Y) = (X^2 + Y^2) \exp(-X^2 - Y^2)$, *local dynamics*

For $F_2(X, Y)$ the point $(X, Y) = (0, 0)$ is unstable.

Another example, $F_3(X, Y) = X \exp(-X^2 - Y^2)$ which has been displayed in Figure (1.3).

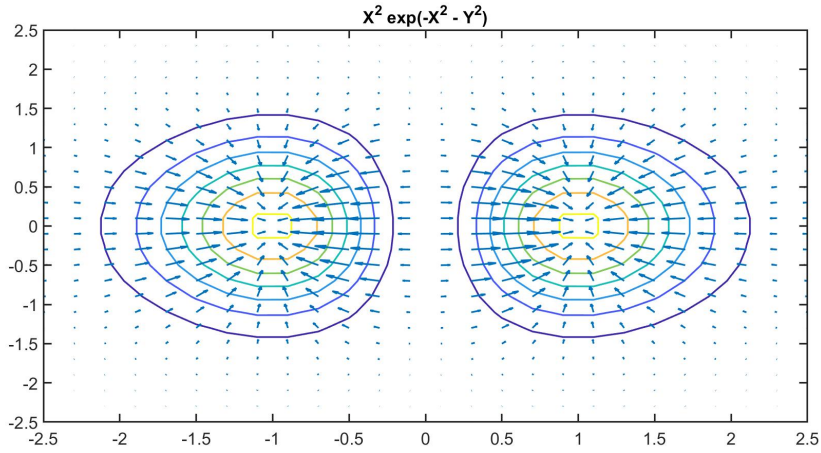


Figure 1.3: $F_3(X, Y) = X^2 \exp(-X^2 - Y^2)$, *local dynamics*

The maximum of $F_3(X, Y)$ occurs at $(X, Y) = (-1, 0)$ and $(X, Y) = (1, 0)$ and it equals to:

$$\max\{X^2 \exp(-X^2 - Y^2)\} = \frac{1}{e} \quad (1.5)$$

In addition, the Taylor expansion for $F_2(X, Y)$ at $X = 0$ has the following form:

$$T_n(X, Y) = X^2 e^{-Y^2} - X^4 e^{-Y^2} + \frac{1}{2} X^6 e^{-Y^2} - \frac{1}{6} X^8 e^{-Y^2} + O(X^9) \quad (1.6)$$

As we can see in Figure (1.3), $(X, Y) = (-1, 0)$ and $(X, Y) = (1, 0)$ are stable.

In Figure (1.4), we can see for $F_4(X, Y) = Y^2 \exp(-X^2 - Y^2)$, $(X, Y) = (0, -1)$ and $(X, Y) = (0, 1)$ are stable.

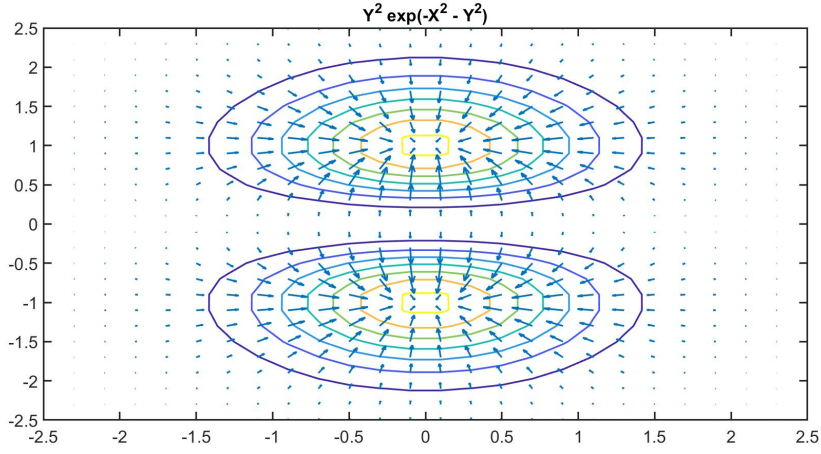


Figure 1.4: $Z = Y^2 \exp(-X^2 - Y^2)$, local dynamics

The maximum of $F_4(X, Y)$ occurs at $(X, Y) = (0, -1)$ and $(X, Y) = (0, 1)$ and equals to

$$\max\{Y^2 \exp(-X^2 - Y^2)\} = \frac{1}{e} \quad (1.7)$$

Moreover, the Taylor expansion for $F_4(X, Y)$ at $X = 0$ has the form

$$T_n(X, Y) = Y^2 e^{-Y^2} - X^2 e^{-Y^2} Y^2 + \frac{1}{2} X^4 e^{-Y^2} Y^2 + O(X^5) \quad (1.8)$$

For $F_5(X, Y) = (X^2 Y^2) \exp(-X^2 - Y^2)$ (Figure (1.5)),

$(X, Y) = (0, 0)$ is a root and Taylor expansion for $F_5(X, Y)$ at $X = 0$ has the form

$$T_n(X, Y) = X^2 e^{-Y^2} Y^2 - X^4 e^{-Y^2} Y^2 + \frac{1}{2} X^6 e^{-Y^2} Y^2 - \frac{1}{6} X^8 e^{-Y^2} Y^2 + O(X^9) \quad (1.9)$$

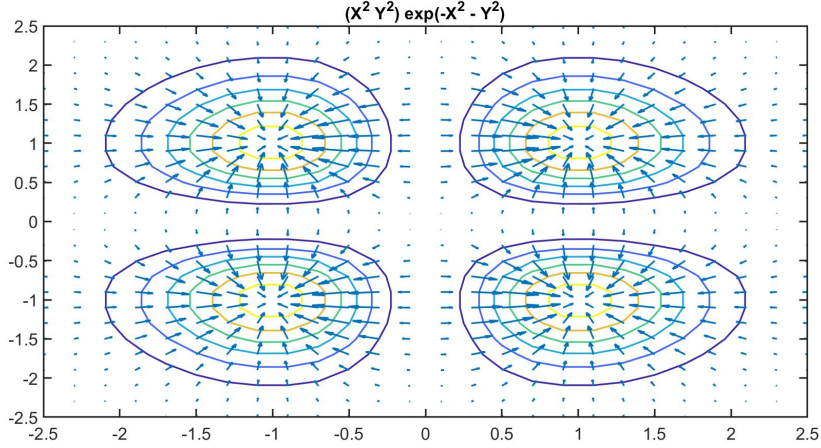


Figure 1.5: $F_5(X, Y) = (X^2 Y^2) \exp(-X^2 - Y^2)$, *local dynamics*

Here, $(X, Y) = (-1, -1)$ and $(X, Y) = (-1, 1)$ give the maximum of $F_5(X, Y)$ which is

$$\max\{X^2 Y^2 \exp(-X^2 - Y^2)\} = \frac{1}{e^2} \quad (1.10)$$

Finally, in Figure (1.6),

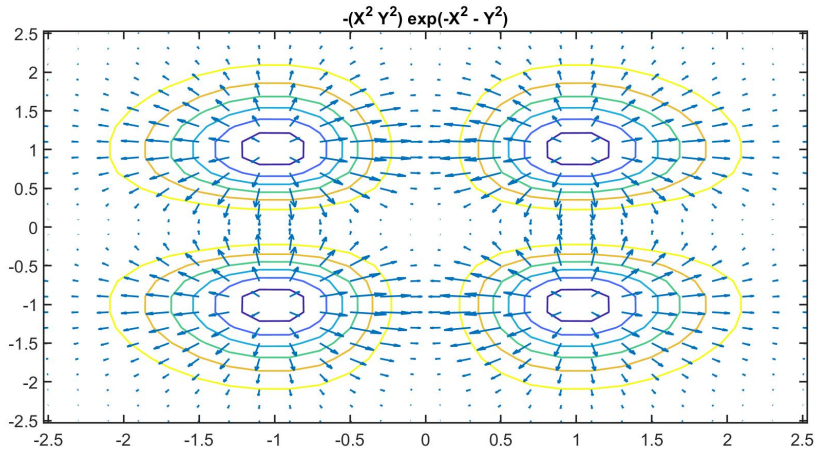


Figure 1.6: $F_6(X, Y) = -(X^2 Y^2) \exp(-X^2 - Y^2)$, *local dynamics*

$F_6(X, Y) = -(X^2 Y^2) \exp(-X^2 - Y^2)$ has a root at $(X, Y) = (0, 0)$ and Taylor expansion for $F_6(X, Y)$ at $X = 0$ has the form

$$T_n(X, Y) = -X^2 e^{-Y^2} Y^2 + X^4 e^{-Y^2} Y^2 - \frac{1}{2} X^6 e^{-Y^2} Y^2 + \frac{1}{6} X^8 e^{-Y^2} Y^2 + O(X^9) \quad (1.11)$$

Here, $(X, Y) = (-1, -1)$ and $(X, Y) = (-1, 1)$ give the minimum of $F_6(X, Y)$ which is

$$\min\{-X^2 Y^2 \exp(-X^2 - Y^2)\} = -\frac{1}{e^2} \quad (1.12)$$

1.3 Application of continuous dynamical systems modeling

1.3.1 Hénon-Heiles system

The Hénon-Heiles potential is one of the simplest examples of classical mechanics and Hamiltonian systems¹⁵⁻¹⁸. The Hénon-Heiles Hamiltonian demonstrates the motion of stars around a galactic center. In 1964, Michael Hénon and Carl Heiles simplified the problem of the motion of stars around a galactic center by using a Hamiltonian to describe the motion of stars near the equilibrium¹⁶. The Hénon-Heiles system has a wide application in studying chaotic dynamics in a system. If the energy of the motion becomes close to the bounding energy of the potential sink which is surrounding the center of the potential, this system displays chaotic dynamics¹⁵.

Consider the following nonlinear system of ordinary differential equations

$$\begin{cases} \frac{dx}{dt} = y \\ \frac{dy}{dt} = x - x^2 \end{cases} \quad (1.13)$$

The Hamiltonian function for this system has the form

$$H(x, y) = \frac{y^2}{2} - \frac{x^2}{2} + \frac{x^3}{2} \quad (1.14)$$

For any x, y satisfying (1.13), we have $\frac{dH}{dt} = 0$. For any solution $(x(t), y(t))$ of system (1.13), the Hamiltonian $H(x(t), y(t))$ is constant, it means $\frac{d}{dt}H(x(t), y(t)) = 0$. This is a very nice property of Hamiltonian function which is a conserved quantity for a system of

ordinary differential equations and it is constant along all solution curves of the system. The solution curves are given by $H(x, y) = C$. Here, there are two non degenerate critical points $(0, 0)$ and $(-1, 0)$. The critical point $(0, 0)$ is a saddle point and the eigenvectors corresponding to this critical points are $(1, -1)^T$ and $(1, 1)^T$. The critical point $(-1, 0)$ is a center. Figure (1.7) displays the level curves or contours of four different Hamiltonian functions.

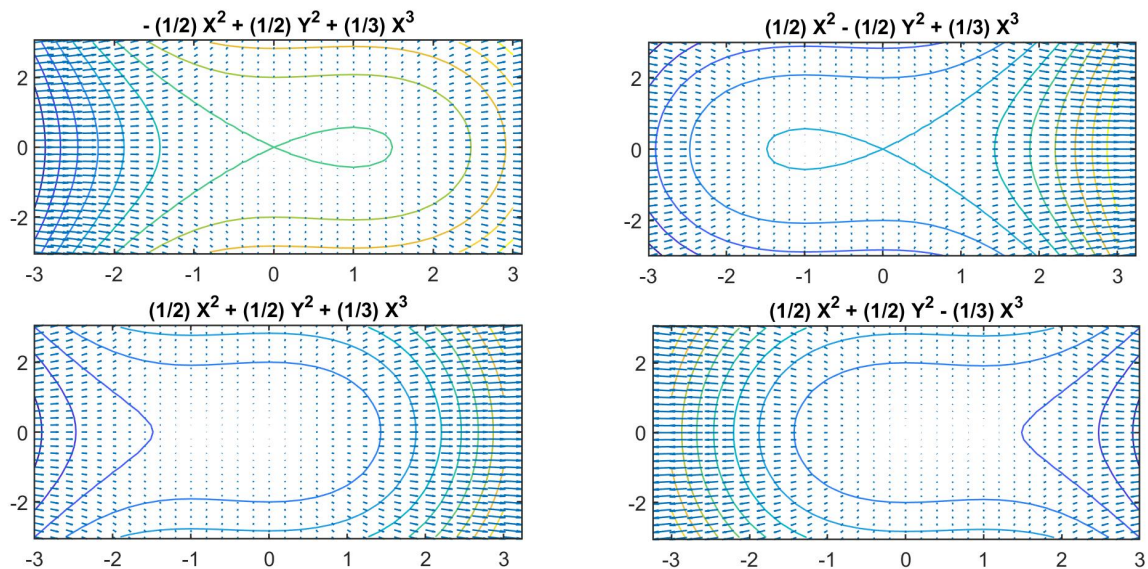


Figure 1.7: *Hénon-Heiles system phase portraits*

Consider the following Hamiltonian functions

$$H_1(x, y) = -\frac{y^2}{2} + \frac{x^2}{2} + \frac{x^3}{2} \quad (1.15)$$

$$H_2(x, y) = \frac{y^2}{2} - \frac{x^2}{2} + \frac{x^3}{2} \quad (1.16)$$

$$H_3(x, y) = \frac{y^2}{2} + \frac{x^2}{2} + \frac{x^3}{2} \quad (1.17)$$

$$H_4(x, y) = \frac{y^2}{2} + \frac{x^2}{2} - \frac{x^3}{2} \quad (1.18)$$

These Hamiltonian functions (1.15)-(1.18), are corresponding to a system of ordinary differential equations. The Hamiltonian function $H_1(x, y)$ has a critical point at $(1, 0)$ and

the Hamiltonian function $H_2(x, y)$ has a critical point at $(-1, 0)$. As we can see in Figure (1.7), the stable and unstable manifolds from the origin for $H_1(x, y)$ and $H_2(x, y)$ form a homoclinic orbit which we can not see this property in Hamiltonian functions $H_3(x, y)$ and $H_4(x, y)$. This homoclinic loop connects the critical point $(0, 0)$ to itself and it takes infinite amount of time to make connection. For Hamiltonian functions $H_1(x, y)$ and $H_2(x, y)$, the critical point $(0, 0)$ is called a saddle-node equilibrium and the Jacobian matrix of the system has a zero eigenvalues at this equilibrium point. However, the critical point $(0, 0)$ for the Hamiltonian functions $H_3(x, y)$ and $H_4(x, y)$ demonstrates another kind of dynamics and it is called the Bogdanov-Takens equilibrium point and the Jaobian matrix in this case has two zero eigenvalues. As it can be seen in Figure (1.7), the critical point $(0, 0)$ is unstable which is the property of Bogdanov-Takens equilibrium point.

1.3.2 Duffing oscillator

The Duffing oscillator is a single ordinary differential equation which represents a nonlinear damped driven oscillator. This simple nonlinear system displays different kinds of dynamical behaviors from periodic and regular behaviors to chaos. When we add a driving force and friction, we can see this simple equation exhibit chaotic behavior¹⁹⁻²¹. The Duffing oscillator equation has the following form

$$y'' + \alpha y' + \beta y + \gamma x^3 = 0, \quad y(0) = A, \quad y'(0) = B \quad (1.19)$$

The law of energy conservation states that this is impossible to see chaotic motion in a single degree of freedom. Therefore, with adding a driving force and damping, the energy conservation would be eliminated. Then, the equations of motion has the form

$$\begin{cases} \frac{dy_1}{dt} = y_2 \\ \frac{dy_2}{dt} = -b y_2 - \alpha y_1 - \beta y_1^3 + amp \sin(w t) \end{cases} \quad (1.20)$$

We have demonstrated different dynamical behaviors of (1.20) in Figures (1.8)-(1.10).

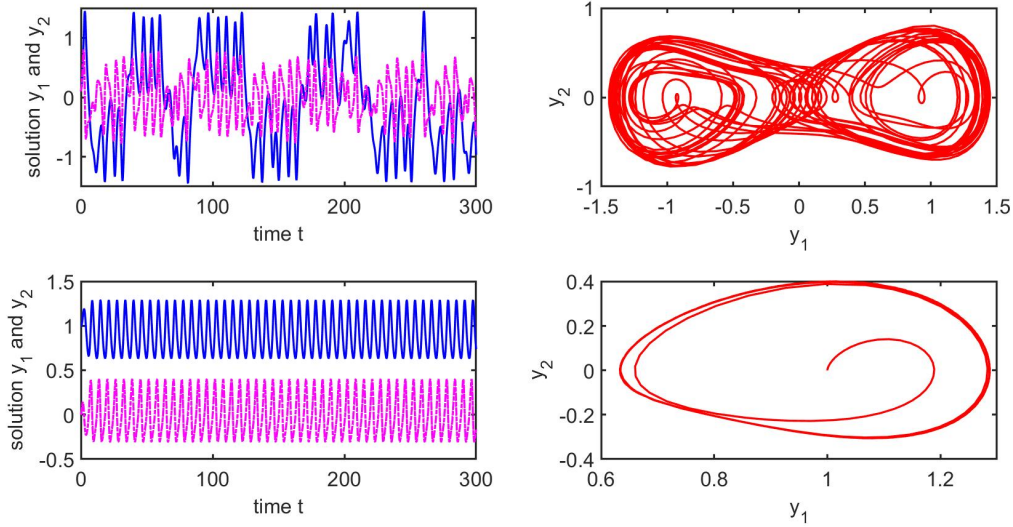


Figure 1.8: *Chaotic solutions of Duffing oscillator (1.20) for $\text{amp} = 0.42$, $b = 0.5$, $\alpha = -1.0$, $\beta = 1.0$, $w = 1.0$, Periodic solutions of Duffing oscillator (1.20) for $\text{amp} = 0.35$, $b = 0.75$, $\alpha = -1.0$, $\beta = 1.0$, $w = 1.0$*

The Duffing oscillator can be used to model different physical phenomenon such as stiffening springs, beam buckling, nonlinear electronic circuits, superconducting Josephson parametric amplifiers, and ionization waves in plasmas²².

1.3.3 The Van der Pol equation

Van der Pol equation which is a well known second order ordinary differential equations with cubic nonlinearity have attracted many researchers in different field of science. This self oscillatory system, Van der Pol oscillator, has been considered as a useful mathematical model for may complicated systems.^{23–25}. Mathematical representation of the Van der Pol system has the form

$$x'' + \mu(x^2 - 1)x' + x = 0 \quad (1.21)$$

where the constant μ is a positive parameter depending on the tube constants. This equation represents the current $x(t)$ in a certain type of vacuum tube. We can write (1.21) as a first

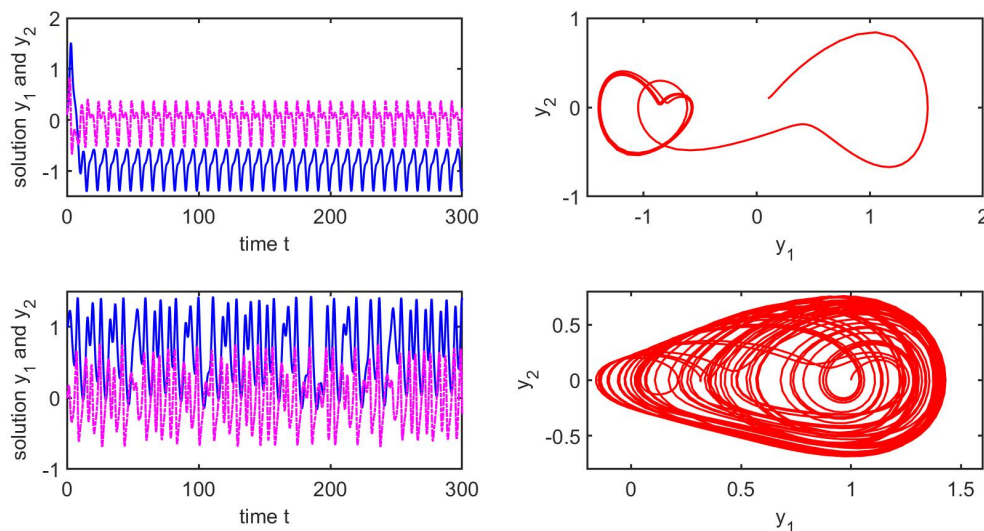


Figure 1.9: *Periodic solutions of Duffing oscillator (1.20) for $\text{amp} = 0.45$, $b = 0.45$, $\alpha = -1.0$, $\beta = 1.0$, $w = 0.75$, Chaotic solutions of Duffing oscillator (1.20) for $\text{amp} = 0.4$, $b = 0.49$, $\alpha = -1.0$, $\beta = 1.0$, $w = 1.1$*

order system of differential equations:

$$\begin{cases} \frac{dx}{dt} = y \\ \frac{dy}{dt} = -\mu(x^2 - 1)y - x \end{cases} \quad (1.22)$$

The numerical integration of equation (1.22) has been represented in Figs. (1.11)-(1.14).

As we can see, depending on different values for μ , solutions look like periodic motion. When μ has small values, this motion is nearly sinusoidal, however for larger values of μ , the solutions seem to be relaxed oscillations which means solutions are similar to a series of step functions and jump twice per cycle between the positive and the negative values.

1.4 Chaos in continuous dynamical systems

In this section, we assume that there is a Hamiltonian function with two degrees of freedom and it is given by $H = H_0 + \epsilon H_1$. Here, we consider ϵ to be a very small parameter, H_0 an integrable Hamiltonian system and H_1 a non-integrable Hamiltonian system (H is a non-

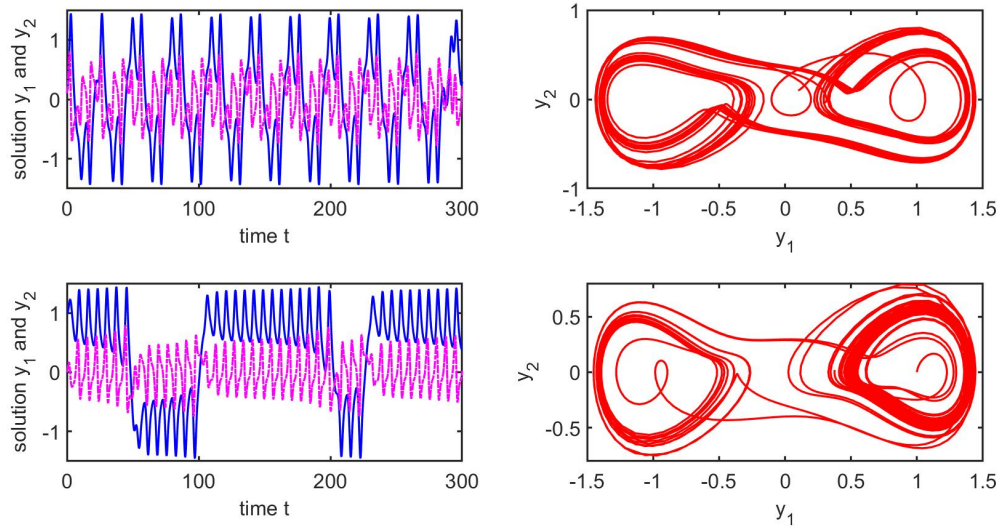


Figure 1.10: *Periodic solutions of Duffing oscillator (1.20) for $\text{amp} = 0.43$, $b = 0.51$, $\alpha = -1.0$, $\beta = 1.0$, $w = 1.05$, Chaotic solutions of Duffing oscillator (1.20) for $\text{amp} = 0.39$, $b = 0.47$, $\alpha = -1.0$, $\beta = 1.0$, $w = 0.9$*

integrable Hamiltonian system). For $\epsilon = 0$ and moreover for $0 < \epsilon \ll 1$, there exist quasi periodic cycles which are known as KAM tori. However, under perturbation, these quasi periodic cycles will be deformed and KAM tori will be dissolved gradually as we increase ϵ . This phenomenon can be observed in Figures (1.15) and (1.16).

According to, KAM theory when x is irrational, then the torus is preserved for small perturbation ϵ . But, proportional tori and adjacent irrational tori would be destroyed. In addition, the stable manifold and unstable manifold of the saddle point which are intersecting transversely, create the Smale horseshoe and chaotic motion. As ϵ increases gradually, these chaotic layers grow and they envelope larger area in phase space^{26;27}.

1.5 Conclusion

Dynamic systems modeling has been frequently used to describe different physical systems and has a very important role in predicting the interactions between multiple components of a system over time. In the present study, we explored different dynamical behaviors of some continuous dynamical systems, from stable and regular motions to periodic and limit cycles,

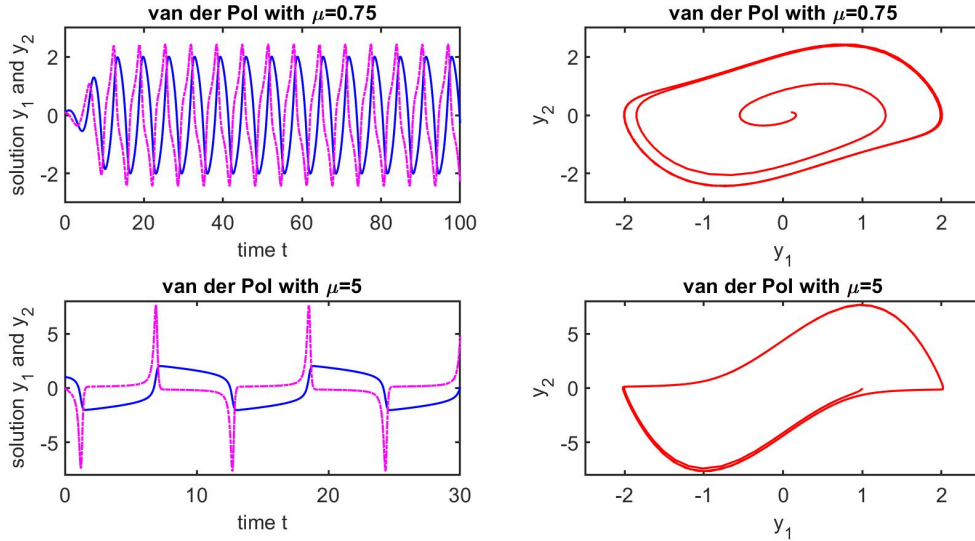


Figure 1.11: *Solutions of Van der Pol equation (1.22) with $\mu = 0.75$ and $\mu = 5$*

and then chaotic and irregular oscillations. We started with studying the local dynamics of some vector fields and we demonstrated the local stable behavior of the system around its critical points. We continued this paper with studying the well known problems which have been used a lot for different physical purposes. Hénon-Heiles system, Duffing oscillator and Van der Pol equation are three important dynamical examples which have been widely studied numerically. We demonstrated the stable and unstable manifolds from the origin form a homoclinic orbit in Hénon-Heiles system and we discussed about the local dynamical behaviors of its critical points. We showed that the critical point $(0, 0)$ is a saddle point and critical point $(-1, 0)$ is a center. For Duffing oscillator, which can be used to model different physical phenomenon, we showed the periodic and chaotic motions of the system using time series. Moreover, for Van der Pol equation, we presented the limit cycle solutions and periodic behavior of the system. We concluded that depending on different values for μ , solutions look like periodic motion. When μ small values, this motion is nearly sinusoidal, however for larger values of μ , the solutions seem to be relaxation oscillations which means solutions are similar to a series of step functions and jump twice per cycle between the positive and the negative values. Finally, we discussed about the chaos in Hamiltonian systems and we provided two interesting and different examples which exhibit chaotic behaviors. We assumed

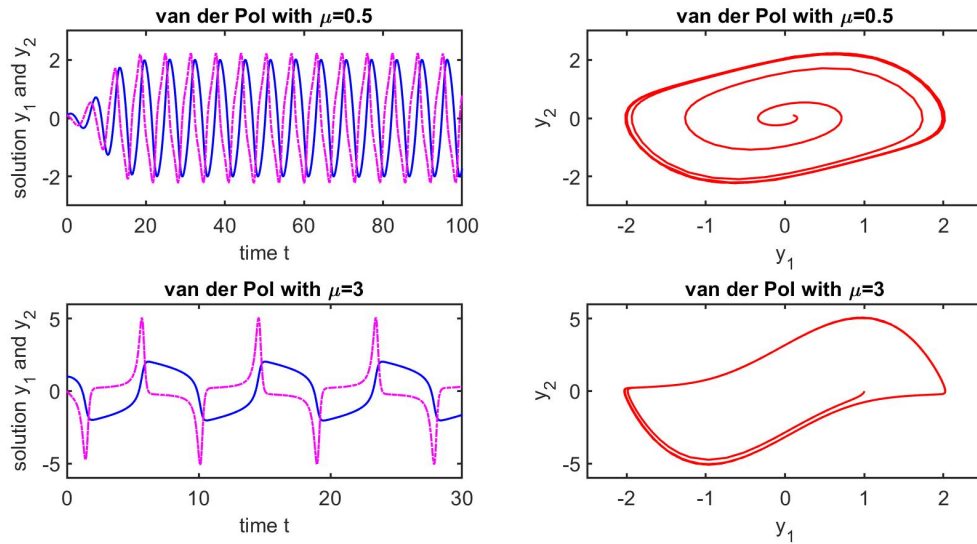


Figure 1.12: *Solutions of Van der Pol equation (1.22) with $\mu = 0.5$ and $\mu = 3$*

a Hamiltonian function with two degrees of freedom and it can be obtained by adding an integrable Hamiltonian system and a non-integrable Hamiltonian system. We showed that for $\epsilon = 0$ and in addition, for $0 < \epsilon \ll 1$, there exist quasi periodic cycles which are known as KAM tori. However, under perturbation, these quasi periodic cycles will be deformed and KAM tori will be dissolved gradually as we increase ϵ .

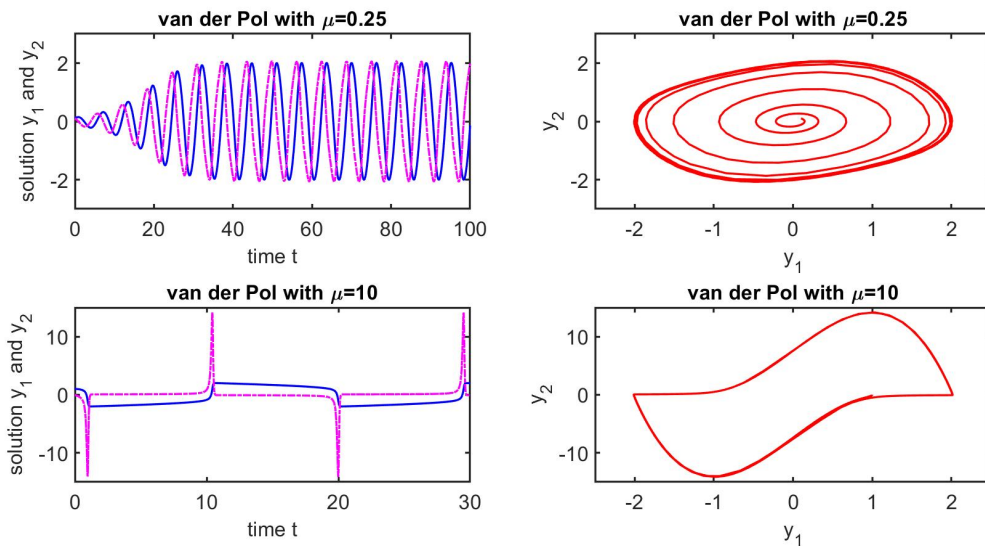


Figure 1.13: Solutions of Van der Pol equation (1.22) with $\mu = 0.25$ and $\mu = 10$

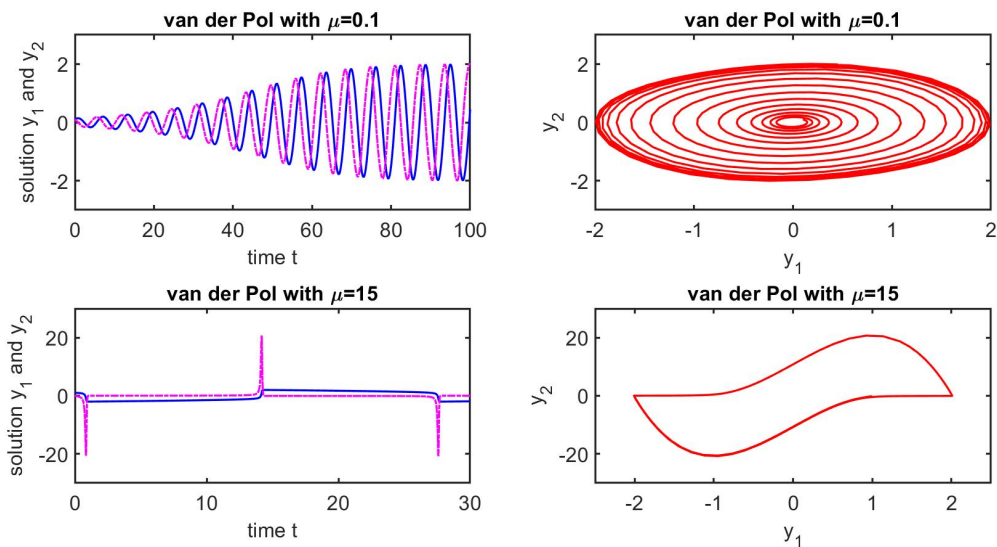


Figure 1.14: Solutions of Van der Pol equation (1.22) with $\mu = 0.1$ and $\mu = 15$

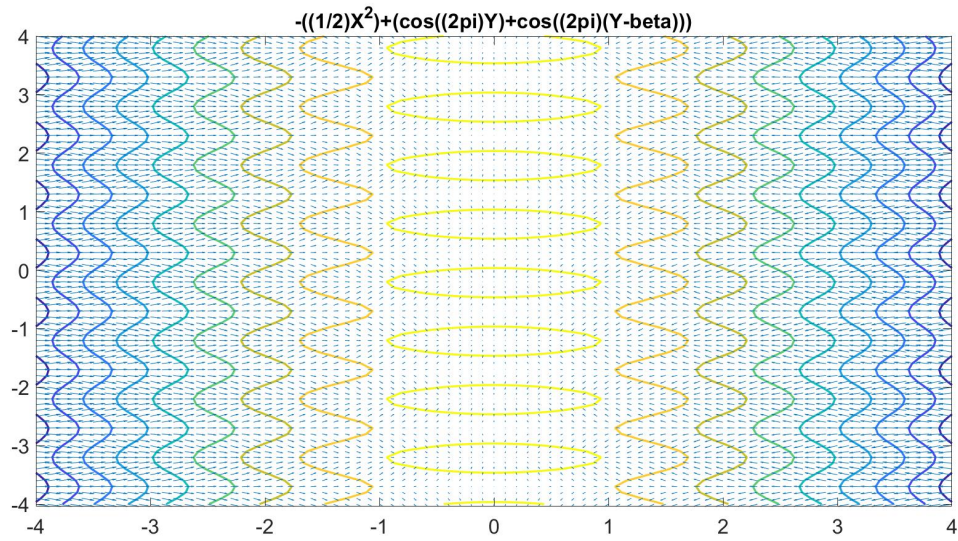


Figure 1.15: *Dissolving the KAM tori caused by perturbation, $H_1(x, y) = -((1/2)x^2) + \epsilon(\sin((\pi/2)y) + \sin((\pi/2)(y - \beta)))$*

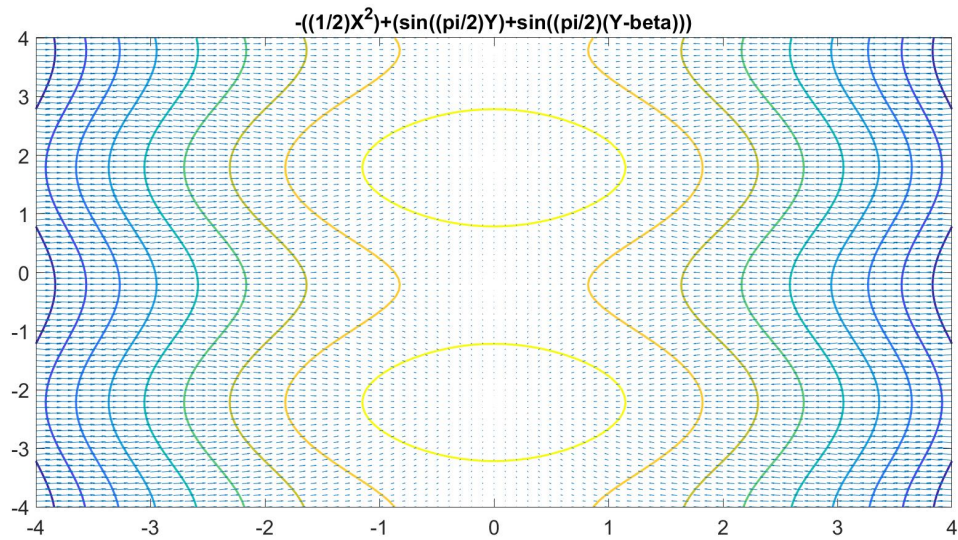


Figure 1.16: *Dissolving the KAM tori caused by perturbation, $H_2(x, y) = -((1/2)x^2) + \epsilon(\cos((2\pi)y) + \cos((2\pi)(y - \beta)))$*

Chapter 2

Neural Bursting and Spiking in Neurons: the Morris-Lecar Model

Abstract

In Chapter Two, we consider some models in computational neuroscience. Due to the complexity of nerve systems, linear modeling methods are not sufficient to understand the various phenomena in neuroscience. We use nonlinear methods and models, which aim at capturing certain properties of the neurons and their complex dynamics. Specifically, we explore the interesting phenomenon of firing spikes and complex dynamics of the Morris-Lecar model. We consider a set of parameters such that the model exhibits a wide range of phenomenon. We investigate the influences of injected current and temperature on the spiking dynamics of Morris-Lecar model. In addition, we study bifurcations, and computational properties of this neuron model. Moreover, we provide a bound for the membrane potential and a certain voltage value or threshold for firing the spikes. Studying the two co-dimension bifurcations demonstrates more complicated behaviors for this single neuron model. Furthermore, we describe the phenomenon of neural bursting and investigate the dynamics of Morris-Lecar model as a square-wave burster, elliptic burster and parabolic burster.

2.1 Introduction

During recent decades, understanding the brain function and exploring its molecular and cellular mechanisms were one of the greatest challenges in different fields of science. Historically, most of the researches in neuroscience focused on only neuronal circuits and synaptic organizations. Indeed, the neurons without considering their electrophysiological properties were divided into excitatory and inhibitory neurons, and sometimes they had been counted to be identical to those in Hodgkin-Huxley's squid axon²⁸⁻³¹. In 1948 Hodgkin injected a *dc*-current of varying amplitude, and discovered that some preparations could show repetitive spiking activities with arbitrarily low frequencies, while the others discharged in a narrow frequency band^{28;32-34}. However, this finding was widely ignored by the scientists until 1989 when Rinzel and Ermentrout published a seminal paper and showed that the difference in behavior is because of different bifurcation mechanisms of excitability^{28;35;36}.

Non-linear dynamical system theory has a very important role in the computational neuroscience research^{28-32;37}. Izhikevich in²⁸ explains how the transition in behavior of a neuron corresponds to a bifurcation from equilibrium to a limit cycle attractor. If we consider the injected current as a bifurcation parameter, when it is small, the cell remains quiescent. However, when the injected current increases, the cell switches to fire repetitive spikes^{28-32;37;38}. In dynamical system theory, the qualitative change in the behavior of a system is called bifurcation. Indeed, when we change the amplitude of the bifurcation parameter (which in this case is the injected current), the cell undergoes a transition from quiescence to repetitive spiking. According to the type of bifurcation which happens for a neuron model, we can divide the neurons into different classes such as the class of excitability, and or we can discuss about the existence of threshold, all-or-none spikes, post-inhibitory rebound spikes, subthreshold oscillations, bistability of rest and spiking states²⁸. For example, the neurons with supercritical and subcritical Hopf bifurcations are called resonator and the neurons with saddle-node bifurcation or SNLC bifurcations are integrator²⁸.

In this chapter, we study the interesting dynamics and fluctuations of spiking patterns of Morris-Lecar model which is a reduced version of Hodgkin-Huxley neuron model. For a

certain range of parameters value, Morris-Lecar model exhibits different types of local bifurcations such as Hopf bifurcation, saddle node on invariant limit cycles and homoclinic bifurcation. Moreover, we demonstrate a temperature bound and injected current range for spiking activity of the neuron. Also, we study co-dimension two bifurcations such as Bautin or generalized Hopf and Bogdanov-Takens bifurcations and we present the normal form of these bifurcations as well. At the end, we look at the complicated dynamics of Morris-Lecar model as a burster.

2.2 Description of model equations

In 1981, Kathleen Morris and Harold Lecar introduced a simple model to generate the action potentials³⁹. The Morris-Lecar model describes the electrical activities of neurons with a system of two non linear ordinary differential equations and includes different channels. This model is a reduction version of the four dimensional Hodgkin-Huxley model keeping the main properties of spike generations with much simpler mathematical and computational analysis^{39;40}. The Morris-Lecar model consists of three channels a potassium channel, a leak and a calcium channel and has the following form

$$\begin{cases} C_M \frac{dV}{dt} = I_{app} - g_L(V - E_L) - g_K n(V - E_K) - g_{Ca} m_\infty(V)(V - E_{Ca}) = I_{app} - I_{ion}(V, n), \\ \frac{dn}{dt} = \phi(n_\infty(V) - n)/\tau_n(V), \end{cases} \quad (2.1)$$

where

$$m_\infty(V) = \frac{1}{2}[1 + \tanh((V - V_1)/V_2)], \quad (2.2)$$

$$\tau_n(V) = 1/\cosh((V - V_3)/(2V_4)), \quad (2.3)$$

$$n_\infty(V) = \frac{1}{2}[1 + \tanh((V - V_3)/V_4)]. \quad (2.4)$$

and

$$I_{ion}(V, n) = g_L(V - E_L) + g_K n(V - E_K) + g_{Ca} m_\infty(V)(V - E_{Ca}) \quad (2.5)$$

where V demonstrates membrane potential, and n the activation variable of the persistent K^+ current, so it is a two-dimensional vector (V, n) . E_K , E_{Ca} , and E_L denote the Nernst equilibrium potentials. I_{app} demonstrates the injected current and I_{ion} the ionic current. Parameter ϕ is a temperature factor. g_L is leak membrane conductance, g_K is potassium membrane conductance and g_{Ca} is calcium membrane conductance. Moreover, C_M is the total membrane capacitance. Also, the voltage-sensitive steady-state activation function $m_\infty(V)$ and $n_\infty(V)$, and the time constant $\tau_n(V)$ can be measured experimentally. A useful way to demonstrate the electrical properties of a neuron is using an equivalent circuit as we can see in Figure (2.1)²⁸. In this case, the total current has the form

$$I = C\dot{V} + I_{Ca} + I_K \quad \text{Kirchhoff's Law}$$

where, $I_k = g_k(V - E_K)$, $I_{Ca} = g_{Ca}(V - E_{Ca})$ are the major ionic currents. Therefore

$$C\dot{V} = I - I_{Ca} - I_K$$

Also, $E_K < V < E_{Ca}$ where I_{Ca} (inward current) is negative and also I_K is positive. Basically, the inward currents depolarize the neuron and outward currents hyperpolarize it.

This simple model shows different types of dynamics such as Hopf bifurcation, saddle node on invariant limit cycles and homoclinic bifurcation. In table (2.2), we can see a list of parameters that cause three types of dynamics in Morris-Lecar model³⁷. As we see, in table (2.1), I_{app} has not been included since we consider it as a bifurcation parameter for bifurcation diagrams.

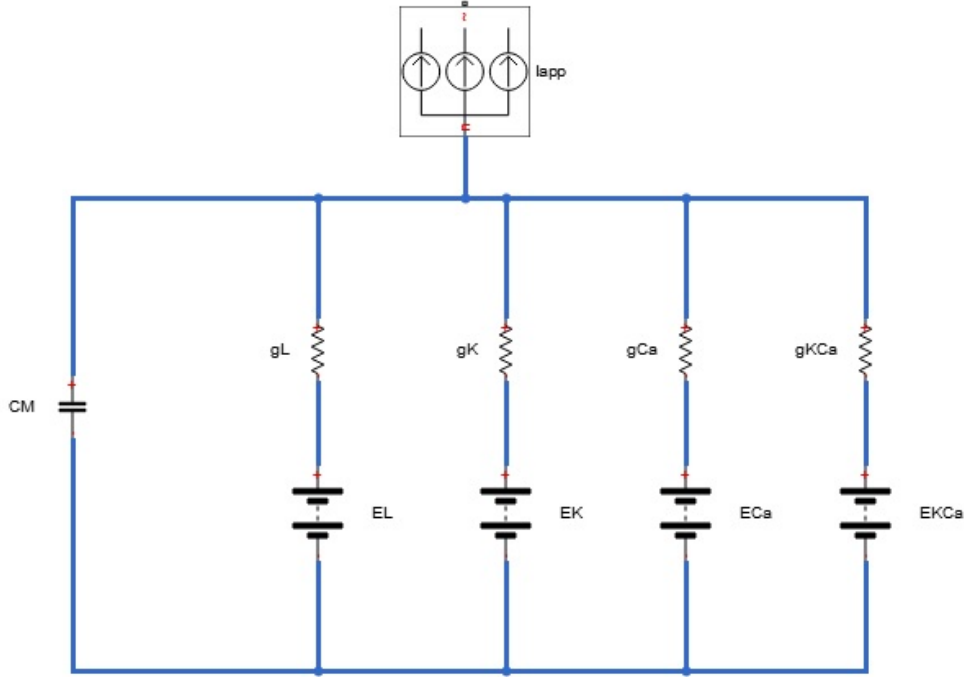


Figure 2.1: *Equivalent circuit for model (2.1). E_K , E_{Ca} , and E_L the Nernst equilibrium potentials. I_{app} the injected current, g_L leak membrane conductance, g_K potassium membrane conductance, g_{Ca} calcium membrane conductance, C_M the total membrane capacitance.*

2.3 The Hopf case

For the case of Hopf parameters, the model (2.1) has one equilibrium point which is intersection point of V nullcline and n nullcline. Indeed, it is not possible to find the explicit solution for any of the cases in table (2.1). In Figure (2.3), we have demonstrated the nullclines of system (2.1) for $I_{app} = 0, 25, 50, 100$ and it shows that there is only one solution for the Hopf case.

In Figure (2.4), we can see different behaviors of the neuron from resting to spiking (the stable constant solutions are corresponding to the resting state and spiking state shows the existence of periodic solutions). Figure (2.5) displays the occurrence of limit cycle corresponding to Hopf bifurcation with increasing I_{app} . As it has been exhibited in Figure (2.6), some trajectories come back to the stable fixed point or resting state after a big counter clockwise excursion but there are some other trajectories that return to the resting state

Parameter	Hopf	SNLC	Homoclinic
\emptyset	0.04	0.067	0.23
g_{Ca}	4.4	4	4
V_3	2	12	12
V_4	30	17.4	17.4
E_{Ca}	120	120	120
E_K	-84	-84	-84
E_L	-60	-60	-60
g_K	8	8	8
g_L	2	2	2
V_1	-1.2	-1.2	-1.2
V_2	18	18	18
C_M	20	20	20

Figure 2.2: *Morris-Lecar parameters*³⁷.

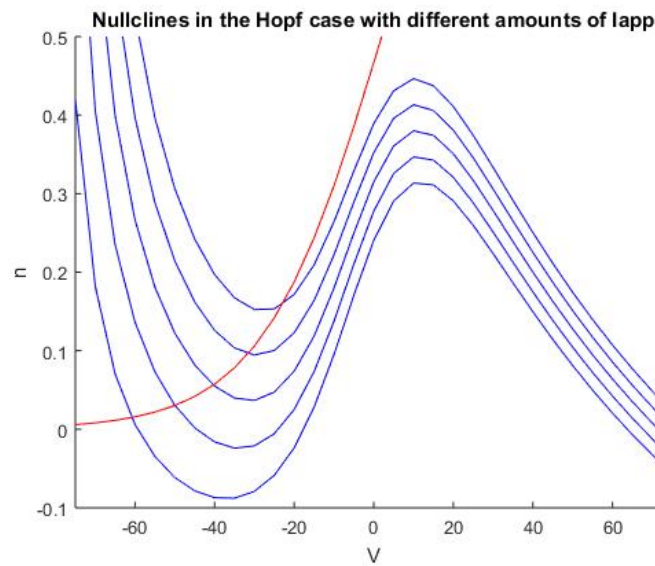


Figure 2.3: *Nullclines of model (2.1) with $I_{app} = 0, 25, 50, 100$.*

without firing a spike. In neuroscience point of view, this kind of behavior is called threshold for firing spike. As a result, model (2.1) has an evident threshold for firing spikes and it has been obtained numerically equals to $V = -20mv$. Also, depends on the initial values of membrane potential, the size of the excursion is different.

Using continuation software Matcont and choosing I_{app} as a bifurcation parameter, we could detect numerically Hopf bifurcation points. For $I_{app} = 93.857569$ and $(V, n) =$

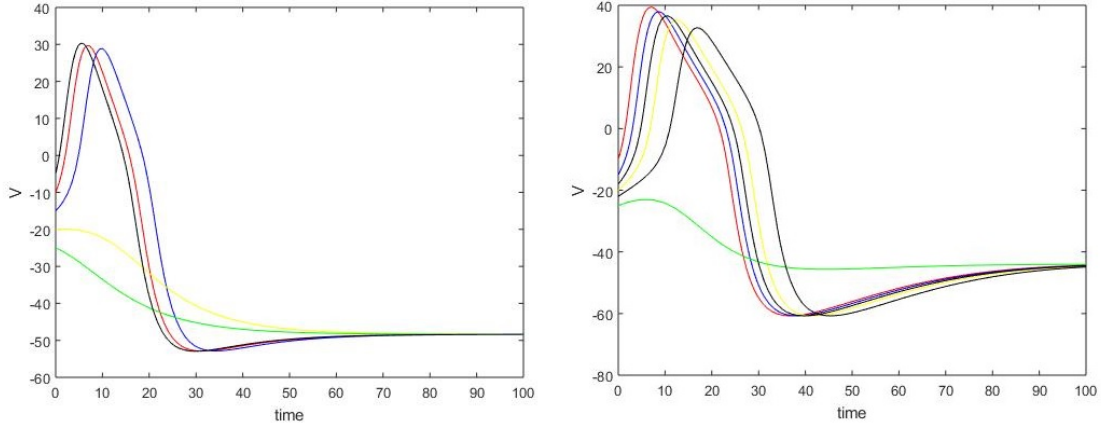


Figure 2.4: Time series of model (2.1) with $I_{app} = 20$ left, and $I_{app} = 40$ right.

$(-25.270122, 0.139673)$ we have the first Hopf point with the first Lyapunov coefficient 5.220161, and for $I_{app} = 212.018818$ and $(V, n) = (7.800664, 0.595491)$ we can see the second Hopf point with the first Lyapunov coefficient 5.451163. Here, the first Lyapunov coefficients for two Hopf points are positive. Thus, there should exist an unstable limit cycle, bifurcating from the equilibrium and it indicates the appearance of subcritical Hopf bifurcation. When the value for injected current I_{app} is small we have a stable equilibrium point. When, we increase the value of injected current, the behavior of system changes and for $I_{app} = 90$, we can see a limit cycle appears. This qualitative changing that causes producing a limit cycle attractor from a stable equilibrium point is called Hopf bifurcation^{41;203}. In model (2.1) the equilibrium point is a stable focus that has a pair of complex conjugate eigenvalues with negative real part. With increasing the injected current, the real part of the eigenvalues changes from negative to zero and with further increasing, to positive. It means that the stable focus loses its stability and a limit cycle appears. With further increasing of the injected current, the amplitude of the limit cycle also increases.

For $(V, n) = (7.800664, 0.595491)$ the eigenvalues are $\lambda_{1,2} = 4.65764 \pm i(0.148602)$. Because the real part of eigenvalues are positive, it implies that equilibrium point is unstable and with further steps we obtain the second Hopf point $(V, n) = (-25.270122, 0.139673)$ with eigenvalues $\lambda_{1,2} = -8.58989 \pm i(0.0797799)$. Since, the real part is negative, it means that the equilibrium point is stable.

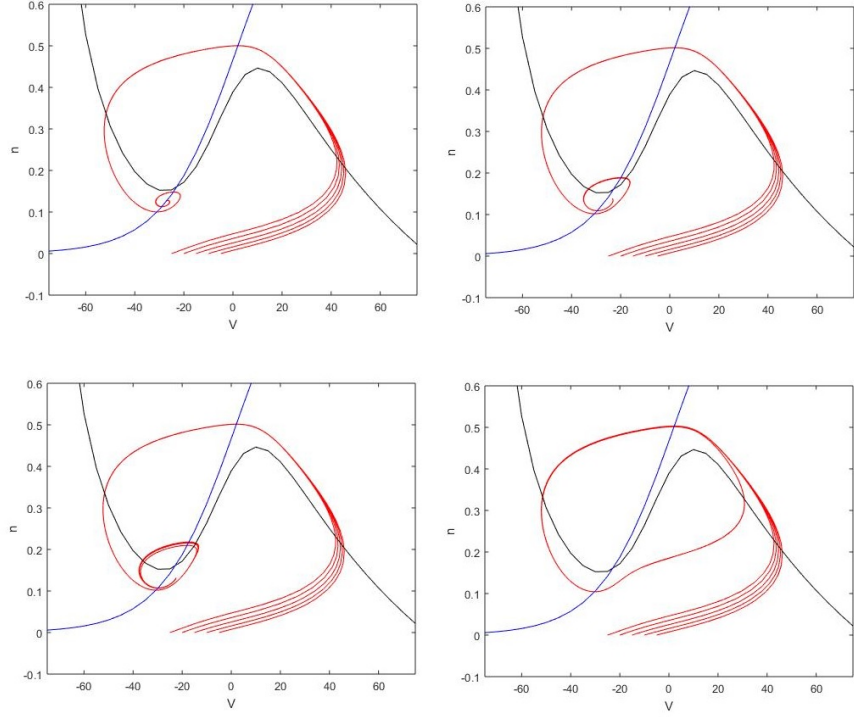


Figure 2.5: Trajectories of model (2.1) with $I_{app} = 87$ (up, left), $I_{app} = 88.25$ (up, right), $I_{app} = 88.3$ (down, left), $I_{app} = 90$ (down, right).

The topological normal form for Hopf bifurcation has the form:

$$\dot{r} = \alpha r + ar^3 \quad (2.6)$$

$$\dot{\theta} = \omega_0 + \beta r^2 \quad (2.7)$$

Here, β does not have any dynamical effect. The normal form for first Hopf point $(V, n) = (7.800664, 0.595491)$ has the form below:

$$\dot{r} = (4.65764)r + (5.451163)r^3 \quad (2.8)$$

$$\dot{\theta} = 0.148602 \quad (2.9)$$

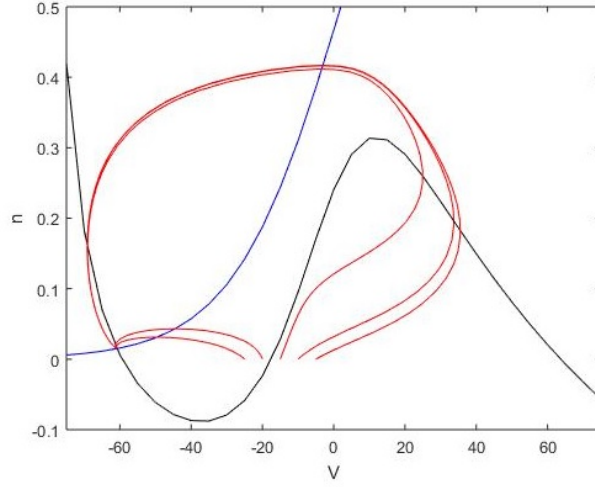


Figure 2.6: *Threshold for firing a spike in model (2.1).*

Moreover

$$\dot{r} = (4.65764)r + (5.451163)r^3 \quad (2.10)$$

$$\dot{\theta} = -0.148602 \quad (2.11)$$

In normal form (2.8), $\dot{\theta} > 0$. θ is the angle of oscillations which is positive and increasing because the frequency of damped or sustained oscillations around this point ω_0 , is positive. But for normal form (2.10), $\dot{\theta} < 0$ which means that the frequency of damped or sustained oscillations around this point ω_0 , is negative.

To analysis the normal form (2.8), we have

$$r((4.65764) + (5.451163)r^2) = 0$$

Therefore,

$$r = 0, \quad (4.65764) + (5.451163)r^2 = 0 \quad (2.12)$$

Here, $r = 0$ is an equilibrium and because for $r = 0$, $\frac{d}{dr}[(4.65764)r + (5.451163)r^3] = 4.65764 > 0$, as a result, this equilibrium is unstable. The equation $(4.65764) + (5.451163)r^2 = 0$ does not give us any periodic solutions or oscillatory behaviors.

For other Hopf point $(V, n) = (-25.270122, 0.139673)$, the normal form can be written as

$$\dot{r} = (-8.58989)r + (5.220161)r^3 \quad (2.13)$$

$$\dot{\theta} = 0.0797799 \quad (2.14)$$

Here, $\dot{\theta} > 0$ means that the frequency of damped or sustained oscillations around this point ω_0 , is positive and increasing. But for the othe normal form:

$$\dot{r} = (-8.58989)r + (5.220161)r^3 \quad (2.15)$$

$$\dot{\theta} = 0.0797799 \quad (2.16)$$

$\dot{\theta} < 0$ which implies that the frequency of damped or sustained oscillations around this point ω_0 , is negative and decreasing.

To analyze the normal form (2.13):

$$r((-8.58989) + (5.220161)r^2) = 0$$

Therefore

$$r = 0, \quad (-8.58989) + (5.220161)r^2 = 0 \quad (2.17)$$

Here, $r = 0$ is an equilibrium and because for $r = 0$

$$\frac{d}{dr}[(-8.58989)r + (5.220161)r^3] = (-8.58989) < 0$$

As a result, this equilibrium is stable. The equation $(-8.58989) + (5.220161)r^2 = 0$ gives us

the unstable periodic solution with amplitude:

$$r = \sqrt{\frac{8.58989}{5.220161}} \quad (2.18)$$

2.4 The SNLC case

Fold bifurcation of limit cycle or SNLC happens when with increasing the injected current two limit cycles, one stable that is associated to the stable node and another one unstable limit cycle that is associated to a saddle point close to each other, collide and at the bifurcation moment, we only have one limit cycle. With further increasing the injected current, this limit cycle also disappears. Figure (2.7) exhibits the nullclines of system (7.15) using SNLC parameters value in table (2.2). As we see, with increasing the injected current, the numbers of equilibrium point change from 3 to only one fixed point.

Figure (2.8) demonstrates the trajectories of system (2.1) with the SNLC parameters in

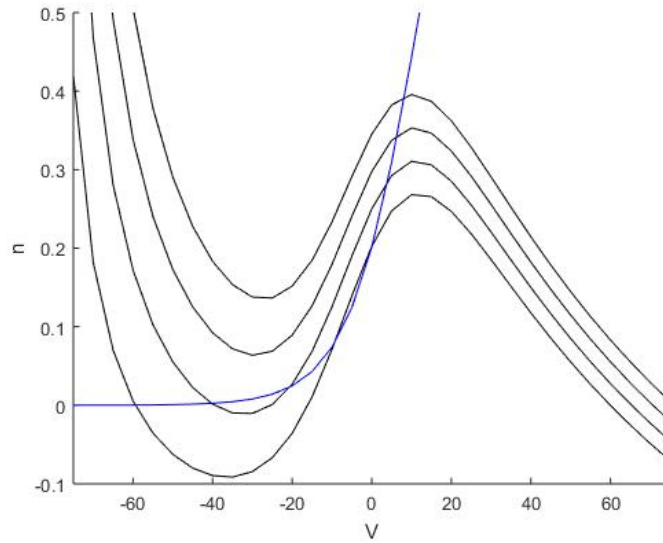


Figure 2.7: *The Nullclines of model (2.1) in the case of SNLC bifurcation.*

table (2.2), and for different values for injected current I_{app} .

When we do the continuation of equilibrium point of SNLC case, we detect the first Hopf point for $I_{app} = 97.646159$ and $(V, n) = (8.334122, 0.396190)$ and first Lyapunov coefficient

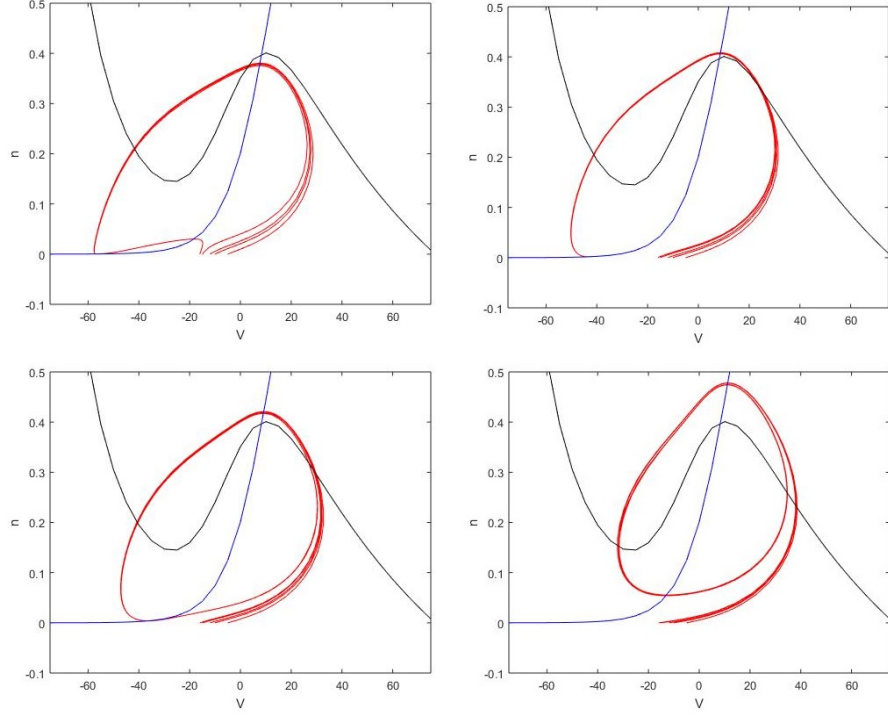


Figure 2.8: Trajectories of model (2.1) in the case of SNLC bifurcation for (up, left) $I_{app} = 5$, (up, right) $I_{app} = 30$, (down, left) $I_{app} = 42$, (down, right) $I_{app} = 100$.

5.317042 and two complex conjugate eigenvalues $\lambda_{1,2} = (6.13675) \pm i(0.252728)$. Here, similar to the Hopf case, Hopf bifurcation is subcritical since the first Lyapunov coefficient is positive and its normal form has the following form

$$\dot{r} = (6.13675)r + (5.317042)r^3 \quad (2.19)$$

$$\dot{\theta} = -0.252748 \quad (2.20)$$

Since, $\dot{\theta} < 0$, the frequency of damped or sustained oscillations around this point ω_0 , is negative and decreasing.

However, the analysis of normal form is just limited to the first equation of normal form (2.19):

$$r((6.13675) + (5.317042)r^2) = 0$$

Therefore,

$$r = 0, \quad (6.13675) + (5.317042)r^2 = 0 \quad (2.21)$$

Here, $r = 0$ is an equilibrium and because for $r = 0$, $\frac{d}{dr}[(6.13675)r + (5.317042)r^3] = 6.13675 > 0$, this equilibrium point is unstable. The equation $(6.13675) + (5.317042)r^2 = 0$ does not give us any periodic solutions or oscillatory behaviors.

Also, the continuation of equilibrium point gives a limit point bifurcation for $I_{app} = -9.949039$ and at the point $(V, n) = (-4.048524, 0.136501)$ with the normal form coefficient $a = 4.772860$ and the eigenvalues $(\lambda_1, \lambda_2) = (-5.61265, 0.359026)$. The normal form for this bifurcation can be written as:

$$\dot{V} = a \pm V^2 \quad (2.22)$$

and for this case, we can write the following normal form:

$$\dot{V} = 4.772860 - V^2 \quad (2.23)$$

Thus, $V = \pm\sqrt{4.772860}$. Here, we find an equilibrium manifold which is the parabola $(4.772860) = V^2$ and gives the appearance of two equilibria. The same analysis can be done for other normal form and it gives the parabola $-4.772860 = V^2$ but in this case, we have a singularity of the fold type.

The third point which has been detected by continuation is a Neutral saddle corresponding to $\lambda_1 + \lambda_2 = 0$ for $I_{app} = 36.639168$ at $(V, n) = (-23.5341020, 0.016555)$ with eigenvalues $(\lambda_1, \lambda_2) = (-0.0792728, 0.0792728)$. Further continuation gives us another limit point bifurcation for $I_{app} = 39.963153$ and at the point $(V, n) = (-29.389788, 0.008514)$ for which a stable and an unstable limit cycle collide and create a non hyperbolic cycle. The real eigenvalues are

$(\lambda_1, \lambda_2) = (-0.0990488, -(1.10511))$. For this fold bifurcation, the normal form would be

$$\dot{V} = -(5.212474) + V^2 \quad (2.24)$$

Thus, $V = \pm\sqrt{(5.212474)}$. Here, we have an equilibrium manifold which is the parabola $(5.212474) = V^2$ and it implies to the appearance of two equilibria. The same analysis can be done for the second normal form and we get the parabola $-(5.212474) = V^2$ which gives a singularity of the fold type.

2.5 The Homoclinic case

Saddle-Homoclinic bifurcation happens when a saddle point and a limit cycle collide as we are increasing the control parameter. At the moment of bifurcation, we have a periodic orbit such that its period goes to infinity and finally, this periodic orbit disappears. The trajectories of system (2.1) for homoclinic case have been demonstrated in Figure (2.9). Also, as we can see in Figure (2.10) the numbers of fixed points of model (2.1) with increasing $I_{app} = 0$ to $I_{app} = 100$, reduce from 3 equilibrium point to one equilibrium point. Indeed, changing the numbers of fixed point means that a qualitative changes or bifurcation happens in the system.

When we do continuation of equilibrium points, we detect a Hopf point for $I_{app} = 36.316266$ and $(V, n) = (4.410760, 0.294770)$ with the first Lyapunov coefficient 3.765575. For this Hopf point the eigenvalues are complex conjugate: $\lambda_1 = (-1.3955) \pm i(0.378861)$. Therefore, this is a subcritical Hopf bifurcation. The normal form of this bifurcation would be

$$\dot{r} = (-1.3955)r + (3.765575)r^3 \quad (2.25)$$

$$\dot{\theta} = -0.378861 \quad (2.26)$$

Since, $\dot{\theta} < 0$, the frequency of damped or sustained oscillations around this point ω_0 , is negative and decreasing.

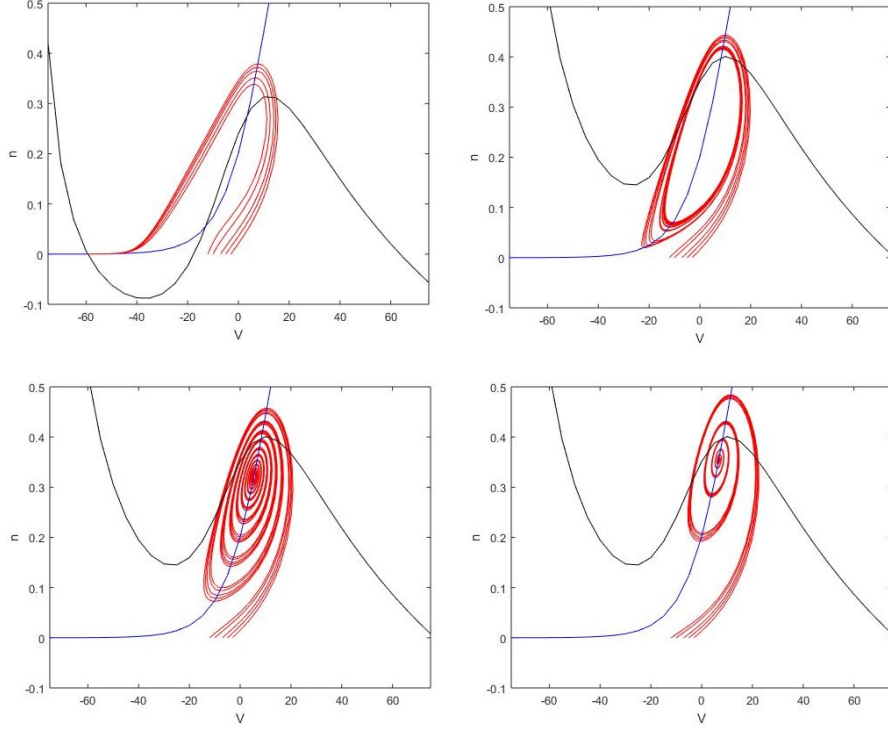


Figure 2.9: Trajectories of model (2.1) in the case of Saddle-Homoclinic bifurcation for (up, left) $I_{app} = 0$, (up, right) $I_{app} = 40$, (down, left) $I_{app} = 50$, (down, right) $I_{app} = 70$.

Analysis of normal form gives us

$$r((-1.3955) + (3.765575)r^2) = 0$$

Therefore

$$r = 0, \quad (-1.3955) + (3.765575)r^2 = 0 \quad (2.27)$$

Here, $r = 0$ is an equilibrium and because for $r = 0$, $\frac{d}{dr}[(-1.3955)r + (3.765575)r^3] = -1.3955 < 0$, this equilibrium point is stable. The equation $(-1.3955) + (3.765575)r^2 = 0$ gives us periodic solution or oscillatory behaviors with amplitude:

$$r = \sqrt{\frac{1.3955}{3.765575}} \quad (2.28)$$

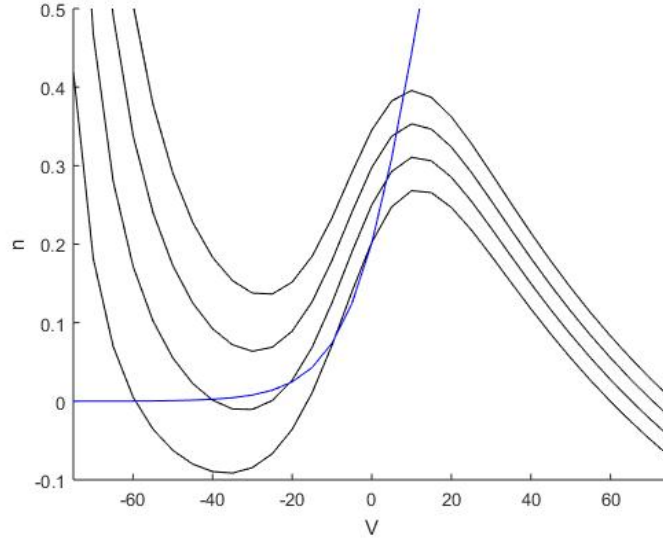


Figure 2.10: *Nullclines of model (2.1) with $I_{app} = 0, 25, 50, 100$.*

When we continue along the curve of equilibrium points, we detect a limit point bifurcation for $I_{app} = -9.949039$ and at the point $(V, n) = (-4.048518, 0.136501)$, with the normal form coefficient $a = 3.297636$. In this case, the eigenvalues are $(\lambda_1, \lambda_2) = (-1.3742, 0.178384)$. The normal form for this limit point bifurcation has the following form

$$\dot{V} = (3.297636) - V^2 \quad (2.29)$$

Consequently, $V = \pm\sqrt{(3.297636)}$. The equilibrium manifold would be the parabola $(3.297636) = V^2$. The same analysis can be done for other normal form and it gives us the parabola $-(3.297636) = V^2$, but in this case, we have a singularity of the fold type.

We can define the type of the saddle homoclinic bifurcation by looking at the sign of the sum of the eigenvalues which is called saddle quantity. If $\lambda_1 + \lambda_2 < 0$, then the saddle homoclinic bifurcation is called supercritical which is corresponding to the appearance or disappearance of a stable limit cycle, and if $\lambda_1 + \lambda_2 > 0$, we have the subcritical saddle homoclinic orbit bifurcation and it is corresponding to the appearance or disappearance of a unstable limit cycle. As a result, since here $\lambda_1 + \lambda_2 < 0$, we have a supercritical saddle homoclinic bifurcation.

By further continuation the equilibrium curve, we obtain a limit point bifurcation for $I_{app} = 39.963153$ and at the point $(V, n) = (-29.389788, 0.008514)$, with normal form coefficient $a = -4.526064$. The eigenvalues are $(\lambda_1, \lambda_2) = (-0.391585, 1.96656)$. Also, the normal form would be

$$\dot{V} = (-4.526064) + V^2 \quad (2.30)$$

and we have $V = \pm\sqrt{4.526064}$. Therefore, we have an equilibrium manifold which is the parabola $(4.526064) = V^2$ and two equilibria appear. The same analysis gives the parabola $-(4.526064) = V^2$ but in this case, we have a singularity of the fold type.

Because here $\lambda_1 + \lambda_2 > 0$, we have the subcritical saddle homoclinic orbit bifurcation. In neuroscience point of view, the saddle homoclinic bifurcation implies to the appearance or disappearance of spiking behavior.

2.6 Two co-dimension bifurcations

In this section, we focus on co-dimension two bifurcations with I_{app} and ϕ as bifurcation parameters. The purpose is exploring the influences of temperature and injected current simultaneously on neuron model (2.1). At first, we discover Bautin or generalized Hopf (GH) points for which the first Lyapunov coefficient vanishes. Then, we study another type of co-dimension two bifurcation which is called Bogdanov-Takens (BT) for which the system has an equilibrium with a double zero eigenvalue⁴¹.

We start with the continuation of Hopf curve that bifurcates from the BT point and continues to reach a Bautin point named GH. With further continuation, we can see another BT point after the second GH. Here, two GH points are non degenerate because the second Lyapunov coefficients l_2 are non zero, $l_2 = -1.556360$.

Here, for $(V, n) = (-11.785736, 0.285152)$, and parameters value $(\phi, I_{app}) = (0.306345, 124.470639)$, we have the first Bautin point. In generalized Hopf (Bautin) bifurcation, the equilibrium has a pair of complex conjugate eigenvalues and also at generalized Hopf point the first Lyapunov

coefficient for the Hopf bifurcation becomes zero. The bifurcation point separates branches of subcritical and supercritical Hopf bifurcations. For the parameter values near bifurcation, the system demonstrates two limit cycles that collide and disappear via a saddle-node bifurcation. Basically, in Bautin bifurcation we have changing the type of bifurcation from subcritical to super critical Hopf bifurcation. It means that the sign of the first coefficient Lyapunove changes from positive to negative. When the first Lyapunov coefficient becomes zero, the bifurcation becomes degenerate and the dynamics of system satisfies the following topological normal form⁴¹:

$$\dot{z} = (\lambda + i\omega)z + l_1 z|z|^2 + l_2 z|z|^4$$

Here, $z \in \mathbb{C}$ is a complex number, l_1 called the first Lyapunov coefficient and l_2 called the second Lyapunov coefficient, and λ is the real part of eigenvalues and ω demonstrates the imaginary part of eigenvalues. At the moment of Bautin bifurcation $\lambda = l_1 = 0$ and $l_2 \neq 0$. Likewise, when $l_2 > 0$, we have subcritical Bautin bifurcation and when $l_2 < 0$, we have supercritical Bautin bifurcation. To begin bifurcation analysis, at first when $\lambda = 0$, we have a Hopf bifurcation and depending on the sign of l_1 we have supercritical or subcritical Hopf bifurcation. Also, when the first and the second Lyapunov coefficients have different sign, the solutions branch collide and disappear at the half parabola $l_1^2 - 4\lambda l_2 = 0$ and they undergo the fold limit cycle.

Here, for $(V, n) = (-11.785736, 0.285152)$ and parameters value $(\phi, I_{app}) = (0.306345, 124.470639)$, we have a Bautin point with eigenvalues $\lambda_{1,2} = (-5.0307) + i(0.156687)$ and the system satisfies the following normal form:

$$\dot{V} = ((-5.0307) + i(0.156687))V + (-1.556360)V|V|^4 \quad (2.31)$$

Because, $l_2 < 0$, we have supercritical Bautin bifurcation. The other Bautin point happens for $(V, n) = (2.472096, 0.507868)$, and $(\phi, I_{app}) = (0.253856, 165.685695)$ with eigenvalues

$\lambda_{1,2} = (-2.67147) \pm i(0.28612)$ and the system satisfies the following normal form

$$\dot{V} = ((-2.67147) + i(0.28612))V + (-3.920527)V|V|^4 \quad (2.32)$$

Because, $l_2 < 0$, we have supercritical Bautin bifurcation.

Generalized Hopf (Bautin) bifurcation in polar coordinates has the following normal form⁴¹:

$$\begin{aligned} \dot{r} &= r(l_1 + l_2 r^2 - r^4), \\ \dot{\phi} &= 1 \end{aligned}$$

In our simulation, the curve LPC corresponds to the saddle-node bifurcation of periodic orbits. As we can see in Figure (2.11), for $\phi = 0.30634507$, we have Limit point cycle with Normal form coefficient = 1.604795.

Moreover, from Figure (2.12), it can be easily observed that, Bogdanov-Takens bifurcation

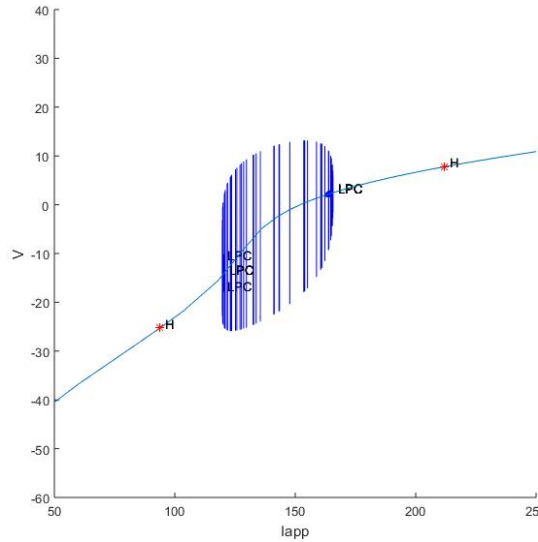


Figure 2.11: Continuation of equilibrium point in generalized Hopf bifurcation with $\phi = 0.30634507$.

can be located along a Hopf bifurcation curves, and as we approach to Bogdanov-Takens point, two purely imaginary eigenvalues collide and we have a double zero eigenvalue^{41;203}. Bogdanov-Takens bifurcation occurs when an equilibrium undergoes Hopf bifurcation and

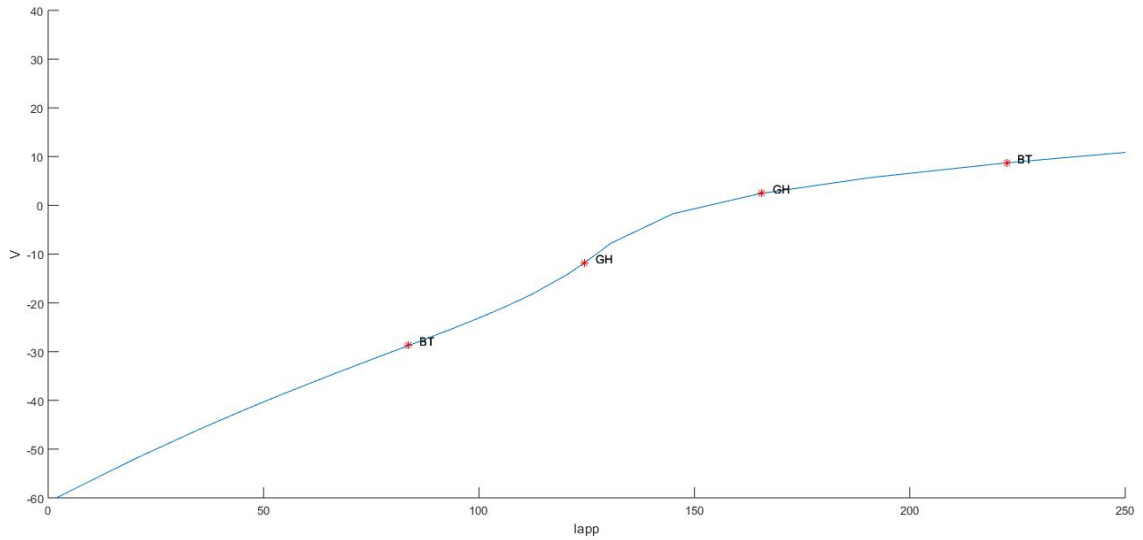


Figure 2.12: Continuation of equilibrium point in generalized Hopf bifurcation with $\phi = 0.30634507$.

saddle-node bifurcation simultaneously and also it occurs when we have at least a two-dimensional system. In this case, the Jacobian matrix of an equilibrium has these properties: $\det(J) = 0$ corresponding to saddle-node bifurcation, and $\text{tr}(J) = 0$ corresponding to Hopf bifurcation and it has the form:

$$J|_{(k,0)} = \begin{pmatrix} 0 & 1 \\ 0 & 0 \end{pmatrix}$$

Because of these two conditions, Bogdanov-Takens is a codimension two bifurcation that has the following normal form

$$\begin{aligned} \dot{u} &= v \\ \dot{v} &= a + bu + u^2 + \sigma uv \end{aligned}$$

where, a, b are the normal form coefficients, and the parameter σ takes the values 1 and -1, negative shows that it is supercritical and positive, when it is sub critical Bogdanov-Takens bifurcation. Two Bogdanov-Takens points in Figure (2.12) are: $(V, n) = (-28.744348, 0.114090)$, $(\phi, I_{app}) = (0.000000, 83.645532)$ with $(a, b) = (-5.341083, -1.363867)$ and the second

Bogdanov-Takens bifurcation happens at $(V, n) = (8.717678, 0.610127)$, with the parameter values $(\phi, I_{app}) = (-0.000000, 222.452534)$ with $(a, b) = (-1.185987, 3.751062)$. Finally, we compared the effect of injected current and temperature in Figures (2.13) and (2.14). In Figure (2.13), we can easily find a lower bound and upper bound for injected current and a maximum and minimum voltage bound corresponding to spiking activity of this single neuron. Also, Figure (2.14) gives us a range for temperature and a maximum and minimum voltage bound corresponding to firing spike for Morris-Lecar model.

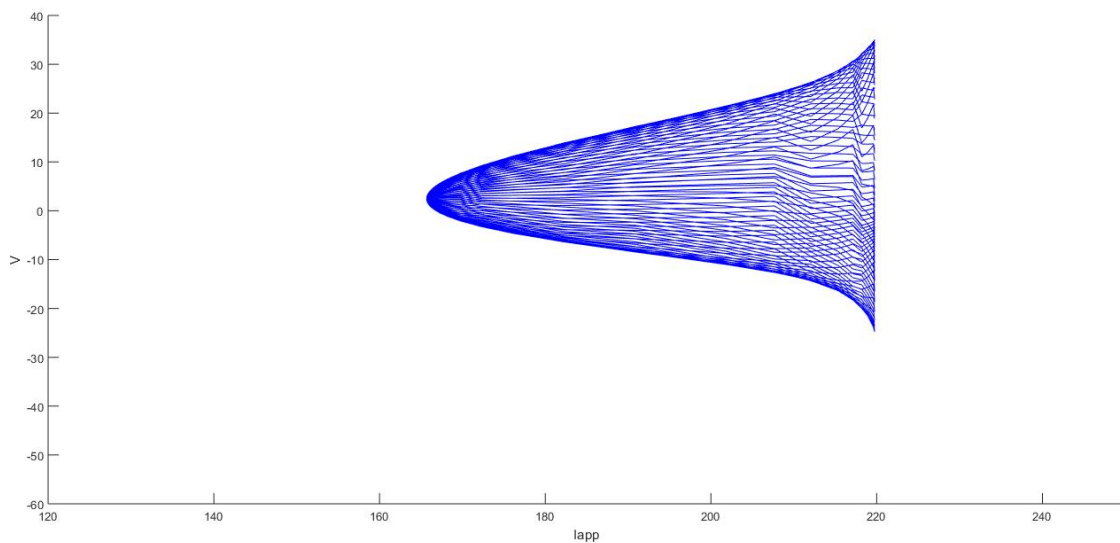


Figure 2.13: *Continuation of limit point cycles. Influence of injected current on neuron activities, maximum and minimum voltage bound.*

2.7 Bursting behaviors of the Morris-Lecar model

For some neurons that have spiking behavior, by applying some changes, they may also exhibit bursting behavior. For a neuron with ability to fire the spike, by adding a slow resonant current or gating variable we can change the neuron state to be a burster. The reason for this type of behavior is modulating the spiking and slow activity by the help of a slow negative feedback. Using the slow parameters, a burster can control the fast subsystem that has spiking state. Classification of bursters depends on the type of bifurcation of

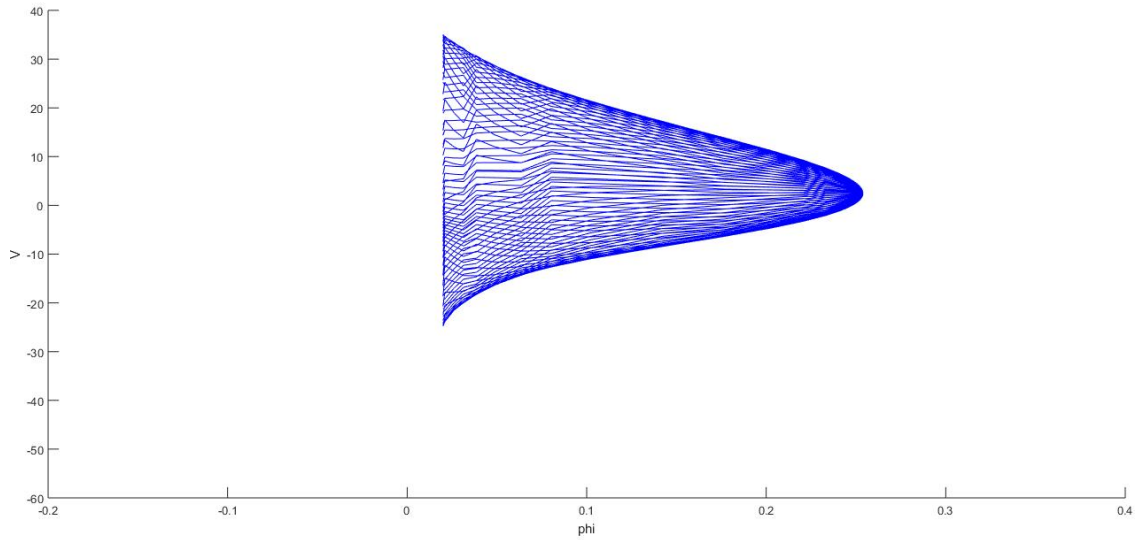


Figure 2.14: *Continuation of limit point cycles. Influence of temperature on neuron activities, maximum and minimum voltage bound.*

equilibrium points and limit cycles³⁷.

2.7.1 Morris-Lecar model as a Square-Wave burster

The first type of bursting is square wave bursting which has two important properties³⁷:

1. The repetitive spikes at membrane potential is more depolarized than the silent state.
2. The frequency of spiking decreases during the spiking state.

Bursting occurs for systems with at least three dimension. For Morris-Lecar model, we consider I_{app} decreases during the repetitive firing state process and increases during the silent state. Then, this burster demonstrates slow negative feedback together with hysteresis in the fast dynamics which specifically happens for square-wave bursting. In this case, we

add a calcium dependent potassium current and the system obtains the form³⁷:

$$\left\{ \begin{array}{l} C_M \frac{dV}{dt} = I_{app} - g_L(V - E_L) - g_K n(V - E_K) - g_{Ca} m_\infty(V)(V - E_{Ca}) - I_{KCa}, \\ \frac{dn}{dt} = \phi(n_\infty(V) - n)/\tau_n(V), \\ \frac{d[Ca]}{dt} = \varepsilon(-\mu I_{Ca} - K_{Ca}[Ca]). \end{array} \right. \quad (2.33)$$

where

$$\begin{aligned} m_\infty(V) &= \frac{1}{2}[1 + \tanh((V - V_1)/V_2)], \\ \tau_n(V) &= 1/\cosh((V - V_3)/(2V_4)), \\ n_\infty(V) &= \frac{1}{2}[1 + \tanh((V - V_3)/V_4)]. \end{aligned}$$

where, I_{KCa} demonstrates the calcium dependent potassium current and equals $I_{KCa} = g_{KCa} z(V - E_K)$. Here, g_{KCa} is the maximal conductance for I_{KCa} and z is a gating variable with a Hill-like dependence on the near membrane calcium concentration, $[Ca]$, and $z = \frac{[Ca]^p}{[Ca]^{p+1}}$. Without loss of generality, we assume $p = 1$. The last equation of system (2.33) is a balance equation for $[Ca]$. The parameter μ has been used to convert current into a concentration flux and includes the ratio of the cell's surface area to the calcium compartment's volume. The parameter K_{Ca} implies to the calcium removal rate and ε represents the ratio of free to total calcium in the cell. Because calcium is highly buffered, ε is small and the calcium dynamics is slow. The two first equations in of system (2.33) are called the fast subsystem and the third equation is called the slow equation³⁷.

Here, I_{KCa} called outward current. If conductance $g_{KCa} z$ is large, the cell has hyperpolarization state which is corresponding to resting behavior. Conversely, if $g_{KCa} z$ is small, the cell fires spikes. We have demonstrated the model (2.33) as a circuit in Figure (2.15)). Also, we have the required bursting parameters for different types of bursters in table (2.16))³⁷. Moreover, we have demonstrated the dynamics of this burster for different I_{app} in

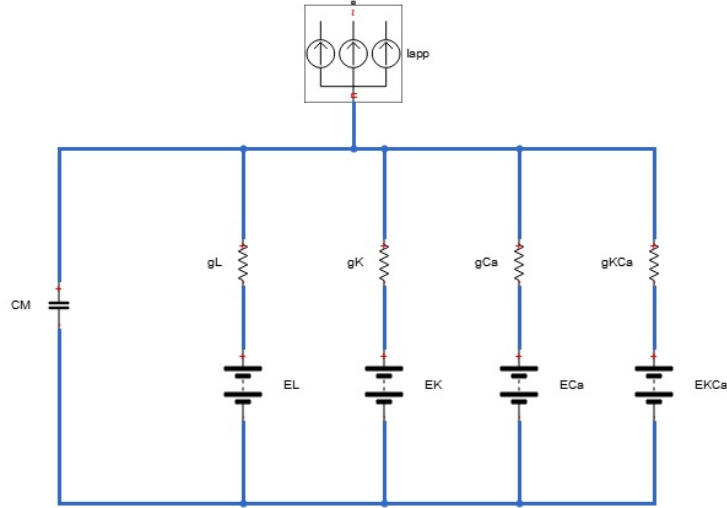


Figure 2.15: *Equivalent circuit for model (2.33). E_K , E_{Ca} , and E_L the Nernst equilibrium potentials. I_{app} the injected current, g_L leak membrane conductance, g_K potassium membrane conductance, g_{Ca} calcium membrane conductance, C_M the total membrane capacitance.*

Figure (2.17).

2.7.2 Morris-Lecar model as an Elliptic burster

For Morris-Lecar model as an elliptic burster, we used the model (2.33) with parameters for Elliptic bursting as we have in table (2.16). Also, we have demonstrated the dynamics of Morris-Lecar model as an elliptic burster for different I_{app} in Figure (2.18).

2.7.3 Morris-Lecar model as a Parabolic burster

Unlike two previous bursters which we need only one slow variable for bursting behavior and the occurrence of the bistability in time series for fast subsystem, in parabolic burster, we need at least two slow variables and the bursting is not because of the bistability and

Parameter	Square wave	Elliptic	Parabolic
\emptyset	0.04	0.067	0.23
g_{Ca}	4	4.4	4
g_{KCa}	0.75	1	1
V_3	12	2	12
V_4	17.4	30	17.4
E_{Ca}	120	120	120
E_K	-84	-84	-84
E_L	-60	-60	-60
g_K	8	8	8
g_L	2	2	2
V_1	-1.2	-1.2	-1.2
V_2	18	18	18
C_M	1	1	1
I_{app}	45	120	65
K_{Ca}	1	1	1
ε	0.1	0.04	0.01
μ	0.02	0.01667	0.025
τ, g_{Cas}			0.05,1

Figure 2.16: *Bursting parameters*³⁷.

hysteresis loop. In parabolic burster, the model has the form:

$$\left\{ \begin{array}{l} C_M \frac{dV}{dt} = I_{app} - g_L(V - E_L) - g_K n(V - E_K) - g_{Ca} m_\infty(V)(V - E_{Ca}) - I_{KCa} \\ \frac{dn}{dt} = \phi(n_\infty(V) - n)/\tau_n(V) \\ \frac{d[Ca]}{dt} = \varepsilon(-\mu I_{Ca} - K_{Ca}[Ca]) \\ \frac{ds}{dt} = \varepsilon(s_\infty(V) - s)/\tau_s \end{array} \right. \quad (2.34)$$

where

$$m_\infty(V) = \frac{1}{2}[1 + \tanh((V - V_1)/V_2)]$$

$$\tau_n(V) = 1/\cosh((V - V_3)/(2V_4))$$

$$n_\infty(V) = \frac{1}{2}[1 + \tanh((V - V_3)/V_4)]$$

$$s_\infty(V) = 0.5(1 + \tanh(V - 12)/24)$$

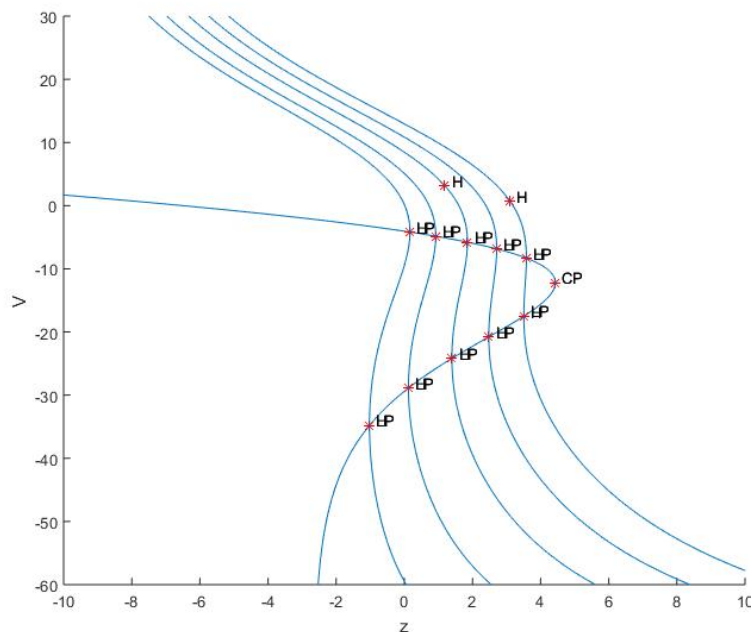


Figure 2.17: Continuation of equilibrium points for $I_{app} = 0, 50, 100, 150, 200$ and occurrence of cusp bifurcation with considering 2 free parameters, the horizontal curve corresponding to co-dimension two bifurcation and the vertical curves are corresponding to co-dimension one bifurcation with increasing I_{app} from left to right. Morris-Lecar model as a Square-Wave burster.

and calcium dependent potassium current I_{KCa} is $I_{KCa} = g_{KCa}z(V - E_K)$ and also a new calcium current $I_{Cas}S(V - E_{Ca})$ that is depending on the gating variable s , and considering the parameters in table (2.16) for parabolic bursting. Here, V, n are two fast variables and $[Ca], s$ are two slow variables. The circuit corresponding to this neuron is presented in Figure (2.19). Finally, we have demonstrated the dynamics of this burster for different I_{app} in Figure (2.20).

2.8 Conclusion

Understanding of the structure of the brain and its dynamics has been facilitated using computer simulations. During the recent decades, our understanding about brain dynamics and the mechanisms of different neuron cells has been greatly improved. Indeed, the field of computational neuroscience has been started with the work of Hodgkin and Huxley in 1952

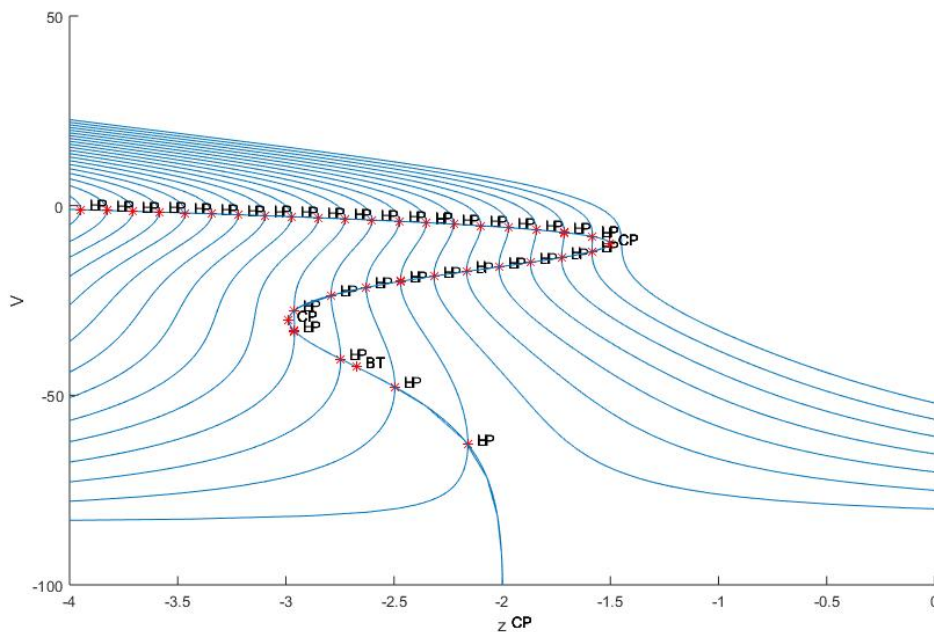


Figure 2.18: Continuation of equilibrium points for $I_{app} = -50, 0, 45, 100, 150, 200, 250, 300$, the horizontal curve corresponding to co-dimension two bifurcation and the vertical curves are corresponding to co-dimension one bifurcation with increasing I_{app} from left to right. Morris-Lecar model as an Elliptic burster.

using nonlinear partial differential equations. The Hodgkin-Huxley model and its reduction related models developed and improved many different areas in mathematics. Recently, dynamical systems theory and computational methods have been used frequently to study neuron activities in a many of neuronal models. The collaboration between experimentalists and theoreticians in analysis of neuronal models provides many progresses in the area of neuroscience⁴³⁻⁴⁵. In this chapter we studied spiking dynamics of a single neuron model which is a reduction of well-known Hodgkin-Huxley model and consists of a system of ordinary differential equations. Depending on the different parameters value, the model reproduces quiescent, spiking and bursting activities. We numerically discovered the Hopf bifurcation, SNLC bifurcation and homocinic bifurcation and we presented their normal form for each case separately. Through bifurcation analysis and continuation of equilibrium point, we explored the complicated dynamics which happened by changing the injected current or changing the temperature in this neuron model. We could find a range for spiking activities

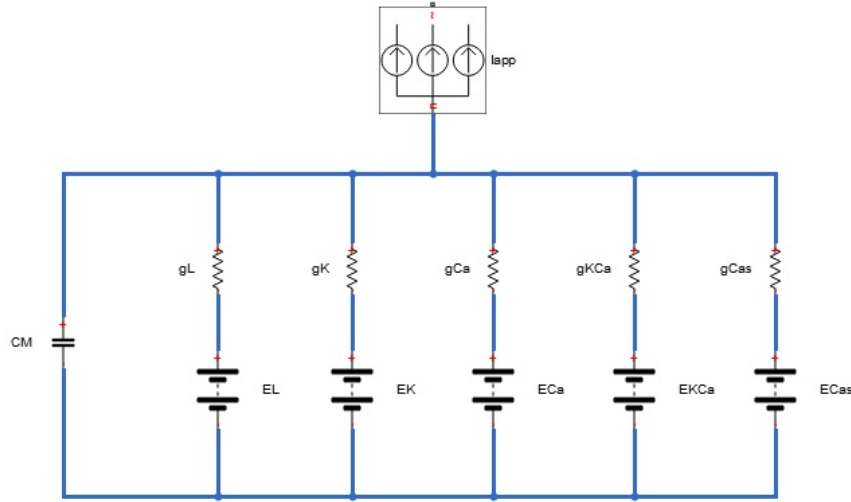


Figure 2.19: Equivalent circuit for model (2.34), Morris-Lecar model as a Parabolic burster. E_K , E_{Ca} , and E_L the Nernst equilibrium potentials. I_{app} the injected current, g_L leak membrane conductance, g_K potassium membrane conductance, g_{Ca} calcium membrane conductance, C_M the total membrane capacitance.

of the neuron for injected current I_{app} and temperature ϕ . We also discovered co-dimension two bifurcations such as Bautin or generalized Hopf, Bogdanov-Takens and limit point cycles and we demonstrated their normal forms. We also described the phenomenon of neural bursting, and we used the continuation method to discover different bifurcations for three types of bursting behaviors. We have found new two co-dimension bifurcations compared to two dimensional Morris-Lecar model, cusp bifurcation and zero-Hopf bifurcation. We presented the Morris-Lecar bursting model for square-wave, elliptic and parabolic burster and we displayed the circuit model corresponding to each type of burster. Finding other types of bursting for Morris-Lecar model can be a new research project which needs to further study about the phenomenon of neuronal bursting.

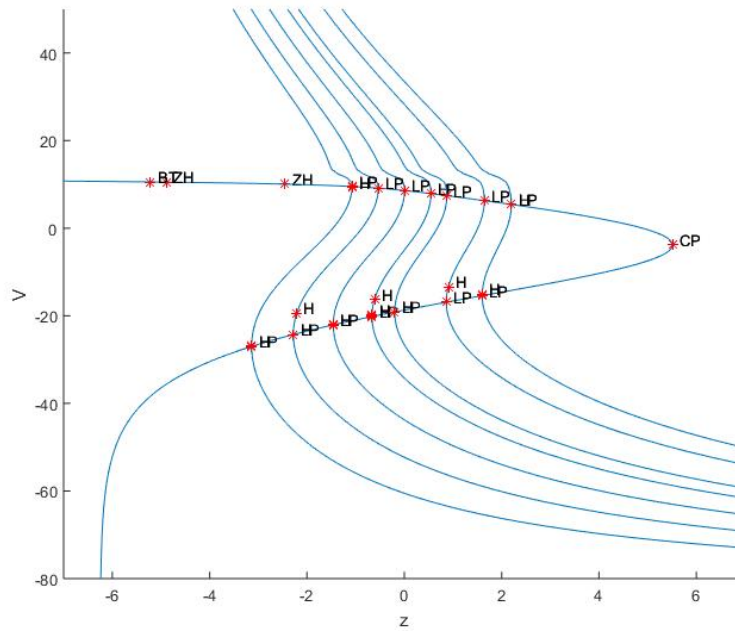


Figure 2.20: Continuation of equilibrium points for $I_{app} = 0, 50, 100, 150, 200$ and occurrence of the zero-Hopf and Bogdanov-Takens and cusp bifurcation with considering 2 free parameters for model (2.34), the horizontal curve corresponding to co-dimension two bifurcation and the vertical curves are corresponding to co-dimension one bifurcation with increasing I_{app} from left to right. Morris-Lecar model as a Parabolic burster.

Chapter 3

Global Sensitivity Analysis in Physiological Systems

Abstract

Pharmacokinetic models are mathematical models, which provide insights into the interaction of chemicals with certain biological processes. In Chapter Three, we consider the process of drug and nanoparticle (NPs) distribution throughout the body. We use a tri-compartmental model to study the perfusion of NPs in tissues and a six-compartmental model to study drug distribution in different body organs. We perform global sensitivity analysis by LHS Monte Carlo method using Partial Rank Correlation Coefficient (PRCC). We identify the key parameters that contribute most significantly to the absorption and distribution of drugs and NPs in different organs in the body.

3.1 Introduction

Nanotechnology is the study of materials, devices, and systems at the nanometer scale. Nanotechnology and nanoscience have been used widely in many areas of research and applications⁴⁶⁻⁵⁰. One of the most important advantages of nanotechnology is that the drug can be targeted to a precise location which would make the drug much more effective and it also reduces the possible side effects. The application of nanotechnology in the field of nanomedicine and health care has grown a huge attention in recent times. Nanomedicine is a branch of nanotechnology. Basically, we can define nanomedicine as the medical application of nanotechnology^{46;47;51}. Nanomedicine has many advantages over conventional drug delivery approaches and has been used frequently in anticancer research. There are some techniques which help in the detection of tumors in the body and nanoparticles are one of them⁵¹. Nanoparticles (NPs) help us to see cells and molecules that cannot be otherwise detected through conventional imaging. The abilities to understand what happens inside the cell and to observe therapeutic intervention and or to see when a cancer cell is lethally injured or is stimulated are important to the effective diagnosis and then better treatment of the disease^{51;52}. Nanoparticles (NPs) have unique physicochemical properties, such as small size, large surface area to mass ratio, and high reactivity, which are different from bulk materials of the same composition⁴⁶. Indeed, because of these unique properties, NPs have very important role in anticancer therapy⁴⁷.

Mathematical and statistical modeling helps us to understand the interaction between the components of systems biology and prediction of the future of different biological models^{56;112-114;215}. Basically, building a mathematical and computational model needs to perform different experiments and obtain different data which depicts the evolution of system^{48;49}. To understand the process of drug distribution through different body organs, we need to develop a comprehensive model which covers completely the experimental data⁵⁸⁻⁶⁰. These models transform all the information into a system of ordinary differential equations to do more analysis based on some mathematical useful tools and are flexible to analysis, updates and modifications of pharmacology and physiology of agents and drugs. A mathe-

mathematical model for drug or NP distributions is a structural model, consisting of compartments such as adipose, tissues, brain, gut, heart, kidney, liver, lung, muscle, spleen, skin, and bone and gastrointestinal tract including mouth, esophagus, and abdomen which are connected by the cardiovascular system. In mathematical perspective, they describe biological systems by converting into mathematical and theoretical equations and parameters and then using computer code to solve the model system computationally.

To check the accuracy of any mathematical model, we need to use different methods and because of existence of uncertainty in experimental data, it can be often complicated. Uncertainty and sensitivity analysis are useful techniques which help us to identify these uncertainties in data and then control them^{113;114;116;117}. Sensitivity analysis allows us to identify the parameter or set of parameters that have the greatest impact on the model output. It then provides useful information about which parameter or input makes the most variability in the model output. Generally, local sensitivity analysis allows us to clarify the impact of each parameter on model outputs individually. However, global sensitivity analysis overcomes the limitations which the local sensitivity analysis creates by examining the sensitivity of model output over the entire range of parameters at the same time.

Current work studies the process of drug distribution throughout the body which consists of a system of ordinary differential equations. There are several biological parameters related to distribution of drug through different body organs. We start with a simple three compartmental model to demonstrate NP distribution from capillary to tissue. Globally sensitivity analysis LHS Monte Carlo method using Partial Rank Correlation Coefficient (PRCC) has been performed to investigate the key parameters in model equations. Also, we study a six compartmental system for which we assume the specific drug has been distributed through different rout of drug administrations, such as intravenous injection, intramuscular injection, water and or feed. We have used the same global sensitivity analysis PRCC method to compare different physiological parameters. We have used the parameters variations based on different studies^{49;63-65}.

3.2 A simple three compartmental model example for NP distribution

There are some efforts to develop physiologically based pharmacokinetic models for nanoparticles distribution through the body, which will be useful tools for predicting nanoparticle distribution in different organs to assist with extrapolation of responses from in vitro and in vivo⁶⁶. However, since the blood-flow limited model which have been used for chemicals⁶⁷ cannot be used for nanoparticles, we need to explain the distribution of the nanoparticles in the tissues to develop a model^{66;68;69}. There are many studies about the effects of Nanomaterials on biological procedures like isolated in vitro cell system and or in vivo effects. But, there are only a few studies about vascular effects of Nanomaterials of different compositions^{49;70-72}. In some studies, researchers have considered Endothelial cells (EC) as in vitro model system for different physiological processes⁷³⁻⁷⁶. According to these works, primary EC have a limited life span and demonstrate distinct characteristics that are different from each other. All vessels in body are covered with a line of Endothelial cells and these cells have different rolls based on their size and location in blood vessels. Some of their important tasks in our body are transporting small molecules and hormones like insulin, and degrading lipoprotein particles. Moreover, they affect blood pressure regulation and transport inflammatory cells into target tissue. Also, they have key role in blood coagulation and fibrinolysis. Endothelial cells are like barriers between blood cells and tissue cells⁷². They may help to some disorders like bleeding disorders, autoimmune disorders, or in pathological processes. As we can see in Figure (3.1), EC or endothelial cells have covered blood vessels and they transport NPs from capillary to target tissue. We have used a tri compartmental model for NPs infusion to tissue. For NPs that move from blood vessels into different tissues this tri-compartmental model is needed to characterize NPs infusion in the body. For simplicity, we have supposed that there is no interaction between Endothelial cells and their surrounding cells.

As we can see in Figure (3.2), NPs enter from artery to the second compartment by a con-

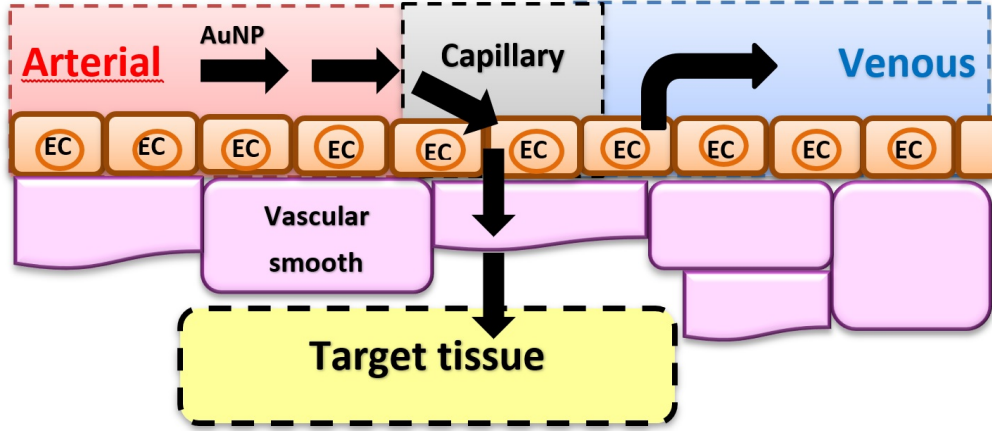


Figure 3.1: *Endothelial cells as barriers between blood vessels and target tissue.*

stant rate k_{12} , we call this rate as absorption rate constant to capillary bed. After this step, NPs distribute to the third compartment by a constant rate k_{23} . Then, we have distribution of NPs into fixed or deep tissue compartment by the constant rate k_{34} . So far, we have finished two phases, absorption and distribution, and the last phase would be NPs leakage or NPs elimination. If we apply the mass balance laws to this tri-compartmental model, we have:

$$\begin{cases} \frac{d A_{Cap}}{dt} = k_{12} A_{Art} - k_{23} A_{Cap} - k_{25} A_{Cap} + k_{32} A_{EC} \\ \frac{d A_{EC}}{dt} = k_{23} A_{Cap} - k_{34} A_{EC} - k_{32} A_{EC} \\ \frac{d A_{DT}}{dt} = k_{34} A_{EC} \end{cases} \quad (3.1)$$

We have two possible routes for NPs in compartment two. First possibility, they can distribute to compartment 3 and or they leave compartment two via venous efflux. Here, also we have assumed that the uptake depends on NP concentration in compartment two and it does not depend on perforce blood flow^{49;77}. For the first compartment, we can easily obtain the following equality:

$$J_{25} = J_{12} - k_{23} A_{Cap} + k_{32} A_{EC} \quad (3.2)$$

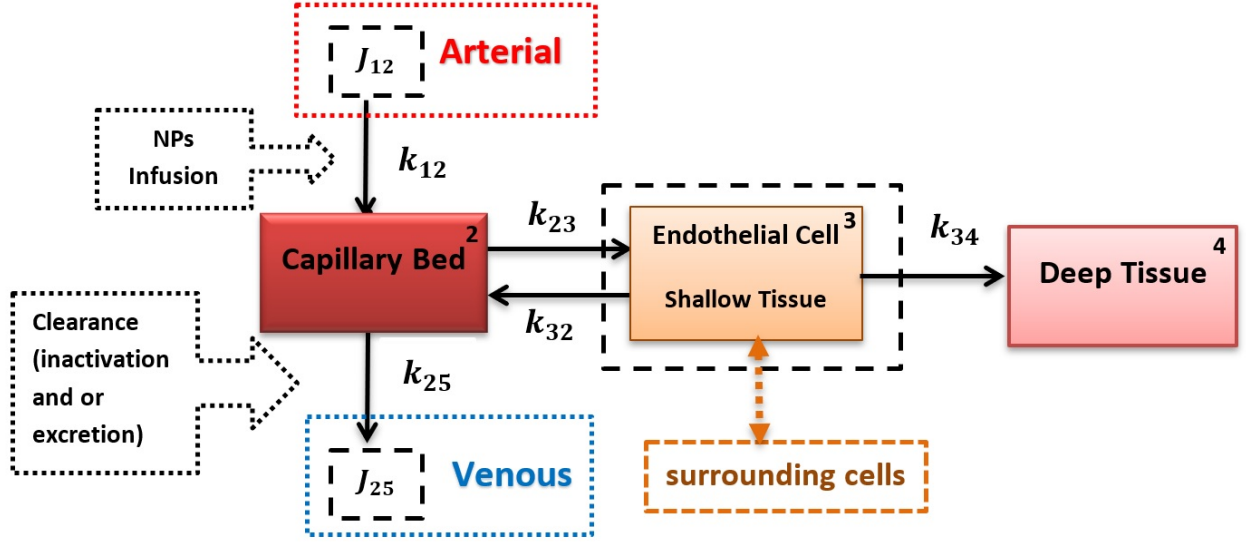


Figure 3.2: Structure of the tri-compartment pharmacokinetic model for nanoparticle disposition with considering NPs infusion, where k_{23} , k_{32} and k_{34} are transfer rate constants, k_{25} describes the rate of mass transfer from vascular (2) compartment to the venous effluent, J_{12} is the infusion drug flux, which is the product of flow (Q) and concentration (C_{12}).

Where $J_{25} = k_{25}A_{Cap}$ and $J_{12} = QC_{12}$ (k_{25} is a variable rate function).

Physiologically speaking, we have considered that at starting time $t = 0$ NPs enter from artery to compartment 2 and then they leave capillary bed to shallow tissue. Before the time for the venous effluent, venous efflux of NPs is zero, and at this moment, $t = \tau$, and then after that the sum of NPs fluxes to shallow tissue compartment and venous effluent should be equal to arterial flux or J_{12} . By this assumption that τ is small at steady state, we can compute the initial mass M_2 for capillary bed compartment that would be $M_2 = C_{12}V_2$. Here, C_{12} is the concentration of infused NPs, and V_2 is the vascular volume. Also, we can calculate the capillary transit time by the following equality $\tau = V_2/Q$, where, Q is perfusate flow through skin flap and we consider it as a constant approximately equal $1 \text{ mL}/\text{min}$. The value of k_{25} as a variable rate function after the time that flux $k_{32}A_{EC}$ reaches to compartment two increased and we will prove it by some computations later⁴⁹. After solving model (3.1)

for A_{Cap} and A_{EC} we have,

$$A_{Cap} = M_2 \quad (3.3)$$

$$A_{EC} = \frac{M_2 k_{23}}{k_{32} + k_{34}} (1 - e^{-(k_{32}+k_{34})t}) + A_{EC}(0) e^{-(k_{32}+k_{34})(t-\Gamma)} \quad (3.4)$$

$$A_{DT} = \frac{M_2 k_{23} k_{34}}{k_{32} + k_{34}} \left(t - \frac{1 - e^{-(k_{32}+k_{34})t}}{k_{32} + k_{34}} \right) + \frac{k_{34} A_{EC}(0)}{k_{32} + k_{34}} [1 - e^{-(k_{32}+k_{34})t(t-\Gamma)}] + A_{DT}(0) \quad (3.5)$$

where we consider Γ as the beginning time of washout phase that is zero during dosing phase⁷⁷. Also, $A_{EC}(0)$ is the initial mass of compartment three and $A_{DT}(0)$ is the initial mass of compartment four. During dosing phase, $A_{EC}(0) = 0$ and $A_{DT}(0) = 0$. During washout phase, the initial mass of NPs in all compartments and Γ are non-zero. In decay or washout phase, we can calculate k_{25} at $t = 0$ by the following equation⁷⁷:

$$k_{25}^0 = \frac{J_{12} + k_{32} A_{EC}(0)}{A_{Cap}(0)} - k_{23} \quad (3.6)$$

Because at $t = 0$, $A_{EC}(0) = 0$ and $A_{Cap}(0) = M_2$, so we have:

$$k_{25}^0 = \frac{J_{12}}{M_2} - k_{23} \quad (3.7)$$

Therefore, k_{25} at steady-state has the following value:

$$k_{25}^{ss} = \frac{J_{12} + k_{32} A_{EC}(ss)}{A_{Cap}(ss)} - k_{23} \quad (3.8)$$

such that $A_{Cap}^{ss} = M_2$ and

$$A_{EC}^{ss} = \lim_{t \rightarrow \infty} A_{EC}(t) = \frac{k_{23} M_2}{k_{32} + k_{34}} \quad (3.9)$$

If we substitute the value of A_{Cap}^{ss} and A_{EC}^{ss} into k_{25}^{ss} , then we have:

$$k_{25}^{ss} = \frac{(k_{32} + k_{34}) J_{12} + k_{32} k_{23} M_2}{(k_{32} + k_{34}) M_2} - k_{23} \quad (3.10)$$

and because we have, $\frac{J_{12}}{M_2} = \tau^{-1}$, so;

$$k_{25}^{ss} = \tau^{-1} + \frac{k_{32} k_{23}}{k_{32} + k_{34}} - k_{23} \quad (3.11)$$

and when $k_{34} = 0$, we have $k_{25}^{ss} = \tau^{-1}$. Moreover, we can write $k_{25}^0 = \tau^{-1} - k_{23}$. When we compare k_{25}^0 and k_{25}^{ss} , we see that k_{25}^0 is less than k_{25}^{ss} by the following result:

$$k_{25}^{ss} = k_{25}^0 + \frac{k_{32} k_{23}}{k_{32} + k_{34}} \quad (3.12)$$

During dosing phase $A_{Cap} = 0$. At $t = \Gamma$, A_{Cap} changes from M_2 to 0, and also $A_{EC}(0)$ from 0 to $A_{EC}(\Gamma)$. During decay phase J_{12} is non-zero. Figure (3.3) displays the evolution of the solutions of (3.1) in time and also with respect to other solutions in separate plots.

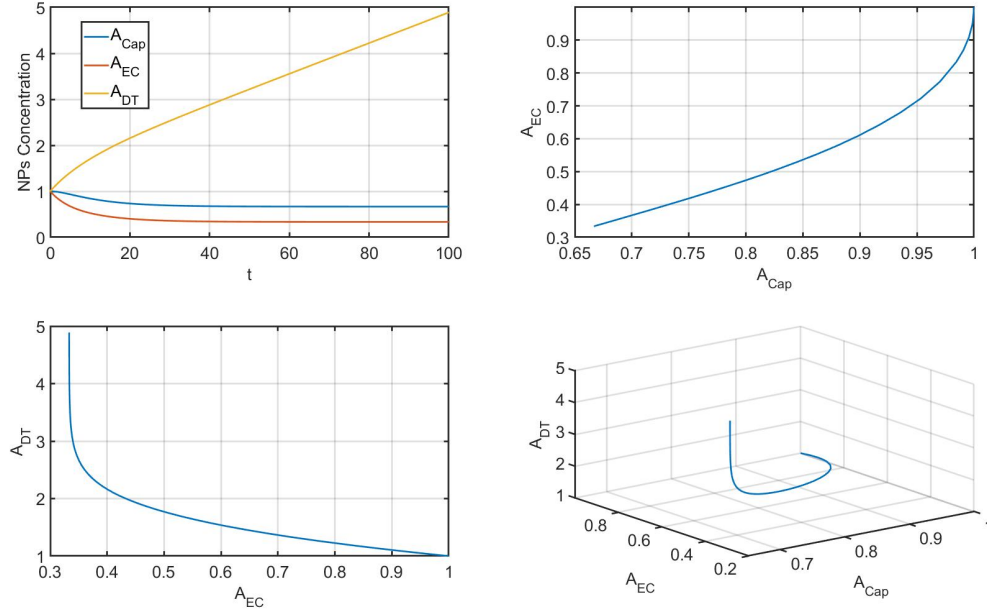


Figure 3.3: A_{Cap} , A_{EC} and A_{DT} in model (3.1).

3.3 A six compartmental model example for drug distribution through body organs

Physiological and pharmacokinetic models are useful to determine drug distribution into different target tissues, which helps for the evaluation of drug efficacy and drug safety. We study a six-compartmental pharmacokinetic model with application in food safety and we use the physiological parameters variations based on different studies^{63;64}.

Cardiac output and blood flows to tissues (L/h):

$$\left\{ \begin{array}{l} QC = QCC \times BW, \quad \text{Cardiac output} \\ QL = QLC \times QC, \quad \text{Liver} \\ QK = QKC \times QC, \quad \text{Kidney} \\ QLu = QLuC \times QC, \quad \text{Lung} \\ QF = QFC \times QC, \quad \text{Fat} \\ QM = QMC \times QC, \quad \text{Muscle} \\ QR = QRC \times QC, \quad \text{Rest of body} \end{array} \right. \quad (3.13)$$

where, $QCC = 4.944$ is cardiac output ($L/h/kg$), $QLC = 0.2725$ is fraction of blood flow to the liver (unitless), $QKC = 0.12$ is fraction of blood flow to the kidneys (unitless), $QFC = 0.1275$ fraction of blood flow to the fat (unitless), $QMC = 0.251$ is fraction of blood flow to the muscle (unitless), $QLuC = 1$ is fraction of blood flow to the Lung (unitless), $QRC = 1 - QLC - QKC - QFC - QMC$; $-QLuC$ is fraction of blood flow to the rest of body and BW is body weight⁶³.

Tissue volumes (L):

$$\left\{ \begin{array}{l} V_{ven} = V_{venC} \times BW, \\ V_{art} = V_{artC} \times BW, \\ VL = VLC \times BW, \quad \text{Liver} \\ VK = VKC \times BW, \quad \text{Kidney} \\ VLu = VLuC \times BW, \quad \text{Lung} \\ VF = VFC \times BW, \quad \text{Fat} \\ VM = VMC \times BW, \quad \text{Muscle} \\ VRB = VRC \times BW, \quad \text{Rest of body} \end{array} \right. \quad (3.14)$$

where, $VLC = 0.0245$ Fractional liver tissue (unitless), $VKC = 0.004$ fractional kidney tissue, $VFC = 0.32$ fractional fat tissue (unitless), $VMC = 0.4$ fractional muscle tissue (unitless), $VLuC = 0.010$ fractional Lung tissue (unitless), $VvenC = 0.044$ venous blood volume, fraction of blood volume (unitless), $VartC = 0.016$ Arterial blood volume, fraction of blood volume (unitless) and $VRC = 1 - VLC - VKC - VFC - VMC - VLuC - VvenC - VartC$ fractional rest of body tissue (unitless).

Permeability surface area coefficients:

$$\left\{ \begin{array}{l} PAF = PAFC \times VF, \\ PAM = PAMC \times VM, \end{array} \right. \quad (3.15)$$

where, permeability constants ($L/h/kg$ tissue) (Permeation area cross products) are: $PAFC = 0.012$ fat tissue permeability constant, $PAMC = 0.225$ muscle tissue permeability constant⁶³.

Volume of tissue as blood:

$$\left\{ \begin{array}{l} VFb = FVBF \times VF, \quad \text{Fat compartment blood volume} \\ VFt = VF - VFb, \quad \text{Fat compartment tissue volume} \end{array} \right. \quad (3.16)$$

where, $FVBF = 0.02$ blood volume fraction of fat⁶⁵.

Muscle:

$$\begin{cases} VMb = FVBM \times VM, & \text{Muscle compartment blood volume} \\ VMt = VM - VMb, & \text{Muscle compartment tissue volume} \end{cases} \quad (3.17)$$

where, $FVBM = 0.01$ blood volume fraction of muscle⁶⁵.

Dosing:

$$\begin{cases} DOSEoral = PDOSEoral \times BW, & (mg) \text{ Oral dose} \\ DOSEiv = PDOSEiv \times BW, & (mg) \text{ IV dose} \\ DOSEim = PDOSEim \times BW, & (mg) \text{ IM dose} \\ DOSEoralw = PDOSEoralw \times BW, & (mg) \text{ Oral through water dose} \\ DOSEoralf = PDOSEoralf \times BW, & (mg) \text{ Oral through feed dose} \end{cases} \quad (3.18)$$

where, $PDSEoral$, $PDSEiv$, $PDSEim$, $PDSEoralw$ and $PDSEoralf$ are parameters for exposure scenario.

Intramuscular (IM) injection equations:

$$\begin{cases} Rim = Kim \times Amtsite \\ \frac{d}{dt}(\text{Absorb}) = Rim \\ Rsite = -Rim + Kdiss \times \text{Doseimremain} \\ \frac{d}{dt}(\text{Amtsite}) = Rsite \\ Rdoseimremain = -Kdiss \times \text{Doseimremain} \\ \frac{d}{dt}(\text{Doseimremain}) = Rdoseimremain \end{cases} \quad (3.19)$$

where, $Kim = 0.15$ or $Kim = 0.3$ IM IM absorption rate constant ($/h$), $Kdiss = 0.02$ IM absorption rate constant⁶³.

Intravascular (IV) injection to the venous equations:

$$\left\{ \begin{array}{l} IVR = DOSE_{iv}/Time_{iv} \\ Riv = IVR \times (1 - heaviside(T - Time_{iv})) \\ \frac{d}{dt}(A_{iv}) = Riv \end{array} \right. \quad (3.20)$$

where, $Time_{iv}$ is IV injection/infusion time (h).

Urinary elimination rate constant:

$$K_{urine} = K_{urineC} \times BW \quad (3.21)$$

Liver compartment:

$$\left\{ \begin{array}{l} RL = QL \times (CA - CVL) + RAO, \\ \frac{d}{dt}(AL) = RL, \\ CL = AL/VL, \\ CVL = AL/(VL \times PL), \\ \frac{d}{dt}(AUCCL) = CL, \end{array} \right. \quad (3.22)$$

Blood compartment:

$$\left\{ \begin{array}{l} RV = (QL \times CVL + QK \times CVK + QF \times CVF + QM \times CVM + QR \times CVRB + Riv + Rim) - \\ -QC \times CV, \quad (mg) \quad RV \text{ the changing rate in the venous blood (mg/h)} \\ \frac{d}{dt}(AV) = RV, \quad AV \text{ the amount of the drug in the venous blood (mg)} \\ CV = AV/V_{ven}, \quad CV \text{ drug concentration in the venous blood (mg/L)} \\ RA = QC \times (CVLu - CA), \quad RA \text{ the changing rate in the arterial blood (mg/h)} \\ \frac{d}{dt}(AA) = RA, \quad AV \text{ the amount of the drug in the venous blood (mg)} \\ CA = AA/V_{art} \\ \frac{d}{dt}(AUCCV) = CV, \quad AUCCV \text{ AUC of drug} \\ ABlood = AA + AV \end{array} \right.$$

Kidney compartment:

$$\left\{ \begin{array}{l} RK = QK \times (CA - CVK) - R_{urine}, \\ \frac{d}{dt}(AK) = RK, \\ CK = AK/VK, \\ CVK = AK/(VK \times PK), \\ \frac{d}{dt}(AUCCK) = CK, \\ R_{urine} = K_{urine} \times CVK, \\ \frac{d}{dt}(A_{urine}) = R_{urine}, \end{array} \right. \quad (3.23)$$

Muscle compartment:

$$\left\{ \begin{array}{l}
 RMB = QM \times (CA - CVM) - PAM \times CVM + PAM \times CMt/PM, \\
 \frac{d}{dt}(AMB) = RMB, \\
 CVM = AMB/VMB, \\
 RMt = PAM \times CVM - PAM \times CMt/PM, \\
 \frac{d}{dt}(AMt) = RMt, \\
 CMt = AMt/VMt, \\
 AMtotal = AMt + AMB, \\
 CM = AMtotal/VM, \\
 \frac{d}{dt}(AUCCM) = CM,
 \end{array} \right. \quad (3.24)$$

Lung compartment:

$$\left\{ \begin{array}{l}
 RLu = QLu \times (CV - CVLu), \\
 \frac{d}{dt}(ALu) = RLu, \\
 CLu = ALu/VLu, \\
 CVLu = ALu/(VLu \times PLu), \\
 \frac{d}{dt}(AUCCLU) = CLu,
 \end{array} \right. \quad (3.25)$$

Fat compartment:

$$\left\{ \begin{array}{l} RFB = QF \times (CA - CVF) - PAF \times CVF + PAF \times CFt/PF, \\ \frac{d}{dt}(AFB) = RFB, \\ CVF = AFB/VFB, \\ Rft = PAF \times CVF - PAF \times CFt/PF, \\ \frac{d}{dt}(AFt) = Rft, \\ CFt = AFt/VFt, \\ Aftotal = AFt + AFB, \\ CF = Aftotal/VF, \end{array} \right. \quad (3.26)$$

Rest of body:

$$\left\{ \begin{array}{l} RRB = QR \times (CA - CVRB), \\ \frac{d}{dt}(AR) = RRB, \\ CR = AR/VRB, \\ CVRB = AR/(VRB \times PR), \\ \frac{d}{dt}(AUCCR) = CR, \end{array} \right. \quad (3.27)$$

Mass balance equation:

$$\left\{ \begin{array}{l} Qbal = QC - QL - QK - QM - QF - QR, \\ Tmass = Ablood + AL + AK + AMtotal + Aftotal + AR + Aurine + ALu, \\ Bal = AAO + Aiv + Absorb - Tmass, \quad \text{Permeability-limited model mass balance} \end{array} \right. \quad (3.28)$$

3.4 Global sensitivity analysis

Global sensitivity analysis allows us to change all parameters simultaneously over the entire parameter interval. This is a way to evaluate the relative effects of each input parameter and also to identify the interactions between parameters to the model output. In global

sensitivity analysis we determine that with variation of input parameters in a certain range, which parameters and interactions have the most influential impact on the overall behavior of our model^{56;112-114;116;117}.

There are several types of global sensitivity analyses, such as weighted average of local sensitivity analysis, partial rank correlation coefficient, multi parametric sensitivity analysis, Fourier amplitude sensitivity analysis (FAST) and Sobol's method, which can be used for systems pharmacology models¹¹². The Latin hypercube sampling (LHS) method has been used frequently for global sensitivity analysis. There are also some other methods for calculating main effect and total effect sensitivity indices and one of the most important one is the method of Sobol¹¹⁶.

LHS method is a sampling method and requires fewer samples compare to simple random sampling to achieve the same accuracy¹¹². In LHS method, we divide the random parameter distributions into N equal probability intervals. Here, N is the sample size. The choice for N should be at least $k + 1$, where k is the number of parameters which are varied. For the case that the interval of variation for some parameter is very large, the sampling can be done on a *log* form.

In LHS method, sampling is independent for each parameter and can be done by randomly selecting values from each *pdf*. We may sample each interval once for each parameter without any replacement. The LHS matrix is consisting of N rows corresponding to the number of simulations or sample size and also it includes k columns corresponding to the number of varied parameters. Then, N model solutions may be simulated, using each combination of parameter values which they represent each row of the LHS matrix¹¹².

3.4.1 Partial Rank Correlation Coefficient (PRCC) results for tri-compartmental model (3.1)

Here, a parameter sensitivity analysis has been conducted to identify the pharmacokinetic parameters that have the most significant effect on our model system by the LHS Monte Carlo method using PRCC with uniform distributions for the 95 percent confidence intervals. The

global sensitivity results with p- values corresponding to capillary compartment, endothelial cell compartment and deep tissue compartment have been demonstrated in Figure (3.4), Figure (3.5) and Figure (3.6) respectively.

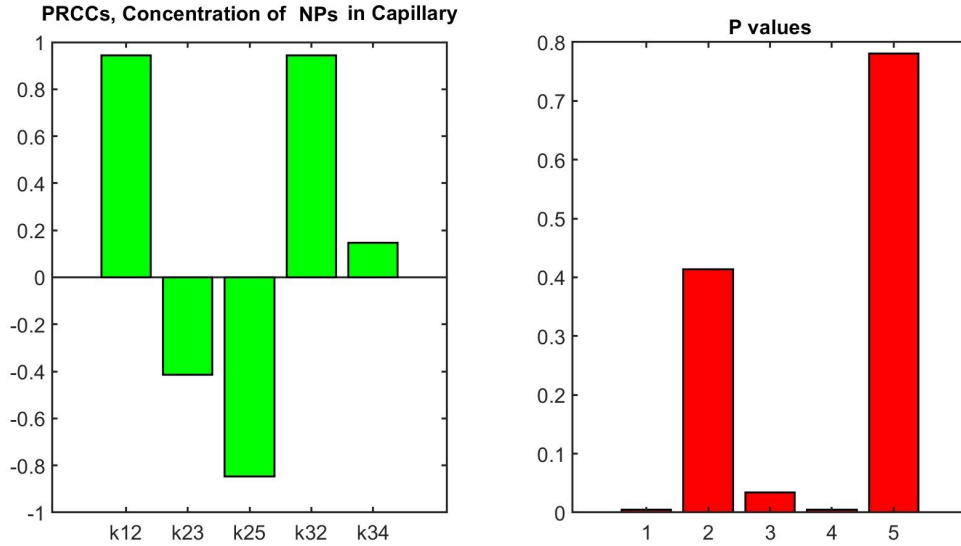


Figure 3.4: Global uncertainty and sensitivity analysis of calculated different parameters for capillary compartment of model (3.1).

3.4.2 Partial Rank Correlation Coefficient (PRCC) results for six-compartmental model (3.1)-(3.25)

According to LHS, we simulated the responses of the model for each organ by randomly selecting values for the parameter set from the 95 percent confidence intervals. These analyses were done by developing a *LHS/PRCC* method with uniform distributions for the 95percent confidence intervals. We found that some parameters illustrate significant performance in terms of sensitivity of the output to the variations of these parameters in some organs while they do not have this effect for other organs. These results have been depicted in Figure (3.7) for kidney tissue, Figure (3.8) for liver tissue, Figure (3.9) for lung tissue, Figure (3.10) for fat tissue, Figure (3.11) for muscle tissue and Figure (3.12) for plasma, are statistically significant with p- values much smaller than 0.01.

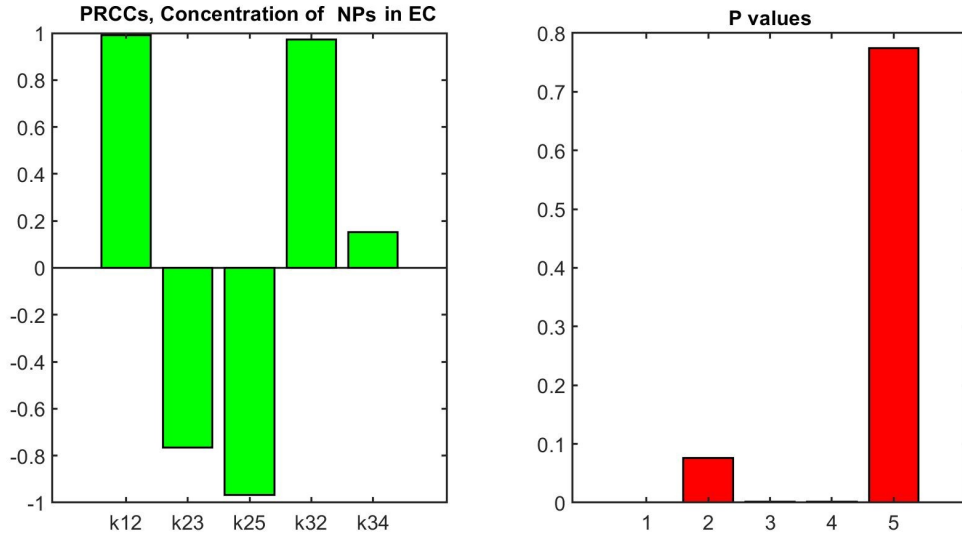


Figure 3.5: *Global uncertainty and sensitivity analysis of calculated different parameters for endothelial cell compartment of model (3.1).*

3.5 Conclusion

Recently, nanoparticles have a growing use in industry specially medicine. There are some studies about applications of NPs in therapeutic areas, however, the number of these studies is not a lot. Increasing the importance of studies about tumors and concentration of drugs and NPs in tumors or other tissues has enhanced the role of in vitro models to simulate absorption process of drugs and NPs. Pharmacokinetic and physiological models are useful means to demonstrate the relationships between different drug administrations, and drug exposure or concentration.

An uncertainty analysis may be applied on the physiological and pharmaceutics models to investigate the uncertainty in system output that is generated from uncertainty in parameter inputs. Sensitivity analysis assesses how variations in model outputs can be apportioned, qualitatively or quantitatively, to different inputs.

In this research we reviewed two physiological systems which have been reported by different authors and we have used the presented physiological parameters from different published works. In the first case, we presented a three compartmental model which can be used to exhibit the distribution of drug and or NPs from capillary compartment to endothelial cells

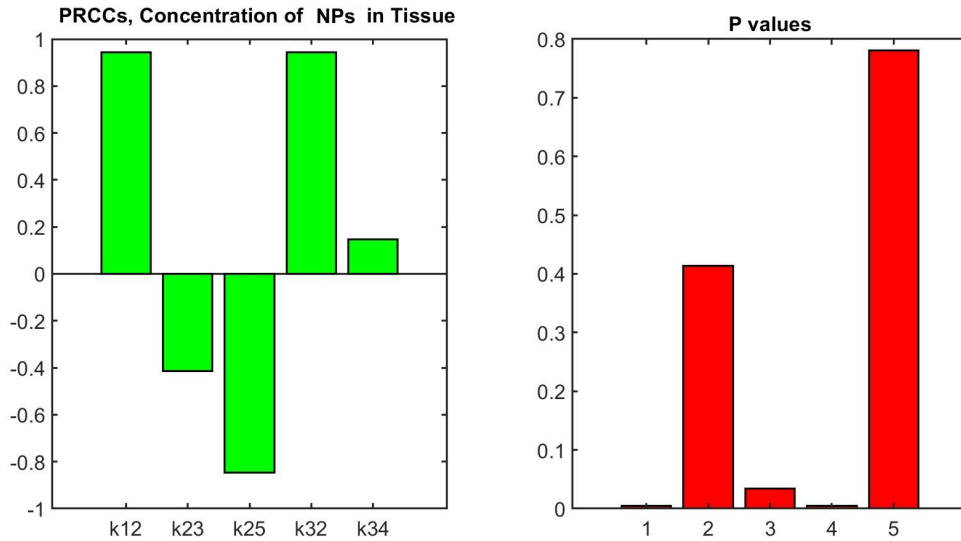


Figure 3.6: *Global uncertainty and sensitivity analysis of calculated different parameters for deep tissue compartment of model (3.1).*

compartment and then tissue compartment. The objective of this study was to determine the key parameters in NPs infusion from blood vessels to target tissue in the ex vivo tissue perfusion system using sampling-based method (Partial Rank Correlation Coefficient-PRCC). As we have seen, some parameters have positively and some others negatively affected NPs infusion process.

We have presented another physiological model with six compartments, such as kidney, liver, lung, fat, muscle and plasma compartment. We identified the key parameters that contribute most significantly to the absorption and distribution of drugs in different organs in body using PRCC. Our findings imply that this identification is clearly dependent upon the dose and target tissues but not on the exposure route.

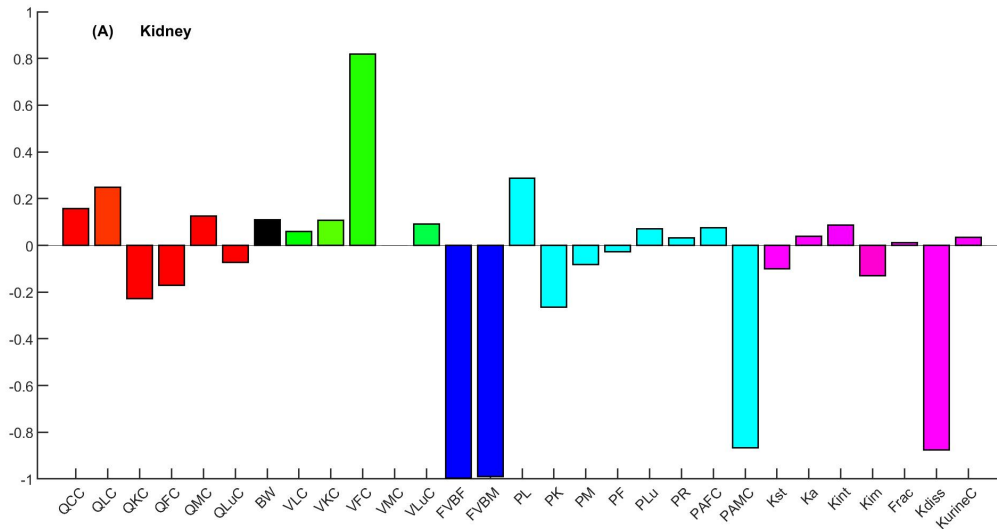


Figure 3.7: Global uncertainty and sensitivity analysis of calculated different parameters for kidney. Analysis based on parameter effects for C_k (concentration of drug in kidney). The PRCCs are compiled within the pharmacokinetic parameters ranges obtained from⁶³⁻⁶⁵.

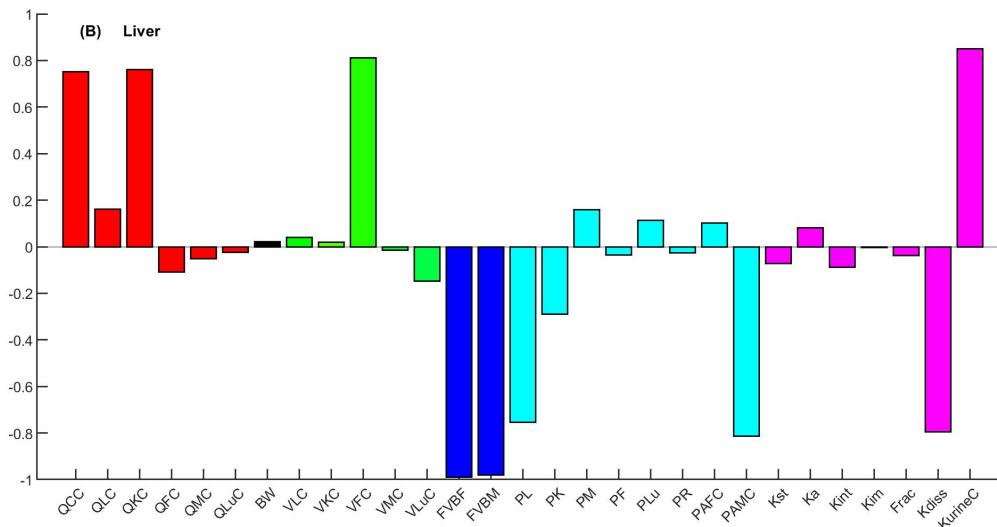


Figure 3.8: Global uncertainty and sensitivity analysis of calculated different parameters for kidney. Analysis based on parameter effects for C_L (concentration of drug in liver). The PRCCs are compiled within the pharmacokinetic parameters ranges obtained from⁶³⁻⁶⁵.

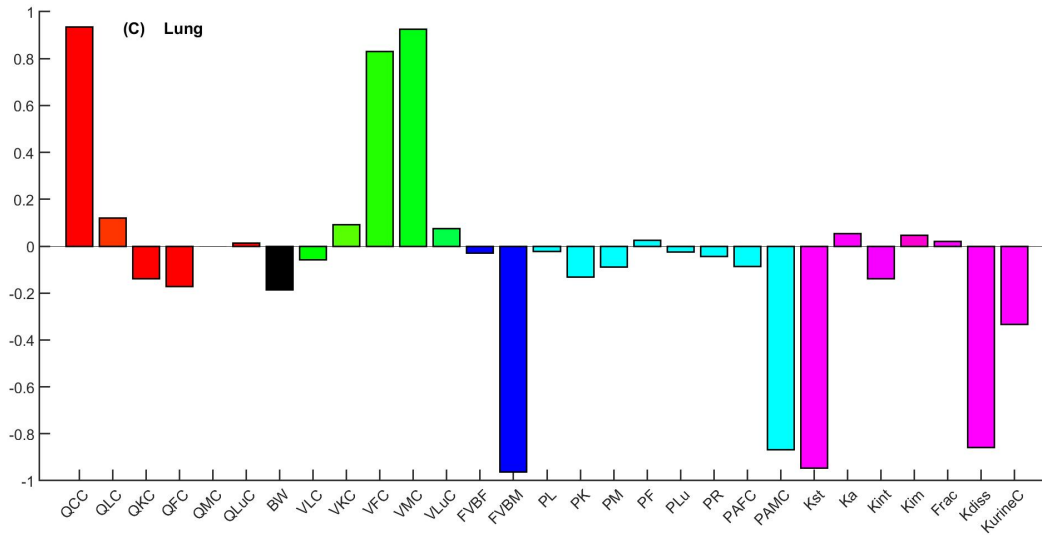


Figure 3.9: Global uncertainty and sensitivity analysis of calculated different parameters for kidney. Analysis based on parameter effects for C_{Lu} (concentration of drug in lung). The PRCCs are compiled within the pharmacokinetic parameters ranges obtained from ⁶³⁻⁶⁵.

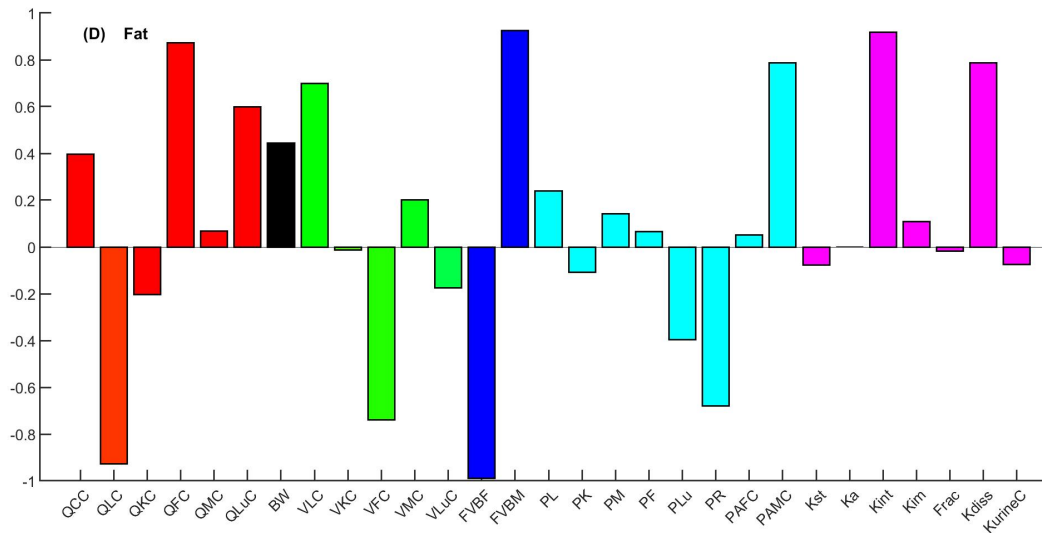


Figure 3.10: Global uncertainty and sensitivity analysis of calculated different parameters for kidney. Analysis based on parameter effects for C_F (concentration of drug in fat). The PRCCs are compiled within the pharmacokinetic parameters ranges obtained from ⁶³⁻⁶⁵.

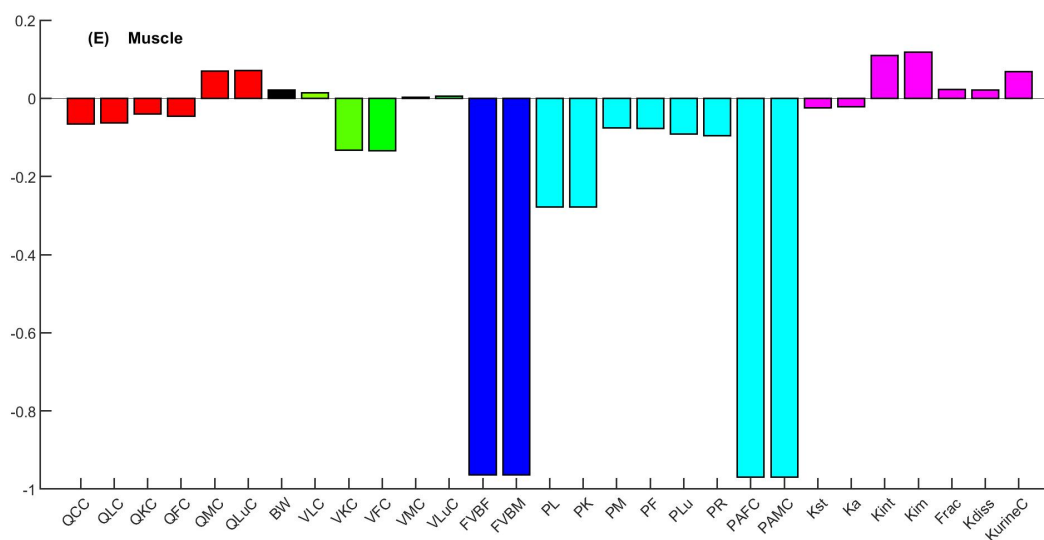


Figure 3.11: Global uncertainty and sensitivity analysis of calculated different parameters for kidney. Analysis based on parameter effects for C_M (concentration of drug in muscle). The PRCCs are compiled within the pharmacokinetic parameters ranges obtained from⁶³⁻⁶⁵.

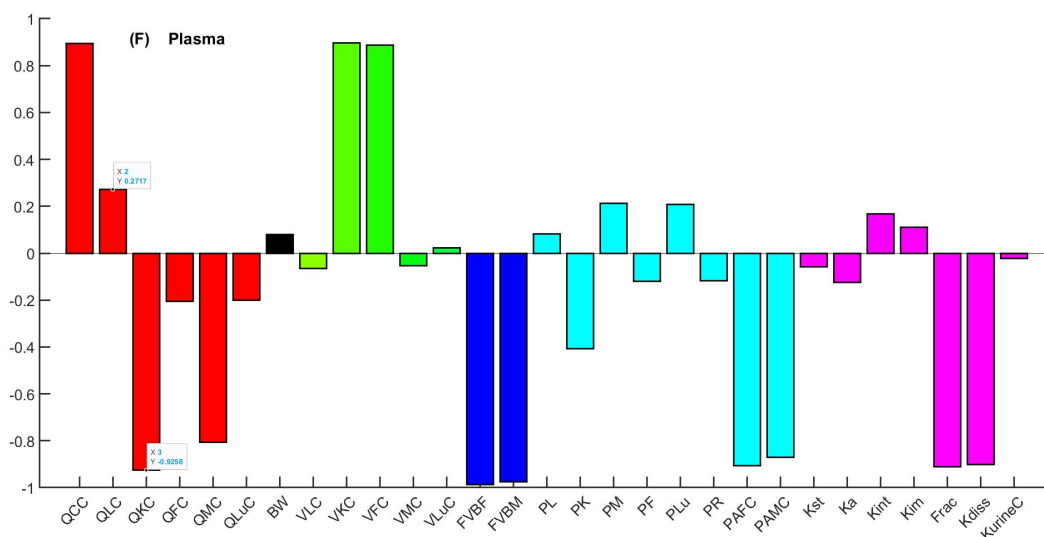


Figure 3.12: Global uncertainty and sensitivity analysis of calculated different parameters for kidney. Analysis based on parameter effects for C_V (concentration of drug in plasma). The PRCCs are compiled within the pharmacokinetic parameters ranges obtained from⁶³⁻⁶⁵.

Chapter 4

Impact of Vaccination Strategies and Key Parameters on Infectious Disease Models

Abstract

In Chapter Four, we study two infectious disease models and use nonlinear optimization and optimal control theory to help in identifying strategies for transmission control and forecasting the spread of infectious diseases. We analyze the effect of vaccination on the disease transmission in these models. Moreover, we perform global sensitivity analysis to investigate the key parameters in these models.

4.1 Introduction

Recently, due to the fast spread of pandemic diseases, mathematical modeling in the field of epidemiology has attracted many scientists in different areas. Many mathematical models have been developed to describe the transmission of communicable diseases⁹³⁻⁹⁵. These mathematical models describe the mechanisms of infectious diseases as well as they are helpful to analysis the effect of public health interventions to control the spreading of diseases. In mathematical perspective, we describe biological systems by converting them into mathematical and theoretical framework with biological parameters and then using computer code to solve the model system computationally To predict the future of infectious diseases, one needs to study the behavior of each individual which plays a key role to understand the behavior epidemiology of infectious diseases⁹⁶.

One of the new approaches in modeling dynamic systems is the theory of optimal control. For the first time, R. E. Bellman introduced a new method to solve dynamic systems by using the principle of optimality which reduces significantly the computation of the optimal controls⁹⁷. In optimal control (OC) theory, for a dynamic system we define a control problem and its state trajectories over a period of time to minimize a performance index⁹⁸. In optimal control theory, the problem of determining the control would be turned to an extension of the calculus of variations⁹⁹. One of the most interesting applications of the calculus of variations was in the Hamilton's principle or the Principle of Least Action. The Russian mathematician Lev S. Pontryagin and his colleagues V. G. Boltyanskii, R. V. Gamkrelidz and E. F. Misshchenko generalized the the calculus of variations to optimal control theory by proposing the Pontryagin Maximum Principle¹⁰⁰ which defines appropriate conditions for optimization problems with differential equations as constraints. OC can be used for the problems where the calculus of variations is not applicable, such as the problems which include constraints on the derivatives of functions¹⁰¹. With increasing the number of variables and parameters of system, optimal control problems can not be solved analytically and one may need to apply numerical methods.

To model a dynamic system, we usually use a set of ordinary differential equations. A system

of ODEs for $t_0 \leq t \leq t_f$ can be described by

$$\dot{y} = \begin{bmatrix} \dot{y}_1 \\ \dot{y}_2 \\ \vdots \\ \dot{y}_n \end{bmatrix} = \begin{bmatrix} f_1(y_1(t), \dots, y_n(t), t) \\ f_2(y_1(t), \dots, y_n(t), t) \\ \vdots \\ f_n(y_1(t), \dots, y_n(t), t) \end{bmatrix}$$

Based on how the conditions at the endpoints of the domain are specified, we classify an ODE solving problem into initial value problems (IVP) and boundary value problems (BVP). For an initial-value problem, all the conditions are specified at the initial point. For a boundary-value problem the conditions are needed for both initial and final points. There are many numerical methods to solve initial value problems such as Euler, Runge-Kutta or adaptive methods and boundary value problems, such as shooting methods^{102;103}.

Euler method is the most common used single-step method. In this discretization technique, for differential equation $\dot{x} = f(x(t), t)$, we can make a convenient approximation of this:

$$x_{n+1} \simeq x_n + h f(x(t_n), t_n) :$$

The approximation x_{n+1} of $x(t)$ at the point t_{n+1} has an error of order h^2 . There exists a trade-off between accuracy and complexity of calculation which depends heavily on the chosen value for h . As h is decreasing, the calculation would be longer however more exact. One of the disadvantages of this method is for many higher order systems, it is very difficult to have an effective Euler approximation. Thus, we need to use more accurate and elaborate methods and one of them is the Runge-Kutta method.

Runge-Kutta method is a multiple-step method. In this technique, we obtain the solution at time t_{k+1} from the values t_{j-k}, \dots, t_k and j is the number of steps. To approximate a differential equation of the form $\dot{x} = f(x(t), t)$, we can use the second order Runge-Kutta

method

$$x_{n+1} \simeq x_n + \frac{h}{2} [f(x_n(t), t_n) + f(x_{n+1}(t), t_{n+1})];$$

or the fourth order Runge-Kutta method

$$x_{n+1} \simeq x_n + \frac{h}{6} (k_1 + 2k_2 + 2k_3 + k_4)$$

where

$$\begin{aligned} k_1 &= f(x(t), t) \\ k_2 &= f\left(x(t) + \frac{h}{2} k_1, t + \frac{h}{2}\right) \\ k_3 &= f\left(x(t) + \frac{h}{2} k_2, t + \frac{h}{2}\right) \\ k_4 &= f(x(t) + h k_3, t + h) \end{aligned}$$

For the second and fourth order Runge-Kutta method, the approximation x_{n+1} of $x(t)$ at the point t_{n+1} has an error of order h_3 and h_5 .

In this research, we study the most basic epidemiological models S-I-R model (composed by Susceptible-Infected-Recovered) and S-E-I-R model (Susceptible-Exposed-Infected-Recovered). For these models, we develop some analytical results that are useful in understanding of simple epidemic diseases. We continue this study by proposing the equivalent optimal control problems of the mentioned epidemic models and we numerically solve them using the backward-forward sweep method with fourth order Runge-Kutta. Finally, we perform global sensitivity analysis by LHS Monte Carlo method using PRCC to identify the key parameters that contribute most significantly to the spread or control of the infectious diseases.

4.2 Kermack-McKendrick SIR epidemic model (S-I-R Model)

Recently, due to the fast spread of pandemic diseases, mathematical modeling in the field of epidemiology has attracted many scientists in different areas. Many mathematical models have been developed to describe the transmission of communicable diseases and among these models, the classical Kermack-McKendrick SIR epidemic model builds the basic skeleton of all of them¹⁰⁴.

S:=Susceptible (People who could potentially catch the disease)

I:= Infective (People who currently have the disease)

R:= Removed (People recovered or have died)

Assumptions:

1. Total population remains constant;
2. Rate of increase in the infectives is proportional to the contact between susceptible and infective;
3. Removal rate (death rate) is constant;

Using these assumptions, the classical S-I-R model has the following form:

$$\left\{ \begin{array}{l} \frac{dS}{dt} = -\beta I S + \delta R \\ \frac{dI}{dt} = \beta I S - \gamma I \\ \frac{dR}{dt} = \gamma I - \delta R \end{array} \right. \quad (4.1)$$

Where, β demonstrates rate of infection, γ implies to rate of recovery and δ represents rate of immunity loss. If $\delta = 0$ we assume a model without immunity loss. In the first equation of system (4.1), susceptible S decreases according to the number of contacts between infective I and susceptible S . Therefore, because of decreasing the rate of change of susceptible over time, in the first equation we get $-\beta I S$. The rate of change of infective I inncreases by

IS and decreases by γI . The term βIS has been added to the second equation of system (4.1) which is due to the increasing the contact between S and I . The negativity of γI is showing decreasing the rate of change in infective I by moving to the next stage which is recovered or died. The term γI has been added to the third equation which means that the rate of changing the recovered R is increasing by this factor. The time-evolution of system (4.1) over 300 days have been demonstrated in Figures (4.1)-(4.4).

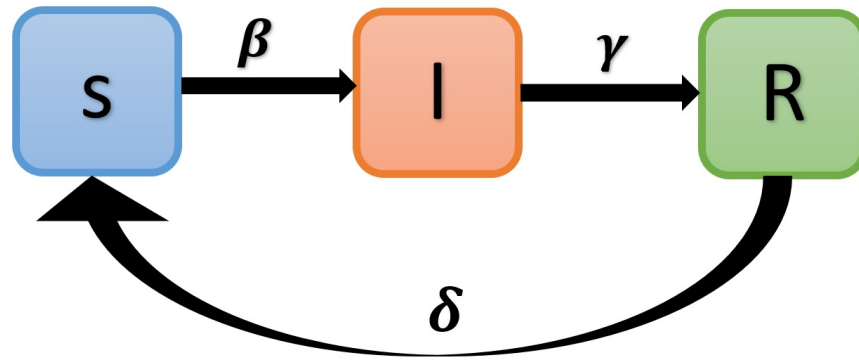


Figure 4.1: *The SIR schematic model for system (4.1). $S:=$ Susceptible Compartment, $I:=$ Infective Compartment, $R:=$ Removed Compartment.*

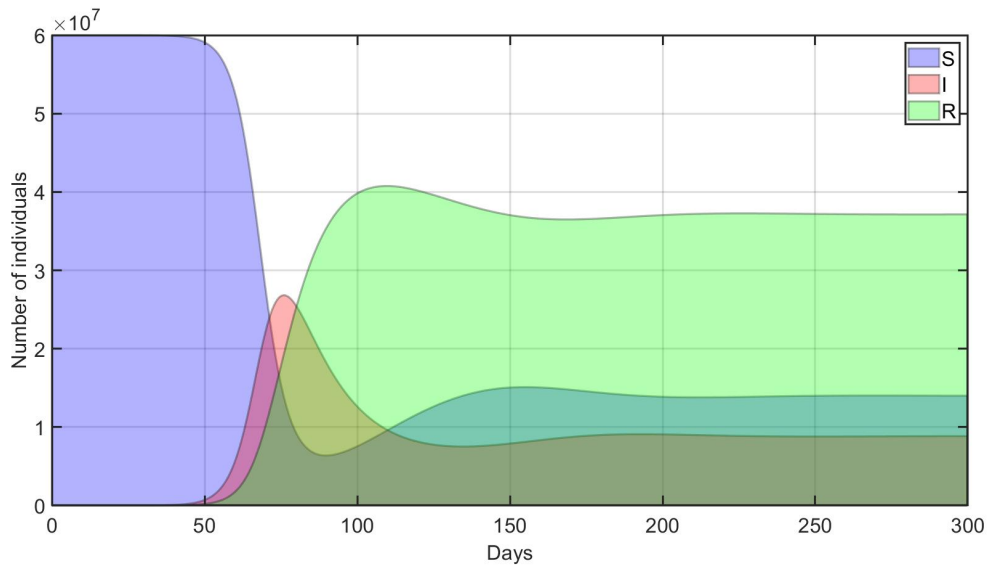


Figure 4.2: *The time-evolution of disease over 300 days $\beta = 5 \times 10^{-9}$, $\gamma = 0.12$, $\delta = 0.016$.*

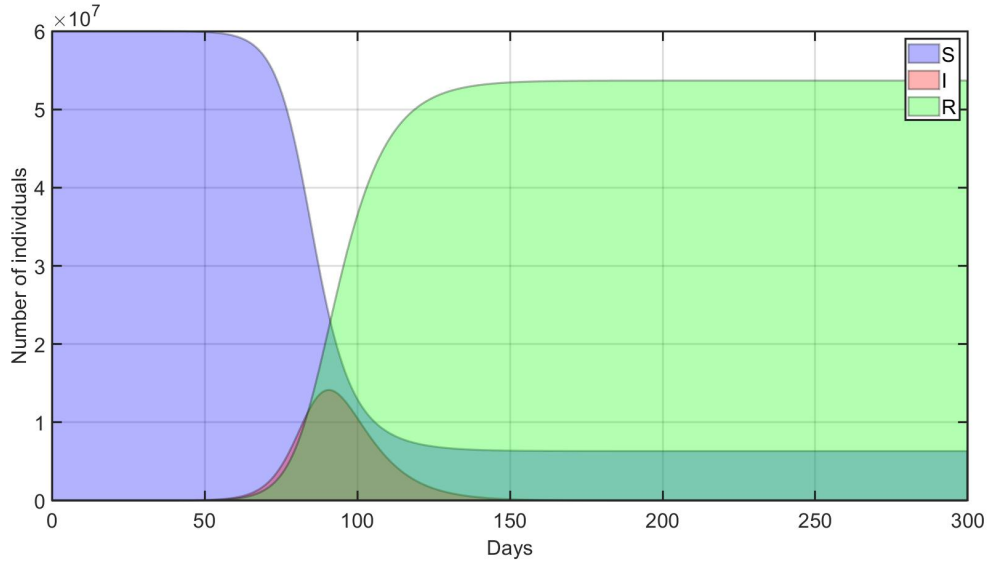


Figure 4.3: *The time-evolution of disease over 300 days $\beta = 5 \times 10^{-9}$, $\gamma = 0.12$, $\delta = 0.0$.*

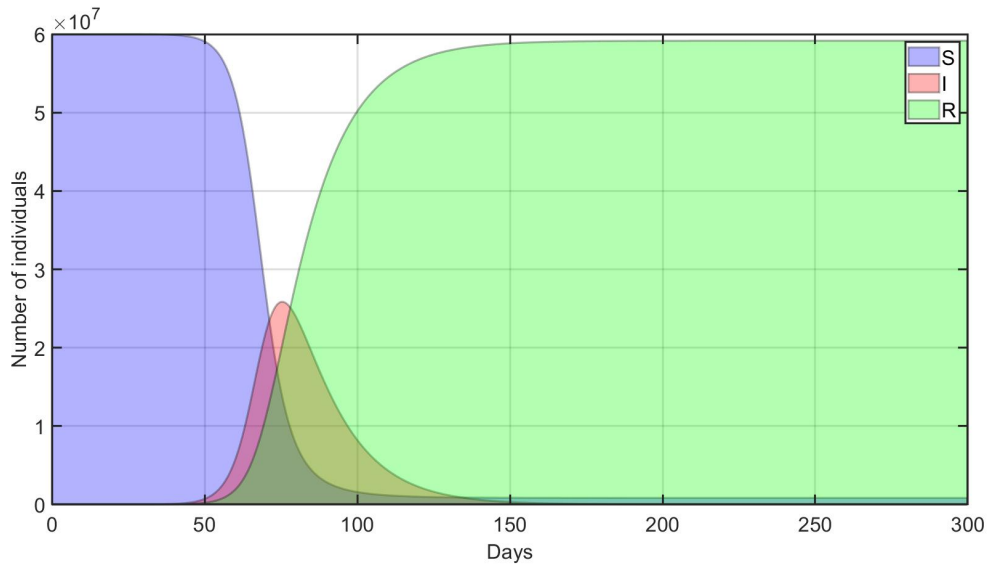


Figure 4.4: *The time-evolution of disease over 300 days $\beta = 5 \times 10^{-9}$, $\gamma = 0.07$, $\delta = 0.0$.*

4.2.1 Will the disease spread? What is the max number of infectives I_{max} ? How many people catch the disease?

To answer these questions consider the following general S-I-R model:

$$\begin{cases} \frac{dS}{dt} = -\beta I S \\ \frac{dI}{dt} = \beta I S - \gamma I \\ \frac{dR}{dt} = \gamma I \end{cases} \quad (4.2)$$

At the start of outbreak we have $S = S_0$, $I = I_0$ and $R = 0$. Total population size remains constant during epidemic, therefore, the rate of change of $S + I + R$ must be zero:

$$\frac{d}{dt}(S + I + R) = 0, \quad S + I + R = S_0 + I_0 \quad (4.3)$$

To find out if the disease will spread, we need to check that

$$\frac{dI}{dt} = I(\beta S - \gamma) < 0, \quad S \leq S_0$$

Therefore, if $S_0 > \frac{\gamma}{\beta} = \frac{1}{q}$, then disease will spread. Here, $\frac{1}{q}$ is the contact ration which is the fraction of population that comes to contact with individual during the period of infectious. However, if the reproductive number or the ratio number $R_0 = \frac{\beta S_0}{\gamma} > 1$, we have epidemic. This ratio represents the number of secondary infection in the population caused by initial primary infection, i.e. how many other people get the disease.

To find the maximum number of infectives or I_{max} , we combine $\frac{dS}{dt}$ and $\frac{dI}{dt}$:

$$\frac{dI}{dS} = \frac{\beta I S - \gamma I}{-\beta I S} = -1 + \frac{\gamma}{\beta S} = -1 + \frac{1}{q S}$$

Assuming

$$I + S - \frac{1}{q} \ln S = I_0 + S_0 - \frac{1}{q} \ln S_0 \quad (4.4)$$

Then

$$I_{max} = I_0 + S_0 - \frac{1}{q}(1 + \ln(q S_0))$$

Here, I_{max} represents the maximum number of people who have the disease at a given time. For COVID-19, or similar worldwide diseases the value for q (contact parameter) is high since disease easily transmits. When q is large, it means that the number of people get infected is a lot.

To reduce the reproduction rate, one can reduce the number of susceptible, S_0 . One way to decrease the number of susceptible is using vaccination which is a common method to eradicate of infectious diseases. Vaccination can go further than being used for just individuals, but it can be beneficial in large scale communities by preserving the effective reproduction rate below the level which would allow an epidemic to spread. However, an epidemic can start and spread very quickly if the reproduction rate rises beyond the critical value for an epidemic¹⁰⁵.

To find out how many people catch the disease, based on the first assumption, the total population is constant and to end the disease, the number of infected need to go down to zero (end of out break):

$$S + I + R = S_0 + I_0$$

and

$$R(end) = -S(end) + I_0 + S_0$$

Here, $S(end)$ is unknown. From (4.4), we have

$$S(end) - \frac{1}{q} \ln(S(end)) = I_0 + S_0 - \frac{1}{q} \ln S_0$$

The graph of $S(end)$ is decreasing and shows at small value of $S(end)$ and larger q , we have larger value for $R(end)$.

4.3 The S-E-I-R model

An SIR model is an epidemiological model that represents the number of people infected with a contagious illness in a closed population over time. In other word, there are some other important infections which include a significant latency or incubation period during which individuals have been infected but are not yet infectious themselves (for example this latency period is zero for cold). During incubation period the individual is exposed. See Figure (4.5).

Here, we write the total population as $N = S + E + I + R$. So, the S-E-I-R model has the

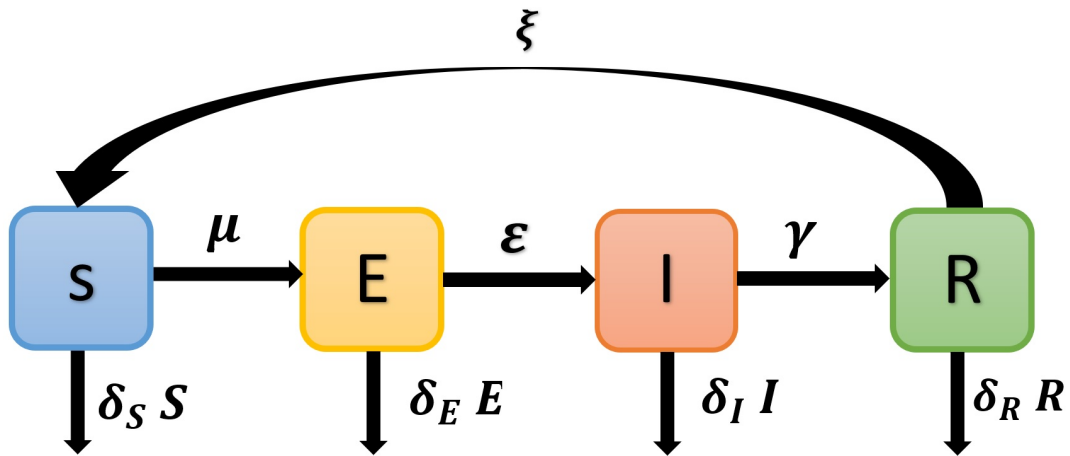


Figure 4.5: The transport diagram for S-E-I-R model (7.15). S :=Susceptible Compartment, E := Exposed Compartment, I := Infective Compartment, R := Removed Compartment.

form

$$\left\{ \begin{array}{l} \frac{dS}{dt} = \Lambda - \beta I S - \delta S \\ \frac{dE}{dt} = \beta I S - \epsilon E - \delta E \\ \frac{dI}{dt} = \epsilon E - \gamma I - \delta I \\ \frac{dR}{dt} = \gamma I - \delta R \end{array} \right. \quad (4.5)$$

where

S:=Susceptible (People who could potentially catch the disease)

E:= Exposed (People who are infected but are not yet infectious)

I:= Infective (People who currently have the disease)

R:= Removed (People recovered or have died)

δ := Constant death rate

$\Lambda = \mu \times N$:= Constant influx of new susceptible (μ Constant birth rate)

ϵ := Latency transfer rate to infectious

γ := Recovery rate of infectious

$\beta I S$:= The bilinear (mass action) incidence.

For simplicity, we assume that the death rates are equal $\delta_S = \delta_E = \delta_I = \delta_R$.

If we have $S > 0$ and $E = I = R = 0$, we have a disease free population or disease free equilibrium, which means that there is no disease. To find disease or endemic equilibrium point, we look for a feasible region Σ such that:

$$\frac{dN}{dt} > 0 \quad \rightarrow \quad \frac{d(S + E + I + R)}{dt} = \frac{dS}{dt} + \frac{dE}{dt} + \frac{dI}{dt} + \frac{dR}{dt} > 0$$

Therefore, from (4.5) we have

$$\begin{aligned} & (\Lambda - \beta I S - \delta S) + (\beta I S - \epsilon E - \delta E) + (\epsilon E - \gamma I - \delta I) + (\gamma I - \delta R) = \\ & \Lambda - \delta S - \delta E - \delta I - \delta R = \Lambda - \delta (S + E + I + R) = \Lambda - \delta N > 0 \end{aligned}$$

Thus

$$\frac{dN}{dt} = \Lambda - \delta N \geq 0 \quad \Rightarrow \quad \Lambda \geq \delta N \quad \Leftrightarrow \quad \frac{\Lambda}{\delta} \geq N = S + E + I + R$$

Therefore, the feasible region Σ would be:

$$\Sigma = \{(S, E, I, R) \in \mathbb{R}^4 \mid S + E + I + R \leq \frac{\Lambda}{\delta}\}$$

From equation three we have,

$$\epsilon = (\delta + \gamma) I \quad \Rightarrow \quad I^* = \left(\frac{\epsilon}{\delta + \gamma}\right) E$$

From equation four,

$$\gamma I - \delta R = 0 \quad \Rightarrow \quad R^* = \frac{\gamma}{\delta} \left(\frac{\epsilon}{\delta + \gamma}\right) E$$

1. Case 1: If $E^* = 0$ No Exposed. So, $I^* = 0$ and $R^* = 0$.

From equation one,

$$0 = \Lambda - \delta S^* \quad \Rightarrow \quad S^* = \frac{\Lambda}{\delta}$$

Therefore, the diseases free equilibrium would be:

$$P_0 = \left(\frac{\Lambda}{\delta}, 0, 0, 0\right)$$

2. Case 2: If $E^* \neq 0$, then $I^* \neq 0$ and $R^* \neq 0$.

$$\begin{aligned}
& (\beta I^* S^* - \epsilon E^* - \delta E^*) + (\epsilon E^* - \gamma I^* - \delta I^*) = 0 + 0 = 0 \\
\Rightarrow & \beta I^* S^* - (\delta + \gamma) I^* - \delta E^* = 0 \\
\Rightarrow & \beta I^* S^* - (\epsilon + \delta) E^* = 0 \\
\Rightarrow & \beta \left(\frac{\epsilon}{\delta + \gamma} \right) E^* S^* - (\epsilon + \delta) E^* = 0 \\
\Rightarrow & \left[\beta \left(\frac{\epsilon}{\delta + \gamma} \right) S^* - (\epsilon + \delta) \right] E^* = 0 \\
\Rightarrow & \left(\frac{\epsilon \beta}{\delta + \gamma} \right) S^* - (\epsilon + \delta) = 0 \\
\Rightarrow & S^* = \frac{(\epsilon + \delta)(\delta + \gamma)}{\epsilon \beta}
\end{aligned}$$

General replication number R_0 is the number of new cases any single infected individual is going to create and produce or infect susceptible. To find R_0 , at equilibrium we have $S^* \geq \frac{\Lambda}{\delta}$. For $S^* = \frac{(\epsilon + \delta)(\delta + \gamma)}{\epsilon \beta}$, we have:

$$\frac{(\epsilon + \delta)(\delta + \gamma)}{\epsilon \beta} \geq \frac{\Lambda}{\delta} \quad \iff \quad 1 \geq \frac{\Lambda \epsilon \beta}{\delta (\epsilon + \delta)(\delta + \gamma)} = R_0$$

1. $R_0 \leq 1 \Rightarrow$ Disease Free equilibrium $P_0 = \left(\frac{\Lambda}{\delta}, 0, 0, 0 \right)$; we can control and there is no disease.

2. $R_0 > 1 \Rightarrow$ Endemic equilibrium $P^* = (S^*, E^*, I^*, R^*) > 0$.

The time-evolution of system (4.5) over 300 days have been demonstrated in Figure (4.6).

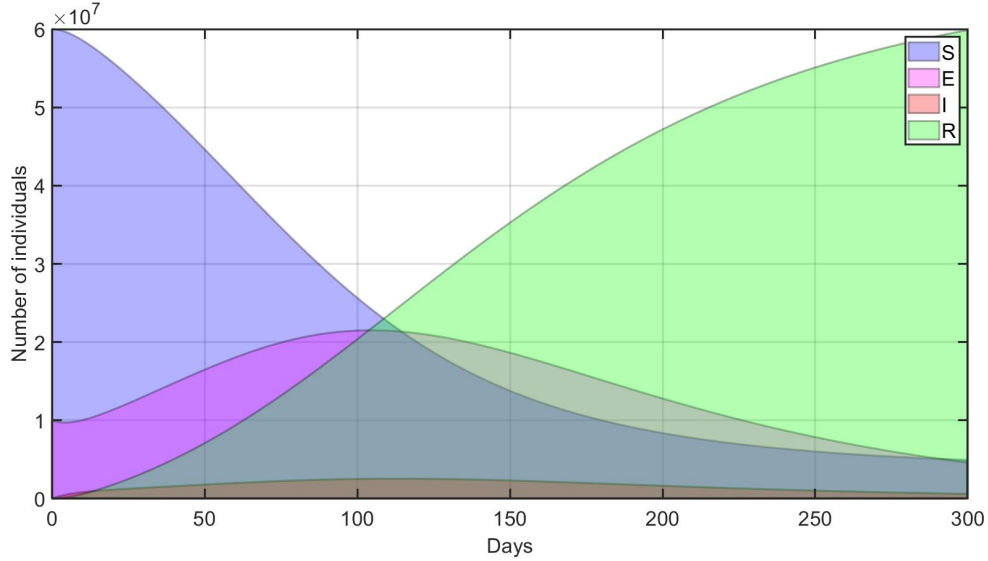


Figure 4.6: *The time-evolution of system (4.5) over 300 days $\beta = 5 \times 10^{-9}$, $\gamma = 0.07$, $\delta = 1/60$ and $\mu = 1/50$.*

4.4 Optimal control problem

A general optimal control (OC) problem needs a cost functional ($J[x(t), u(t)]$), a set of state variables ($x(t) \in X$), a set of control variables ($u(t) \in U$) in a time t , with $t_0 \leq t \leq t_f$. The main goal is finding a piecewise continuous control $u(t)$ and the associated state variable $x(t)$ to maximize a given objective functional.

Definition 4.4.1 (Basic optimal control Problem in Lagrange formulation). *An OC problem is in the form*

$$\begin{aligned} \max_u J[x(t), u(t)] &= \int_{t_0}^{t_f} f(t, x(t), u(t)) dt \\ \text{s.t. } \dot{x}(t) &= g(t, x(t), u(t)) \\ x(t_0) &= x_0 \end{aligned}$$

$x(t_f)$ could be free, which means that the value of $x(t_f)$ is unrestricted, or could be fixed, i.e., $x(t_f) = x^{106}$.

We consider f and g to be continuously differentiable functions. We suppose that the

control set U is a Lebesgue measurable function. Therefore, as long as the controls will always be piecewise continuous, the associated states will be piecewise differentiable.

We can change the maximization problem to a minimization problem by making the cost functional negative:

$$\min\{J\} = -\max\{J\}$$

Definition 4.4.2 (Bolza formulation). *The Bolza formulation of the OC problem can be defined as*

$$\begin{aligned} \max_u J[x(t), u(t)] &= \Phi((t_0, x(t_0), t_f, x(t_f))) + \int_{t_0}^{t_f} f(t, x(t), u(t))dt \\ \text{s.t. } \dot{x}(t) &= g(t, x(t), u(t)) \\ x(t_0) &= x_0 \end{aligned}$$

where Φ is a continuously differentiable function¹⁰⁷.

Definition 4.4.3 (Mayer formulation).¹⁰⁸ *The Mayer formulation of the OC problem can be defined as*

$$\begin{aligned} \max_u J[x(t), u(t)] &= \Phi((t_0, x(t_0), t_f, x(t_f))) \\ \text{s.t. } \dot{x}(t) &= g(t, x(t), u(t)) \\ x(t_0) &= x_0 \end{aligned}$$

4.4.1 Pontryagin's Maximum Principle

Pontryagin proposed the idea of adjoint functions to append the differential equation to the objective functional which was one of the most important results of Mathematics in the 20th century and illustrates the necessary conditions to find the optimal control. Similar to Lagrange multipliers in multivariate calculus, Adjoint functions append constraints to the

function of several variables to be maximized or minimized⁹⁹.

Definition 4.4.4 (Hamiltonian). *Consider the OC problem in definition (4.4.1). The function*

$$H(t, x(t), u(t), \lambda(t)) = f(t, x(t), u(t)) + \lambda(t)g(t, x(t), u(t))$$

is called Hamiltonian function and λ is the adjoint variable.

Theorem 4.4.5 (Pontryagin's Maximum Principle).^{100;109} *Let $u^*(t)$ and $x^*(t)$ be optimal for problem in definition (4.4.1), then there exists a piecewise differentiable adjoint variable $\lambda(t)$ such that*

$$H(t, x^*(t), u(t), \lambda(t)) \leq H(t, x^*(t), u^*(t), \lambda(t))$$

for all controls u at each time t , where H is the Hamiltonian previously defined and

$$\begin{aligned} \lambda'(t) &= \frac{\partial H(t, x^*(t), u^*(t), \lambda(t))}{\partial x} \\ \lambda(t_f) &= 0 \end{aligned}$$

The last condition, $\lambda(t_f) = 0$, called transversality condition, is only used when the OC problem does not have terminal value in the state variable, i.e., $x(t_f)$ is free.

This Pontryagin's Maximum Principle converts the problem of finding a control which maximizes the objective functional subject to the state ODE and initial condition into the problem of optimizing the Hamiltonian pointwise. Therefore, with this adjoint equation and Hamiltonian, we have

$$\frac{\partial H}{\partial u} = 0$$

at u^* for each t , meaning that the Hamiltonian has a critical point and we call this condition as optimality condition. Therefore, to find the necessary conditions, we do not need to

calculate the integral in the objective functional and we only use the Hamiltonian.

4.4.2 Existence of a finite objective functional value at the optimal control and state variables

Theorem 4.4.6. ^{110;111} *Consider*

$$\begin{aligned} \max_u J[x(t), u(t)] &= \int_{t_0}^{t_f} f(t, x(t), u(t)) dt \\ \text{s.t. } \dot{x}(t) &= g(t, x(t), u(t)) \\ x(t_0) &= x_0 \end{aligned}$$

Suppose that $f(t, x, u)$ and $g(t, x, u)$ are both continuously differentiable functions in their three arguments and concave in x and u . Suppose u^ is a control with associated state x^* , and λ a piecewise differentiable function, such that u^* , x^* and λ together satisfy on $t_0 \leq t \leq t_f$:*

$$\begin{aligned} f_u + \lambda g_u &= 0, \\ \lambda' &= -(f_x + \lambda g_x), \\ \lambda(t_f) &= 0, \\ \lambda(t) &\geq 0. \end{aligned}$$

Then for all controls u , we have $J(u^) \geq J(u)$*

Based on how the conditions at the endpoints of the domain are specified, we classify an ODE solving problem into initial value problems (IVP) and boundary value problems (BVP). For an initial-value problem, all the conditions are specified at the initial point. For a boundary-value problem the conditions are needed for both initial and final points. There are many numerical methods to solve initial value problems such as Euler, Runge-Kutta or adaptive methods and boundary value problems, such as shooting methods ^{102;103}.

Numerical methods for solving OC problems started from the 1950s with the works of

Bellman¹⁰². We can divide these method into two major groups: direct methods and indirect methods. Indirect methods indirectly solve the problem by converting the optimal control problem to a boundary-value problem, using the PMP. However, direct method solves the OC by transcribing an infinite-dimensional optimization problem to a finite-dimensional optimization problem.

4.5 An optimal control problem for S-I-R model

In this section, we present an optimal control (OC) problem to study the dynamics of S-I-R model, using a vaccination process (u) as a measure to control the disease. Let x_1 represents the susceptible population, x_2 represents the proportion of population that is infected and x_3 represents the proportion of population that is recovered or dead. The optimal control problem can be defined as:

$$\min_u J[x(t), u(t)] = \int_{t_0}^{t_f} (x_2 + u^2) dt \quad (4.6)$$

$$s.t \quad \frac{dx_1}{dt} = -\beta x_1 x_2 + \delta x_3 - u x_1 \quad (4.7)$$

$$\frac{dx_2}{dt} = \beta x_1 x_2 - \gamma x_2 \quad (4.8)$$

$$\frac{dx_3}{dt} = \gamma x_2 - \delta x_3 \quad (4.9)$$

$$x(t_0) = (x_1(0), x_2(0), x_3(0)) \quad (4.10)$$

With $x(t) = (x_1(t), x_2(t), x_3(t))$ and $\lambda(t) = (\lambda_1(t), \lambda_2(t), \lambda_3(t))$, with initial conditions $x_1(0) = 0.0555$, $x_2(0) = 0.0003$, $x_3(0) = 0.0004$ and the parameters $\beta = 5 \times 10^{-9}$, $\gamma = 0.12$, $\delta = 1/60$.

Let consider the problem (4.6) and constraints (4.7)-(4.9). With $x(t) = (x_1(t), x_2(t), x_3(t))$

and $\lambda(t) = (\lambda_1(t), \lambda_2(t), \lambda_3(t))$, the Hamiltonian of this problem can be written as

$$\begin{aligned}
 H(t, x(t), u(t), \lambda(t)) = & A x_2 + u^2 \\
 & + \lambda_1 (-\beta x_1 x_2 + \delta x_3 - u x_1) \\
 & + \lambda_2 (\beta x_1 x_2 - \gamma x_2) \\
 & + \lambda_3 (\gamma x_2 - \delta x_3)
 \end{aligned}$$

A is a weight parameter describing the comparative importance of the two terms in the functional. Using the PMP the optimal control problem can be studied with the state variables

$$\begin{aligned}
 \dot{x}_1 &= -\beta x_1 x_2 + \delta x_3 - u x_1 \\
 \dot{x}_2 &= \beta x_1 x_2 - \gamma x_2 \\
 \dot{x}_3 &= \gamma x_2 - \delta x_3
 \end{aligned}$$

The adjoint variables are:

$$\begin{aligned}
 \dot{\lambda}_1 &= \lambda_1 (u + \beta x_2) + \lambda_2 \beta x_2 \\
 \dot{\lambda}_2 &= -A + \lambda_1 \beta x_1 - \lambda_2 (\beta x_1 - \gamma) - \lambda_3 \gamma \\
 \dot{\lambda}_3 &= \lambda_3 \delta - \lambda_1 \delta
 \end{aligned}$$

with transversality conditions $\lambda(t_f) = 0$. Figure (4.7) demonstrates the optimal curves for the states variables and optimal control corresponding the to S-I-R model (4.1).

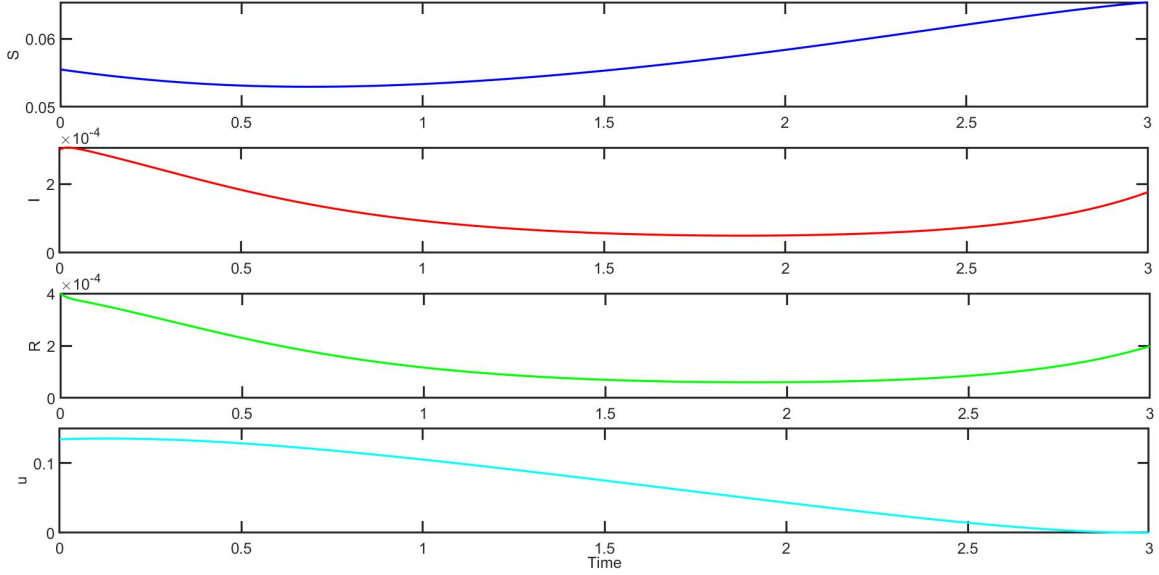


Figure 4.7: Solutions of optimal control problem for $S - E - I - R$ model (4.1). $u :=$ Vaccination related variable, $S :=$ Susceptible Population, $I :=$ Infective Population, $R :=$ Removed Population.

4.6 An optimal control problem for S-E-I-R model

In this section, we present an optimal control (OC) problem to study the dynamics of S-E-I-R model, using a vaccination process (u) as a measure to control the disease. Let x_1 represents the susceptible population, x_2 represents the proportion of population that is in the incubation period, x_3 represents the proportion of population that is infected and x_4 represents the proportion of population that is recovered or dead. The optimal control

problem can be defined as:

$$\min_u J[x(t), u(t)] = \int_{t_0}^{t_f} (x_3 + u^2) dt \quad (4.11)$$

$$s.t \quad \frac{dx_1}{dt} = \Lambda - \beta x_1 x_3 - \delta x_1 - u x_1 \quad (4.12)$$

$$\frac{dx_2}{dt} = \beta x_1 x_3 - \epsilon x_2 - \delta x_2 \quad (4.13)$$

$$\frac{dx_3}{dt} = \epsilon x_2 - \gamma x_3 - \delta x_3 \quad (4.14)$$

$$\frac{dx_4}{dt} = \gamma x_3 - \delta x_4 \quad (4.15)$$

$$x(t_0) = (x_1(0), x_2(0), x_3(0), x_4(0)) \quad (4.16)$$

With initial conditions $x_1(0) = 0.0555$, $x_2(0) = 0.0003$, $x_3(0) = 0.0004$, $x_4(0) = 1$ and the parameters $\beta = 5 \times 10^{-9}$, $\gamma = 0.12$, $\delta = 1/60$.

Let consider the problem (4.11) and constraints (4.12)-(4.15). With $x(t) = (x_1(t), x_2(t), x_3(t), x_4(t))$ and $\lambda(t) = (\lambda_1(t), \lambda_2(t), \lambda_3(t), \lambda_4(t))$, the Hamiltonian of this problem can be written as

$$\begin{aligned} H(t, x(t), u(t), \lambda(t)) = & A x_3 + u^2 \\ & + \lambda_1 (\Lambda - \beta x_1 x_3 - \delta x_1 - u x_1) \\ & + \lambda_2 (\beta x_1 x_3 - \epsilon x_2 - \delta x_2) \\ & + \lambda_3 (\epsilon x_2 - \gamma x_3 - \delta x_3) \\ & + \lambda_4 (\gamma x_3 - \delta x_4) \end{aligned}$$

A is a weight parameter describing the comparative importance of the two terms in the functional. Using the PMP the optimal control problem can be studied with the state

variables

$$\dot{x}_1 = \Lambda - \beta x_1 x_3 - \delta x_1 - u x_1$$

$$\dot{x}_2 = \beta x_1 x_3 - \epsilon x_2 - \delta x_2$$

$$\dot{x}_3 = \epsilon x_2 - \gamma x_3 - \delta x_3$$

$$\dot{x}_4 = \gamma x_3 - \delta x_4$$

The adjoint variables are:

$$\dot{\lambda}_1 = \lambda_1 (u + \beta x_3 + \delta) - \lambda_2 \beta x_3$$

$$\dot{\lambda}_2 = \lambda_2 (\epsilon + \delta) - \lambda_3 \epsilon$$

$$\dot{\lambda}_3 = -A - \lambda_4 \gamma + \lambda_3 (\gamma + \delta) - \lambda_2 \beta x_1 + \lambda_1 \beta x_1$$

$$\dot{\lambda}_4 = \lambda_4 \delta$$

with transversality conditions $\lambda(t_f) = 0$. Figure (4.8) displays the optimal curves for the states variables and optimal control corresponding to the S-E-I-R model (4.5).

4.7 Global sensitivity analysis

Global sensitivity analysis allows us to change all parameters simultaneously over the entire parameter interval. This is a way to evaluate the relative effects of each input parameter and moreover to identify the interactions between parameters to the model output. In global sensitivity analysis we determine that with variation of input parameters in a certain range, which parameters and interactions have the most influential impact on the overall behavior of our model^{56;112-117}.

There are several types of global sensitivity analyses, such as weighted average of local sensitivity analysis, partial rank correlation coefficient, multi parametric sensitivity analysis, Fourier amplitude sensitivity analysis (FAST) and Sobol's method, which can be used for

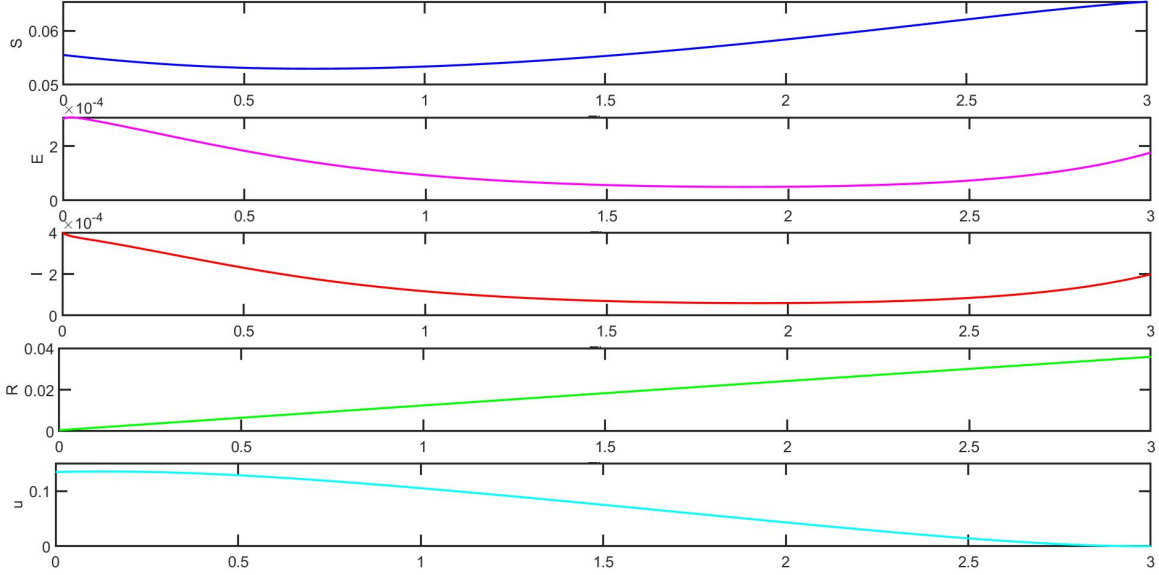


Figure 4.8: Solutions of optimal control problem for S - E - I - R model (4.5). u := Vaccination related variable, S :=Susceptible Population, E := Exposed Population, I := Infective Population, R := Removed Population

systems pharmacology models¹¹². The Latin hypercube sampling (LHS) method has been used frequently for global sensitivity analysis. There are some other methods for calculating main effect and total effect sensitivity indices and one of the most important one is the method of Sobol¹¹⁶.

LHS method is a sampling method and requires fewer samples compare to simple random sampling to achieve the same accuracy¹¹². In LHS method, we divide the random parameter distributions into N equal probability intervals. Here, N is the sample size. The choice for N should be at least $k + 1$, where k is the number of parameters which are varied. For the case that the interval of variation for some parameter is very large, the sampling can be done on a *log* form.

In LHS method, sampling is independent for each parameter and can be done by randomly selecting values from each *pdf*. We may sample each interval once for each parameter without any replacement. The LHS matrix is consisting of N rows corresponding to the number of simulations or sample size and moreover it includes k columns corresponding to the number of varied parameters. Then, N model solutions may be simulated, using each combination of parameter values which they represent each row of the LHS matrix¹¹².

4.7.1 Partial Rank Correlation Coefficient (PRCC) results for S-I-R model (4.1)

Here, a parameter sensitivity analysis has been conducted to identify the biological parameters that have the most significant effect on our model system by the LHS Monte Carlo method using PRCC with uniform distributions for the 95 percent confidence intervals. The global sensitivity results with p-values corresponding to S compartment, I compartment and R compartment have been demonstrated in Figure (4.9).

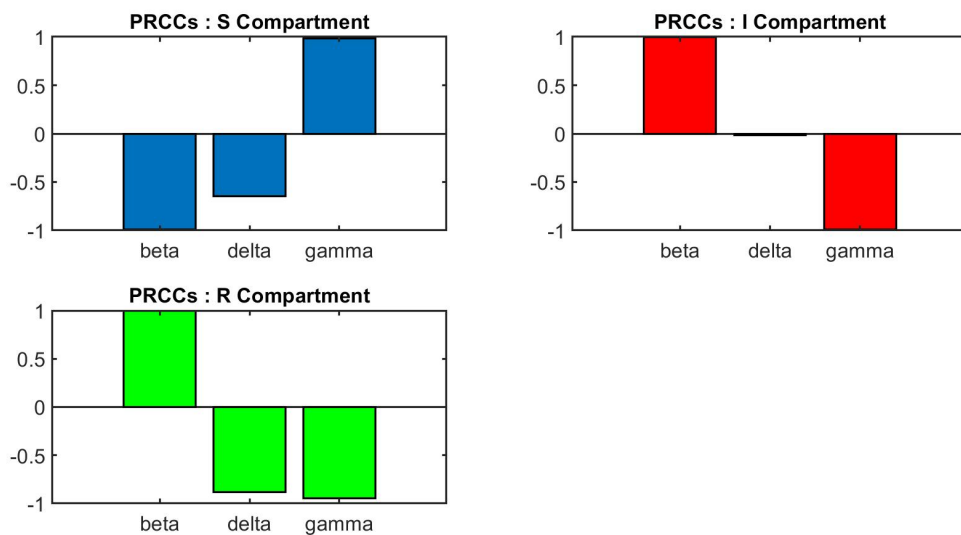


Figure 4.9: Global uncertainty and sensitivity analysis of calculated different parameters for S-I-R model (4.1).

4.7.2 Partial Rank Correlation Coefficient (PRCC) results for S-E-I-R model (4.5)

According to LHS, we simulated the responses of the model for each organ by randomly selecting values for the parameter set from the 95 percent confidence intervals. These analyses were done by developing a *LHS/PRCC* method with uniform distributions for the 95 percent confidence intervals. We found that some parameters illustrate significant performance in terms of sensitivity of the output to the variations of these parameters in some compartments

while they do not have this effect for others. These results have been depicted in Figure (4.10), are statistically significant with p- values much smaller than 0.01.

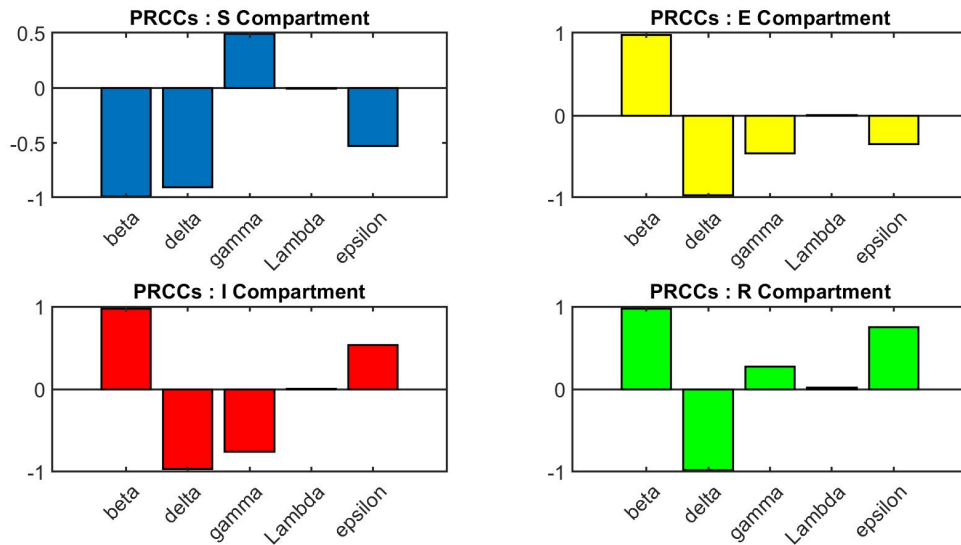


Figure 4.10: Global uncertainty and sensitivity analysis of calculated different parameters for S-E-I-R model (4.5).

4.8 Conclusion

Infectious diseases can be defined as diseases that can be transmitted from human to human, from human to animal, or from animal to animal. The mathematical modeling of infectious disease spread has been studied for many years and recently it has been widely discussed due to the spread of the COVID-19 pandemic. To build up an appropriate infectious disease dynamic model we may need to use a system of ordinary differential equations that cover the spread process, spread law, and spread trend of infectious diseases.

In this chapter we considered the S-I-R and S-E-I-R models and for these, we could develop some analytical results which can be useful in studying the simple epidemics. We displayed the evolution of these two compartmental models over time, Susceptible-Infected-Recovered and Susceptible-Exposed-Infected-Recovered for interesting values of parameters. We followed the optimal control perspective to study these models and because of the complexity

of the presented optimal control problems, we could no longer solve them analytically and we ended up looking at the numerical solutions. The optimal curves for the states variables and optimal control were obtained and demonstrated for each control problem separately. An uncertainty analysis can be applied on the epidemiological models to investigate the uncertainty in system output that is generated from uncertainty in parameter inputs. Sensitivity analysis assesses how variations in model outputs can be apportioned, qualitatively or quantitatively, to different inputs. The final objective of this study was to determine the key parameters in spread of infectious diseases using sampling-based method (Partial Rank Correlation Coefficient-PRCC). In this research we applied LHS/PRCC method with uniform distributions for the 95percent confidence intervals on the model equations (7.15) and (5.7). As we have seen, some parameters have positively and some others negatively affected the spread of disease.

Chapter 5

Chaos Induced by Snap-Back Repeller in a Two Species Competitive Model

Abstract

In Chapter Five, we investigate the complex dynamics of two-species Ricker-type discrete-time competitive model. We perform local stability analysis for the fixed points of the system and discuss about its persistence for boundary fixed points. This system inherits properties of the dynamics of a one-dimensional Ricker model such as the cascade of period-doubling bifurcation, periodic windows, and chaos. We explore the existence of chaos for the equilibrium points for a specific case of this system using Marotto theorem and show the existence of snap-back repeller.

5.1 Introduction

When we study the evolution of population dynamics, two major types of mathematical models can be used, the continuous-time dynamical systems and the discrete-time dynamical systems. For the purpose of modeling small size population and non overlapping generations, the discrete time systems are the appropriate model¹¹⁸. There are so many studies that have been worked on discovering complex behaviors of discrete competitive model during the last decades¹¹⁹⁻¹²². There are not many of these studies which are concerning about the existence of chaos in higher dimensional discrete dynamical systems. Chaos and chaos synchronizations have attracted many researchers for many years^{123;124}. In 1975, Li and York provided a simple criterion for chaos in one dimensional discrete dynamical systems, "period three implies chaos"¹²⁵. This definition is the first description of chaos. Although, a precise definition of chaos was presented by their work, however, F.R. Marotto mentioned that the essential properties of chaos are the following: (i) there exist an infinite number of periodic solutions of various periods (ii) there exists an uncountably infinite set of points which exhibit random behavior and (iii) there is a highly sensitivity to initial conditions¹²⁶⁻¹²⁸. Marotto extended Li-York's chaos in one-dimension to multi-dimension through introducing the notion of snapback repeller by his famous theorem in 1978 a few years after Li and York definition for chaos. To explain more we have mentioned the Marotto's definition for "Snap-back repeller" and then his theorem¹²⁶:

Definition 5.1.1 (Marotto-1978). *Let f be differentiable in $B_{r'}(z)$. The point $z \in \mathbb{R}^n$ is an expanding fixed point of f in $B_{r'}(z)$, if $f(z) = z$ and all eigenvalues of $Df(x)$ exceed 1 in norm for all $x \in B_{r'}(z)$.*

Definition 5.1.2 (Marotto-1978). *Assume that z is an expanding fixed point of f in $B_{r'}(z)$ for some $r' > 0$. Then z is said to be an snap-back repeller of f if there exists a point $z_0 \in B_{r'}(z)$ with $z_0 \neq z$ and $f^M(z_0) = z$ and $|Df^M(z_0)| \neq 0$ for some positive integer M ¹²⁶.*

Figure (5.1) demonstrates the schematic diagram of snap-back repeller point.

Under the assumptions for definitions (5.1.1) and (5.1.2), the following theorem by Marotto

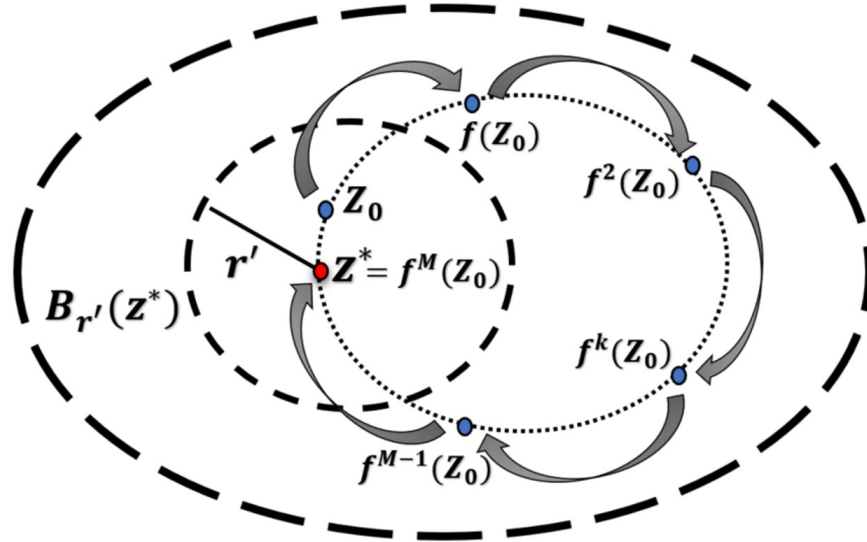


Figure 5.1: Snap-Back repeller schematic diagram.

holds.

Theorem 5.1.3 (Marotto-1978). *If f possesses a snap back repeller, then f is chaotic in the following sense: There exist (i) a positive integer N , such that f has a point of period p , for each integer $p \geq N$, (ii) a scrambled set of f , i.e., an uncountable set S containing no periodic points of f , such that*

1. $f(S) \subset S$,
2. $\limsup_{n \rightarrow \infty} \|f^n(x) - f^n(y)\| > 0$, for all $x, y \in S$, with $x \neq y$,
3. $\limsup_{n \rightarrow \infty} \|f^n(x) - f^n(y)\| > 0$, for all $x \in S$ and periodic point y of f ,

(iii) an uncountable subset S_0 of S , such that $\liminf_{n \rightarrow \infty} \|f^n(x) - f^n(y)\| = 0$, for every $x, y \in S_0$ ¹²⁶.

However, there was a minor technical flaw in his work¹²⁸⁻¹³⁰. Although he wanted to apply his theorem to any repelling fixed point, some of the conditions that he considered in the proof of his theorem were associated with only expanding fixed points. He incorrectly mentioned that if the absolute value for all eigenvalues of $Df(z)$ is larger than 1, then the fixed point z is an expanding fixed point of f . As we know all expanding fixed points are

repelling and its converse is not true. Therefore, Marotto definition for snap-back repeller and then his proof about existence of snap-back repeller implies chaos had a minor error. Chen et al., 1998; Lin et al., 2002; Li and Chen, 2003a; discussed about the flaws of Marotto's theorem and some of them provided several counterexamples to say that if all eigenvalues of the Jacobian $Df(z)$ at the fixed point z are greater than one in norm, we can not say always there exists some $s > 1$ and $r' > 0$ such that for all $x, y \in B_{r'}(z)$, $\|f(x) - f(y)\| > s\|x - y\|$. Then they redefined the Marotto's Theorem as the following form¹³⁰:

Theorem 5.1.4 (Marotto-Li-Chen Theorem (2003)). *Consider the following n -dimensional discrete dynamical system:*

$$x_{n+1} = f(x_n), \quad x_n \in \mathbb{R}^n, n = 0, 1, 2, \dots$$

Where $f : \mathbb{R}^n \rightarrow \mathbb{R}^n$ and z is a fixed point. Moreover, assume that

1. $f(x)$ is continuously differentiable in $B_{r'}(z)$ for some $r' > 0$,
2. All eigenvalues of $(Df(z))^T Df(z)$ are greater than 1,
3. There exists a point $z_0 = \{x \mid \|x - z\| \leq r' \text{ and all eigenvalues of } (Df(x))^T Df(x) \text{ are larger than } 1\}$, with $z_0 \neq z$, such that $f^M(z_0) = z$ where $f^i(z_0) \in B_{r'}(z)$, $i = 0, 1, 2, \dots, M$, and the determinant $|Df^M(z_0)| \neq 0$, for some positive integer M .

Then, the system is chaotic in the sense of Li-York¹³⁰.

Marotto refined his theorem in 2005 and he explained that a fixed point z is called a repelling fixed point under differentiable function $f : \mathbb{R}^n \rightarrow \mathbb{R}^n$ if all eigenvalues of $Df(z)$ exceed 1 in magnitude, but z is expanding only if

$$\|f(x) - f(y)\| > s\|x - y\|$$

Where $s > 1$, for all x, y sufficiently close to z with $x \neq y$ (for $x, y \in B_{r'}(z)$). This implies that f is a 1-1 function in $B_{r'}(z)$ ¹²⁸.

Definition 5.1.5 (Marotto-2005). *Suppose z is a fixed point of f with all eigenvalues of $Df(z)$ exceeding 1 in magnitude and suppose that there exists a point $z_0 \neq z$ in a repelling neighborhood of z and an integer $M > 1$, such that $x_M = z$ and $\det(Df(x_k)) \neq 0$ for $1 \leq k \leq M$ where $x_k = f^k(z_0)$. Then z is called a snapback repeller of f ¹²⁸.*

He claimed that since $\det(Df(x_k)) \neq 0$ for all $1 \leq k \leq M$, then the homoclinic orbit is transversal in the sense that f for all $k \leq M$ is 1-1 map in a neighborhood of x_k .

As Marotto explained in 1978, the condition $\det(Df(x_k)) \neq 0$ guarantees the existence of the inverse of f^M in $B_{r'}(z)$. He mentioned that functions exhibit chaos and complex behavior when they possess snap-back repeller.

But what will happen that existence of a transverse homoclinic map convince us that we have chaos? As it is mentioned by many authors, a point which is in intersection of stable manifold and unstable manifold of a hyperbolic fixed point is called homoclinic point^{127;131;132;134;135;203}. If stable manifolds and unstable manifold of the hyperbolic fixed point, intersect transversally, then we have transverse homoclinic point in the intersection of both manifolds. In a neighborhood of a transverse homoclinic point, our map possesses an invariant cantor set on which it is topologically conjugate to a shift map. Shift map acting on the space of bi-infinite sequences of 0's and 1's and it has the following properties:

A countable infinity of periodic orbits consisting of orbits of all periods.

1. An uncountable infinity of non-periodic orbits.
2. A dense orbit.

Although, Wiggins in²⁰³ mentioned that understanding the orbit structure of a map in that invariant Cantor set is impossible, he could show that the map in that invariant set behaves the same as shift map.

There are some researches which have more details about small neighborhood of a point on the homoclinic orbit^{136-139;203}. The homoclinic orbits and homoclinic bifurcations which occur in continuous time dynamical systems has been studied widely by^{140;141} are using in discrete time systems by defining the Poincare map¹³². In 2011, L. Gardini et al. showed

that critical homoclinic orbits lead to snap-back repellers and chaos too¹³².

As Gardini. et al discussed, in non-invertible maps homoclinic orbits may be associate with expanding fixed points and or expanding cycles. In addition, they mentioned that in the neighborhood of such homoclinic orbits, there exists an invariant set on which the map is chaotic. They even for the case that They proved that even if $\det(Df(x_k)) = 0$, there are some situations in which the map is chaotic although Marotto theorem does not work. Laura. et all, provide a definition for non-critical expanding fixed points and then they defined when a homoclinic orbit is critical. They used those definitions to prove a generalization of Marotto theorem in the case that we do not need the homoclinic orbit to be non-degenerate¹³²:

Theorem 5.1.6 (L. Gardini. et. all, (2011)). *Let f be a piecewise smooth non-invertible map, $f : X \rightarrow X$, $X \in \mathbb{R}^n$. Let p be an expanding fixed point of f and $O(p)$ a noncritical homoclinic orbit of p . Then in any neighborhood of $O(p)$, there exists an invariant cantor like set Λ on which the f is chaotic¹³².*

In¹³¹, Gardini. studied the homoclinic bifurcations in n dimensional endomorphisms (maps with a nonunique inverse) which are associated to expanding periodic orbits. The study of chaos for these kinds of map in one dimension was studied by Mira in 1987¹⁴². Since, this topic is out of the discussion for this chapter, so we avoid going through that. In this chapter, we study the local dynamics of a two-species Ricker competitive model with four biological parameters. We will conduct a local stability analysis to study the local dynamics of the steady states of the system. We will use the persistence theory to study the global dynamics of the system. To study the chaotic dynamics of the system, we focus on a specific case with only three biological parameters. We provide the condition under which Marotto theorem works for positive fixed points of this new system. Furthermore, this model does not have a Neimark-Sacker bifurcation and inherits the same dynamics as one dimensional Ricker model. We will numerically demonstrate the local and qualitative dynamics of the system using several dynamical system tools.

5.2 The two-species Ricker competitive model and its local dynamics

The Ricker model is a well known population model which demonstrates stable, periodic and non-periodic and complex nonlinear dynamics^{214;215}. Here, we consider a two-species Ricker model which is a special case of model (2) in¹²⁰ and has the following form:

$$f_1 = X_1(n+1) = X_1(n) e^{r_1 \left(1 - \frac{X_1(n)}{k} - X_2(n)\right)} \quad (5.1)$$

$$f_2 = X_2(n+1) = X_2(n) e^{r_2 \left(1 - \frac{X_2(n)}{l} - X_1(n)\right)} \quad (5.2)$$

Here, X_1 demonstrates the population size of the first species, X_2 represents the population size of the second species, r_1 and r_2 are the intrinsic growth rate, k and l the carrying capacity of the environment.

The Jacobian matrix for (5.1)-(5.2) has the form

$$J := \begin{bmatrix} \frac{\partial f_1}{\partial X_1} & \frac{\partial f_1}{\partial X_2} \\ \frac{\partial f_2}{\partial X_1} & \frac{\partial f_2}{\partial X_2} \end{bmatrix} \quad (5.3)$$

where

$$\begin{aligned} \frac{\partial f_1}{\partial X_1} &= \left(1 - \frac{r_1 X_1}{k}\right) \exp\left(r_1 \left(1 - \frac{X_1}{k} - X_2\right)\right) \\ \frac{\partial f_1}{\partial X_2} &= -r_1 X_1 \exp\left(r_1 \left(1 - \frac{X_1}{k} - X_2\right)\right) \\ \frac{\partial f_2}{\partial X_1} &= -r_2 X_2 \exp\left(r_2 \left(1 - \frac{X_2}{l} - X_1\right)\right) \\ \frac{\partial f_2}{\partial X_2} &= \left(1 - \frac{r_2 X_2}{l}\right) \exp\left(r_2 \left(1 - \frac{X_2}{l} - X_1\right)\right) \end{aligned}$$

Then, at the origin we have

$$J|_{(0,0)} = \begin{pmatrix} e^{r_1} & 0 \\ 0 & e^{r_2} \end{pmatrix}$$

and for the fixed point $(k, 0)$ we have

$$J|_{(k,0)} = \begin{pmatrix} 1 - r_1 & -k r_1 \\ 0 & e^{r_2(1-l)} \end{pmatrix}$$

and for the fixed point $(0, l)$ we have

$$J|_{(0,l)} = \begin{pmatrix} e^{r_1(1-k)} & 0 \\ -l r_2 & 1 - r_2 \end{pmatrix}$$

and for the positive fixed point $(X_1^*, X_2^*) = \left(\frac{k(1-l)}{1-kl}, \frac{l(1-k)}{1-kl} \right)$, we have

$$J|_{(X_1^*, X_2^*)} = \begin{pmatrix} \frac{-1 + kl + r_1 - r_1 l}{-1 + kl} & \frac{-k(-1 + l) r_1}{-1 + kl} \\ \frac{-k(-1 + k) r_2}{-1 + kl} & \frac{-1 + kl + r_2 - r_2 k}{-1 + kl} \end{pmatrix} \quad (5.4)$$

Proposition 5.2.1. *The local stability analysis results for the fixed points $(0, 0)$, $(k, 0)$, $(0, l)$ of (5.1)-(5.2) are summarized as below:*

1. *The equilibrium point $(0, 0)$ is always an unstable fixed point.*
2. *The equilibrium point $(k, 0)$ for $l < 1$ and $0 < r_1 < 2$, has a stable manifold in X_1 direction and an unstable manifold in X_2 direction and is a saddle point. Moreover, $(k, 0)$ for $l > 1$ and $0 < r_1 < 2$, has a stable manifold in X_1 direction and a stable manifold in X_2 direction and is a stable node. Moreover, $(k, 0)$ for $l < 1$ and $r_1 > 2$, has an unstable manifold in X_1 direction and an unstable manifold in X_2 direction and is an unstable node. Finally, $(k, 0)$ for $l > 1$ and $r_1 > 2$, has an unstable manifold in*

X_1 direction and a stable manifold in X_2 direction and is a saddle point.

3. The equilibrium point $(0, l)$ for $k < 1$ and $0 < r_1 < 2$, has a stable manifold in X_2 direction and an unstable manifold in X_1 direction and is a saddle point. In addition, $(0, l)$ for $k > 1$ and $0 < r_2 < 2$, has a stable manifold in X_1 direction and a stable manifold in X_2 direction and is a stable node. Moreover, $(0, l)$ for $k < 1$ and $r_2 > 2$, has an unstable manifold in X_1 direction and an unstable manifold in X_2 direction and is an unstable node. Finally, $(0, l)$ for $k > 1$ and $r_1 > 2$, has an unstable manifold in X_2 direction and a stable manifold in X_1 direction and is a saddle point.

5.3 Global stability analysis using persistence theory

5.3.1 Boundedness of the system solutions

To study the global stability of the equilibrium points of system, at first we prove that all solutions in the first quadrant \mathbb{R}_+^2 are eventually bounded.

Theorem 5.3.1. For $r_1, r_2 > 0, k, l > 0$ and initial conditions in the first quadrant \mathbb{R}_+^2 , i.e. $X_1(0) > 0$ and $X_2(0) > 0$, for the system of (5.1)-(5.2) we have: $X_1 > 0$ and $X_2 > 0$ for all $n \in \mathbb{Z}^+$. In addition, we can find some positive number M , such that $\max_{n \in \mathbb{Z}^+} \{X_1(n), X_2(n)\} \leq M$.

Proof. By induction.

Since $X_1(0) > 0$ we have $\exp\left(r_1\left(1 - \frac{X_1(0)}{k}\right)\right) > 0$, hence

$$X_1(1) = X_1(0) e^{r_1\left(1 - \frac{X_1(0)}{k} - X_2(0)\right)} < X_1(0) e^{r_1\left(1 - \frac{X_1(0)}{k}\right)} > 0$$

Assume that for $n \leq j$, we have $X_1(j) > 0$. Then for $n = j + 1$ we have

$$X_1(j + 1) = X_1(j) e^{r_1\left(1 - \frac{X_1(j)}{k} - X_2(j)\right)} > 0$$

Therefore $X_1(n) > 0$ for any $n \in \mathbb{Z}^+$. Similarly, since $X_1(0) > 0$ and $X_2(0) > 0$, we automatically have $\exp\left(r_2\left(1 - \frac{X_2(0)}{j}\right)\right) > 0$ is positive. Hence,

$$X_2(1) = X_2(0) e^{r_2\left(1 - \frac{X_2(0)}{j} - X_1(0)\right)} < X_2(0) e^{r_2\left(1 - \frac{X_2(0)}{j}\right)} > 0$$

Assume that for $n \leq j$, we have $X_2(j) > 0$. Then for $n = j + 1$ we have

$$X_2(j + 1) = X_2(j) e^{r_2\left(1 - \frac{X_2(j)}{j} - X_1(j)\right)} > 0$$

Therefore $X_2(n) > 0$ for any $n \in \mathbb{Z}^+$.

To find an upper bound, we know,

$$X_1(n + 1) = X_1(n) e^{r_1\left(1 - \frac{X_1(n)}{k}\right)} \leq \max_{x \in \mathbb{R}^+} \{f(x)\}$$

If we define $f_1(x) = x e^{r_1\left(1 - \frac{x}{k}\right)}$, then $f_1'(x) = \left(1 - \frac{r_1 x}{k}\right) e^{r_1\left(1 - \frac{x}{k}\right)}$ and $f_1(x)$ has critical points at $x = \frac{k}{r_1}$. Since $f_1'(x) > 0$ if $x < \frac{k}{r_1}$ and $f_1'(x) < 0$ if $x > \frac{k}{r_1}$, then $x = \frac{k}{r_1}$ is the maximal point of $f_1(x)$, i.e. $\max_{x \in \mathbb{R}^+} \{f_1(x)\} = f_1\left(\frac{k}{r_1}\right)$. Hence,

$$x_1(n + 1) = X_1(n) e^{r_1\left(1 - \frac{X_1(n)}{k} - X_2(n)\right)} \leq f_1\left(\frac{k}{r_1}\right) = \frac{k e^{r_1 - 1}}{r_1} = M_1$$

Similarly, we define $f_2(x) = x e^{r_2\left(1 - \frac{x}{l}\right)}$, then $f_2'(x) = \left(1 - \frac{r_2 x}{l}\right) e^{r_2\left(1 - \frac{x}{l}\right)}$ and $f_2(x)$ has critical points at $x = \frac{l}{r_2}$. Since $f_2'(x) > 0$ if $x < \frac{l}{r_2}$ and $f_2'(x) < 0$ if $x > \frac{l}{r_2}$, then $x = \frac{l}{r_2}$ is the maximal point of $f_2(x)$, i.e. $\max_{x \in \mathbb{R}^+} \{f_2(x)\} = f_2\left(\frac{l}{r_2}\right)$.

$$X_2(n + 1) = X_2(n) e^{r_2\left(1 - \frac{X_2(n)}{l} - X_1(n)\right)} \leq f_2\left(\frac{l}{r_2}\right) = \frac{l e^{r_2 - 1}}{r_2} = M_2$$

Therefore, we can find some positive number $M = \max\{M_1, M_2\}$, such that $\max_{n \in \mathbb{Z}^+} \{X_1(n), X_2(n)\} \leq M$. □

5.3.2 Persistence of the species

To work on global stability, we need to study the persistence theory^{146;182}. Here, we consider two cases:

1. Persistence of system corresponding to $(k, 0)$.
2. Persistence of system corresponding to $(0, l)$.

Case 1: Persistence of system corresponding to $(k, 0)$

For the first case, we have:

$$\begin{aligned}
 P &= \{(X_1, X_2) : X_1 \geq 0, X_2 \geq 0\} \\
 P_{k,0} &= \{(X_1, X_2) \in P : X_1 > 0\} \\
 \partial P_{k,0} &= P \setminus P_{k,0}
 \end{aligned}$$

Proposition 5.3.2. *The system is uniformly persistent with respect to $(P_{k,0}, \partial P_{k,0})$.*

Proof. Here, $\partial P_{k,0}$ is closed in P . For any positive solution of $(X_1(n), X_2(n))$ of the system, as we proved in theorem (6.3.2), we have

$$X_1(n+1) \leq X_1(n)e^{r_1(1-\frac{X_1(n)}{k})} \leq \max_{X_1 \in \mathbb{R}^+} \{f_1(X_1)\} = \frac{ke^{r_1-1}}{r_1} = M_1$$

And for large enough n

$$X_2(n+1) \leq X_2(n)e^{r_2(1-\frac{X_2(n)}{l})} \leq \max_{X_2 \in \mathbb{R}^+} \{f_2(X_2)\} = \frac{le^{r_2-1}}{r_2} = M_2$$

Therefore, system (5.1)-(5.2) is point dissipative. Assume for all $n \geq 0$

$$Y_\partial = \{(X_1(0), X_2(0)) : (X_1(n), X_2(n)) \text{ satisfies the system equations and } (X_1(n), X_2(n)) \in \partial P_{k,0}\}$$

We see that

$$Y_{\partial} = \{(0, X_2) : X_2 \geq 0\} = \partial P_{k,0}$$

Moreover, $(0, 0)$ is the unique equilibrium in Y_{∂} . Define $W^s(0, 0)$ to be the stable manifold for $(0, 0)$. We show that

$$W^s(0, 0) \cap P_{k,0} = \emptyset$$

Assume that in contradiction, there exist a solution $(X_1(n), X_2(n))$ of system with $X_1(n) > 0$ such that

$$(X_1(n), X_2(n)) \rightarrow (0, 0) \quad \text{as } n \rightarrow \infty$$

Then, for large n we have

$$X_1(n+1) > X_1(n)e^{r_1/2}$$

Since $r_1 > 0$, it follows that $X_1(n) \rightarrow \infty$ as $n \rightarrow \infty$ and contradiction. Moreover, every orbit in Y_{∂} tends to $(0, 0)$ as $n \rightarrow \infty$. It means that $(0, 0)$ is an isolated invariant set in P and acyclic in Y_{∂} . Note that Y_{∂} repels uniformly the solution of systems with positive $X_1(n)$ ^{147;148}. It follows that there is $s_1 > 0$ such that $X_1(n) > s_1$ for large enough n . \square

Theorem 5.3.3. *There exists $s_1 > 0$ such that for any $X_1(0) > 0$ we have*

$$s_1 < X_1(n) < \frac{k e^{r_1-1}}{r_1}$$

Proof. By proposition (5.3.2). \square

Theorem 5.3.4. *All solutions $\{(X_1(n), X_2(n))\}$ of system with $X_1(0) > 0$ and $X_2(0) \geq 0$,*

for $l > 1$ and $0 < r_1 < 2$, are decreasing to the fixed point $(k, 0)$, i.e.

$$\lim_{n \rightarrow +\infty} X_1(n) = k, \quad \lim_{n \rightarrow +\infty} X_2(n) = 0$$

Proof. By proposition (5.3.2) and theorem (5.3.3). □

Case 2: Persistence of system corresponding to $(0, l)$

For this case, we have:

$$\begin{aligned} Q &= \{(X_1, X_2) : X_1 \geq 0, X_2 \geq 0\} \\ Q_{0,l} &= \{(X_1, X_2) \in Q : X_2 > 0\} \\ \partial Q_{0,l} &= Q \setminus Q_{0,l} \end{aligned}$$

Proposition 5.3.5. *The system is uniformly persistent with respect to $(Q_{0,l}, \partial Q_{0,l})$.*

Proof. Here, $\partial Q_{0,l}$ is closed in Q . Similarly, for any positive solution of $(X_1(n), X_2(n))$ of the system (5.1)-(5.2), similar to theorem (6.3.2), we can write

$$X_1(n+1) \leq X_1(n)e^{r_1(1-\frac{X_1(n)}{k})} \leq \max_{X_1 \in \mathbb{R}^+} \{f(X_1)\} = \frac{k e^{r_1-1}}{r_1} = M_1$$

For large enough n

$$X_2(n+1) \leq X_2(n)e^{r_2(1-\frac{X_2(n)}{l})} \leq \max_{X_2 \in \mathbb{R}^+} \{f(X_2)\} = \frac{l e^{r_2-1}}{r_2} = M_2$$

Thus, system (5.1)-(5.2) is point dissipative. Now, for all $n \geq 0$, we set

$$L_\partial = \{(X_1(0), X_2(0)) : (X_1(n), X_2(n)) \text{ satisfies the system equations and } (X_1(n), X_2(n)) \in \partial Q_{0,l}\}$$

for which

$$L_{\partial} = \{(X_1, 0) : X_2 \geq 0\} = \partial Q_{0,l}$$

Moreover, $(0, 0)$ is the unique equilibrium in L_{∂} . Set $W^s(0, 0)$ to be the stable manifold for $(0, 0)$. We prove that

$$W^s(0, 0) \cap Q_{0,l} = \emptyset$$

By contradiction, there exist a solution $(X_1(n), X_2(n))$ of system with $X_2(n) > 0$ such that

$$(X_1(n), X_2(n)) \rightarrow (0, 0) \quad \text{as } n \rightarrow \infty$$

For large n we have

$$X_2(n+1) > X_2(n)e^{r_2/2}$$

Since $r_2 > 0$, it leads to $X_2(n) \rightarrow \infty$ as $n \rightarrow \infty$ which is a contradiction. In addition, every orbit in L_{∂} tends to $(0, 0)$ as $n \rightarrow \infty$. It implies that $(0, 0)$ is an isolated invariant set in Q and acyclic in L_{∂} . Here, l_{∂} repels uniformly the solutions of system with positive $X_2(n)$ ^{147;148}. It follows that there is $s_2 > 0$ such that $X_2(n) > s_2$ for large enough n . \square

Theorem 5.3.6. *There exists $s_2 > 0$ such that for any $X_2(0) > 0$ we have*

$$s_2 < X_2(n) < \frac{l e^{r_2-1}}{r_2}$$

Proof. By proposition (5.3.5). \square

Theorem 5.3.7. *All solutions $\{(X_1(n), X_2(n))\}$ of system with $X_1(0) \geq 0$ and $X_2(0) > 0$,*

for $k > 1$ and $0 < r_2 < 2$, are decreasing to the fixed point $(0, l)$, i.e.

$$\lim_{n \rightarrow +\infty} X_1(n) = 0, \quad \lim_{n \rightarrow +\infty} X_2(n) = l$$

Proof. By proposition (5.3.5) and theorem (5.3.6). □

Finally, we have the following result

Theorem 5.3.8. *If there are positive constants $s_1, s_2 > 0$ and $M_1, M_2 > 0$ such that the solution $(X_1(n), X_2(n))$ of system satisfies*

$$\begin{aligned} 0 < s_1 &\leq \liminf_{n \rightarrow +\infty} X_1(n) \leq \limsup_{n \rightarrow +\infty} X_1(n) \leq M_1 = \frac{k e^{r_1-1}}{r_1} \\ 0 < s_2 &\leq \liminf_{n \rightarrow +\infty} X_2(n) \leq \limsup_{n \rightarrow +\infty} X_2(n) \leq M_2 = \frac{l e^{r_2-1}}{r_2} \end{aligned}$$

Then, system (5.1)-(5.2) is persistent. If system is not persistent, it is called non-persistent¹⁸².

5.4 Application of snap-back repeller and Marroto chaos in study of chaotic dynamics of system

In this section, we explore analytically chaos in the sense of Marotto for a specific case of model (5.1)-(5.2). Without loss of generality, we consider $k = l$, then we have

$$F := \begin{cases} g_1(X_1(n), X_2(n)) = X_1(n) \exp\left(r_1 \left(1 - \frac{X_1(n)}{k} - X_2(n)\right)\right) \\ g_2(X_1(n), X_2(n)) = X_2(n) \exp\left(r_2 \left(1 - \frac{X_2(n)}{k} - X_1(n)\right)\right) \end{cases} \quad (5.5)$$

The Jacobian matrix for (5.5) has the form

$$J := \begin{bmatrix} \frac{\partial g_1}{\partial X_1} & \frac{\partial g_1}{\partial X_2} \\ \frac{\partial g_2}{\partial X_1} & \frac{\partial g_2}{\partial X_2} \end{bmatrix} \quad (5.6)$$

where

$$\frac{\partial g_1}{\partial X_1} = \left(1 - \frac{r_1 X_1}{k}\right) \exp\left(r_1 \left(1 - \frac{X_1}{k} - X_2\right)\right) \quad (5.7)$$

$$\frac{\partial g_1}{\partial X_2} = -r_1 X_1 \exp\left(r_1 \left(1 - \frac{X_1}{k} - X_2\right)\right) \quad (5.8)$$

$$\frac{\partial g_2}{\partial X_1} = -r_2 X_2 \exp\left(r_2 \left(1 - \frac{X_2}{k} - X_1\right)\right) \quad (5.9)$$

$$\frac{\partial g_2}{\partial X_2} = \left(1 - \frac{r_2 X_2}{k}\right) \exp\left(r_2 \left(1 - \frac{X_2}{k} - X_1\right)\right) \quad (5.10)$$

For this specific case, we have four fixed points $(0, 0)$, $(k, 0)$, $(0, k)$ and $(X_1^*, X_2^*) = \left(\frac{k}{k+1}, \frac{k}{k+1}\right)$.

At $(0, 0)$ we have

$$J|_{(0,0)} = \begin{pmatrix} e^{r_1} & 0 \\ 0 & e^{r_2} \end{pmatrix}$$

and at $(k, 0)$ we have

$$J|_{(k,0)} = \begin{pmatrix} 1 - r_1 & -k r_1 \\ 0 & e^{r_2(1-k)} \end{pmatrix}$$

Furthermore, for the fixed point $(0, k)$ we have

$$J|_{(0,k)} = \begin{pmatrix} e^{r_1(1-k)} & 0 \\ -k r_2 & 1 - r_2 \end{pmatrix}$$

and finally for the positive fixed point $(X_1^*, X_2^*) = \left(\frac{k}{k+1}, \frac{k}{k+1}\right)$, we have

$$J|_{(X_1^*, X_2^*)} = \begin{pmatrix} \frac{k+1-r_1}{k+1} & \frac{-k r_1}{k+1} \\ \frac{-k r_2}{k+1} & \frac{k+1-r_2}{k+1} \end{pmatrix} \quad (5.11)$$

where

$$\det(J|_{(X_1^*, X_2^*)}) = -\frac{k r_1 r_2 - r_1 r_2 - k + r_1 + r_2 - 1}{k + 1} \quad (5.12)$$

$$\operatorname{tr}(J|_{(X_1^*, X_2^*)}) = \frac{2k + 2 - r_2 - r_1}{k + 1} \quad (5.13)$$

In addition, characteristic polynomial has the form

$$P(X) := X^2 - \frac{2k + 2 - r_2 - r_1}{k + 1} X - \frac{k r_1 r_2 - r_1 r_2 - k + r_1 + r_2 - 1}{k + 1} \quad (5.14)$$

Proposition 5.4.1. *The local stability analysis results for the fixed points $(0, 0)$, $(k, 0)$, $(0, k)$ of (5.5) are summarized as below:*

1. *The equilibrium point $(0, 0)$ is always an unstable fixed point.*
2. *The equilibrium point $(k, 0)$ for $k < 1$ and $0 < r < 2$, has a stable manifold in X_1 direction and an unstable manifold in X_2 direction and is a saddle point. Moreover, $(k, 0)$ for $k > 1$ and $0 < r < 2$, has a stable manifold in X_1 direction and a stable manifold in X_2 direction and is a stable node. Moreover, $(k, 0)$ for $k < 1$ and $r > 2$, has an unstable manifold in X_1 direction and an unstable manifold in X_2 direction and is an unstable node. Finally, $(k, 0)$ for $k > 1$ and $r > 2$, has an unstable manifold in X_1 direction and a stable manifold in X_2 direction and is a saddle point.*
3. *The equilibrium point $(0, k)$ for $k < 1$ and $0 < r < 2$, has a stable manifold in X_2 direction and an unstable manifold in X_1 direction and is a saddle point. Furthermore, $(0, k)$ for $k > 1$ and $0 < r < 2$, has a stable manifold in X_1 direction and a stable manifold in X_2 direction and is a stable node. Moreover, $(0, k)$ for $k < 1$ and $r > 2$, has an unstable manifold in X_1 direction and an unstable manifold in X_2 direction and is an unstable node. Finally, $(0, k)$ for $k > 1$ and $r > 2$, has an unstable manifold in X_2 direction and a stable manifold in X_1 direction and is a saddle point.*

Proposition 5.4.2. *The local stability analysis results for the fixed points $(X_1^*, X_2^*) = (\frac{k}{k+1}, \frac{k}{k+1})$ of (5.5) are summarized as below:*

1. The equilibrium point (X_1^*, X_2^*) is an unstable fixed point if and only if

$$r_1 r_2 (1 - k) + 2(k + 1) < (r_1 + r_2), \quad 4(k + 1) - 2(r_1 + r_2) + r_1 r_2 (1 - k) > 0, \quad k < 1$$

or

$$k < \frac{r_1 r_2 - r_1 - r_2}{r_1 r_2}, \quad 4(k + 1) - 2(r_1 + r_2) + r_1 r_2 (1 - k) > 0, \quad k < 1$$

2. The equilibrium point (X_1^*, X_2^*) is a stable fixed point if and only if

$$k > \frac{r_1 r_2 - r_1 - r_2}{r_1 r_2}, \quad 4(k + 1) - 2(r_1 + r_2) + r_1 r_2 (1 - k) > 0, \quad k < 1$$

3. The equilibrium point (X_1^*, X_2^*) is a saddle point if and only if

$$4(k + 1) - 2(r_1 + r_2) + r_1 r_2 (1 - k) < 0, \quad k > 1$$

Proof. Using Theorem 1.1.1 (Linearized Stability) in ¹⁴⁹.

The equilibrium point (X_1^*, X_2^*) is an unstable fixed point if and only if $|\det(J)| > 1$ and $|\operatorname{tr}(J)| < |1 + \det(J)|$. $\operatorname{tr}(J|_{(X_1^*, X_2^*)}) - \det(J|_{(X_1^*, X_2^*)}) - 1 < 0$ gives us:

$$\frac{r_1 r_2 (k - 1)}{k + 1} < 0 \quad \rightarrow \quad k < 1 \tag{5.15}$$

Moreover, $\operatorname{tr}(J|_{(X_1^*, X_2^*)}) + \det(J|_{(X_1^*, X_2^*)}) + 1 < 0$ gives us:

$$\frac{4(k + 1) - 2(r_1 + r_2) + r_1 r_2 (1 - k)}{k + 1} > 0 \tag{5.16}$$

and $\det(J|_{(X_1^*, X_2^*)}) > 1$ gives us

$$\frac{r_1 r_2 (1 - k) - (r_1 + r_2)}{k + 1} < 0$$

that is to say

$$k > \frac{r_1 r_2 - r_1 - r_2}{r_1 r_2}$$

Moreover, $\det(J|_{(X_1^*, X_2^*)}) < -1$ gives us

$$\frac{r_1 r_2 (1 - k) + 2(k + 1) - (r_1 + r_2)}{k + 1} < 0$$

The positive fixed point of system (5.5) is asymptotically stable if and only if

$$|\operatorname{tr}(J)| < 1 + \det(J) < 2 \quad (5.17)$$

We check (5.17) using (5.12) and (5.13). $\operatorname{tr}(J|_{(X_1^*, X_2^*)}) - \det(J|_{(X_1^*, X_2^*)}) - 1 < 0$ and $\operatorname{tr}(J|_{(X_1^*, X_2^*)}) + \det(J|_{(X_1^*, X_2^*)}) + 1 < 0$ give us (5.15) and (5.16). and $\det(J|_{(X_1^*, X_2^*)}) < 1$ gives us

$$\frac{r_1 r_2 (1 - k) - (r_1 + r_2)}{k + 1} < 0$$

that is to say

$$k > \frac{r_1 r_2 - r_1 - r_2}{r_1 r_2}$$

Finally, The equilibrium point (X_1^*, X_2^*) is a saddle point if and only if $\operatorname{tr}^2(J) - 4 \det(J) > 0$ and $|\operatorname{tr}(J)| > |1 + \det(J)|$. The first condition gives us

$$\frac{(r_1 - r_2)^2 + 4k^2}{(k + 1)^2} > 0$$

which is always true. Another conditions to check are: $\operatorname{tr}(J|_{(X_1^*, X_2^*)}) - \det(J|_{(X_1^*, X_2^*)}) - 1 > 0$ gives us:

$$\frac{r_1 r_2 (k - 1)}{k + 1} > 0 \quad (5.18)$$

and, $\text{tr}(J|_{(X_1^*, X_2^*)}) + \det(J|_{(X_1^*, X_2^*)}) + 1 < 0$ which gives us:

$$\frac{4(k+1) - 2(r_1 + r_2) + r_1 r_2 (1 - k)}{k + 1} < 0 \quad (5.19)$$

□

Numerical simulations, including bifurcation diagrams and time series display that this model demonstrates chaotic oscillations after a cascade of period-doubling bifurcations. As we can see in Figure (5.2), there are chaotic regions which are embedded in periodic windows regions. The periodic behaviors which appear alternately in the chaotic area, contain a copy of bifurcation diagram and it is repeating when we are changing the bifurcation parameter r . The bifurcation diagram for system (5.5) with respect to r displays the same qualitative dynamics for different values of k . Moreover, we have run bifurcation analysis with respect to k with different r values in Figure (5.3).

In addition, if we look at Figure (5.4), at first, the equilibrium point is stable, when we increase r , it loses stability, from one cycle to two cycles, and produces a flip bifurcation. As r continues to increase, periodic oscillations are observed with periods 4, \dots , which eventually leads to chaos.

To prove the existence of chaos for the map (5.5) in the sense of Marotto, we need to find the conditions under which the fixed point $Z^* = (X_1^*, X_2^*)$ of the system is a snap-back repeller. According to definition (5.1.5) and Figure (5.1), we need to find a neighborhood $B_r(Z^*)$ of Z^* in which all eigenvalues have absolute value more than one. Now, we give the following lemma which we need that to prove chaos in the sense of Marotto for positive fixed point $Z^* = (X_1^*, X_2^*)$ of map (5.5).

Lemma 5.4.3. *Assume that the conditions of the first part of the proposition (5.4.2) are satisfied. The fixed point $Z^* = (X_1^*, X_2^*)$ of map F is called snap-back repeller if there exists a point $Z_0 = (X_1, X_2)$ in the neighborhood of Z^* such that $Z_0 \neq Z^*$, $F(Z_0) = Z^*$, $|\det(J|_{(X_1, X_2)})| \neq 0$, that is to say, at first, the following system of equations has a unique*

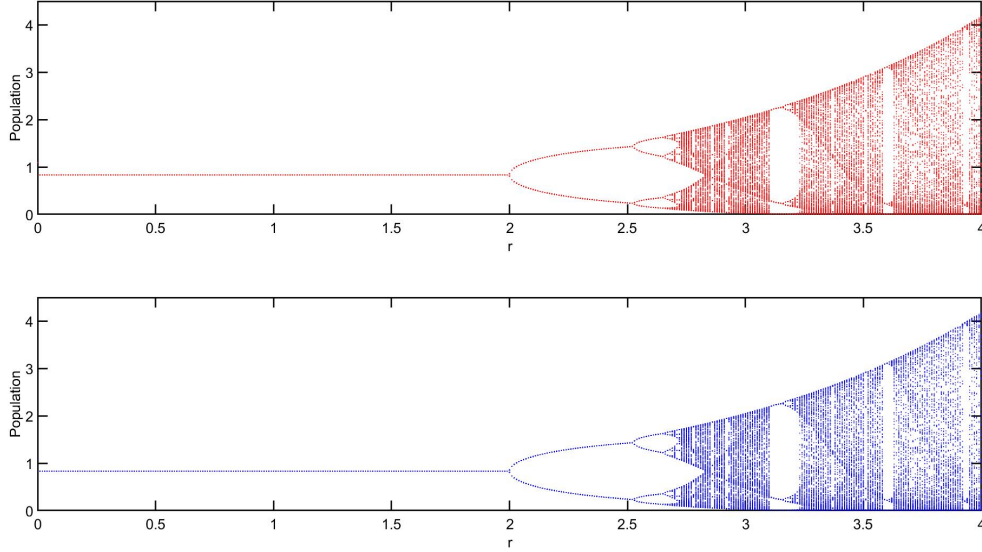


Figure 5.2: Bifurcation diagram of system (5.5) when $k = 10$ and $r_1 = r_2 = r$.

solution

$$\begin{cases} X_1^* = X_1 \exp\left(r_1\left(1 - \frac{X_1}{k} - X_2\right)\right) \\ X_2^* = X_2 \exp\left(r_2\left(1 - \frac{X_2}{k} - X_1\right)\right) \end{cases} \quad (5.20)$$

and

$$k^2 - k(r_2 X_2 + r_1 X_1 + r_1 r_2 X_1 X_2) + r_1 r_2 X_1 X_2 \neq 0 \quad (5.21)$$

Then Z^* for some parameter values (r_1, r_2) and k , is a snap-back repeller for map (5.5).

Proof. From $|\det(J|_{(X_1, X_2)})| \neq 0$, we have:

$$\frac{\partial g_1}{\partial X_1} \frac{\partial g_2}{\partial X_2} - \frac{\partial g_1}{\partial X_2} \frac{\partial g_2}{\partial X_1} \neq 0$$

which

$$\left(\left(1 - \frac{r_1 X_1}{k}\right)\left(1 - \frac{r_2 X_2}{k}\right) - r_1 r_2 X_1 X_2\right) e^{\left(r_1\left(1 - \frac{X_1}{k} - X_2\right) + r_2\left(1 - \frac{X_2}{k} - X_1\right)\right)} \neq 0$$

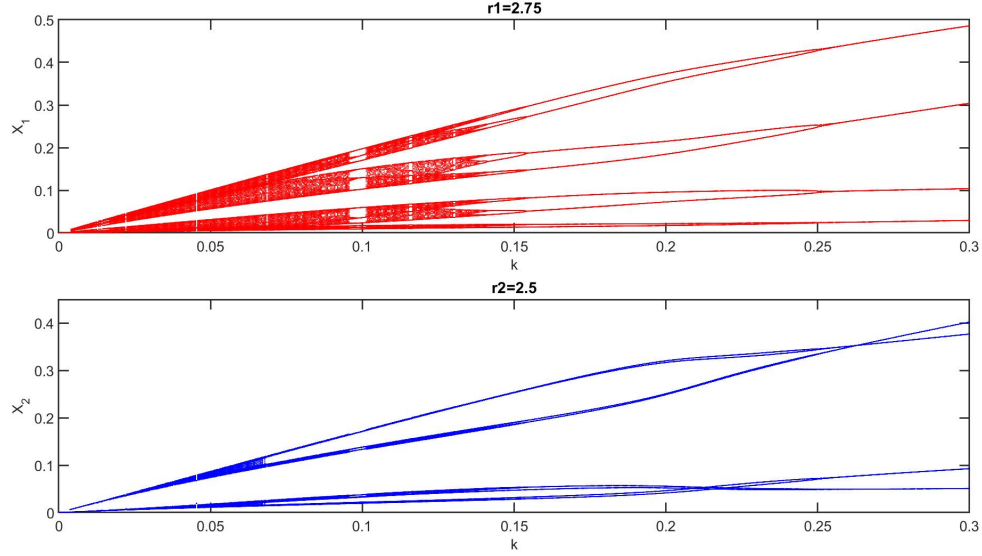


Figure 5.3: *Bifurcation diagram of system (5.5) when $r_1 = 2.75$ and $r_2 = 2.5$.*

and it gives us

$$k^2 - k(r_2 X_2 + r_1 X_1 + r_1 r_2 X_1 X_2) + r_1 r_2 X_1 X_2 \neq 0$$

Therefore, any solution $Z^* = (X_1^*, X_2^*) \neq (X_1, X_2) = Z_0$ of system (5.20) which satisfies the first part of the proposition (5.4.2) and (5.21), is snap-back repeller for system (5.5). \square

Theorem 5.4.4. *Under the assumptions of the first part of proposition (5.4.2) and lemma (5.4.3), the map (5.5) is chaotic in the sense of Li-York, which means that: There exist (i) a positive integer N , such that map (5.5) has a point of period p , for each integer $p \geq N$, (ii) a scrambled set of F , i.e., an uncountable set S containing no periodic points of F , such that*

1. $F(S) \subset S$,

2. $\limsup_{n \rightarrow \infty} \|F^n(x) - F^n(y)\| > 0$, for all $x, y \in S$, with $x \neq y$,

3. $\limsup_{n \rightarrow \infty} \|F^n(x) - F^n(y)\| > 0$, for all $x \in S$ and periodic point y of f ,

(iii) an uncountable subset S_0 of S , such that $\liminf_{n \rightarrow \infty} \|F^n(x) - F^n(y)\| = 0$, for every $x, y \in S_0$.

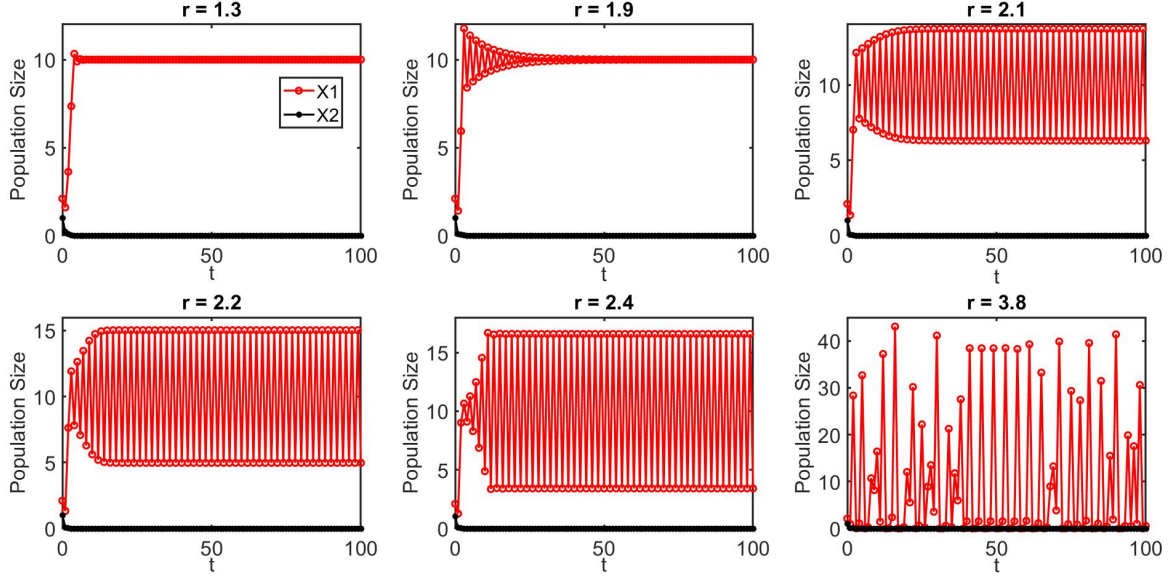


Figure 5.4: Evolution of host population X_1 and its coupled X_2 in time for system (5.5) when $k = 10$.

Proof. By theorem (5.1.3). □

5.5 Conclusion

Studying the evolution of population models and complex dynamics of competitive models has attracted many researchers during several past decades. In this chapter, we studied the complex dynamics of a two-species Ricker model which consists of four different biological parameters. We explored the stability of the origin and two other boundary fixed points using local stability theorem. Furthermore, we provided the condition under which the solutions are bounded. We have seen that this model undergoes period doubling bifurcation but it does not show Neimark-Sacker bifurcation. We used the persistence theory to reveal the global behavior of system and we discovered the persistence of the system for two boundary fixed points. Afterward, we changed the model to a specific case with only three biological parameters and we discussed about the local stability of extinction and boundary fixed points of the system. Moreover, we discovered the chaotic dynamics of the new model using Marotto theorem. As we discussed, Marotto theorem is a rigorous theorem to study chaotic dynamics for systems with higher dimensions and can be used to study the chaotic dynamics

of competitive models. We presented the conditions under which the new system undergoes snap-back repeller and as a result, it is chaotic in the sense of Li-York. Finally, we used bifurcation diagram to demonstrate the interesting dynamics of new system and the role of biological parameters r and k in appearance of different types of complicated dynamics. The new system has the same number of fixed points as the first system and the bifurcation analysis displayed the same qualitative dynamics for both species as we expected.

Chapter 6

Chaos Synchronization in Population Dynamics

Abstract

In Chapter Six, we study the problem of chaos synchronization in certain discrete-time dynamical systems. We introduce a drive-response discrete-time dynamical system, which is coupled using convex link function. We investigate a synchronization threshold, after which, the drive-response system uncouples and loses its synchronized behaviors. We apply this method to the synchronized cycles of the Ricker model and show that this model displays a rich cascade of complex dynamics from a stable fixed point and cascade of period-doubling bifurcation to chaos. We numerically verify the effectiveness of the proposed scheme and demonstrate how this type of coupling affects the synchronization of the system.

6.1 Introduction

Population dynamics can be modeled through the continuous-time system and the discrete-time system. However, when population size is small or that population does not overlap, discrete-time systems are more appropriate to use. Discrete-time population models are widely used to describe the dynamics of hosts and parasitoids interactions^{150–152}. There are many simple nonlinear discrete-time biological models which create rich and complex spectrum of dynamics from coexistence of species through periodic cycles to irregular and chaotic behaviors^{153–157}. Chaos and synchronization are two widespread phenomena with application in many disciplines which have been considered as a central topic in nonlinear dynamics^{158–160}. The presence of chaos in population models has been extensively reported by different researchers^{153–157}. The main property of chaotic dynamics is its critical sensitivity to initial conditions, which is responsible for initially neighboring trajectories separating from each other exponentially in the course of time. Synchronization implies that there is a strong correlation between coupled systems and intuitively, it refers to a phenomenon which makes the systems have the same dynamical behavior. Traditionally, synchronization was based upon periodic signals. However, after coming to the chaotic signals, more possibilities and flexibilities have been entered in this area.

Chaos synchronization has been started by the work of Fujisaka and Yamada¹⁹¹ in 1983. After 1990, when the possibility of chaos synchronization was understood by researchers, this idea has received many attractions by people in different areas^{162;164–166;193}. Synchronized chaos means that for any two chaotic systems for which any two nearby initial points in phase space quickly diverge and become unpredictable, it is possible that these two converge toward each other and evolve with each other in time. Complete synchronization takes place if there is a perfect linking of the chaotic solutions such that they remain in step with each other in time. In 1990, L.M. Pecora and L. Carroll, described a coupling method which constructs a real set of chaotic synchronization circuits¹⁶². They have applied this common signal to several well-known continuous-time dynamical systems such as Lorenz and Rossler and they claimed that it is possible to use this method with a slight variation for

discrete-time dynamical systems. Chaos synchronization has great interest and application in different disciplines like physics¹⁵⁸ and biology¹⁵⁹, and it has been observed in a huge variety of phenomena in nature¹⁶⁰. Synchronization has an important role in self-organization of organisms' groups in various biological systems,¹⁶⁷. There are several types of synchronization, such as complete synchronization¹⁹³, generalized synchronization^{168, 169, 170}, phase synchronization¹⁷¹, lag synchronization¹⁷², antisynchronization and projective synchronization¹⁷³ and¹⁷⁴.

This study proposes a new way to couple of discrete-time dynamical systems. We study three different types of synchronization for this new coupled system and we present the results related to the local stability of drive response system and we find the attractive set of this novel coupled system. This chapter moreover studies the interesting dynamics of a drive-response Ricker model which has been coupled by convex link function. Our goal is to build an appropriate response system which traces the drive system and finally they evolve in time even in chaotic regime. We explain that how this coupling method can be applied on a general discrete-time dynamical system to get a complete synchronization. Finally, the long term analysis through bifurcation diagrams and in addition, time-series analysis exhibit that this drive-response system which reveals complex dynamics including cascade of period doubling to chaotic solutions, for smaller synchronization threshold, get completely synchronized.

6.2 Description of the coupling method

In this section, we study the complete synchronization in a general discrete-time drive-response system. Here, we use a convex function to build the proposed drive-response system. To begin with, consider the following discrete-time dynamical system:

$$X_{n+1} = f(X_n) \tag{6.1}$$

Where $X \in \mathbb{R}^n$ is the state vector of drive system at time n , f is a mapping from \mathbb{R}^n to itself and is continuously differentiable. Next step is to find a perfect linking such that the system (6.1) and new coupled one remain in step with each other in time. To model the response system or coupled system, we use a convex link function as the form $H(X, Y) := (1 - s)X + sY$ where $H : \mathbb{R}^{2n} \rightarrow \mathbb{R}^n$ and $X, Y \in \mathbb{R}^n$ are the state vectors of response system at time n , and $0 < s \leq 1$ is synchronization threshold. Therefore, for $H_n := (1 - s)X_n + sY_n$, the response system has the form:

$$Y_{n+1} := f(H_n) = f((1 - s)X_n + sY_n) \quad (6.2)$$

and we demonstrate the error between the solutions of the drive system (6.1) and the response system (6.2) by $e(n) = \|Y_n - X_n\|$.

6.2.1 Complete synchronization using contraction mapping theorem

To explain the complete synchronization between two systems (6.1) and (6.2), we need to recall some known concepts which are crucial part of the proposed coupling method:

Definition 6.2.1. *We say that the drive system (6.1) and response system (6.2) are in complete synchronization if*

$$\lim_{n \rightarrow \infty} e(n) = \lim_{n \rightarrow \infty} \|Y_n - X_n\| = 0 \quad (6.3)$$

means that two systems eventually evolve identically in time.

Definition 6.2.2. *Let E be a Banach space. Then, the map $F : E \rightarrow E$ is called a contraction mapping if there exists a constant $0 \leq \alpha < 1$ such that for every pair of points $X, Y \in E$, we have $\|F(X) - F(Y)\| \leq \alpha\|X - Y\|$, where α is called a contraction constant of F on E ²⁰².*

The error between the drive and response system (6.1) and (6.2) has the following form:

$$e(n+1) = Y_{n+1} - X_{n+1} = f((1-s)X_n + sY_n) - f(X_n) \quad (6.4)$$

We can easily see that for $0 < s \leq 1$:

$$\|((1-s)X_n + sY_n) - X_n\| \leq s \|Y_n - X_n\|$$

Here, we assume that f is a contraction mapping. Then, for the equation (6.4) we can write:

$$\|e(n+1)\| = \|f((1-s)X_n + sY_n) - f(X_n)\| \leq \beta \|Y_n - X_n\| = \beta \|e(n)\|$$

where, β is a contraction constant.

As we defined before, to get complete synchronization, we need to have $\lim_{n \rightarrow \infty} \|e(n)\| = 0$.

Therefore, for contraction constant $0 \leq \beta < 1$,

$$\lim_{n \rightarrow \infty} \|e(n+1)\| = \lim_{n \rightarrow \infty} \|Y_{n+1} - X_{n+1}\| = 0$$

which means that the drive-response system (6.1)-(6.2) satisfies the complete synchronization properties. We will find β in theorem (6.2.3).

Theorem 6.2.3. *Given the non-linear coupled dynamical system (6.1) and (6.2), where the map $f : \mathbb{R}^{2n} \rightarrow \mathbb{R}^n$, and for the values $s < \tilde{s} = \frac{1}{\rho_A + \alpha}$, we get*

$$\lim_{n \rightarrow \infty} \|Y_{n+1} - X_{n+1}\| = 0$$

means that passing the synchronization threshold \tilde{s} makes the drive-response system (6.1) and (6.2) lose the complete synchronization properties.

Proof. Suppose the following C^r maps which have a fixed point at the origin:

$$X_{n+1} = A X_n + F(X_n), \quad (6.5)$$

$$Y_{n+1} = A((1-s)X_n + sY_n) + F((1-s)X_n + sY_n), \quad (6.6)$$

where the contraction mapping $F(X_n) = F_2(X_n) + \dots + F_{r-1}(X_n) + O(\|X_n\|^r)$, includes the vector-valued homogeneous polynomials of degree $2, \dots, r$. Consider the following equation for the error:

$$\begin{aligned} e(n+1) &= Y_{n+1} - X_{n+1} = (1-s)A X_n + sA Y_n - A X_n + F((1-s)X_n + sY_n) - F(X_n) \\ &= sA(Y_n - X_n) + F((1-s)X_n + sY_n) - F(X_n) \end{aligned}$$

Since, we assumed that F is a contraction mapping, it satisfies the following inequality:

$$\|F(Y) - F(X)\| \leq \alpha \|Y - X\|$$

where, α is a contraction constant. By triangular inequality we can write:

$$\begin{aligned} \|e(n+1)\| &= \|sA(Y_n - X_n) + F((1-s)X_n + sY_n) - F(X_n)\| \\ &\leq s\rho_A \|Y_n - X_n\| + s\alpha \|Y_n - X_n\| = s\rho_A \|e(n)\| + s\alpha \|e(n)\| \end{aligned}$$

where, $0 < s \leq 1$ and ρ_A is the spectral radius of A which is equal to $\rho_A = \max |\lambda_i|$ where λ is the root of characteristic polynomial or eigenvalue for A . Since, $0 \leq \alpha < 1$, therefore

$$\|e(n+1)\| \leq s\rho_A \|e(n)\| + s\alpha \|e(n)\| = s(\rho_A + \alpha) \|e(n)\|$$

We know that for complete synchronization, the error between the solutions should converge toward zero. Thus, $\lim_{n \rightarrow \infty} \|e(n)\| = \lim_{n \rightarrow \infty} \|Y_n - X_n\| = 0$. As a result, for $s(\rho_A + \alpha) < 1$

we have

$$\lim_{n \rightarrow \infty} \|e(n+1)\| = \lim_{n \rightarrow \infty} \|Y_{n+1} - X_{n+1}\| = 0$$

for which, $s < \frac{1}{\rho_A + \alpha} = \tilde{s}$. Here, $\tilde{s} = \beta$, which we discussed in the beginning of this section. After passing \tilde{s} , we lose the complete synchronization between (6.1) and (6.2). \square

Remark 1. Consider the drive system (6.1) becomes periodic with period ℓ , i.e, $X_{n+\ell} = X_n$. Then, for the values $s < \frac{1}{\rho_A + \alpha}$, the non-linear coupled dynamical system (6.1) and (6.2) become completely synchronized. In other word,

$$\lim_{n \rightarrow \infty} \|Y_{n+1} - X_{n+1}\| = 0$$

Here, similar to the proof of theorem (6.2.3), we decompose the nonlinear dynamical system (6.1) and (6.2) into linear and non-linear part. In this case, using triangular inequality we have:

$$\|e(n+1)\| \leq (s(\rho_A + \alpha))^\ell \|e(n)\|$$

We know that

$$\lim_{n \rightarrow \infty} \|e(n)\| = \lim_{n \rightarrow \infty} \|Y_n - X_n\| = 0$$

Therefore, for $(s(\rho_A + \alpha))^\ell < 1$ we have

$$\lim_{n \rightarrow \infty} \|e(n+1)\| = 0$$

for which, $s < \frac{1}{\rho_A + \alpha} = \tilde{s}$.

6.2.2 Local dynamics, attractors and attracting set of drive-response system

We continue this section by seeking appropriate closed subset $\Omega \in \mathbb{R}^n$ in which for drive and response system (6.1) and (6.2); where $X = (X_0, X_1, \dots, X_n)$ and $Y = (Y_0, Y_1, \dots, Y_n)$, the following conditions hold:

1. for all $X, Y \in \Omega$, then $f(X) \in \Omega$, $f(H) \in \Omega \times \Omega$.
2. f is a contraction on Ω .

The Jacobian matrix for drive-response system (6.1)-(6.2) has the following form:

$$J := \begin{bmatrix} \frac{\partial f(X)}{\partial X} & 0 \\ \frac{\partial f(H)}{\partial X} & \frac{\partial f(H)}{\partial Y} \end{bmatrix} \quad (6.7)$$

We can immediately obtain the following result:

Proposition 6.2.4. *Given Jacobian matrix (6.7), for which the following inequality holds:*

$$\|J\| := \rho_J = \max |\lambda_i| \leq \beta < 1 \quad (6.8)$$

where β is the contraction constant, ρ_J is the spectral radius of J and λ_i for $i = 1, \dots, n$ are the eigenvalues of Jacobian matrix J . Then, the mapping f is a contraction and the drive-response system (6.1)-(6.2) satisfies the complete synchronization properties, i.e.

$$\lim_{n \rightarrow \infty} \|e(n+1)\| = \lim_{n \rightarrow \infty} \|Y_{n+1} - X_{n+1}\| = 0$$

Proof. By contraction mapping theorem. Assume that the eigenvalues of the Jacobian matrix (6.7) have absolute values less than one. Then, using the contraction mapping theorem, f satisfies the contraction properties and would be a contraction mapping. Therefore, for the

equation (6.4) we can write:

$$\|e(n+1)\| = \|f((1-s)X_n + sY_n) - f(X_n)\| \leq \beta \|Y_n - X_n\| = \beta \|e(n)\|$$

where, β is a contraction constant. Thus, for contraction constant $0 \leq \beta < 1$,

$$\lim_{n \rightarrow \infty} \|e(n+1)\| = \lim_{n \rightarrow \infty} \|Y_{n+1} - X_{n+1}\| = 0$$

which means that the drive-response system (6.1)-(6.2) satisfies the complete synchronization properties. \square

The schematic representation for this type of coupling to obtain complete synchronization has been demonstrated in Figure (6.1).

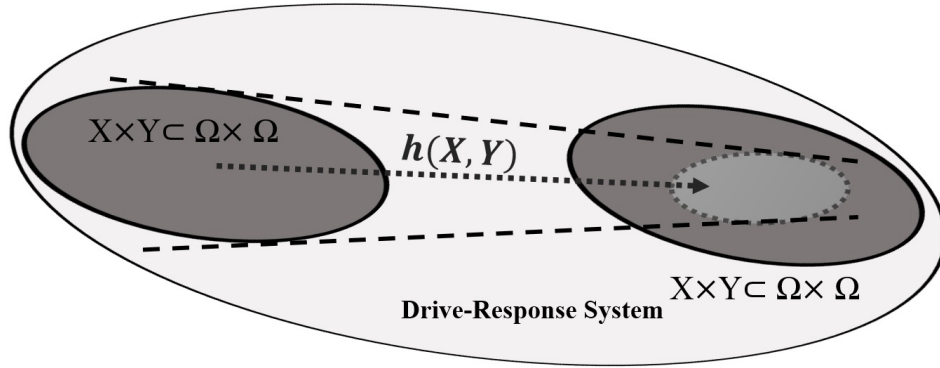


Figure 6.1: The schematic diagram for complete synchronization in a discrete-time drive-response dynamical system.

Recall from the theorem (6.2.3) that the linearization of a given autonomous drive-response problem discrete dynamical system can be written as the form:

$$Z_{n+1} := h(Z_n) = J Z_n + \tilde{h}(Z_n), \quad (6.9)$$

where, $Z = (X, Y)$ and $h : \mathbb{R}^{2n} \rightarrow \mathbb{R}^{2n}$ is a sufficiently smooth governing transition function.

Remark 2. For drive-response system (6.9), the following hold:

1. For all $Z \in \Omega \times \Omega$, then $h(Z) \in \Omega \times \Omega$.

2. h is a contraction on $\Omega \times \Omega$.

Therefore, we have the following statements for system (6.9).

Proposition 6.2.5. *Consider the drive-response system $h : \mathbb{R}^{2n} \rightarrow \mathbb{R}^{2n}$ which is defined on a closed subset $\Omega \times \Omega \subset \mathbb{R}^{2n}$ and satisfies the conditions in remark (2). Then, there exists a unique Z^* with $h(Z^*) = Z^*$. In another word, if (6.8) holds, then the drive-response system (6.9) has a unique fixed point.*

Remark 3. *According to the well known contraction mapping theorem, the converse of proposition (6.2.5) does not necessarily hold.*

For drive-response system (6.9), we can establish notions of sequential convergence and hence of stability for drive-response system (6.9). We now provide a general theorem which is the result of proposition (6.2.4).

Theorem 6.2.6. *Let $h : \mathbb{R}^{2n} \rightarrow \mathbb{R}^{2n}$ be a continuously differentiable map defined on a closed subset $\Omega \times \Omega \subset \mathbb{R}^{2n}$ and let J satisfying the form (6.8) be the Jacobian matrix of drive-response system (6.9) with $\left| \frac{\partial f(X)}{\partial X} \right| < 1$ and $\left| \frac{\partial f(H)}{\partial Y} \right| < 1$. Then, the following hold:*

1. *The solutions $Z = (X, Y) \in \Omega \times \Omega$ of drive-response system (6.9) completely synchronized.*

2. *Equilibrium Z^* of drive-response system (6.9) is stable; i.e.*

for any $\epsilon > 0$, there exists $\delta > 0$ such that $\|Z^ - Z\| < \delta$ implies that $\|h^\ell(Z) - Z^*\| < \epsilon$ for $\ell > 0$.*

Proof. The proof is straightforward. □

Remark 4. *In theorem (6.2.6), hyperbolicity is a robust property and it is one of the most important assumptions.*

It has been experimentally observed that there may be some situations in which the response system is stable but the response system has complex dynamics and the reason is using non differentiable link function or any non-differentiable transport system. In this study, we take the advantages of using a continuous convex link function which can completely control over the behavior of response system and we will numerically show that the response system inherits the same qualitative dynamics as its drive system and even for smaller synchronization threshold, the response system and drive system are almost completely equivalent.

6.3 Application of chaos synchronization in population dynamics

The chaotic behavior may be observed experimentally in natural systems in many scientific areas. Chaos can be defined as irregular and unpredictable time evolution of non linear systems. Main characteristic of chaos is sensitivity on initial conditions and that system does not repeat its past behavior. Despite the fact that chaotic systems are sensitive to initial conditions, it has been experimentally shown that the chaotic oscillators could be coupled. Chaos synchronization occurs when a chaotic oscillator drives another chaotic oscillator and is a very important phenomenon which has been occurred widely in ecological systems¹⁷⁶⁻¹⁷⁹. Because of importance of synchronization and its consequences on population dynamics, we study Ricker model and its synchronized system and we present their qualitative dynamics using different dynamical system tools.

The Ricker model is one of the most widely-used ecological models which displays regular and irregular complex nonlinear dynamics^{214;215} and its coupled system as the following form:

$$R_1 := x_1(n + 1) = x_1(n) e^{r\left(1 - \frac{x_1(n)}{k}\right)} \quad (6.10)$$

$$R_2 := x_2(n + 1) = H e^{r\left(1 - \frac{H}{k}\right)} \quad (6.11)$$

where

$$H(x_1, x_2) := (1 - s)x_1 + s x_2 \quad (6.12)$$

Here, x_1 demonstrates the population size of drive system, x_2 represents the population size of response system, r is the intrinsic growth rate, k is the carrying capacity of the environment, $s \in (0, 1]$ is synchronization threshold and $H(x_1, x_2) : \mathbb{R}^2 \rightarrow \mathbb{R}$ is a link function which has been used to couple (6.10) and (6.11). Thus, if drive system $R_1 : \mathbb{R} \rightarrow \mathbb{R}$, the corresponding response system would be $R_2 : \mathbb{R}^2 \rightarrow \mathbb{R}$, where H is a function of x_1 and x_2 .

For drive-response (6.10)-(6.11), the steady states are $(0, 0)$, $(0, x_2^*)$, and (k, k) . The Jacobian matrix for (6.10)-(6.11) has the form

$$J := \begin{bmatrix} \frac{\partial R_1}{\partial x_1} & 0 \\ \frac{\partial R_1}{\partial x_1} & \frac{\partial R_1}{\partial x_2} \end{bmatrix} \quad (6.13)$$

where

$$\begin{aligned} \frac{\partial R_1}{\partial x_1} &= \left(1 - \frac{r x_1}{k}\right) \exp\left(r \left(1 - \frac{x_1}{k}\right)\right) \\ \frac{\partial R_1}{\partial x_1} &= (1 - s) \exp\left(r \left(1 - \frac{(1 - s)x_1 + s x_2}{k}\right)\right) \left(1 - \frac{((1 - s)x_1 + s x_2) r}{k}\right) \\ \frac{\partial R_1}{\partial x_2} &= s \exp\left(r \left(1 - \frac{(1 - s)x_1 + s x_2}{k}\right)\right) \left(1 - \frac{(1 - s)x_1 + s x_2}{k}\right) \end{aligned}$$

Then, at the origin we have

$$J|_{(0,0)} = \begin{pmatrix} e^r & 0 \\ (1 - s) e^r & s e^r \end{pmatrix}$$

and for the positive fixed point (k, k) we have

$$J|_{(k,k)} = \begin{pmatrix} 1-r & 0 \\ 1-s-r+rs & s-rs \end{pmatrix}$$

Furthermore, for $(0, x_2^*)$,

$$J|_{(0,x_2^*)} = \begin{pmatrix} e^r & 0 \\ (1-s) \exp\left(r\left(1-\frac{x_2^*}{k}\right)\right) \left(1-\frac{x_2^*r}{k}\right) & s \exp\left(r\left(1-\frac{x_2^*}{k}\right)\right) \left(1-\frac{x_2^*}{k}\right) \end{pmatrix}$$

Proposition 6.3.1. *The local stability analysis results for the fixed points of (6.10)-(6.11) are summarized as below:*

1. *The equilibrium point $(0,0)$ for $r < -\ln s$ is a saddle point, and for $r > -\ln s$ is an unstable fixed point.*
2. *The equilibrium point (k,k) is a stable point in the interior of positive quadratic if $s < 1/(1-r)$, $0 < r < 1$ and $s > 1/(1-r)$, $1 < r < 2$, or $s < 1/(r-1)$, $0 < r < 1$ and $s < -1/(1-r)$, $1 < r < 2$. (k,k) is a saddle point if $s > 1/(1-r)$, $r > 2$ or $s < -1/(1-r)$, $r > 2$.*
3. *The equilibrium point $(0, x_2^*)$ for $s > k \exp[r(x_2^* - k)/k]/(k - x_2^*)$ or $s < k \exp[r(x_2^* - k)/k]/(x_2^* - k)$ is an unstable point, and for $|s| < k \exp[r(x_2^* - k)/k]/(k - x_2^*)$ is a saddle point.*

To study the global stability of the equilibrium points of both systems, at first we prove that all solutions in the first quadrant \mathbb{R}_+^2 are eventually bounded.

Theorem 6.3.2. *For $r > 0$, $k > 0$ and initial conditions in the first quadrant \mathbb{R}_+^2 , i.e. $x_1(0) > 0$ and $x_2(0) > 0$, for system of (6.10)-(6.11) we have: $x_1 > 0$ and $x_2 > 0$ for all $n \in \mathbb{Z}^+$. In addition, we can find some positive number M , such that $\max_{n \in \mathbb{Z}^+} \{x_1(n), x_2(n)\} \leq M$.*

Proof. By induction.

Since $x_1(0) > 0$ we have $\exp\left(r\left(1 - \frac{x_1(0)}{k}\right)\right) > 0$, hence

$$x_1(1) = x_1(0) e^{r\left(1 - \frac{x_1(0)}{k}\right)} > 0$$

Assume that for $n \leq l$, we have $x_1(l) > 0$. Then for $n = l + 1$ we have

$$x_1(l + 1) = x_1(l) e^{r\left(1 - \frac{x_1(l)}{k}\right)} > 0$$

Therefore $x_1(n) > 0$ for any $n \in \mathbb{Z}^+$. Similarly, since $x_1(0) > 0$ and $x_2(0) > 0$, we have $e^{r\left(1 - \frac{((1-s)x_1(0) + sx_2(0))}{k}\right)}$ is positive. Hence,

$$x_2(1) = ((1 - s)x_1(0) + sx_2(0)) e^{r\left(1 - \frac{((1-s)x_1(0) + sx_2(0))}{k}\right)} > 0$$

Assume that for $n \leq l$, we have $x_2(l) > 0$. Then for $n = l + 1$ we have

$$x_2(l + 1) = ((1 - s)x_1(l) + sx_2(l)) e^{r\left(1 - \frac{((1-s)x_1(l) + sx_2(l))}{k}\right)} > 0$$

Therefore $x_2(n) > 0$ for any $n \in \mathbb{Z}^+$. To find an upper bound, we know,

$$x_1(n + 1) = x_1(n) e^{r\left(1 - \frac{x_1(n)}{k}\right)} \leq \max_{x \in \mathbb{R}^+} \{f(x)\}$$

If we define $f(x) = x e^{r\left(1 - \frac{x}{k}\right)}$, then $f'(x) = \left(1 - \frac{rx}{k}\right) e^{r\left(1 - \frac{x}{k}\right)}$ and $f(x)$ has critical points at $x = \frac{k}{r}$. Since $f'(x) > 0$ if $x < \frac{k}{r}$ and $f'(x) < 0$ if $x > \frac{k}{r}$, then $x = \frac{k}{r}$ is the maximal point of $f(x)$, i.e. $\max_{x \in \mathbb{R}^+} \{f(x)\} = f\left(\frac{k}{r}\right)$. Hence,

$$x_1(n + 1) = x_1(n) e^{r\left(1 - \frac{x_1(n)}{k}\right)} \leq \max_{x \in \mathbb{R}^+} \{x e^{r\left(1 - \frac{x}{k}\right)}\} = f\left(\frac{k}{r}\right) = \frac{k e^{r-1}}{r} = M$$

Similarly,

$$\begin{aligned} x_2(n+1) &= ((1-s)x_1(n) + sx_2(n)) e^{r\left(1 - \frac{((1-s)x_1(n) + sx_2(n))}{k}\right)} = H e^{r\left(1 - \frac{H}{k}\right)} \\ &\leq \max_{H \in \mathbb{R}^+} \left\{ H e^{r\left(1 - \frac{H}{k}\right)} \right\} = \frac{k e^{r-1}}{r} = M \end{aligned}$$

Therefore, we can find some positive number M , such that $\max_{n \in \mathbb{Z}^+} \{x_1(n), x_2(n)\} \leq M$. \square

Theorem 6.3.3. *If there are positive constants $m > 0$ and $M > 0$ such that the solution $(x_1(n), x_2(n))$ of system satisfies*

$$\begin{aligned} 0 < m &\leq \liminf_{n \rightarrow +\infty} x_1(n) \leq \limsup_{n \rightarrow +\infty} x_1(n) \leq M = \frac{k e^{r-1}}{r} \\ 0 < m &\leq \liminf_{n \rightarrow +\infty} x_2(n) \leq \limsup_{n \rightarrow +\infty} x_2(n) \leq M = \frac{k e^{r-1}}{r} \end{aligned}$$

Then, system (6.10)-(6.11) is persistent. If system is not persistent, it is called non-persistent¹⁸².

Theorem 6.3.4. *Given $r > 0$, $k > 0$ and initial conditions $x_1(0) > 0$ and $x_2(0) > 0$ in system (6.10)-(6.11), if the following conditions hold:*

1. $\left| \left(1 - \frac{r x_1}{k}\right) \exp\left(r \left(1 - \frac{x_1}{k}\right)\right) \right| < 1$
2. $\left| s \left(1 - \frac{(1-s)x_1 + s x_2}{k}\right) \exp\left(r \left(1 - \frac{(1-s)x_1 - s x_2}{k}\right)\right) \right| < 1$

Then for drive-response system (6.10)-(6.11) for $(x_1, x_2) \in \Omega \times \Omega$ we have,

$$\lim_{n \rightarrow \infty} \|e(n+1)\| = \lim_{n \rightarrow \infty} \|x_2(n+1) - x_1(n+1)\| = 0$$

where

$$\Omega \times \Omega = \left\{ (x_1, x_2) \left| \max_{n \in \mathbb{Z}^+} \{x_1(n), x_2(n)\} \leq \frac{k e^{r-1}}{r} \right. \right\} \quad (6.14)$$

Proof. Using theorem (6.2.6), since $\Omega \times \Omega$ is closed and the conditions of proposition (6.2.4)

are satisfied, therefore the solutions of drive-response system (6.10)-(6.11) are completely synchronized and the error between the solutions converges toward zero. \square

6.3.1 Phase and amplitude synchronization in population dynamics

We begin with two important concepts in theory of synchronization of chaotic systems: (a) mean phase difference, (b) mean amplitude difference. We analyze these two types of synchronizations for drive-response population model (6.10)-(6.11) which have been coupled using the proposed link function. We consider the oscillations of this discrete-time population system as being synchronized if their phases coincide repeatedly and they have identical mean amplitude. These two types of synchronization have been studied widely in science, nature, engineering, or social life^{183–188} and before using them, we briefly define them.

Definition 6.3.5. *We call two systems are in phase synchronization if they have equivalent mean phase or they have a constant difference in phase. We define mean phase for two oscillators as*

$$\Phi_n \equiv ||X_{n+1} - X_n|| \Rightarrow \langle \Phi_\tau \rangle = \frac{\sum_{n=1}^{N_\tau} \Phi_n}{N_\tau} \quad (6.15)$$

where, N_τ is the number of cycles within a time τ .

In fact, for two non identical oscillators, phase synchronization happens when their phases evolve in synchrony but their amplitude remain unsynchronized.

Definition 6.3.6. *We call two systems are in amplitude synchronization if they have identical mean amplitude. We define mean amplitude for two oscillators as*

$$\langle A \rangle = \frac{\sum_{n=1}^{N_\tau} A_n}{N_\tau} \quad (6.16)$$

Remark 5. *The mean amplitude and mean phase are qualitatively similar with each other.*

Figure (6.2) demonstrates the mean phase difference, i.e. $|\Phi_{R_2} - \Phi_{R_1}|$ and the mean amplitude difference, i.e. $|A_{R_2} - A_{R_1}|$ corresponding to Ricker model and its synchronized

model (6.10) and (6.11). As we can see, using these two tools, we can numerically catch the threshold at which the systems (6.10) and (6.11) satisfy the phase synchronization and amplitude synchronization properties.

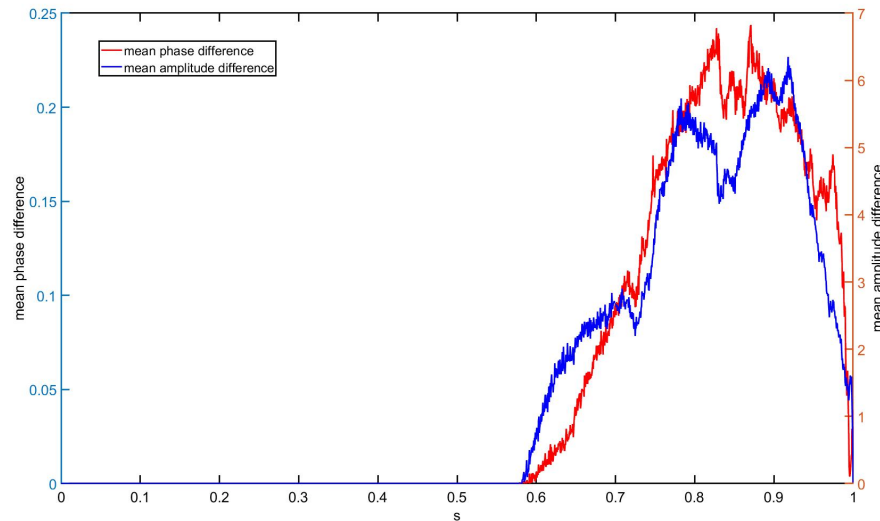


Figure 6.2: *The mean phase difference and the mean amplitude difference for drive-response system (6.10)-(6.11) when $r = 3$.*

6.3.2 Complete synchronization in population dynamics

In this section, we study the complete synchronization for drive-response system (6.10)-(6.11) using some qualitative methods which have been used frequently to detect chaos. In order to understand some dynamical behaviors of systems including period doubling bifurcations and chaotic oscillations, we picked a single parameter bifurcation, which can demonstrate how dependence is the dynamics of the systems on a certain parameter.

Figure (6.3) demonstrates the solutions of drive system (6.10) (red color) and response system (6.11) (black color) with different initial conditions and some interesting r values while $s = 0.5$.

For $r = 1.3$ and $s = 0.5$ both drive and response system (6.10)-(6.11) evidently, exhibit

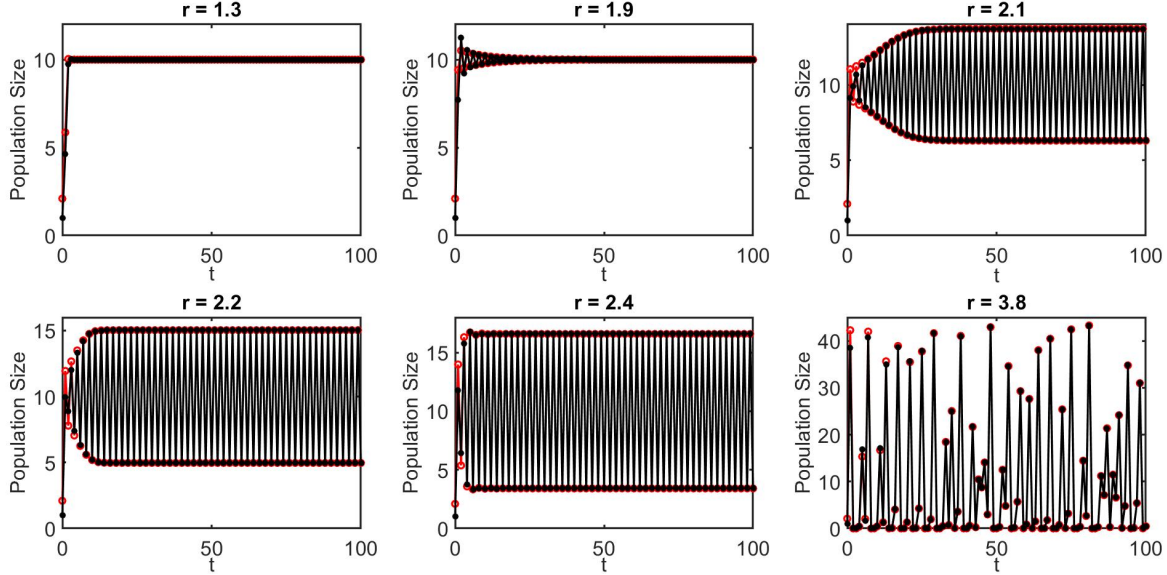


Figure 6.3: Evolution of host population x_1 and its coupled x_2 in time with two different initial conditions for drive-response system (6.10)-(6.11) when $s = 0.5$ and $k = 10$, drive system (red color) and response system (black color).

the sigmoidal approach to carrying capacity reminiscent of the logistic model. For $r = 1.9$, we have damped oscillations toward steady state which is because of two biological phenomena: at first, the population which started below carrying capacity does not smoothly approach steady state through a phenomenon called as overcompensation and then this follows by the second phenomenon called undershooting, which is due to further overshooting. If we increase r further, for the value $r = 2.1$ we see that these damped oscillations follows by a 2-cycle pattern and they are diverging from the steady states. Similarly, for $r = 2.2$ and $r = 2.4$, the oscillations follow a 2-cycle pattern. Finally, for $r = 3.8$ we can see the occurrence of unpredictable, irregular and chaotic oscillations.

In Figure (6.4) and for the case $s = 0.95$, we have almost the same dynamics as we had for $s = 0.5$. As we can see, for larger values of threshold s , we do not get completely synchronized cycles.

Indeed, displayed dynamics in Figures (6.3) and (6.4) are not special to the Ricker model, but are common features of discrete time population models.

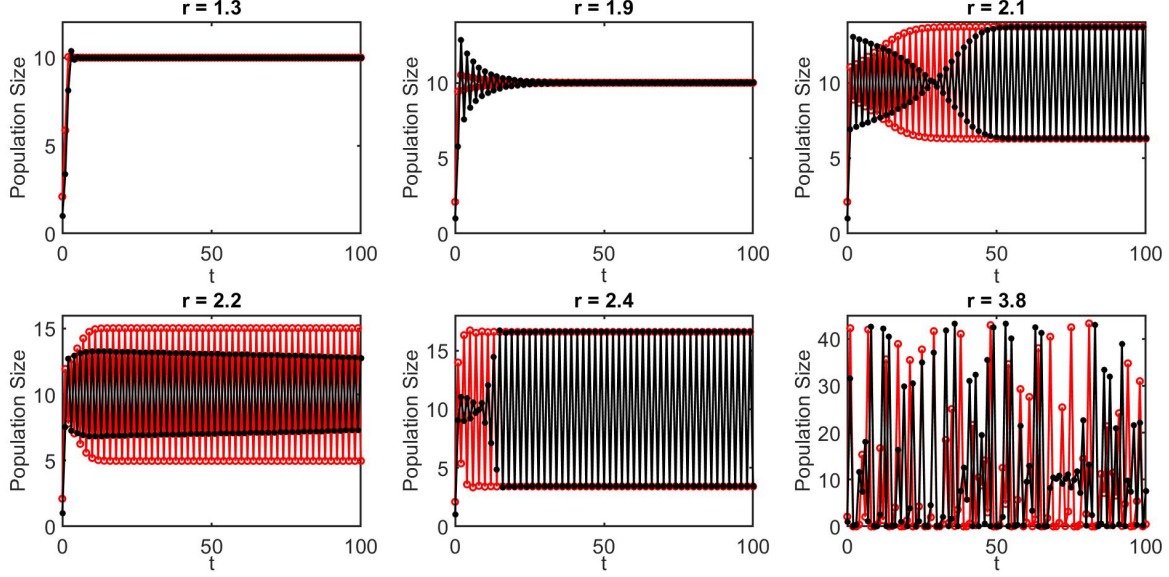


Figure 6.4: Evolution of host population x_1 and its coupled x_2 in time with two different initial conditions for drive-response system (6.10)-(6.11) when $s = 0.95$ and $k = 10$, drive system (red color) and response system (black color).

For the Figure (6.5), we explain some general properties which have been shared between the drive-response system (6.10)-(6.11) in common. As we can see, with increasing r the value of carrying capacity k is increasing. However, for $r \approx 2$ the branch corresponding to stable steady states bifurcates through period-doubling bifurcation into a 2-cycle. As we increase r further, the interval over which we have a new period reduces, and as we know this smaller and smaller windows are called Feigenbaum cascade which after them the dynamics become aperiodic. As we expected, the bifurcation diagram of drive-response system (6.10)-(6.11) for greater values of s , shows the same types of dynamics for drive and response system, but not completely synchronized.

The Poincare section and power spectrum of drive-response system (6.10)-(6.11) have been displayed in Figure (6.6) for the case $s = 0.95$, $r = 3$ and $k = 10$. Basically, the Poincare section can be constructed by sampling the phase portrait which helps to simplify the complicated dynamical systems. It is known that periodic behavior corresponds to a fixed point in Poincare section and any chaotic dynamics can be detected by set of distinct points in Poincare map. Moreover, the wideband chaotic signals and periodic signals can be easily distinguished from each other using the frequency spectra. Therefore, as we understood

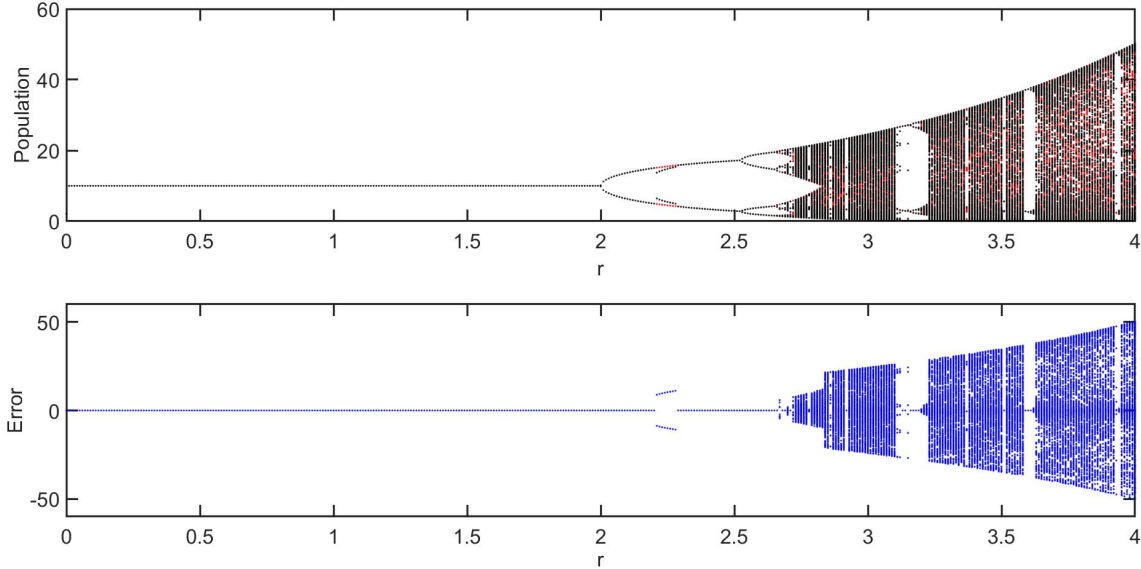


Figure 6.5: *Bifurcation diagram of Ricker model and its coupled with the error between their attractors for $s = 0.95$ and $k = 10$, drive system (red color) and response system (black color).*

from bifurcation diagram, drive-response system (6.10)-(6.11) experiences the chaotic dynamics for $r = 3$ and as we expected for large values of s we can not establish a complete synchronization.

6.4 Conclusion

Synchronization in population dynamics can lead to arising complex dynamics and understanding the synchronization of oscillations is crucially important in this area. In this study, we developed a new drive-response system by defining a convex continuous link function which maps the orbits of the drive system keeping the same qualitative properties such as stability and periodicity into the orbits of its coupled system. As has been shown by n L. M. Pecora and T. L. Carroll showed, in 1990, two Lorenz systems with the property of sensitive dependence on the initial conditions could be synchronized starting from different initial states. We extended this result into discrete-time dynamical systems and we have shown that by using the concept of convex function, we can force the orbits of a discrete-time drive-response system starting from different initial conditions get synchronized and we

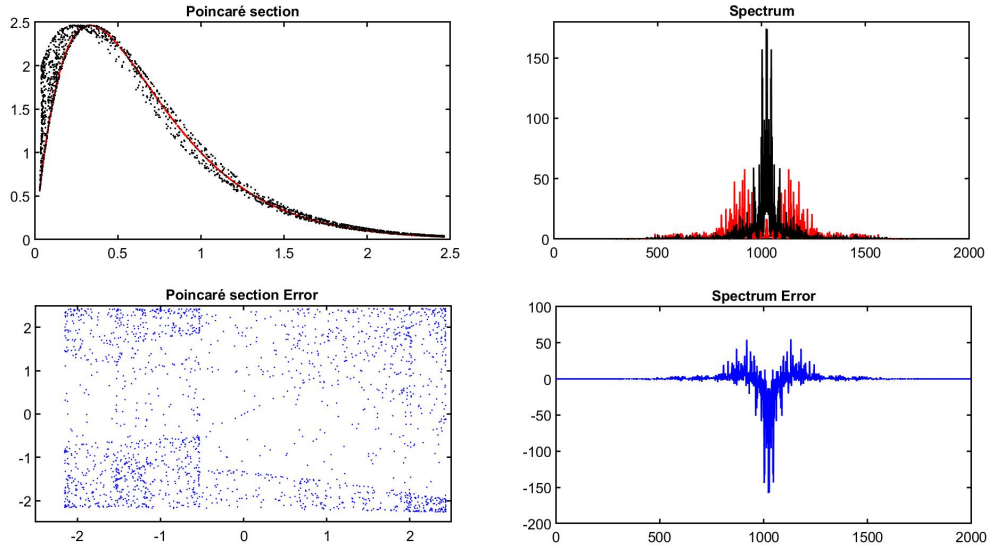


Figure 6.6: *Poincaré section and spectrum for Ricker model and its coupled with corresponding error for $s = 0.95$, $r = 3$ and $k = 10$, drive system (red color) and response system (black color).*

observed that this coupling method can be successful for drive-response system (6.10)-(6.11) to get a complete synchronization when the synchronization threshold has smaller values, closer to zero. In addition, we changed the values of synchronization threshold s in its range between (0,1) and we observed that the response system (6.11) for larger values of synchronization threshold s is not completely synchronized with its original drive system (6.10) and when we increased the values of synchronization threshold s , we noticed that the qualitative behaviors of both systems remain the same, even though, we do not get a complete synchronization between the solutions of drive and response system (6.10)-(6.11). In chaotic regime, for larger values of synchronization threshold s , closer to one, we could not get a complete synchronization. But, for smaller synchronization threshold s , closer to zero, we have shown that two systems are in complete synchronization even though the dynamics is chaotic.

Chapter 7

Synchronized Cycles of Generalized Nicholson-Bailey Model

Abstract

In Chapter Seven, we study the synchronized cycles of a generalized Nicholson-Bailey model. This model demonstrates a rich cascade of complex dynamics from a stable fixed point to periodic orbits, quasi periodic orbits and chaos. We introduce a coupling of these two chaotic systems with different initial conditions and show how they synchronize over a short time. We investigate the qualitative behavior of Generalized Nicholson-Bailey model and its synchronized model using time series analysis and its long-time dynamics by using its bifurcation diagram.

7.1 Introduction

Traditionally, the study of long time behavior of a dynamical systems was based on the examples of ordinary differential equations with regular solutions and those solutions which remained in a bounded region of the phase space could be divided into two different types based on their local behavior: first a stable equilibrium point and second a periodic (or quasi-periodic) oscillation. Edward Lorenz in 1961, by working on a simplified version of atmospheric transfer model which was consisting of three nonlinear ordinary differential equations, numerically observed that a very small changing in the initial conditions of the system equations makes a huge difference on the long term behavior of their solutions¹⁸⁹. Indeed, his finding was due to one of the major properties of chaotic dynamical systems which later called as sensitive dependence on initial conditions or butterfly effect.

Chaos is a complex nonlinear phenomenon that has been increasingly studied in the last three decades. During those years, many fields of science and engineering have been affected by chaos studies. One of the most important achievements in nonlinear and complex dynamics is the discovery of synchronized chaos. Synchronization happens when two events take place in synchrony at the same time and when time approaches infinity, the error between solutions of the first system and its synchronized one vanishes and approaches to zero. The synchronization between two dynamical systems is a well known phenomena occurring in Physics, Biology or Engineering and refers to a phenomenon that may occur when two or more oscillators are coupled. For the first time, Christiaan Huygens discovered synchronization of coupled pendulum clocks in 1665¹⁹⁰. Occurrence of synchronization in coupled chaotic system composed of identical chaotic oscillators has been detected for the first time by Fujisaka and Yamada¹⁹¹ and¹⁹² and after that it has been reported by Pecora and Carroll¹⁹³.

The dynamics of coupled chaotic systems show properties which we cannot detect in the behavior of the individual elements¹⁹⁴. Someone can find the same spatial synchronized fluctuations in biology, ecology and epidemiology¹⁹⁵⁻¹⁹⁹. Synchronization of complex population oscillations in natural systems has been examined widely by some researchers²⁰⁰.

Bernd Blasius and Lewi Stone worked on a chaotic UPCA foodweb model and they claimed that the spatio-temporal structures associated with phase synchronization have important implications for conservation ecology. They proposed that even though perturbation of a local patch population can bring them to the brink of extinction, however, the periodicity of spatial phase synchronization can help to buffer the endangered population by colonizers. They moreover asserted that unlike this thought that population synchronization can cause global population extinction²⁰¹, however, phase synchronization can be useful for maintaining species persistence. Their finding indicated that synchronization can shape the distribution and abundance of species even in continental scale.

As we have already discussed, there are many varieties of synchronization. In this research, instead of exploring all of these different types of synchronization which have been proposed for different purposes and with various applications, we simply focus on the most fundamental case, and we will develop our new approach based on a basic mathematical concept. Indeed, the purpose of this chapter is that after defining and setting the fundamental concepts which we need to establish the basis of our study, to demonstrate that such configurations under a suitable coupling method is possible. Moreover, we explore the dynamical and ecological effects of synchronization of a host-parasitoid model which is a generalization of Nicholson-Bailey model (GNB). The GNB model demonstrates regular and irregular or chaotic oscillations. We define a lift function which is technically a convex function and maps the orbits of the drive system into the orbits of the response system. Using this convex function, we drive the response system which inherits all the complex qualitative dynamics of GNB model and mimics that certain properties of the motion which is shared between them. We investigate numerically that this method of coupling, synchronizes completely the stable and periodic cycles and even the chaotic motions of GNB model and to do that, we need to adjust the synchronization constant to be closer to zero. We demonstrate the complex dynamics of GNB model and its coupled system by conducting some time series and bifurcation analysis.

7.2 Drive-response system derivation

In this section, we derive the coupled system corresponding to the drive system by defining a convex link function. We consider the following drive system:

$$X_{n+1} = g(X_n), \quad (7.1)$$

where $X_n \in \mathbb{R}^n$ is the state vector of a general discrete-time drive system and $g : \mathbb{R}^n \rightarrow \mathbb{R}^n$ is continuous. To find an appropriate response system, we provide the following definition¹²³:

Definition 7.2.1. *Assume $X, Y \in \mathbb{R}^n$ are the state vectors of two non-linear discrete-time dynamical systems and a constant $0 < s \leq 1$. Then, a continuous function $h(X, Y, s) := (1 - s)X + sY$ where $h : \mathbb{R}^{2n+1} \rightarrow \mathbb{R}^n$ is called a link function which maps the orbits of first system keeping the same qualitative dynamics to the orbits of second system.*

Using the definition (7.2.1), we develop a new system which inherits the qualitative features of the system (7.1) and has the following form

$$Y_{n+1} = g((1 - s)X_n + sY_n) \quad (7.2)$$

and it is called response system. Now, for the following non-linear discrete-time dynamical system, we are going to develop a theorem which helps us to find the synchronization threshold. We consider the following drive-response system:

$$\begin{cases} X_{n+1} = g(X_n), \\ Y_{n+1} = g((1 - s)X_n + sY_n). \end{cases} \quad (7.3)$$

Where $X_n, Y_n \in \mathbb{R}^n$ are the state vectors of drive system (7.1) and response system (7.2) respectively, g is a mapping from \mathbb{R}^n to itself and a constant $0 < s \leq 1$. The Jacobian matrix

for drive-response system (7.3) has the following form:

$$J := \begin{bmatrix} \frac{\partial g(X)}{\partial X} & 0 \\ \frac{\partial g(h)}{\partial X} & \frac{\partial g(h)}{\partial Y} \end{bmatrix} \quad (7.4)$$

Definition 7.2.2. *We say that the drive system (7.1) and response system (7.2) are in complete synchronization if*

$$\lim_{n \rightarrow \infty} \|Y_n - X_n\| = 0 \quad (7.5)$$

Here, we imply to a general definition in synchronization theory which is crucial for proposed coupling method.

Definition 7.2.3. *Let E be a Banach space. Then, the map $g : E \rightarrow E$ is called a contraction mapping if there exists a constant $0 \leq \alpha < 1$ such that for every pair of points $X, Y \in E$, we have $\|g(X) - g(Y)\| \leq \alpha \|X - Y\|$, where α is called a contraction constant of g on E ²⁰².*

Now, we have the following result for drive-response system (7.3).

Proposition 7.2.4. *For drive-response system (7.3) if g is a contraction function, then the solutions eventually evolve identically in time and*

$$\lim_{n \rightarrow \infty} \|e(n+1)\| = 0$$

where $e(n+1) = \|Y_{n+1} - X_{n+1}\|$ is the error between the solutions of the system (7.3).

Proof. For drive-response system (7.3), we have:

$$e(n+1) = Y_{n+1} - X_{n+1} = g((1-s)X_n + sY_n) - g(X_n)$$

We can easily see that for $0 < s \leq 1$:

$$\|((1-s)X_n + sY_n) - X_n\| \leq s\|Y_n - X_n\|$$

for $0 \leq \alpha < 1$ and since g is a contraction mapping, we can write:

$$\|e(n+1)\| = \|g((1-s)X_n + sY_n) - g(X_n)\| \leq \alpha\|Y_n - X_n\| = \alpha\|e(n)\|$$

That is to say

$$\|e(n+1)\| \leq \alpha\|e(n)\|$$

It is obvious that

$$\lim_{n \rightarrow \infty} \|e(n)\| = \lim_{n \rightarrow \infty} \|Y_n - X_n\| = 0$$

Therefore;

$$\lim_{n \rightarrow \infty} \|e(n+1)\| = 0$$

□

To obtain our rigorous results for complete synchronization, we need to find the normal form for drive-response system (7.3), we need to perform a few linear coordinate transformations that will put (7.3) into a form which is easier to work with²⁰³. First we transform the fixed point (X^*, Y^*) of the system (7.3) to the origin by the translation $X = X^* + \bar{X}$ and $Y = Y^* + \bar{Y}$ under which drive-response system (7.3) becomes

$$F := \begin{cases} \bar{X}_{n+1} &= g(\bar{X}_n + X^*) - X^* \equiv G(\bar{X}_n), \\ \bar{Y}_{n+1} &= g((1-s)(\bar{X}_n + X^*) + s(\bar{Y}_n + Y^*)) - Y^* \equiv G(\bar{X}_n, \bar{Y}_n). \end{cases} \quad (7.6)$$

The Jacobian matrix for drive-response system (7.6) has the following form:

$$\tilde{J} := \begin{bmatrix} \frac{\partial G(\bar{X})}{\partial \bar{X}} & 0 \\ \frac{\partial G(\bar{X}, \bar{Y})}{\partial \bar{X}} & \frac{\partial G(\bar{X}, \bar{Y})}{\partial \bar{Y}} \end{bmatrix} \quad (7.7)$$

Then, we split off the linear part of the system (7.6) and write

$$\begin{bmatrix} \bar{X} \\ \bar{Y} \end{bmatrix} = \begin{bmatrix} \frac{\partial G(\bar{X})}{\partial \bar{X}} & 0 \\ \frac{\partial G(\bar{X}, \bar{Y})}{\partial \bar{X}} & \frac{\partial G(\bar{X}, \bar{Y})}{\partial \bar{Y}} \end{bmatrix} \begin{bmatrix} \bar{X} \\ \bar{Y} \end{bmatrix} + \begin{bmatrix} \tilde{G}(\bar{X}) \\ \tilde{G}(\bar{X}, \bar{Y}) \end{bmatrix} = \begin{bmatrix} \frac{\partial G(\bar{X})}{\partial \bar{X}} \bar{X} + \tilde{G}(\bar{X}) \\ \frac{\partial G(\bar{X}, \bar{Y})}{\partial \bar{X}} \bar{X} + \frac{\partial G(\bar{X}, \bar{Y})}{\partial \bar{Y}} \bar{Y} + \tilde{G}(\bar{X}, \bar{Y}) \end{bmatrix} \quad (7.8)$$

where

$$\begin{bmatrix} \tilde{G}(\bar{X}) \\ \tilde{G}(\bar{X}, \bar{Y}) \end{bmatrix} = \begin{bmatrix} G(\bar{X}) \\ G(\bar{X}, \bar{Y}) \end{bmatrix} - \begin{bmatrix} \frac{\partial G(\bar{X})}{\partial \bar{X}} & 0 \\ \frac{\partial G(\bar{X}, \bar{Y})}{\partial \bar{X}} & \frac{\partial G(\bar{X}, \bar{Y})}{\partial \bar{Y}} \end{bmatrix} \begin{bmatrix} \bar{X} \\ \bar{Y} \end{bmatrix} \quad (7.9)$$

Let Q be the matrix that transforms the matrix \tilde{J} into (real) Jordan canonical form which has the following form

$$Q = \begin{bmatrix} \frac{\partial G(\bar{X}, \bar{Y})}{\partial \bar{Y}} - \frac{\partial G(\bar{X})}{\partial \bar{X}} & 0 \\ \frac{\partial G(\bar{X}, \bar{Y})}{\partial \bar{X}} & 1 \end{bmatrix}, \quad Q^{-1} = \begin{bmatrix} 1 & 0 \\ \frac{\partial G(\bar{X}, \bar{Y})}{\partial \bar{Y}} - \frac{\partial G(\bar{X})}{\partial \bar{X}} & \\ \frac{\partial G(\bar{X}, \bar{Y})}{\partial \bar{X}} & \\ \frac{\partial G(\bar{X})}{\partial \bar{X}} - \frac{\partial G(\bar{X}, \bar{Y})}{\partial \bar{Y}} & 1 \end{bmatrix}$$

Then, under the transformation

$$\begin{bmatrix} \bar{X} \\ \bar{Y} \end{bmatrix} = \begin{bmatrix} \frac{\partial G(\bar{X}, \bar{Y})}{\partial Y} - \frac{\partial G(\bar{X})}{\partial X} & 0 \\ \frac{\partial G(\bar{X}, \bar{Y})}{\partial X} & 1 \end{bmatrix} \begin{bmatrix} U \\ V \end{bmatrix} \quad (7.10)$$

(7.8) becomes

$$\begin{bmatrix} U \\ V \end{bmatrix} = \hat{J} \begin{bmatrix} U \\ V \end{bmatrix} + Q^{-1} \begin{bmatrix} \tilde{G}(U) \\ \tilde{G}(U, V) \end{bmatrix} \quad (7.11)$$

where $\hat{J} = Q^{-1} \tilde{J} Q$. We remark that the transformation (7.10) has simplified the linear part of (7.8) as much as possible. One can continue the task of simplifying the nonlinear part. However, for our purpose, we only need to focus on the linear part of the system. The schematic representation of the procedure of complete synchronization in a general discrete-time drive-response dynamical system has been demonstrated in Figure (7.1).

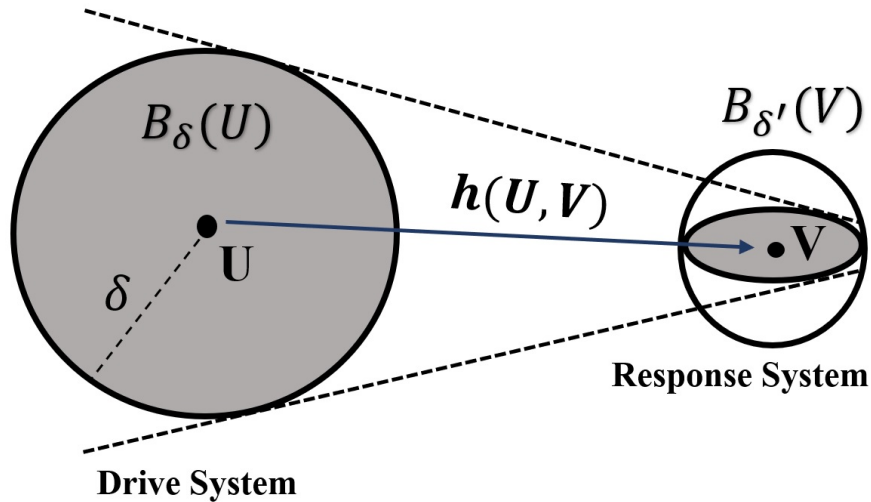


Figure 7.1: The schematic diagram for complete synchronization in a discrete-time drive-response dynamical system.

Hartman [1960] and Grobman [1959] proved that the orbit structure near a hyperbolic fixed point has the same qualitative structure of associated linearized system²⁰⁴⁻²⁰⁶. According to Hartman-Grobman theorem, the dynamical systems behave similar to their linearization part around the fixed point. However, this theorem needs the linearization part without eigenvalues with real part zero for continuous-time system and for discrete-time systems, it needs the absolute value of the eigenvalues of linearized part not become one.

Remark 6. *Because of the nature of the contraction mapping theorem and therefore the proposed coupling method, the Hartman-Grobman theorem can be applied directly into our problem.*

Lemma 7.2.5. *Using Hartman-Grobman theorem, to find the condition under which the drive-response system (7.11) achieves complete synchronization, we only need to look at the linear part of (7.11) which is*

$$L(U, V) \equiv Q^{-1} \tilde{J} Q \quad (7.12)$$

Theorem 7.2.6. *Given Jacobian matrix $\hat{J} = Q^{-1} \tilde{J} Q$, for which the following inequality holds:*

$$\|\hat{J}\| := \rho_{\hat{J}} = \max |\lambda_i| \leq \alpha < 1 \quad (7.13)$$

where α is the contraction constant, $\rho_{\hat{J}}$ is the spectral radius of \hat{J} and λ_i for $i = 1, \dots, n$ are the eigenvalues of Jacobian matrix \hat{J} . Then, the mapping G is a contraction and the drive-response system (7.11) satisfies the complete synchronization properties, i.e.

$$\lim_{n \rightarrow \infty} \|e(n+1)\| = \lim_{n \rightarrow \infty} \|\bar{Y}_{n+1} - \bar{X}_{n+1}\| = 0$$

Proof. Using the contraction mapping theorem²⁰⁷. □

In dynamical system point of view, it is possible for a point arbitrarily close to fixed point $Z^* = (U^*, V^*)$ of system (7.11) to generate an orbit which stays arbitrarily close to Z^* .

An orbit which could circle around the equilibrium Z^* staying within the proposed bounded region, for initial conditions sufficiently close to Z^* , could eventually approach Z^* . In this case, Z^* and all invariant set of points which demonstrating the same attractive property called attractor. Using this statement, we define an attractor of drive-response system (7.11):

Definition 7.2.7. *Let $\Lambda \subset \mathbb{R}^n$ such that Λ is invariant under the function G ; i.e, $G(\Lambda) \subseteq \Lambda$. We define the distance between Λ and a point Z , as $d(\Lambda, Z) = \min_{z \in \Lambda} \|Z - z\|$. If there exists an $\epsilon > 0$ such that $d(\Lambda, Z) < \epsilon$ implies $\lim_{\ell \rightarrow \infty} d(\Lambda, G^\ell(Z)) = 0$, then Λ is called an attractor for drive-response system (7.11).*

For a stable fixed point, it is of special interest to determine the set of initial conditions whose subsequent orbits end up at this fixed point and we call this set as the basin of attraction of stable fixed point which achieves by the following definition:

Definition 7.2.8. *Given $G : \mathbb{R}^{2n+1} \rightarrow \mathbb{R}^{2n}$ a continuously differentiable map, then, the compact and invariant set Γ is called the attracting set of drive-response system (7.11) if there exists an open neighborhood B of Γ such that $G(B) \subset B$ and $\cap_{\ell=0}^{\infty} G^\ell(B) = \Gamma$. The largest such B is called the basin of attraction for system.*

7.2.1 Stable threshold for synchronization in discrete-time dynamical systems

We continue this section by defining a new concept in synchronization theory of discrete-time dynamical systems. The concept of stability in this study is similar to the one that we have in contraction mapping theorem which is different from the relative stability of equilibrium point and some nominal motion. We say that a system is stable if the final state of the system is independent on initial conditions and we call a system is attracting if the orbits of that system get pulled in or converge towards each other²⁰⁸. In general, stability can be interpreted as a property of solutions of a dynamical systems which means all solutions converge towards each other²⁰⁹.

Definition 7.2.9. A variable response system to the dynamical system $\bar{X}_0, \bar{X}_1, \dots, \bar{X}_n$, with the map $\Phi : D \subseteq \mathbb{R}^n \rightarrow D \subseteq \mathbb{R}^n$ with respect to the sequence $s = (s_0, s_1, \dots, s_n)$ where $0 < s_i \leq 1$ is the sequence $\tilde{Y}_0 = (\bar{Y}_1, \dots, \bar{Y}_n), \dots, \tilde{Y}_{n+1} = \Phi(\text{Cont}_{\bar{X}_n}^{s_n}(\bar{Y}_n))$ where the map $\text{Cont}_u^s : \mathbb{R}^n \rightarrow \mathbb{R}^n$ can be represented via $\text{Cont}_u^s(v) = (1 - s) \vec{u} + s \vec{v}$.

Definition 7.2.10. The threshold for the coupled dynamical system with drive system $\bar{X}_0, \bar{X}_1, \dots, \bar{X}_n$, with the map $\Phi : D \subseteq \mathbb{R}^n \rightarrow D \subseteq \mathbb{R}^n$ is s if given any $\tilde{s} < s$ and any \bar{Y}_0 , there exists a sequence $s = (s_0, s_1, \dots, s_n)$ with $0 < s_i \leq 1$ and $s_i = \tilde{s}$ for $i \gg 0$ such that

$$\lim_{n \rightarrow \infty} \|\bar{Y}_n - \bar{X}_n\| = 0 \quad (7.14)$$

Using the definitions (7.2.9) and (7.2.10), we state the main results of this section.

Theorem 7.2.11. Consider a linear discrete-time dynamical system (drive-response system) as following form:

$$X_{n+1} = A X_n. \quad (7.15)$$

$$Y_{n+1} = A((1 - s) X_n + s Y_n). \quad (7.16)$$

where matrix A is similar to a diagonal matrix. For the values $s < \tilde{s}_1 = \frac{1}{\rho(A)}$ where \tilde{s}_1 represents the synchronization threshold, we have

$$\lim_{n \rightarrow \infty} \|Y_n - X_n\| = 0$$

and passing this threshold decreases the stability of synchronization and consequently, the drive-response system (7.15) and (7.16) lose the complete synchronization properties.

Proof. Considering the drive system (7.15) and (7.16), we have

$$\|Y_{n+1} - X_{n+1}\| \leq s A \|Y_n - X_n\|. \quad (7.17)$$

To have a complete synchronization, at first we need to clarify the concept of the norm of a

matrix. To find the behavior of the sequence of $\{A\}$, we need to look at the modulus of the largest eigenvalue of A . But, for the initial value $X_0 = \bar{0}$, we have $X_0 = X_1 = X_2 = \dots = X_n = \bar{0}$. So, (7.16) can be written as $Y_{n+1} = A(s Y_n)$. Thus, for \mathbb{R}^n to be the direct sum of $\mathbb{R}^n = V_{\lambda_1} \oplus V_{\lambda_2} \oplus \dots \oplus V_{\lambda_n}$ where λ_i are the eigenvalues of the matrix A , we have $Y_{n+1} = s A Y_n$. For the sequences Y_1, Y_2, \dots, Y_n , we have:

$$\begin{aligned} Y_1 &= s A Y_0 \\ Y_2 &= s A Y_1 = s A (s A) Y_0 = (s A)^2 Y_0 \\ &\vdots \\ Y_n &= (s A)^n Y_0 \end{aligned}$$

we need to find minimal k where $Y_0 \in V_{\lambda_{i_1}} \oplus V_{\lambda_{i_2}} \oplus \dots \oplus V_{\lambda_{i_k}}$. So, for $Y_0 = \sum_{j=1}^k v_j$ and for all $v_j \in V_{\lambda_{i_j}}$, we have $Y_n = \sum_{j=1}^k (s \lambda_{i_j})^n v_j$. So, for $A v_i = \lambda_{i_j} v_i$, we can write, $\lim_{n \rightarrow \infty} Y_n = 0$ if and only if $\lim_{n \rightarrow \infty} (s \lambda_{i_j})^n v_j = 0$ which gives us $|s \lambda_{i_j}| < 1$ if and only if $s \leq \frac{1}{|\lambda_{i_j}|}$. If Y_0 is generic, we get $s \leq \frac{1}{|\lambda|}$ for all λ which gives $s < \frac{1}{\rho(A)}$, where, $\rho(A)$ is the spectral radius of A and can be written as $\rho(A(n)) = \max |\lambda_i|$. Therefore, the threshold for (7.15) and (7.16) to be completely synchronized is $s < \frac{1}{\rho(A)} = \tilde{s}_1$. When we pass this threshold, two systems (7.15) and (7.16) cannot be completely synchronized anymore. \square

Now, for the non-linear discrete-time dynamical system, we are going to develop a theorem which helps us to find the synchronization threshold.

Theorem 7.2.12. *Given the non-linear coupled dynamical system (7.3), where the map $g : D \subseteq \mathbb{R}^n \rightarrow D \subseteq \mathbb{R}^n$, for the values $s < \tilde{s}_2 = \frac{1}{(\rho_A + \alpha)}$, we get*

$$\lim_{n \rightarrow \infty} \|Y_n - X_n\| = 0$$

means that passing the synchronization threshold \tilde{s}_2 makes the drive-response system (7.3) lose the complete synchronization properties.

Proof. Suppose the following C^r maps which have a fixed point at the origin:

$$X_{n+1} = A X_n + \hat{F}(X_n), \quad (7.18)$$

$$Y_{n+1} = A((1-s)X_n + sY_n) + \hat{F}((1-s)X_n + sY_n), \quad (7.19)$$

and the $\hat{F}(X_n) = \hat{F}_2(X_n) + \dots + \hat{F}_{r-1}(X_n) + O(\|X_n\|^r)$, which including the vector-valued homogeneous polynomials of degree $2, \dots, r$. Consider the following equation for the error:

$$\begin{aligned} e(n+1) &= Y_{n+1} - X_{n+1} = (1-s)AX_n + sAY_n - AX_n + \hat{F}((1-s)X_n + sY_n) - \hat{F}(X_n) \\ &= sA(Y_n - X_n) + \hat{F}((1-s)X_n + sY_n) - \hat{F}(X_n) \end{aligned}$$

By triangular inequality we can write:

$$\begin{aligned} \|e(n+1)\| &= \|sA(Y_n - X_n) + \hat{F}((1-s)X_n + sY_n) - \hat{F}(X_n)\| \\ &\leq s\rho_A \|Y_n - X_n\| + s\alpha \|Y_n - X_n\| \\ &= s\rho_A \|e(n)\| + s\alpha \|e(n)\| \end{aligned}$$

where, ρ_A is the spectral radius of A which is equal to $\rho_A = \max |\lambda_i|$ where λ is the root of characteristic polynomial or eigenvalue for A and $0 \leq \alpha < 1$ and $0 < s_i \leq 1$ (to find the behavior of the sequence of $\{A\}$, we need to look at the modulus of the largest eigenvalue of A). So,

$$\|e(n+1)\| \leq s\rho_A \|e(n)\| + s\alpha \|e(n)\|$$

We know that

$$\lim_{n \rightarrow \infty} \|e(n)\| = \lim_{n \rightarrow \infty} \|Y_n - X_n\| = 0$$

Therefore,

$$\|e(n+1)\| \leq s(\rho_A + \alpha) \|e(n)\|$$

Thus, for $s(\rho_A + \alpha) < 1$ we have

$$\lim_{n \rightarrow \infty} \|Y_n - X_n\| = 0$$

for which, $s < \frac{1}{(\rho_A + \alpha)} = \tilde{s}_2$. Here, $\tilde{s}_2 = \beta$, which we discussed in the beginning of this section. After passing \tilde{s}_2 , we lose the complete synchronization in system (7.3). \square

Lemma 7.2.13. *If drive system (7.15) becomes periodic. Then, for the values $s < \left(\frac{1}{\rho_A + \alpha}\right)^{\frac{1}{k}} := \tilde{s}_3$, where \tilde{s}_3 implies to the synchronization threshold, the non-linear coupled dynamical system (7.3) becomes completely synchronized. In other word,*

$$\lim_{n \rightarrow \infty} \|Y_n - X_n\| = 0$$

7.3 Synchronized cycles in Generalized Nicholson Bailey (GNB) model: Description of the Model

Generalized Nicholson Bailey (GNB) model is a generalization of the work presented by Beddington, Free and Lawton in 1975²¹⁰. They have investigated the complex dynamics of a host-parasitoid model which was an extension work of Nicholson-Bailey model in 1935²¹¹. This model depends on three biological parameters a , k and r and has the following form

$$H(n+1) = H(n) e^{r\left(1 - \frac{H(n)}{k}\right) - aP(n)} \quad P(n+1) = H(n) (1 - e^{-aP(n)}) \quad (7.20)$$

Where $H(n)$ presents the host population after being attacked by the parasitoid and $P(n)$ implies to the parasitoids population before they die because of biological reasons like short-

age of food and or some other natural biological reasons at the end of the season n . k is the carrying capacity and shows maximum population size that can be supported by availability of all the potentially limiting resources. It is usually limited by the intensity of light and space. The fractions of hosts not parasitized is $\exp(-aP(n))$ where a is called the searching efficiency which is the probability that a given parasitoid confronts a host whole of the life-time.

Here, we focus on the above model including a new parameter b which has the following form

$$H(n+1) = H(n) e^{r\left(1-\frac{H(n)}{k}\right)-bP(n)} \quad P(n+1) = H(n) (1 - e^{-aP(n)}) \quad (7.21)$$

Without loss of generality, we assume $b = r$ and follow the same model assumptions as Asheghi in 2014²¹². Therefore, (7.21) can be written as the form:

$$H(n+1) = H(n) e^{r\left(1-\frac{H(n)}{k}\right)-rP(n)} \quad P(n+1) = H(n) (1 - e^{-aP(n)}) \quad (7.22)$$

The local dynamics of system (7.22), have been studied by different authors numerically and analytically^{212;213}. We replace H, P in(7.22) with x, y respectively and re wright (7.22) as the following form

$$x(n+1) = x(n) e^{r\left(1-\frac{x(n)}{k}\right)-ry(n)} \quad y(n+1) = x(n) (1 - e^{-ay(n)}) \quad (7.23)$$

Now, we apply this coupling method on the system (7.23). Consider the following drive-response system:

$$x_1(n+1) = x_1(n) e^{r\left(1-\frac{x_1(n)}{k}\right)-ry_1(n)} \quad (7.24)$$

$$y_1(n+1) = x_1(n) (1 - e^{-ay_1(n)}) \quad (7.25)$$

$$x_2(n+1) = p e^{r\left(1-\frac{p}{k}\right)-rq} \quad (7.26)$$

$$y_2(n+1) = p (1 - e^{-aq}) \quad (7.27)$$

where

$$p = (1 - s)x_1(n) + sx_2(n) \quad (7.28)$$

$$q = (1 - s)y_1(n) + sy_2(n) \quad (7.29)$$

Here, $p : \mathbb{R}^2 \rightarrow \mathbb{R}$ and $q : \mathbb{R}^2 \rightarrow \mathbb{R}$ are two continuous functions. So, if we consider the drive system $G_1(x_1, y_1) : \mathbb{R}^2 \rightarrow \mathbb{R}^2$, the synchronized system would be $G_2(p, q) : \mathbb{R}^4 \rightarrow \mathbb{R}^2$, where $p = (x_1, x_2)$ and $q = (y_1, y_2)$. The local stability results for the drive system (7.24)-(7.25) and (7.26)-(7.27) are the same. To investigate the qualitative dynamics of the solutions of system (7.24)-(7.27), we use several dynamical systems tools.

7.3.1 Synchronized cycles in GNB model without parasitoid

Here, we show that in system (7.23), when the parasitoid populations go extinct (because of severe intraspecific competition or due to external factors), the dynamics of (7.23) inherits all different behaviors of Ricker curves from stable fixed point to cascade of period doubling bifurcations and then chaos^{214;215}. We rewrite the drive-response system (7.24)-(7.27) in one dimension as the following form:

$$x_1(n+1) = x_1(n) e^{r\left(1 - \frac{x_1(n)}{k}\right)} \quad (7.30)$$

$$x_2(n+1) = p e^{r\left(1 - \frac{p}{k}\right)} \quad (7.31)$$

where

$$p = (1 - s)x_1(n) + sx_2(n) \quad (7.32)$$

Here, $p : \mathbb{R}^2 \rightarrow \mathbb{R}$ is a continuous function. So, if we consider the drive system $R_1(x_1) : \mathbb{R} \rightarrow \mathbb{R}$, the synchronized system would be $R_2(p) : \mathbb{R}^2 \rightarrow \mathbb{R}$, where p is a function of x_1 and x_2 .

We have demonstrated the time-series corresponding to the solution of the drive-response system (7.30)-(7.31) in Figure (7.2). As we can see, with increasing the growth rate r , the

behavior of system changes from stable equilibrium point to periodic behavior and then to irregular and chaotic dynamics which was expected since the system (7.30)-(7.31) has the same form and so dynamics of Ricker model.

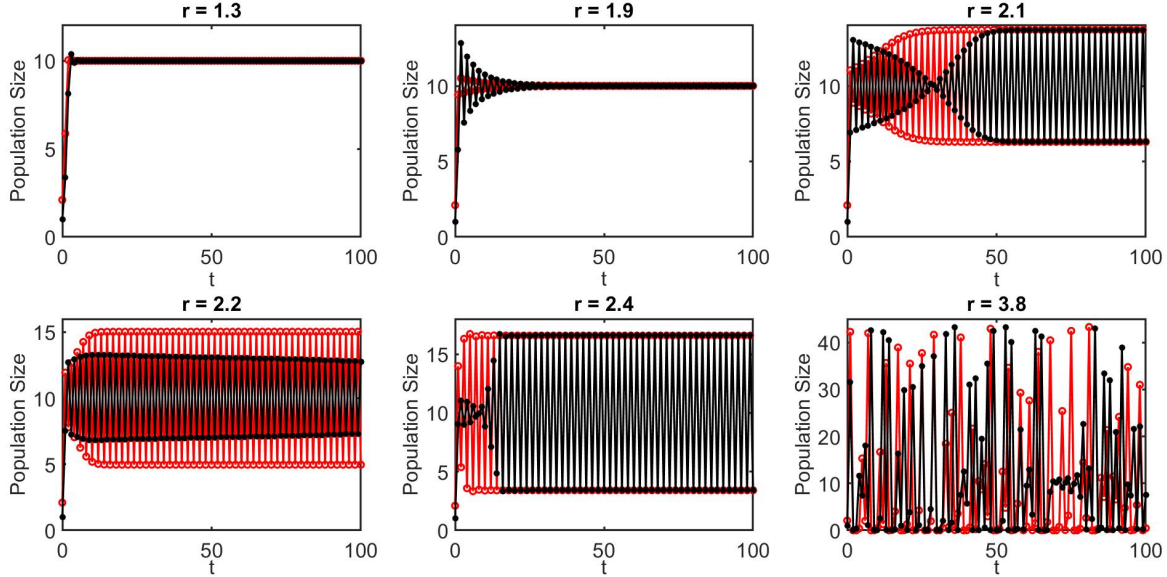


Figure 7.2: Evolution of host population x_1 and its coupled x_2 in time for for drive-response system (7.30)-(7.31) when $s = 0.95$, $k = 10$.

Furthermore, we performed a one co-dimensional bifurcation analysis for system (7.30)-(7.31) with respect to growth rate r in Figure (7.3)-a to discover the long term behavior of the system and we have compared the solution of drive system (7.30) with the response system (7.31) by showing the error between the solutions in Figure (7.3)-b. As we will discuss in section (7.4), when synchronization constant s is larger, the drive-response system can not be synchronized completely. Moreover, we have shown the Lyapunov Exponent corresponding the drive-response system (7.30)-(7.31) in Figure (7.3)-c which is the best place to investigate the stability or chaotic behavior of system (7.30)-(7.31). As we know, the negative Lyapunov Exponent implies to stable behavior and when it is positive, we expect to see chaotic behavior.

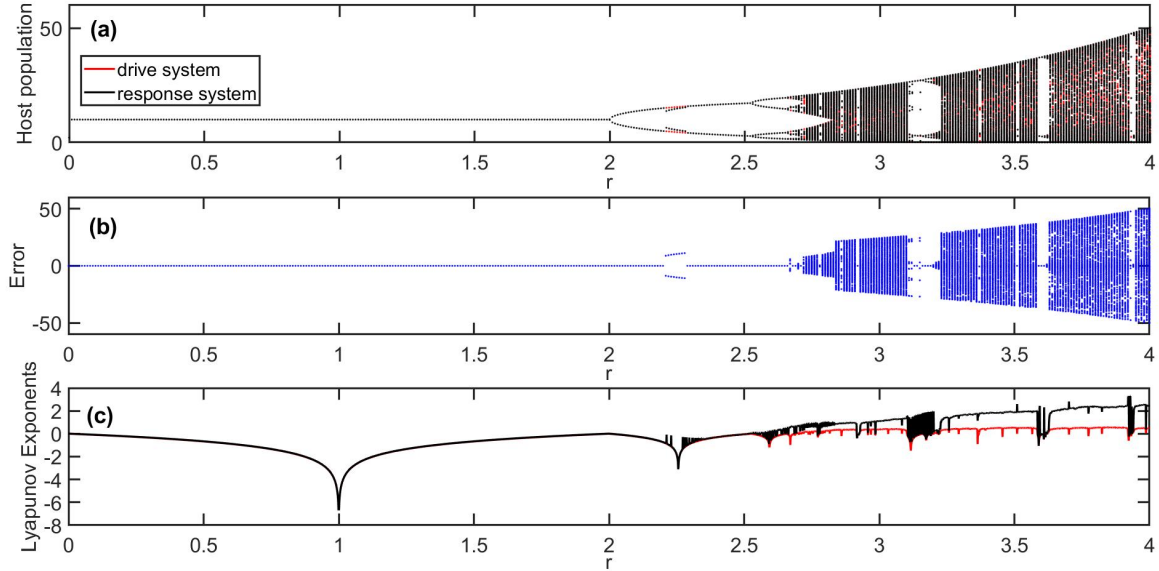


Figure 7.3: (a): bifurcation diagram for drive-response system (7.30)-(7.31) when $s = 0.95$, $k = 10$, red (drive system) and black (response system), (b): the error between the solutions of drive system and response system receptively, (c): the Lyapunov Exponent corresponding to drive-response system (7.30)-(7.31) when $s = 0.95$, $k = 10$, red (drive system) and black (response system).

7.4 Numerical simulations

In chaotic systems, it seems to not being possible to reproduce exactly the same initial conditions and parameters and force the orbits converge. However, in this section, we will numerically show that by using a sufficiently strong coupling method, we can change the track of the orbits to converge. Therefore, there exists a possible way to get a complete synchronization in chaotic systems whereas they have been coupled by a suitable coupling method.

In this section, we demonstrate some numerical simulation to describe the qualitative behavior of drive-response system (7.24) - (7.27). The orbits of the system (7.24) - (7.27) in chaotic regime can be considered as chaotic oscillations. Now we want to study the evolution of the dynamic variables x_1, x_2 corresponding to the host population of drive system and response system, and y_1, y_2 which are corresponding to the parasitoid population of drive system and response system respectively. All analysis and numerical simulations which have been conducted in this section, are expected to reveal the type of attractor from equilibrium

point, periodic and quasi-periodic orbits, and chaotic attractors for which the dynamics will eventually settle down and remain forever.

In Figure (7.4), we can see the evolution of the attractors of drive system (red color) and response system (black color) when we change the growth rate r . As we see, as long as we are increasing r , the dynamics of the system change from the stable equilibrium point which loses stability and arises to a limit cycle. This Figure demonstrates that the drive and response system with different initial conditions, and for the smaller value of the synchronization constant s , become completely synchronized.

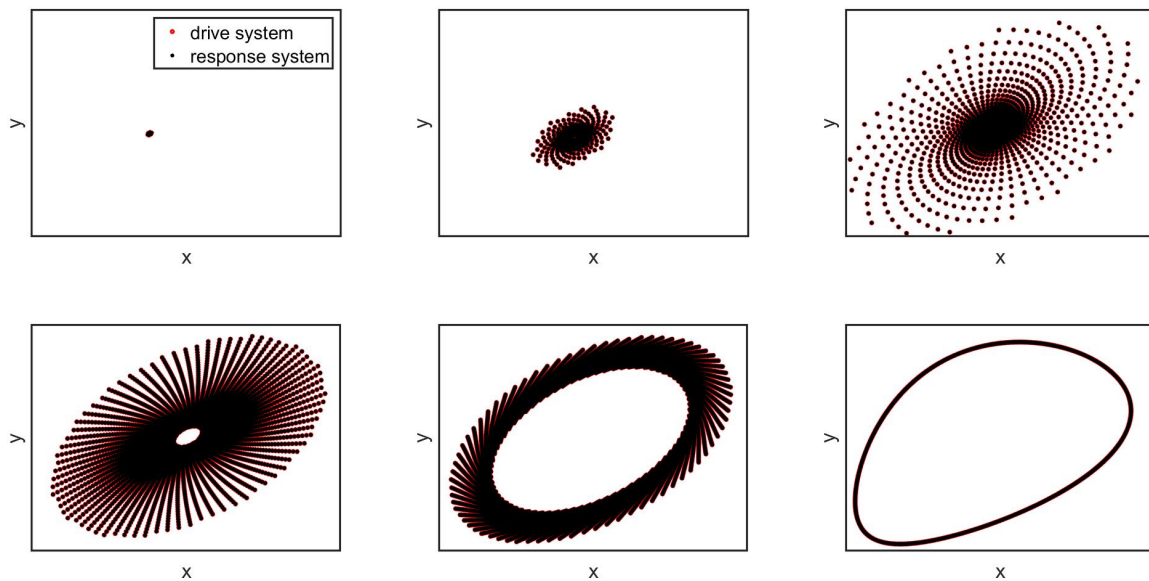


Figure 7.4: *Attractors for drive-response system (7.24)-(7.27) when $s = 0.5$, $a = 40$, $k = 10$, from up left side $r = 1.08, 1.087, 1.095$, and from down left side $r = 1.099, 1.1, 1.15$.*

In Figure (7.5), we increase the value of the synchronization constant s and we notice that two systems keep the same qualitative behavior from stable equilibrium point to limit cycle but they are not completely synchronized.

In Figure (7.6), we demonstrated the evolution of host population for drive-response system (7.24)-(7.27) (The interested parameters values have been selected from the given bifurcation diagram). For fixed parameter values $s = 0.5$, $a = 40$, $k = 10$, and different growth rate r , we can easily see how the time series for x_1, x_2 change from stable and periodic

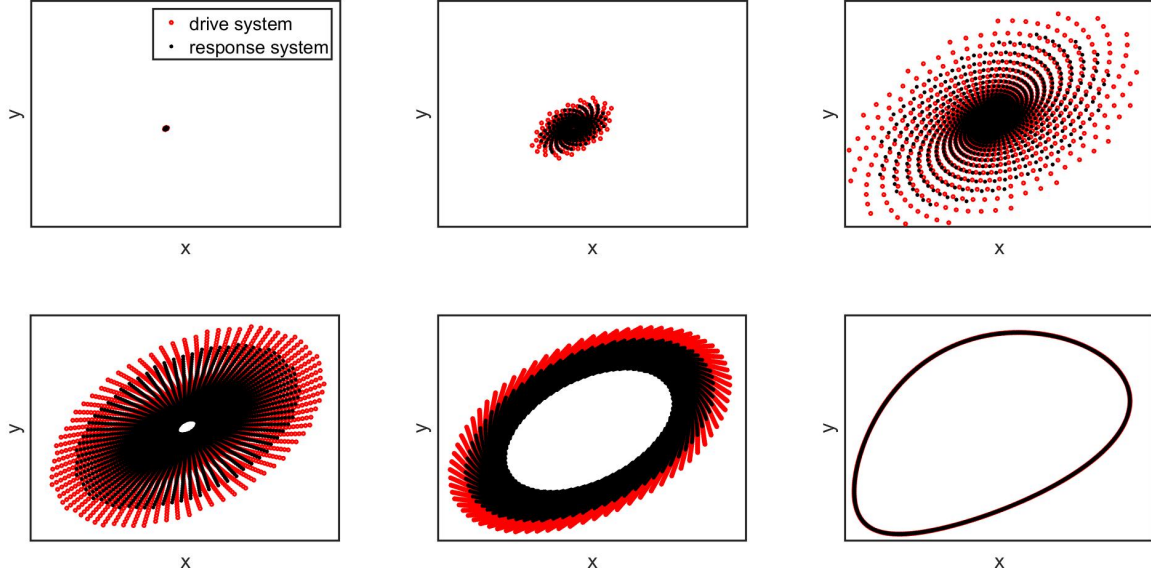


Figure 7.5: *Attractors for drive-response system (7.24)-(7.27) when $s = 0.99995$, $a = 40$, $k = 10$, from up left side $r = 1.08, 1.087, 1.095$, and from down left side $r = 1.099, 1.1, 1.15$.*

oscillations to chaotic motions. However, as we discussed before, for smaller synchronization constant s , both x_1 and its coupled x_2 are completely synchronized. With previous illustration about the chaotic synchronization, we conclude that using this method of coupling, we can expect to get a complete synchronization in chaotic regime for smaller synchronization constant s which this has been demonstrated for growth rate $r = 3.8$ in Figure (7.6).

However, when we compare Figure (7.6) with Figure (7.7), the coupling method which has been explained in section (7.2), is successful when the synchronization constant s has smaller values and is closer to zero. With increasing the synchronization constant s , we noticed that two convex functions (7.28) and (7.29) which we introduced in section (7.2) can not make a complete synchronization between the drive and response systems (7.24)-(7.27).

For different growth rate r , bifurcation diagrams for drive system (7.24), (7.25) and response system (7.26), (7.27), have been demonstrated for fixed synchronization constant $s = 0.5$ in Figure (7.8) and for fixed synchronization constant $s = 0.95$ in Figure (7.9). The one- co-dimensional bifurcation diagram helps us to know about the dependence of the

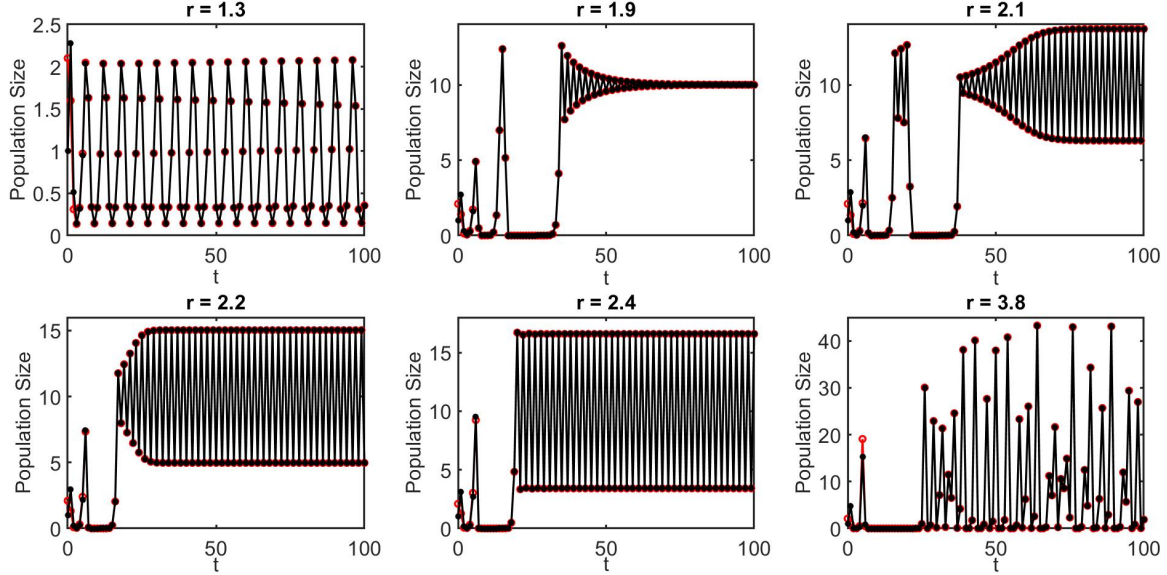


Figure 7.6: Evolution of host population x_1 and its coupled x_2 in time for drive-response system (7.24)-(7.27) when $s = 0.5$, $a = 40$, $k = 10$.

drive-response dynamical systems (7.24)-(7.27) on the certain parameter which here is the growth rate r .

Here, we are expecting to get completely synchronization for $s = 0.5$ (Figure (7.8)) and we do not expect to get a complete synchronization phase for $s = 0.95$ (Figure (7.9)).

As it can be easily seen in Figure (7.8) and Figure (7.9), the dynamics of host population for drive-response system (7.24)-(7.27), for some range of parameter values r and when $(y_1, y_2) = (0, 0)$ (without parasitoid), is similar to classical bifurcation diagram of Ricker model where the routes to chaos happen through the cascade of period-doubling bifurcations and crisis corresponding to the extinction of parasitoid for drive and response system. However, for smaller values of growth rate r , the host and parasitoid in both systems can coexist through the periodic and quasi-periodic cycles of the Neimark-Sacker bifurcation of interior steady states. In addition, we can easily observe that the sudden changes of attractors (crisis) happens frequently when we increase the parameter values of r .

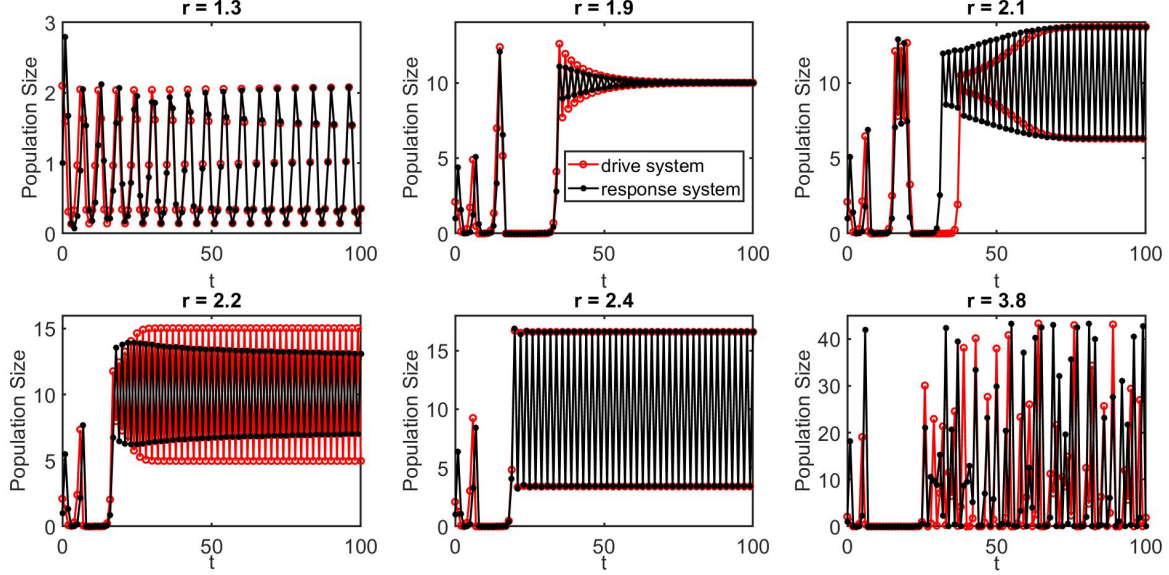


Figure 7.7: Evolution of host population x_1 and its coupled x_2 in time for drive-response system (7.24)-(7.27) when $s = 0.95$, $a = 40$, $k = 10$.

7.5 Conclusion

In this chapter, we developed a drive-response system by defining a convex continuous link function which maps the orbits of the drive system into the orbits of its coupled system and keeps the same qualitative dynamics. We found an appropriate normal form for drive-response system and we obtained the conditions under which the solutions of drive and response system become completely synchronized. We provided a new concept in chaos synchronization, called, synchronization threshold, means that the solutions of drive and response system diverge from each other and lose the complete synchronization properties when they pass the threshold. Furthermore, we studied a coupled discrete-time two dimensional host-parasitoid model which is a generalization of famous Nicholson-Bailey model. One of our objectives in this chapter was to investigate the rich dynamics of drive-response system (7.24)-(7.27) around its equilibrium points and achieving the chaos synchronization. We developed a new drive-response system by defining a convex continuous link function which maps the orbits of the drive system keeping the same qualitative properties such as stability and periodicity into the orbits of its coupled system. We observed that this coupling method can be successful for drive-response system (7.24)-(7.27) to get a complete

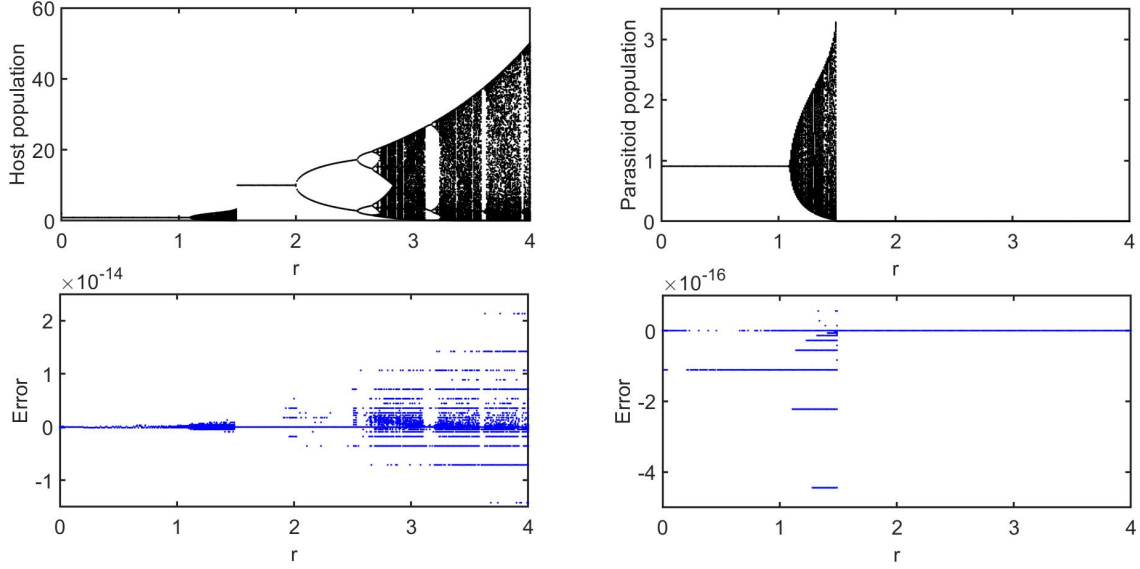


Figure 7.8: *Up: bifurcation diagram for drive-response system (7.24)-(7.27) for $a = 40$, $s = 0.5$, $k = 10$. Down: the error between the solutions of drive system and response system receptively*

synchronization when the synchronization constant has smaller values, closer to zero. Moreover, numerical verification is performed to show the existence of wide range of dynamics of drive-response system (7.24)-(7.27) around the positive equilibrium point. In addition, we changed the values of synchronization constant s in its range between $(0,1)$ and we observed that the response system (7.26)-(7.27) for smaller values of synchronization constant s is completely synchronized with its original drive system (7.24)-(7.25) and when we increased the values of synchronization constant s , we noticed that the qualitative behaviors of both systems remain the same, however, we do not get a complete synchronization between the solutions of drive and response system (7.24)-(7.27). In chaotic regime, for larger values of synchronization constant s , closer to one, we could not get a complete synchronization. But, for smaller synchronization constant s , closer to zero, we have shown that two systems are in complete synchronization when the dynamic is chaotic.

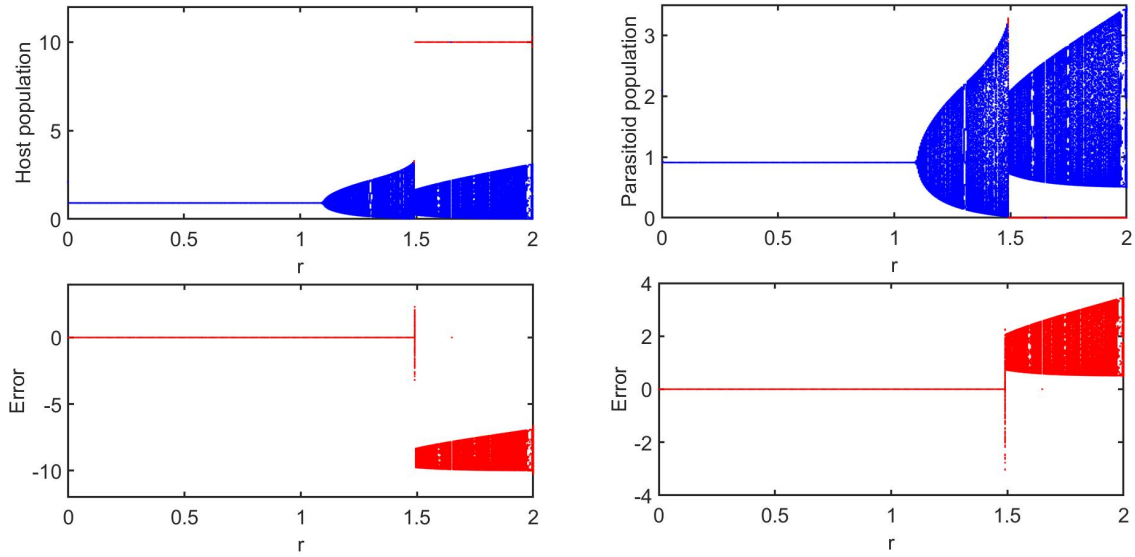


Figure 7.9: *Up: bifurcation diagram for drive-response system (7.24)-(7.27) for $a = 40$, $s = 0.95$, $k = 10$, red (drive system) and blue (response system). Down: the error between the solutions of drive system and response system receptively*

More Numerical Results

We have demonstrated different types of attractors of drive-response system (7.24)-(7.27) in Figure (7.10)-(7.13) when we are changing the threshold s .

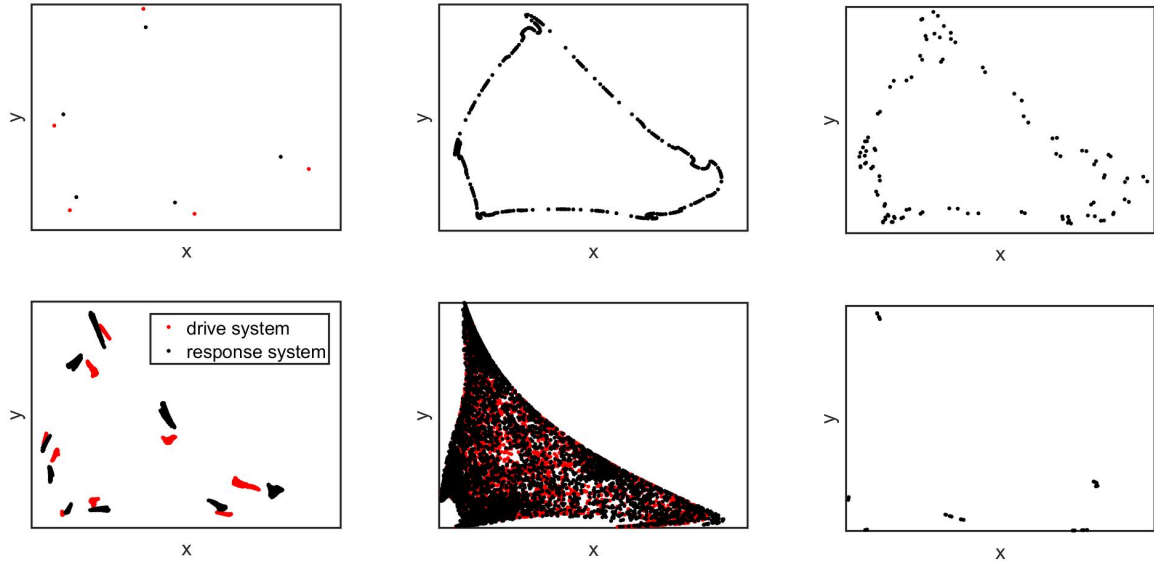


Figure 7.10: *Attractors for drive-response system (7.24)-(7.27) when $s = 0.94$, $a = 5$, $k = 1.5$, from up left side $r = 2.0, 2.2, 2.3$, and from down left side $r = 2.5, 2.7, 2.8$.*

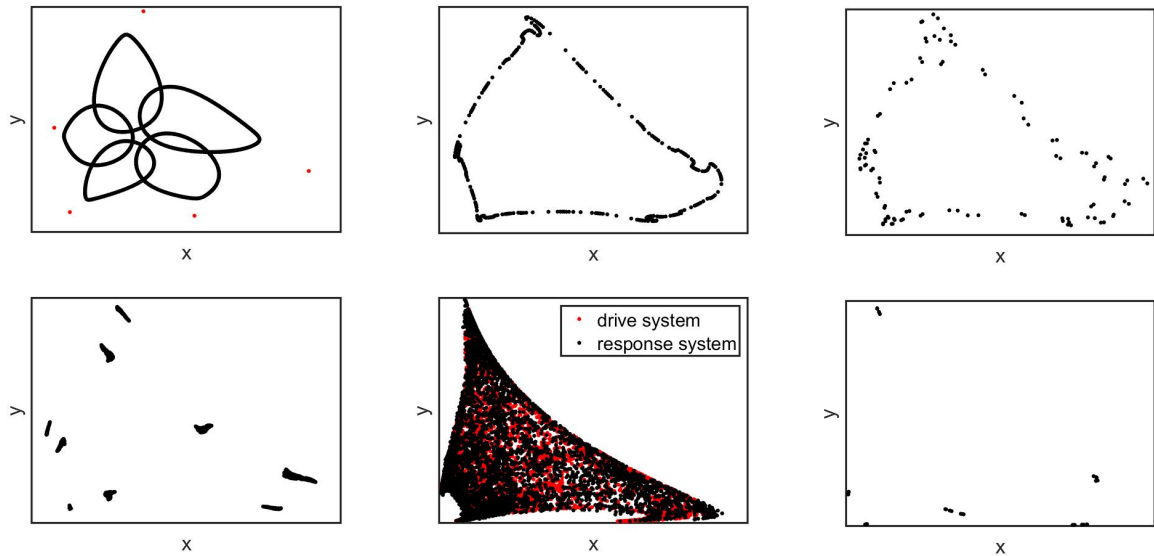


Figure 7.11: *Attractors for drive-response system (7.24)-(7.27) when $s = 0.95$, $a = 5$, $k = 1.5$, from up left side $r = 2.0, 2.2, 2.3$, and from down left side $r = 2.5, 2.7, 2.8$.*

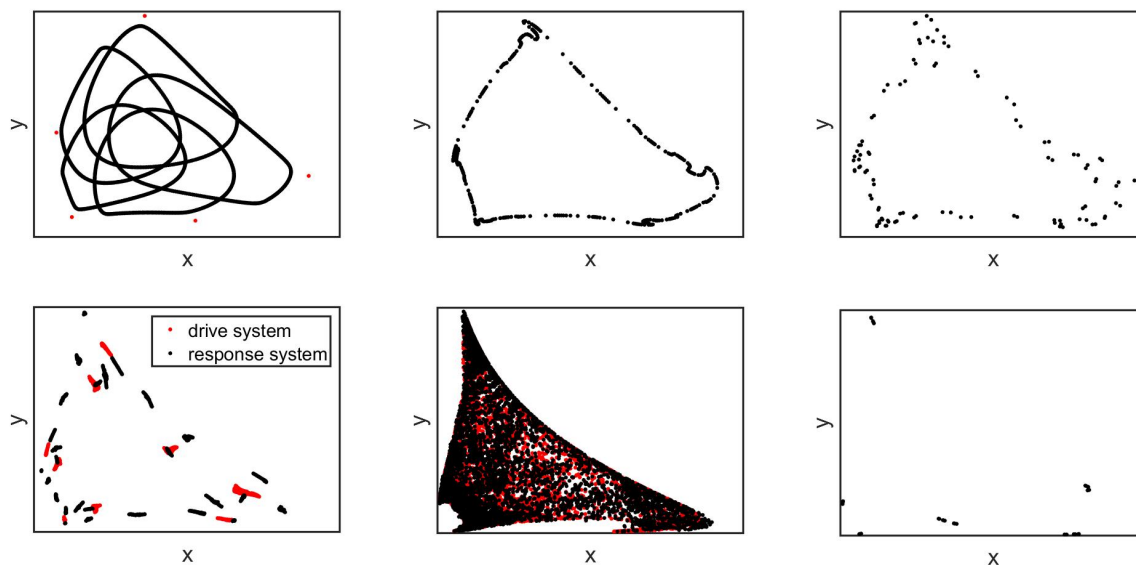


Figure 7.12: *Attractors for drive-response system (7.24)-(7.27) when $s = 0.96$, $a = 5$, $k = 1.5$, from up left side $r = 2.0, 2.2, 2.3$, and from down left side $r = 2.5, 2.7, 2.8$.*

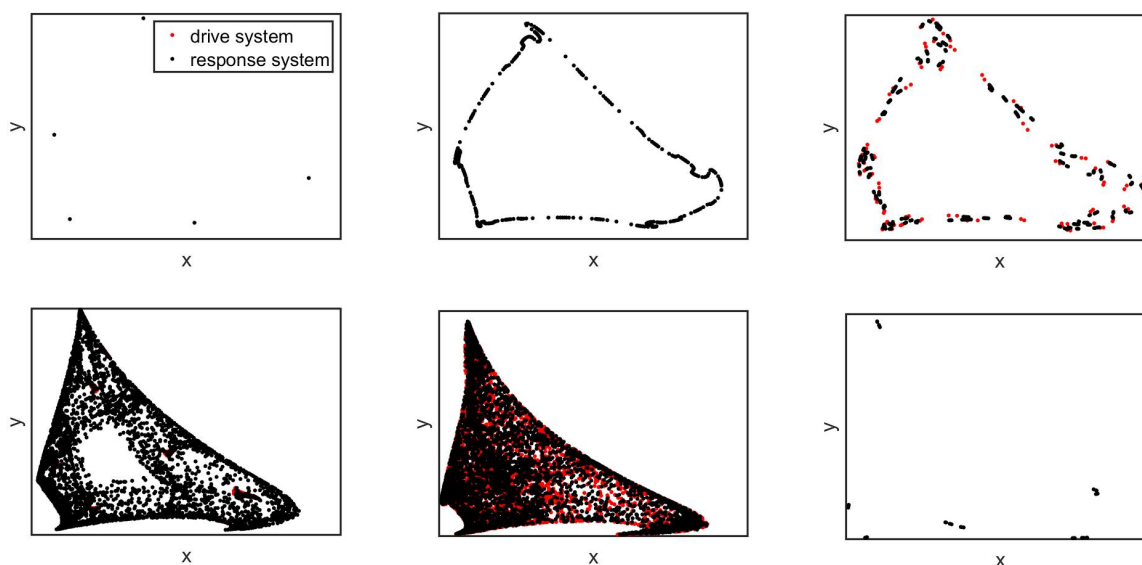


Figure 7.13: *Attractors for drive-response system (7.24)-(7.27) when $s = 0.99$, $a = 5$, $k = 1.5$, from up left side $r = 2.0, 2.2, 2.3$, and from down left side $r = 2.5, 2.7, 2.8$.*

Bibliography

- [1] Strogatz, Stephen. *Nonlinear dynamics and chaos: with applications to physics, biology, chemistry, and engineering (studies in nonlinearity)* 2001.
- [2] Strogatz, Steven H. *Nonlinear dynamics and chaos with student solutions manual: With applications to physics, biology, chemistry, and engineering* CRC press, 2018.
- [3] Rozhdestvensky, Kirill and Ryzhov, Vladimir and Fedorova, Tatiana and Safronov, Kirill and Tryaskin, Nikita and Sulaiman, Shaharin Anwar and Ovinis, Mark and Hassan, Suhaimi. *Computer Modeling and Simulation of Dynamic Systems Using Wolfram System Modeler* Springer, 2020.
- [4] Guckenheimer, John and Holmes, Philip. *Nonlinear oscillations, dynamical systems, and bifurcations of vector fields* Springer Science & Business Media, 42, 2013.
- [5] Wiggins, Stephen. *Introduction to applied nonlinear dynamical systems and chaos* Springer Science & Business Media, 2, 2003.
- [6] LaSalle, Joseph P. *The stability of dynamical systems* Siam, 25, 1976.
- [7] Shub, Michael. *Global stability of dynamical systems* Springer Science & Business Media, 2013.
- [8] Michel, Anthony N and Hou, Ling and Liu, Derong. *Stability of dynamical systems* Springer, 2008.
- [9] Kuznetsov, Yuri A. *Elements of applied bifurcation theory* Springer Science & Business Media, 112, 2013.
- [10] Zhang, Huaguang and Liu, Derong and Wang, Zhiliang. *Controlling chaos: suppression, synchronization and chaotification* Springer Science & Business Media, 2009.

- [11] Wang, Xiao Fan and Chen, Guanrong. *Chaotification via arbitrarily small feedback controls: Theory, method, and applications*. International Journal of Bifurcation and Chaos, World Scientific, 10(03):549-570, 2000.
- [12] Chen, Hsien-Keng and Lin, Tsung-Nan and Chen, Juhn-Horng. *Dynamic analysis, controlling chaos and chaotification of a SMIB power system*. Chaos, Solitons & Fractals, Elsevier, 24(5):1307-1315, 2005.
- [13] Liu, Yi and Anderson, Brian DO. *Singular perturbation approximation of balanced systems*. International Journal of Control, Taylor & Francis, 50(4):1379-1405, 1989.
- [14] Yedavalli, RK. *Perturbation bounds for robust stability in linear state space models*. International Journal of Control, Taylor & Francis, 42(6):1507-1517, 1985.
- [15] Feit, MD and Fleck Jr, JA. *Wave packet dynamics and chaos in the Hénon–Heiles system*. The Journal of chemical physics, American Institute of Physics, 80(6):2578-2584, 1984.
- [16] Ozaki, Jiro and Kurosaki, Satoru. *Periodic Orbits of Hénon Heiles Hamiltonian: Bifurcation Phenomenon*. Progress of theoretical physics, Oxford University Press, 95(3):519-529, 1996.
- [17] Zotos, Euaggelos E. *Classifying orbits in the classical Hénon–Heiles Hamiltonian system*. Nonlinear Dynamics, Springer, 79(3):1665-1677, 2015.
- [18] Zotos, Euaggelos E. *An overview of the escape dynamics in the Hénon–Heiles Hamiltonian system*. Meccanica, Springer, 52(11-12):2615-2630, 2017.
- [19] Kovacic, Ivana and Brennan, Michael J. *The Duffing equation: nonlinear oscillators and their behaviour*. John Wiley & Sons, 2011.
- [20] Wiggins, Stephen. *Chaos in the quasiperiodically forced Duffing oscillator*. Physics Letters A, Elsevier, 124(3): 138-142, 1987.

- [21] Nayfeh, Ali H and Sanchez, Nestor E. *Bifurcations in a forced softening Duffing oscillator*. International Journal of Non-Linear Mechanics, Elsevier, 24(6): 483-497, 1989.
- [22] Korsch, Hans Jürgen and Jodl, Hans-Jörg and Hartmann, Timo. *Chaos: a program collection for the PC*. Springer Science & Business Media, 2007.
- [23] Tsatsos, Marios. *Theoretical and Numerical study of the Van der Pol equation*. Doctoral desertation, Aristotle University of Thessaloniki, 2006.
- [24] Guckenheimer, John. *Dynamics of the van der Pol equation*. IEEE Transactions on Circuits and Systems, IEEE, 27(11): 983-989, 1980.
- [25] Guckenheimer, John and Hoffman, Kathleen and Weckesser, Warren. *The forced van der Pol equation I: The slow flow and its bifurcations*. SIAM Journal on Applied Dynamical Systems, SIAM, 2(1): 1-35, 2003.
- [26] Zaslavsky, George M and Zaslavskij, Georgij Moiseevič. *Hamiltonian chaos and fractional dynamics*. Oxford University Press on Demand, 2005.
- [27] Combescure, M. *Hamiltonian chaos and fractional dynamics*. Journal of Physics. A, Mathematical and General, 38(23): 5380, 2005.
- [28] Izhikevich, Eugene M. *Dynamical systems in neuroscience*. MIT press, 2007.
- [29] Izhikevich, Eugene M. *Simple model of spiking neurons*. IEEE Transactions on neural networks, IEEE, 14(6):11569-1572, 2003.
- [30] Izhikevich, Eugene M. *Which model to use for cortical spiking neurons?*. IEEE transactions on neural networks, , 15(5):1063-1070, 2004. Eugene
- [31] Izhikevich, M. *Neural excitability, spiking and bursting*. International Journal of Bifurcation and Chaos, World Scientific, 10(06):1171-1266, 2000.
- [32] Hoppensteadt, Frank C and Izhikevich, Eugene M. *Weakly connected neural networks*. Nonlinear Analysis: Real World Applications, Springer Science & Business Media, 126, 2012.

- [33] Hodgkin, Alan L. *The local electric changes associated with repetitive action in a non-medullated axon*. The Journal of physiology, Wiley Online Library, 107(2):165-181, 1948.
- [34] Hodgkin, Alan L and Huxley, Andrew F. *A quantitative description of membrane current and its application to conduction and excitation in nerve*. The Journal of physiology, Wiley Online Library, 117(4):500-544, 1952.
- [35] Rinzel, John and Ermentrout, G Bard. *Analysis of neural excitability and oscillations*, MIT Press, Cambridge, MA, 1989.
- [36] Rinzel, John and Ermentrout, G Bard. *Analysis of neural excitability and oscillations*. Methods in neuronal modeling, MIT press Cambridge, MA, 2:251-292, 1998.
- [37] Ermentrout, G Bard and Terman, David H. *Mathematical foundations of neuroscience*. Springer Science & Business Media, 35, 2010.
- [38] Ermentrout, Bard. *Type I membranes, phase resetting curves, and synchrony*. Neural computation, MIT Press, 8(5):979-1001, 1996.
- [39] Morris, Catherine and Lecar, Harold. *Voltage oscillations in the barnacle giant muscle fiber*. Biophysical journal, Elsevier, 35(1):193-213, 1981.
- [40] FitzHugh, Richard. *Impulses and physiological states in theoretical models of nerve membrane*. Biophysical journal, Elsevier, 1(6):445-466, 1961.
- [41] Kuznetsov, Yuri A. *Elements of applied bifurcation theory*. Springer Science & Business Media, 112, 2013.
- [42] Wiggins, Stephen. *Introduction to applied nonlinear dynamical systems and chaos*. Springer Science & Business Media, 2, 2003.
- [43] Gerstner, Wulfram and Kistler, Werner M. *Spiking neuron models: Single neurons, populations, plasticity*. Cambridge university press, 2002.

- [44] Dayan, Peter and Abbott, Laurence F and others. *Theoretical neuroscience*. Cambridge, MA: MIT Press, 806, 2001.
- [45] Nagumo, Jinichi and Arimoto, Suguru and Yoshizawa, Shuji. *An active pulse transmission line simulating nerve axon*. Proceedings of the IRE, IEEE, 50(10):2061-2070, 1962.
- [46] Earn, David JD and Rohani, Pejman and Bolker, Benjamin M and Grenfell, Bryan T. *Polymeric and ceramic nanoparticles in biomedical applications*. Journal of Nanotechnology, Hindawi, 2012, 2012.
- [47] Biswas, Amit Kumer and Islam, Md Reazul and Choudhury, Zahid Sadek and Mostafa, Asif and Kadir, Mohammad Fahim. *Nanotechnology based approaches in cancer therapeutics*. Advances in Natural Sciences: Nanoscience and Nanotechnology, IOP Publishing, 5(4):043001, 2014.
- [48] Pitchaimani, Arunkumar and Nguyen, Tuyen Duong Thanh and Marasini, Ramesh and Eliyapura, Achini and Azizi, Tahmineh and Jaber-Douraki, Majid and Aryal, Santosh. *Biomimetic natural killer membrane camouflaged polymeric nanoparticle for targeted bioimaging*. Advanced Functional Materials, Wiley Online Library, 29(4):1806817, 2019.
- [49] Riviere, Jim E and Jaber-Douraki, Majid and Lillich, James and Azizi, Tahmineh and Joo, Hyun and Choi, Kyoungju and Thakkar, Ravi and Monteiro-Riviere, Nancy A. *Modeling gold nanoparticle biodistribution after arterial infusion into perfused tissue: effects of surface coating, size and protein corona*. Nanotoxicology, Taylor & Francis, 12(10):1093-1112, 2018.
- [50] Moreno-Vega, Aura-Ileana and Gomez-Quintero, Teresa and Nunez-Anita, Rosa-Elvira and Acosta-Torres, Laura-Susana and Castaño, Víctor. *Nanoparticles for radiation therapy enhancement: the key parameters*. Theranostics, Ivyspring International Publisher, 9(5):1030, 2015.

- [51] Shubhika, Kwatra. *Nanotechnology and medicine-The upside and the downside*. Int. J. Drug Dev. Res., Citeseer, 5, 1-10, 2012.
- [52] Mauricio, MD and Guerra-Ojeda, S and Marchio, P and Valles, SL and Aldasoro, M and Escribano-Lopez, I and Herance, JR and Rocha, M and Vila, JM and Victor, VM. *Nanoparticles in medicine: a focus on vascular oxidative stress*. Oxidative medicine and cellular longevity, Hindawi, 2018, 2018.
- [53] Marino, Simeone and Hogue, Ian B and Ray, Christian J and Kirschner, Denise E. *A methodology for performing global uncertainty and sensitivity analysis in systems biology*. Journal of theoretical biology, Elsevier, 254(1):178-196, 2008.
- [54] Blower, Sally M and Dowlatabadi, Hadi. *Sensitivity and uncertainty analysis of complex models of disease transmission: an HIV model, as an example*. International Statistical Review/Revue Internationale de Statistique, JSTOR, 3(5-6):229-243, 1994.
- [55] Zi, Zhike. *Sensitivity analysis approaches applied to systems biology models*. IET systems biology, IET, 5(6):336-346, 2011.
- [56] Dalberg, Jack and Gimenez, Harrison and Keeley, Anna and Azizi, Tahmineh and Xi, Xuan and Jaber-Douraki, Majid. *Local and Global Dynamics of Discrete Type 1 Diabetes Model*. 2019.
- [57] Azizi, T and others. *Dynamics of a discrete-time plant-herbivore model*. Caspian Journal of Mathematical Sciences (CJMS), 4(2):241-256, 2015.
- [58] Zhao, P and Zhang, L and Grillo, JA and Liu, Q and Bullock, JM and Moon, YJ and Song, P and Brar, SS and Madabushi, R and Wu, TC and others. *Applications of physiologically based pharmacokinetic (PBPK) modeling and simulation during regulatory review*. Clinical Pharmacology & Therapeutics, Wiley Online Library, 89(2):259-267, 2011.
- [59] Barrett, JS and Della Casa Alberighi, O and Läer, S and Meibohm, B. *Physiologically*

based pharmacokinetic (PBPK) modeling in children. Clinical Pharmacology & Therapeutics, Wiley Online Library, 92(1):40-49, 2012.

- [60] Wagner, C and Zhao, P and Pan, Y and Hsu, V and Grillo, J and Huang, SM and Sinha, V. *Application of physiologically based pharmacokinetic (PBPK) modeling to support dose selection: report of an FDA public workshop on PBPK.* CPT: pharmacometrics & systems pharmacology, Wiley Online Library, 4(4):226-230, 2015.
- [61] Sobol, Ilya M. *Sensitivity estimates for nonlinear mathematical models.* Mathematical modelling and computational experiments, 4(1):407-414, 1993.
- [62] Saltelli, Andrea and Tarantola, Stefano and Campolongo, Francesca and Ratto, Marco. *Sensitivity analysis in practice: a guide to assessing scientific models.* Wiley Online Library, 1, 2004.
- [63] Lin, Z and Gehring, R and Mochel, JP and Lave, T and Riviere, JE. *Mathematical modeling and simulation in animal health—Part II: principles, methods, applications, and value of physiologically based pharmacokinetic modeling in veterinary medicine and food safety assessment.* Journal of veterinary pharmacology and therapeutics, Wiley Online Library, 39(5):421-438, 2016.
- [64] Lin, Zhoumeng and Li, Mengjie and Gehring, Ronette and Riviere, Jim E. *Development and application of a multiroute physiologically based pharmacokinetic model for oxytetracycline in dogs and humans.* Journal of pharmaceutical sciences, Elsevier, 104(1):233-243, 2015.
- [65] Brown, Ronald P and Delp, Michael D and Lindstedt, Stan L and Rhomberg, Lorenz R and Beliles, Robert P. *Physiological parameter values for physiologically based pharmacokinetic models.* Toxicology and industrial health, Sage Publications Sage CA: Thousand Oaks, CA, 13(4):407-484, 1997.
- [66] Lankveld, Danille PK and Oomen, Agnes G and Krystek, P and Neigh, A and Troost-de Jong, A and Noorlander, CW and Van Eijkeren, JCH and Geertsma, RE and De

- Jong, WH. *The kinetics of the tissue distribution of silver nanoparticles of different sizes*. Biomaterials, Elsevier, 31(32):8350-8361, 2010.
- [67] Meek, ME Bette and Barton, Hugh A and Bessems, Jos G and Lipscomb, John C and Krishnan, Kannan. *Case study illustrating the WHO IPCS guidance on characterization and application of physiologically based pharmacokinetic models in risk assessment*. Regulatory Toxicology and Pharmacology, Elsevier, 66(1):116-129, 2013.
- [68] Lee, Hyun A and Leavens, Teresa L and Mason, Sharon E and Monteiro-Riviere, Nancy A and Riviere, Jim E. *Comparison of quantum dot biodistribution with a blood-flow-limited physiologically based pharmacokinetic model*. Nano letters, ACS Publications, 9(2):794-799, 2009.
- [69] Lin, Pinpin and Chen, Jein-Wen and Chang, Louis W and Wu, Jui-Pin and Redding, Laurel and Chang, Han and Yeh, Teng-Kuang and Yang, Chung Shi and Tsai, Ming-Hsien and Wang, Hsiu-Jen and others. *Computational and ultrastructural toxicology of a nanoparticle, Quantum Dot 705, in mice*. Environmental science & technology, ACS Publications, 42(16):6264-6270, 2008.
- [70] Riviere, J Edmond and Bowman, Karl F and Monteiro-Riviere, Nancy A and Dix, LYNN P and Carver, Michael P. *The isolated perfused porcine skin flap (IPPSF) I. A novel in vitro model for percutaneous absorption and cutaneous toxicology studies*. Toxicological Sciences, Oxford University Press, 7(3):444-453, 1986.
- [71] Riviere, Jim E and Leavens, Teresa L and Brooks, James D and Monteiro-Riviere, Nancy A. *Acute vascular effects of nanoparticle infusion in isolated perfused skin*. Nanomedicine: Nanotechnology, Biology and Medicine, Elsevier, 8(4):428-431, 2012.
- [72] Lee, Hyun A and Imran, Mudassar and Monteiro-Riviere, Nancy A and Colvin, Vicki L and Yu, William W and Riviere, Jim E. *Biodistribution of quantum dot nanoparticles in perfused skin: evidence of coating dependency and periodicity in arterial extraction*. Nano letters, ACS Publications, 7(9):2865-2870, 2007.

- [73] Sacks, Thomas and Moldow, Ch F and Craddock, Ph R and Bowers, TK and Jacob, Harry S. *Oxygen radicals mediate endothelial cell damage by complement-stimulated granulocytes. An in vitro model of immune vascular damage.* The Journal of clinical investigation, Am Soc Clin Investig, 61(5):1161-1167, 1978.
- [74] Blackman, Brett R and Garcí a-Carden a, Guillermo and Gimbrone Jr, Michael A. *A new in vitro model to evaluate differential responses of endothelial cells to simulated arterial shear stress waveforms.* J. Biomech. Eng., Elsevier, 124(4):397-407, 2002.
- [75] Gaillard, Pieter Jaap and Voorwinden, Levina Helena and Nielsen, Jette Lyngholm and Ivanov, Alexei and Atsumi, Ryo and Engman, Helena and Ringbom, Carina and de Boer, Albertus Gerrit and Breimer, Douwe Durk. *Establishment and functional characterization of an in vitro model of the blood–brain barrier, comprising a co-culture of brain capillary endothelial cells and astrocytes.* European journal of pharmaceutical sciences, Elsevier, 12(3):215-222, 2001.
- [76] Kumar, TR Santhosh and Krishnan, Lissy K. *Endothelial cell growth factor (ECGF) enmeshed with fibrin matrix enhances proliferation of EC in vitro.* Biomaterials, Elsevier, 22(20):2769-2776, 2001.
- [77] Williams, Patrick L and Riviere, J Edmond. *Definition of a physiologic pharmacokinetic model of cutaneous drug distribution using the isolated perfused porcine skin flap.* Journal of pharmaceutical sciences, Wiley Online Library, 78(7):550-555, 1989.
- [78] Lenhart, Suzanne and Workman, John T. *Optimal control applied to biological models.* CRC press, 2007.
- [79] Chachuat, Benoit. *Nonlinear and dynamic optimization: From theory to practice.* 2007.
- [80] Zabczyk, Jerzy. *Mathematical control theory, Modern Birkhäuser Classics.* Birkhäuser Boston Inc., Boston, MA, 2008.
- [81] Rodrigues, Helena Sofia. *Optimal control and numerical optimization applied to epidemiological models.* arXiv preprint arXiv:1401.7390, 2014.

- [82] Pontryagin, Lev Semenovich. *Mathematical theory of optimal processes*. Routledge, 2018.
- [83] Clarke, Frank H. *Optimization and nonsmooth analysis*. SIAM, 1990.
- [84] Fleming, WH and Rishel, RW and Marchuk, GI and Balakrishnan, AV and Borovkov, AA and Makarov, VL and Rubinov, AM and Liptser, RS and Shiriyayev, AN and Krassovsky, NN and others. *Applications of mathematics*. Deterministic and Stochastic Optimal Control, Springer-Verlag Berlin 1975.
- [85] Kamien, Morton I and Schwartz, Nancy Lou. *Dynamic optimization: the calculus of variations and optimal control in economics and management*. Courier Corporation, 2012.
- [86] Rao, Anil V. *A survey of numerical methods for optimal control*. Advances in the Astronautical Sciences, Univelt, Inc. 135(1):497-528, 2009.
- [87] Betts, John T. *Practical methods for optimal control and estimation using nonlinear programming*. SIAM, 2010.
- [88] Marino, Simeone and Hogue, Ian B and Ray, Christian J and Kirschner, Denise E. *A methodology for performing global uncertainty and sensitivity analysis in systems biology*. Journal of theoretical biology, Elsevier, 254(1):178-196, 2008.
- [89] Blower, Sally M and Dowlatabadi, Hadi. *Sensitivity and uncertainty analysis of complex models of disease transmission: an HIV model, as an example*. International Statistical Review/Revue Internationale de Statistique, JSTOR, 3(5-6):229-243, 1994.
- [90] Zi, Zhike. *Sensitivity analysis approaches applied to systems biology models*. IET systems biology, IET, 5(6):336-346, 2011.
- [91] Sobol, Ilya M. *Sensitivity estimates for nonlinear mathematical models*. Mathematical modelling and computational experiments, 4(1):407-414, 1993.
- [92] Saltelli, Andrea and Tarantola, Stefano and Campolongo, Francesca and Ratto, Marco. *Sensitivity analysis in practice: a guide to assessing scientific models*. Wiley Online Library, 1, 2004.

- [93] Urabe, Chiyori T and Tanaka, Gouhei and Aihara, Kazuyuki and Mimura, Masayasu. *Parameter scaling for epidemic size in a spatial epidemic model with mobile individuals*. Public Library of Science San Francisco, CA USA, PLoS One, 11(12):e0168127, 2017.
- [94] Li, Gui-Hua and Zhang, Yong-Xin. *Dynamic behaviors of a modified SIR model in epidemic diseases using nonlinear incidence and recovery rates*. Public Library of Science San Francisco, PLoS One, 12(4):e0175789, 2016.
- [95] Huang, Chuangxia and Cao, Jie and Wen, Fenghua and Yang, Xiaoguang. *Stability analysis of SIR model with distributed delay on complex networks*. Public Library of Science San Francisco, PLoS One, 11(8):e0158813, 2016.
- [96] Bauch, Chris and d'Onofrio, Alberto and Manfredi, Piero. *Behavioral epidemiology of infectious diseases: an overview, Modeling the interplay between human behavior and the spread of infectious diseases*. Springer, 1-19, 2013.
- [97] Kirk, Donald E. *Optimal control theory: an introduction*. Courier Corporation, 2004.
- [98] Bryson, Arthur E. *Optimal control-1950 to 1985*. IEEE Control Systems Magazine, IEEE, 16(3):26-33, 1996.
- [99] Rodrigues, Helena Sofia. *Optimal control and numerical optimization applied to epidemiological models*. arXiv preprint arXiv:1401.7390, 2014.
- [100] Pontryagin, Lev Semenovich. *Mathematical theory of optimal processes*. Routledge, 2018.
- [101] Leitmann, George. *The calculus of variations and optimal control: an introduction*. IEEE Control Systems Magazine, Springer Science & Business Media, 24, 2013.
- [102] Rao, Anil V. *A survey of numerical methods for optimal control*. Advances in the Astronautical Sciences, Univelt, Inc. 135(1):497-528, 2009.
- [103] Betts, John T. *Practical methods for optimal control and estimation using nonlinear programming*. SIAM, 2010.

- [104] Kermack, William Ogilvy and McKendrick, Anderson G. *A contribution to the mathematical theory of epidemics*. Proceedings of the royal society of london. Series A, Containing papers of a mathematical and physical character, The Royal Society London, 115(772):700-721, 1927.
- [105] Gallina, Riccardo. *Dynamic models for the analysis of epidemic spreads Modelli dinamici per l'analisi di diffusioni epidemiche*. 2012.
- [106] Lenhart, Suzanne and Workman, John T. *Optimal control applied to biological models*. CRC press, 2007.
- [107] Chachuat, Benoit. *Nonlinear and dynamic optimization: From theory to practice*. 2007.
- [108] Zabczyk, Jerzy. *Mathematical control theory, Modern Birkhäuser Classics*. Birkhäuser Boston Inc., Boston, MA, 2008.
- [109] Clarke, Frank H. *Optimization and nonsmooth analysis*. SIAM, 1990.
- [110] Fleming, WH and Rishel, RW and Marchuk, GI and Balakrishnan, AV and Borovkov, AA and Makarov, VL and Rubinov, AM and Liptser, RS and Shirayayev, AN and Krassovsky, NN and others. *Applications of mathematics. Deterministic and Stochastic Optimal Control*, Springer-Verlag Berlin 1975.
- [111] Kamien, Morton I and Schwartz, Nancy Lou. *Dynamic optimization: the calculus of variations and optimal control in economics and management*. Courier Corporation, 2012.
- [112] Marino, Simeone and Hogue, Ian B and Ray, Christian J and Kirschner, Denise E. *A methodology for performing global uncertainty and sensitivity analysis in systems biology*. Journal of theoretical biology, Elsevier, 254(1):178-196, 2008.
- [113] Blower, Sally M and Dowlatabadi, Hadi. *Sensitivity and uncertainty analysis of complex models of disease transmission: an HIV model, as an example*. International Statistical Review/Revue Internationale de Statistique, JSTOR, 3(5-6):229-243, 1994.

- [114] Zi, Zhike. *Sensitivity analysis approaches applied to systems biology models*. IET systems biology, IET, 5(6):336-346, 2011.
- [115] Azizi, Tahmineh and Mugabi, Robert. *Global Sensitivity Analysis in Physiological Systems*. Applied Mathematics, Scientific Research Publishing, 11(3):119-136, 2020.
- [116] Sobol, Ilya M. *Sensitivity estimates for nonlinear mathematical models*. Mathematical modelling and computational experiments, 4(1):407-414, 1993.
- [117] Saltelli, Andrea and Tarantola, Stefano and Campolongo, Francesca and Ratto, Marco. *Sensitivity analysis in practice: a guide to assessing scientific models*. Wiley Online Library, 1, 2004.
- [118] Liu, Hua and Zhang, Kai and Ye, Yong and Wei, Yumei and Ma, Ming. *Dynamic complexity and bifurcation analysis of a host-parasitoid model with Allee effect and Holling type III functional response*. Advances in Difference Equations, Springer, 2019(1):507, 2019.
- [119] Smith, HL. *Planar competitive and cooperative difference equations*. Journal of Difference Equations and Applications, Taylor & Francis, 3(5-6):335-357, 1998.
- [120] Luís, Rafael and Elaydi, Saber and Oliveira, Henrique. *Stability of a Ricker-type competitive model and the competitive exclusion principle*. Journal of Difference Equations and Applications, Taylor & Francis, 5(6):636-660, 2011.
- [121] Gyllenberg, Mats and Jiang, Jifa and Niu, Lei. *A note on global stability of three-dimensional Ricker models*. Journal of Difference Equations and Applications, Taylor & Francis, 25(1):142-150, 2019.
- [122] Wu, Daiyong and Zhang, Hai. *Bifurcation analysis of a two-species competitive discrete model of plankton allelopathy*. Advances in Difference Equations, Springer, 3(1):70, 2014.

- [123] Azizi, Tahmineh and Kerr, Gabriel. *Chaos Synchronization in Discrete-Time Dynamical Systems with Application in Population Dynamics*. Journal of Applied Mathematics and Physics, Scientific Research Publishing, 8(3):406-423, 2020.
- [124] Azizi, Tahmineh and Kerr, Gabriel. *Synchronized Cycles of Generalized Nicholson-Bailey Model*. American Journal of Computational Mathematics, Scientific Research Publishing, 10(1):147-166, 2020.
- [125] Li, Tien-Yien and Yorke, James A. *Period three implies chaos*. Computational Ecology and Software, International Academy of Ecology and Environmental The American Mathematical Monthly, Taylor & Francis, 82(10):985-992, 1975.
- [126] Marotto, Frederick R. *Snap-back repellers imply chaos in R^n* . Journal of mathematical analysis and applications, Elsevier, 63(1):199-223, 1978.
- [127] Marotto, Frederick R. *Chaotic behavior in the Hénon mapping*. Journal of Mathematical Analysis and Applications, Elsevier, 68(2):187-194, 1979.
- [128] Marotto, FR. *On redefining a snap-back repeller*. Journal of Mathematical Analysis and Applications, Elsevier, 25(1):25-28, 2005.
- [129] Lin, Wei and Ruan, Jiong and Zhao, Weirui. *On the mathematical clarification of the snap-back-repeller in high-dimensional systems and chaos in a discrete neural network model*. International Journal of Bifurcation and Chaos, World Scientific, 12(05):1129–1139, 2002.
- [130] Li, Changpin and Chen, Guanrong. *An improved version of the Marotto theorem*. Chaos, Solitons & Fractals, Elsevier, 18(1):69-77, 2003.
- [131] Gardini, Laura. *Homoclinic bifurcations in n -dimensional endomorphisms, due to expanding periodic points*. Nonlinear Analysis: Theory, Methods & Applications, Elsevier, 23(8):1039-1089, 1994.

- [132] Gardini, Laura and Sushko, Iryna and Avrutin, Viktor and Schanz, Michael. *Critical homoclinic orbits lead to snap-back repellers*. Chaos, Solitons & Fractals, Elsevier, 44(6):433-449, 2011.
- [133] Wiggins, Stephen. *Introduction to applied nonlinear dynamical systems and chaos*. Princeton University Press, Springer Science & Business Media, 2, 2003.
- [134] Balibrea, Francisco and Cascales, Antonio. *Li-Yorke Chaos in Perturbed Rational Difference Equations*. International Conference on Difference Equations and Applications, Springer, 44(6):49-61, 2012.
- [135] Panchuk, Anastasiia. *Some aspects on global analysis of discrete time dynamical systems*. Qualitative theory of dynamical systems, tools and applications for economic modelling, Springer, 161-186, 2016.
- [136] Smale, Stephen. *Diffeomorphisms with many periodic points*. The Collected Papers of Stephen Smale: Volume 2, World Scientific, 44(6):636-653, 2000.
- [137] Moser, Jurgen. *Stable and random motions in dynamical systems: With special emphasis on celestial mechanics*. Princeton university press, 1, 2001.
- [138] Robinson, Clark. *Dynamical systems: stability, symbolic dynamics, and chaos*. CRC press, 1998.
- [139] Guckenheimer, John and Holmes, Philip. *Nonlinear oscillations, dynamical systems and bifurcations of vector fields*. J. Appl. Mech, 51(4):947, 1984.
- [140] Shilnikov, Leonid Pavlovich. *A contribution to the problem of the structure of an extended neighborhood of a rough equilibrium state of saddle-focus type*. Matematicheskii Sbornik, Russian Academy of Sciences, Steklov Mathematical Institute of Russian, 123(1):92-103, 1970.

- [141] Shilnikov, LP and Shilnikov, AL and Turaev, DV and Chua, LO. *Methods Of Qualitative Theory In Nonlinear Dynamics (Part II)*. World Sci. Singapore, New Jersey, London, Hong Kong, 2001.
- [142] Mira, Christian. *Chaotic dynamics: from the one-dimensional endomorphism to the two-dimensional diffeomorphism*. World Scientific, 1987.
- [143] Ricker, William E. *Stock and recruitment*. Journal of the Fisheries Board of Canada, NRC Research Press, 11(5):559-623, 1954.
- [144] Azizi, T and others. *Dynamics of a discrete-time plant-herbivore model*. Caspian Journal of Mathematical Sciences (CJMS), 4(2):241-256, 2015.
- [145] Smith, Hal L and Thieme, Horst R. *Dynamical systems and population persistence*. American Mathematical Soc, 118, 2011.
- [146] Kong, Xiangzeng and Chen, Liping and Yang, Wensheng. *Note on the persistent property of a discrete Lotka-Volterra competitive system with delays and feedback controls*. Advances in Difference Equations, Springer, 2010.
- [147] Thieme, Horst R. *Persistence under relaxed point-dissipativity (with application to an endemic model)*. SIAM Journal on Mathematical Analysis, SIAM, 24(2):407-435, 1993.
- [148] Hirsch, Morris W and Smith, Hal L and Zhao, Xiao-Qiang. *Chain transitivity, attractivity, and strong repellers for semidynamical systems*. Journal of Dynamics and Differential Equations, Springer, 13(1):107-131, 2001.
- [149] Kulenovic, Mustafa RS and Ladas, Gerasimos. *Dynamics of second order rational difference equations: with open problems and conjectures*. Chapman and Hall/CRC, 2001.
- [150] Bellows, TS and Hassell, MP. *The Dynamics of Age-Structured Host-Parasitoid Interactions*. The Journal of Animal Ecology, JSTOR, 259-268, 1988.
- [151] Hawkins, Bradford A. *Pattern and process in host-parasitoid interactions*. Cambridge University Press, 2005.

- [152] Hawkins, Bradford A and Sheehan, William and others. *Parasitoid community ecology*. Oxford University Press Oxford, 1 1994.
- [153] Earn, David JD and Rohani, Pejman and Bolker, Benjamin M and Grenfell, Bryan T. *A simple model for complex dynamical transitions in epidemics*. science, American Association for the Advancement of Science, 287(5453):667-670, 2000.
- [154] Earn, David JD and Rohani, Pejman and Bolker, Benjamin Geritz, Stefan AH and Kisdi, Éva. *On the mechanistic underpinning of discrete-time population models with complex dynamics*. Journal of Theoretical Biology, Elsevier, 228(2):261-269, 2004.
- [155] Frisman, E Ya and Neverova, GP and Revutskaya, OL. *Complex dynamics of the population with a simple age structure*. Ecological Modelling, Elsevier, 222(12):1943-1950, 2011.
- [156] Zeng, Zheng and Nowierski, Robert M and Taper, Mark L and Dennis, Brian and Kemp, William P. *Complex population dynamics in the real world: modeling the influence of time-varying parameters and time lags*. Ecology, Wiley Online Library, 79(6):2193-2209, 1998.
- [157] May, Robert M. *Chaos and the dynamics of biological populations*. Nuclear Physics B-Proceedings Supplements, Elsevier, 2:225-245, 1987.
- [158] Belykh, Igor and Hasler, Martin and Lauret, Menno and Nijmeijer, Henk. *Synchronization and graph topology*. International Journal of Bifurcation and Chaos, World Scientific, 15(11):3423-3433, 2005.
- [159] Cosp, Jordi and Madrenas, Jordi and Alarcón, Eduard and Vidal, Eva and Villar, Gerard. *Synchronization of nonlinear electronic oscillators for neural computation*. IEEE transactions on neural networks, IEEE, 15(5):1315-1327, 2004.
- [160] Porfiri, Maurizio and Pigliacampo, Roberta. *Master-slave global stochastic synchronization of chaotic oscillators*. SIAM Journal on Applied Dynamical Systems, SIAM, 7(3):825-842, 2008.

- [161] Fujisaka, Hirokazu and Yamada, Tomoji. *Stability theory of synchronized motion in coupled-oscillator systems*. Progress of theoretical physics, Oxford University Press, 69(1):32-47, 1983.
- [162] Pecora, Louis M and Carroll, Thomas L and Johnson, Gregg A and Mar, Douglas J and Heagy, James F. *Fundamentals of synchronization in chaotic systems, concepts, and applications*. Chaos: An Interdisciplinary Journal of Nonlinear Science, AIP, 7(4):520-543, 1997.
- [163] Pecora, Louis M and Carroll, Thomas L. *Synchronization in chaotic systems*. Physical review letters, APS, 64(8):821, 1990.
- [164] Boccaletti, Stefano and Kurths, Jürgen and Osipov, Grigory and Valladares, DL and Zhou, CS. *The synchronization of chaotic systems*. Physics reports, Elsevier, 366(1-2):1-101, 2002.
- [165] Li, Guo-Hui. *Modified projective synchronization of chaotic system*. Chaos, Solitons & Fractals, Elsevier, 32(5):1786-1790, 2007.
- [166] Yassen, MT. *Chaos synchronization between two different chaotic systems using active control*. Chaos, Solitons & Fractals, Elsevier, 23(1):131-140, 2005.
- [167] Camazine, Scott and Deneubourg, Jean-Louis and Franks, Nigel R and Sneyd, James and Bonabeau, Eric and Theraula, Guy. *Self-organization in biological systems*. Princeton university press, 2003.
- [168] Tarai, Anindita and Poria, Swarup and Chatterjee, Prasanta. *Synchronization of generalised linearly bidirectionally coupled unified chaotic system*. Chaos, Solitons & Fractals, Elsevier, 40(2):885-892, 2009.
- [169] Kocarev, Ljupco and Parlitz, Ulrich. *Generalized synchronization, predictability, and equivalence of unidirectionally coupled dynamical systems*. Physical review letters, APS, 76(11):1816, 1996.

- [170] Yang, Tao and Chua, Leon O. *Generalized synchronization of chaos via linear transformations*. International Journal of Bifurcation and Chaos, World Scientific, 9(01):215-219, 1999.
- [171] Rosenblum, Michael G and Pikovsky, Arkady S and Kurths, Jürgen. *Phase synchronization of chaotic oscillators*. Physical review letters, APS, 76(11):1804, 1996.
- [172] Rosenblum, Michael G and Pikovsky, Arkady S and Kurths, Jürgen. *From phase to lag synchronization in coupled chaotic oscillators*. Physical Review Letters, APS, 78(22):4193, 1997.
- [173] Khan, Mohammad Ali and Poria, Swarup. *Projective synchronization of bidirectionally coupled chaotic systems via linear transformations*. International Journal of Applied, 1(4):541-548, 2012.
- [174] Mainieri, Ronnie and Rehacek, Jan. *Projective synchronization in three-dimensional chaotic systems*. Physical Review Letters, APS, 82(15):3042, 1999.
- [175] Kolmogorov, Andre Nikolaevich and Fomin, Serge Vasilevich. *Elements of the theory of functions and functional analysis*. 1957.
- [176] Post, Eric and Forchhammer, Mads C. *Synchronization of animal population dynamics by large-scale climate*. Nature Publishing Group, Nature, 420(6912):168, 2002.
- [177] Noble, Andrew E and Machta, Jonathan and Hastings, Alan. *Emergent long-range synchronization of oscillating ecological populations without external forcing described by Ising universality*. Nature communications, Nature Publishing Group, 6:6664, 2015.
- [178] Manica, Vanderlei and Silva, Jacques AL. *Population distribution and synchronized dynamics in a metapopulation model in two geographic scales*. Mathematical biosciences, Elsevier, 250:1-9, 2014.
- [179] Gouhier, Tarik C and Guichard, Frédéric and Menge, Bruce A. *Ecological processes*

- can synchronize marine population dynamics over continental scales*. Proceedings of the National Academy of Sciences, National Acad Sciences 107(18):8281-8286, 2010.
- [180] Ricker, William E. *Stock and recruitment*. Journal of the Fisheries Board of Canada, NRC Research Press, 11(5):559-623, 1954.
- [181] Azizi, T and others. *Dynamics of a discrete-time plant-herbivore model*. Caspian Journal of Mathematical Sciences (CJMS), 4(2):241-256, 2015.
- [182] Smith, Hal L and Thieme, Horst R. *Dynamical systems and population persistence*. American Mathematical Soc, 118, 2011.
- [183] Mormann, Florian and Lehnertz, Klaus and David, Peter and Elger, Christian E. *Mean phase coherence as a measure for phase synchronization and its application to the EEG of epilepsy patients*. Physica D: Nonlinear Phenomena, Elsevier, 144(3-4):358-369, 2000.
- [184] Vinck, Martin and Oostenveld, Robert and Van Wingerden, Marijn and Battaglia, Francesco and Pennartz, Cyriel MA. *An improved index of phase-synchronization for electrophysiological data in the presence of volume-conduction, noise and sample-size bias*. Neuroimage, Elsevier, 55(4):1548-1565, 2011.
- [185] Daume, Jonathan and Gruber, Thomas and Engel, Andreas K and Frieze, Uwe. *Phase-amplitude coupling and long-range phase synchronization reveal frontotemporal interactions during visual working memory*. Journal of Neuroscience, Soc Neuroscience, 37(2):313-322, 2017.
- [186] Lowet, Eric and Roberts, Mark J and Bonizzi, Pietro and Karel, Joël and De Weerd, Peter. *Quantifying neural oscillatory synchronization: a comparison between spectral coherence and phase-locking value approaches*. PloS one, Public Library of Science, 11(1):e0146443, 2016.
- [187] Gambuzza, Lucia Valentina and Gomez-Gardenes, Jesus and Frasca, Mattia. *Amplitude dynamics favors synchronization in complex networks*. Scientific reports, Nature Publishing Group, 6(1):24915, 2016.

- [188] Liu, Hao and Zhang, Puming. *Phase Synchronization Dynamics of Neural Network during Seizures*. Computational and mathematical methods in medicine, Hindawi, 2018, 2018.
- [189] Lorenz, Edward N. *Deterministic nonperiodic flow*. Journal of the atmospheric sciences, 20(2):130-141, 1963.
- [190] Pikovsky, Arkady and Kurths, Jurgen and Rosenblum, Michael and Kurths, Jürgen. *Synchronization: a universal concept in nonlinear sciences*. Cambridge university press, 12, 2003.
- [191] Fujisaka, Hirokazu and Yamada, Tomoji. *Stability theory of synchronized motion in coupled-oscillator systems*. Oxford University Press, 69(1):32-47, 1983.
- [192] Yamada, Tomoji and Fujisaka, Hirokazu. *Stability theory of synchronized motion in coupled-oscillator systems. ii: The mapping approach*. Progress of Theoretical Physics, 70(5):1240-1248, 1983.
- [193] Pecora, Louis M and Carroll, Thomas L. *Synchronization in chaotic systems*. APS, 64(8):821, 1990.
- [194] Balmforth, NJ and Jacobson, A and Provenzale, A. *Synchronized family dynamics in globally coupled maps*. Chaos: An Interdisciplinary Journal of Nonlinear Science, AIP, 9(3):738-754, 1999.
- [195] Moran, Patrick AP. *The statistical analysis of the Canadian lynx cycle*. Australian Journal of Zoology, CSIRO, 1(3):291-298, 1953.
- [196] Bulmer, Martin G. *A statistical analysis of the 10-year cycle in Canada*. The Journal of Animal Ecology, JSTOR, 47(3):701-718, 1974.
- [197] Korpimäki, Erkki and Krebs, Charles J. *Predation and population cycles of small mammals: a reassessment of the predation hypothesis*. BioScience, American Institute of Biological Sciences Circulation, AIBS, 1313 Dolley, 46(10):754-764, 1996.

- [198] Ranta, Esa and Kaitala, Veijo and Lundberg, Per. *The spatial dimension in population fluctuations*. Science, American Association for the Advancement of Science, 278(5343):1621-1623, 1997.
- [199] Gurney, William SC and Crowley, Philip H and Nisbet, Roger M. *Locking life-cycles onto seasons: circle-map models of population dynamics and local adaptation*. Journal of Mathematical Biology, Springer, 30(3):251, 1992.
- [200] Blasius, Bernd and Stone, Lewi. *Chaos and phase synchronization in ecological systems*. International Journal of Bifurcation and Chaos, World Scientific, 10(10):2361-2380, 2000.
- [201] Earn, David JD and Rohani, Pejman and Grenfell, Bryan T. *Persistence, chaos and synchrony in ecology and epidemiology*. Proceedings of the Royal Society of London. Series B: Biological Sciences, The Royal Society, 265(1390):7-10, 1998.
- [202] Kolmogorov, Andre Nikolaevich and Fomin, Serge Vasilevich. *Elements of the theory of functions and functional analysis*. 1957.
- [203] Wiggins, Stephen. *Introduction to applied nonlinear dynamical systems and chaos*. Princeton University Press, Springer Science & Business Media, 2, 2003.
- [204] Grobman, David M. *Homeomorphism of systems of differential equations*. Doklady Akademii Nauk SSSR, MEZHDUNARODNAYA KNIGA 39 DIMITROVA UL., 113095 MOSCOW, RUSSIA, 128(5):880-881, 1959.
- [205] Hartman, Philip. *On local homeomorphisms of Euclidean spaces*. Bol. Soc. Mat. Mexicana, 5(2):220-241, 1960.
- [206] Hartman, Philip. *A lemma in the theory of structural stability of differential equations*. Proceedings of the American Mathematical Society, JSTOR, 11(4):610-620, 1960.
- [207] Conrad, Keith. *The Contraction Mapping Theorem, II*. 2014.

- [208] Russo, Giovanni. *Analysis, Control and Synchronization of nonlinear systems and networks via Contraction Theory: theory and applications*. University of Naples Federico II, Italy, 2010.
- [209] Angeli, David. *A Lyapunov approach to incremental stability properties*. IEEE Transactions on Automatic Control, IEEE, 47(3):410-421, 2002.
- [210] Beddington, JR and Free, CA and Lawton, JH. *Host-parasitoid dynamics of a generalized Thompson model*. Nature Publishing Group, Nature, 255(5503), 1975.
- [211] Nicholson, Alexander J and Bailey, Victor A. *The Balance of Animal Populations Part I*. Proceedings of the Zoological Society of London, 105(3):551-598, 1935.
- [212] Asheghi, Rasoul. *Bifurcations and dynamics of a discrete predator-prey system*. Journal of biological dynamics, Taylor & Francis, 8(1):161-186, 2014.
- [213] Kapçak, Sinan and Ufuktepe, Ünal and Elaydi, Saber. *Stability and invariant manifolds of a generalized Beddington host-parasitoid model*. Journal of biological dynamics, Taylor & Francis, 148(2):233-253, 2013.
- [214] Ricker, William E. *Stock and recruitment*. Journal of the Fisheries Board of Canada, NRC Research Press, 11(5):559-623, 1954.
- [215] Azizi, T and others. *Dynamics of a discrete-time plant-herbivore model*. Caspian Journal of Mathematical Sciences (CJMS), 4(2):241-256, 2015.